University of Catania

Department of Clinical and Sperimental Medicine

PhD Program in Translational Biomedicine

XXXV Cycle

PhD Thesis

Giovanni Lauretta

Study of Novel Approaches in Tissue Engineering for Cartilage Repair and Prevention of Osteoarthritis

Coordinator: *Prof. Carlo Vancheri*

Tutor: *Prof. Giuseppe Musumeci*

Academic year: 2021/2022

Affiliations

Gen 2020- Dec 2022 – PhD Student;

Department of Biomedical and Biotechnological Sciences, Anatomy, Histology and Movement Science Section, University of Catania, Via S. Sofia 87, 95123 Catania, Italy.

Mar 2021 - Nov 2021– Guest PhD Student;

AO Research Institute Davos, Clavadelerstrasse 8, 7270 Davos, Switzerland.

Riassunto

L'osteoartrite (OA) è una patologia degenerativa che colpisce l'intera articolazione, portando ad alterazioni a carico della cartilagine che possono estendersi anche, ai legamenti, osso subcondrale e membrana sinoviale. Quarta causa di disabilità nel mondo, l'OA, il cui carico finanziario e sociale è destinato ad aumentare nel tempo, è la principale ragione alla base degli interventi di artoplastica nei paesi sviluppati. Sebbene precedentemente considerata esclusivamente come una malattia “da usura”, dovuta al fisiologico invecchiamento della cartilagine articolare che ne riduce la capacità nel sostenere i carichi, l'OA è ormai evoluta nella definizione come una patologia multifattoriale e complessa. Si presume infatti che uno squilibrio tra i processi anabolici e catabolici agisca insieme con diversi fattori di rischio, rappresentati da età, sesso, genetica, obesità, stress fisici, traumi e lesioni.

Il trattamento dell’ OA nella pratica clinica è ostacolato dalla scarsa capacità di auto-rigenerazione della cartilagine. L'ingegneria dei tessuti, che si basa sull’uso combinato di matrici biocompatibili, cellule progenitrici e stimoli biologici e biofisici, emerge come una strategia promettente per la rigenerazione della cartilagine articolare.

Uno degli obiettivi di questo lavoro di tesi è stato quello di valutare in vitro, il differenziamento in senso condrogenico di cellule staminali mesenchimali umane primarie isolate da midollo osseo, in pellet e in hydrogels composti da GelMA e acido ialuronico sottoposti a preincubazione con il fattore di crescita TGFβ1 e stimolazione meccanica. Inoltre si è voluto sfruttare le attuali conoscenze in questo campo di ricerca per investigare l’ efficacia di un scaffold cell-free di collagene di tipo I nel promuovere la riparazione cartilaginea dopo l'impianto ortotopico in modelli in vivo di ratto.

Infine, l’attuale letteratura scientifica sottolinea l'importanza della prevenzione e dell'intervento terapeutico precoce al fine di evitare la degenerazione della cartilagine e rallentare la progressione dell’ OA. Per questo motivo, un altro obiettivo di questo lavoro di tesi è stato quello di contribuire alla ricerca nel campo della prevenzione con nuove evidenze scientifiche, sull'effetto dell'esercizio fisico nella cartilagine articolare durante la progressione della patologia, e sulle conseguenze dell'atrofia muscolare dovuta all'inattività, in una popolazione di cellule staminali.

Abstract

Osteoarthritis (OA) is a degenerative disease that affects the entire joint, leading to alterations in articular cartilage, ligaments, subchondral bone, and synovium. Rated as the 4th leading cause of chronic disability worldwide, OA is the most common reason behind joint replacement in developed societies, and its financial and social burden is likely to increase in the next future. Once merely considered as a “wear and tear” disease, due to the physiological decline of cartilage architecture in weight-bearing tolerance, OA is by now evolved into the definition of a multifactorial and complex disease. An imbalance between anabolic and catabolic processes is assumed to act in concert with several risk factors, e.g., age, gender, genetics, obesity, bone metabolism, physical stresses, muscle strength, trauma, and sports injuries.

The treatment of chondral defects in clinical practice is hindered by the poor self-healing ability of cartilage. Tissue engineering, combining the use of biocompatible scaffolds, progenitor cells and biological and biophysical stimuli, emerges as a promising strategy for joint regeneration. One of the aims of this research was to evaluate in vitro, the chondrogenic differentiation of primary human bone-derived mesenchymal stromal cells in pellet cultures and in GelMA/HA hydrogels exposed to TGFβ1 priming and mechanical stimulation. In addition, another aim of this research was to exploit tissue engineering principles by evaluating the capability of a cell-free collagen I-based scaffold to promote cartilaginous repair after orthotopic implantation in vivo rat model.

Furthermore, current literature underlines the importance of prevention and early intervention in order to avoid cartilage disruption and slow down the disease progression. For this reason, another aim of this work focused on contributing to the field of prevention of OA disease with new insights about, the effect of physical exercise in OA articular cartilage and the consequence of muscle atrophy due to inactivity in a population of stem cells.

Index

1 General introduction

1.1 Joints

The joint is anatomically defined as a complex of structures that maintains two or more bone surfaces in mutual contiguity. The human skeletal system exhibits a large number of joints (about 360) which, based on their degree of movement, are classified into synarthrosis (immovable), amphiarthrosis (poorly movable) and diathrosis (movable) also known as synovial joint.

The latter allow to perform a wide range of movements thanks to their complex anatomical organisation. Specifically, they consist of two or more bone ends separated by a cavity of a few millimetres. The surfaces of the bone ends are covered with highly specialised hyaline cartilage (articular cartilage) which provides a smooth surface where the bones meet. The bone ends are held together by a joint capsule, a sleeve of fibrous connective tissue, rich in blood vessels and lined internally with the synovial membrane, capable of filtering synovial fluid from the blood. This fluid, poured into the joint cavity, has a trophic and lubricating function for the articular cartilages and reduces the mechanical friction between the contiguous joint surfaces. Joint capsules can also be reinforced by ligaments with stabilising functions and limit joint movement in some directions. Particular then, is the presence in some cases of fibrocartilaginous discs (such as menisci) interposed between the articular cartilages, whose main function is to make the articular surfaces of the skeletal segments more concordant. Examples of synovial joints include the hip, shoulder, elbow, wrist, and knee (Schunke et al., 2014).

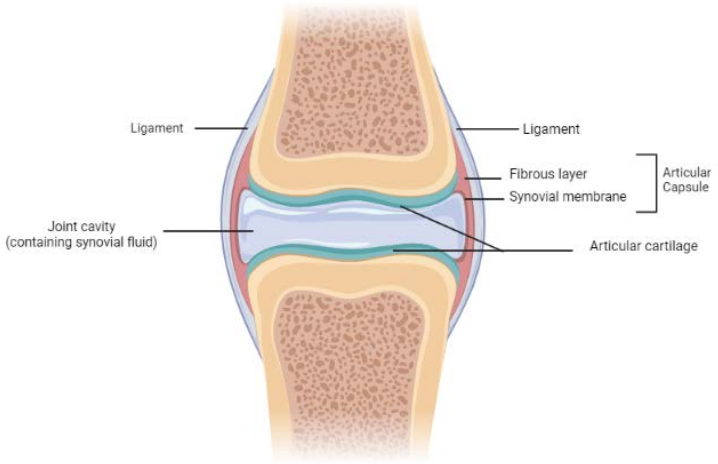

Figure1.1. Schematic representation of synovial joint. Articular cartilage on the ends of the articulating bones acts as buffer against loads and forces that act on the joint. The articular capsule is composed of the synovial membrane and a fibrous capsule. The articular joint capsule contains synovial fluid that is produced by the cells of the synovial membrane. Picture created with BioRender.com.

1.2 The knee joint

The knee joint is one of the biggest synovial joints in the skeletal system which allows for flexion, extension, and some limited degree of leg rotation. Structurally, the knee is composed of three bones and two joints included within a complex joint capsule: the femorotibial joint, between the tibia and femur and the femoralpatellar joint, between the patella and the femur. In the femorotibial joint there is a disproportion between the two articular surfaces since the femoral condyles are rounded and more developed in the sagittal plane, while the tibial surface is almost flat. This irregularity is mediated by the presence of two menisci, medial and lateral, which are fixed on the intercondylar tibial surface. They protect the joint surfaces from shocks and help to cushion the body weight and distribute it, evenly over the entire joint. The patella within the patellofemoral joint has a protective role for the knee joint and also increases the lever arm of quadriceps muscle in order to facilitate the knee extension. Finally, the knee joint is characterised by the presence of numerous ligaments that provide stability and limitation of femur and tibia reciprocal movements. This ligamentous system encompasses: collateral ligaments (tibial and peroneal), cruciate ligaments (anterior and posterior), patella retinacles (lateral and medial), patellar ligament and popliteal ligaments (oblique and arched) (Schunke et al., 2014).

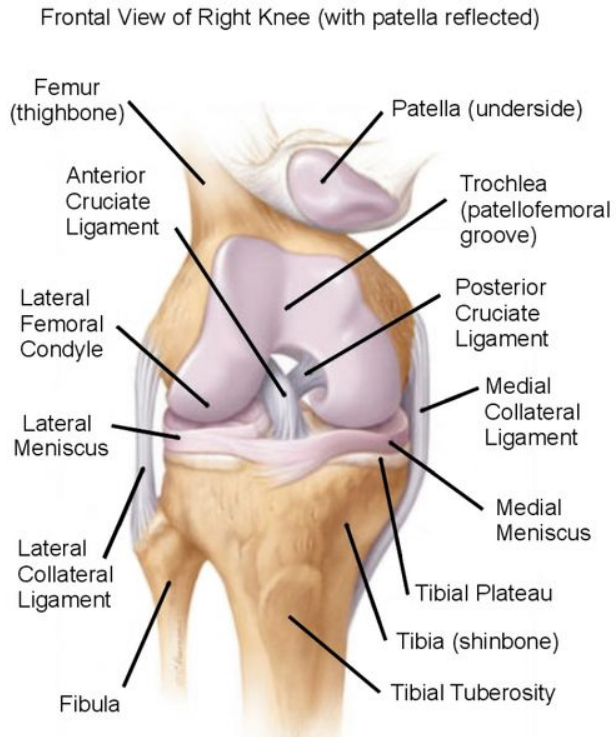

Figure 1.2 Anatomy of knee joint. Schematic representation of the right knee joint with patella reflected.

1.3 Articular Cartilage

Articular cartilage is the highly specialised connective tissue that covers the bone ends of diarthrodial joints. In the knee joint it covers the femur and tibia condyles and under surface of the patella. Its main function is to provide a continuous, lubricated and friction-free surface for the joints and to facilitate the transmission of loads to the underlying subchondral bone (Sophia Fox et al., 2009). The only cells present in the tissue are chondrocytes, embedded in a dense extracellular matrix (ECM). These cells are specialised in the ECM synthesis and maintaining the health of cartilage which is an avascular, alymphatic and aneural tissue. Due to these tissue characteristics, the chondrocytes are not able to draw nourishment from the blood stream, indeed their survival and function depend on the diffusion and transport of nutrients, metabolites and oxygen through the ECM.

Chondrocytes constitute about 2% of the total volume of articular cartilage and originate from mesenchymal stem cells (MSCs) through the process of chondrogenesis during development (Brendan et al., 2018).

The ECM is an organised network of collagens, glycosaminoglycans (GAGs) and proteoglycans immersed in an interstitial fluid composed by water and electrolytes. The collagens represent the 60% of dry weight of cartilage and are responsible of shape and tensile straight of the tissue. The most abundant is the collagen type II (up to 90%) but other collagen isoforms are present in smaller quantities such as collagen type I, IV, V, VI, IX and XI (Bruckner and van der Rest, 1994).

The GAGs (i.e., a long, unbranched polysaccharide), most represented in articular cartilage are chondroitin, keratin sulphate and hyaluronic acid (HA), which forms aggregates where other molecules such as proteoglycan can bind (Fraser et al., 1997).

The proteoglycans present in ECM are aggrecans, decorin, fibronectin, lumican, lubricin and biglycan. Aggrecan is the most abundant in articular cartilage where forms big aggregates with HA (Fig. 1.3). It is highly glycosylated with negatively charged sulfated GAGs, which can bind water molecules and generate a charge density essential to counteract compressive force during mechanical loading via attraction of solute, generating an osmotic resistance crucial to maintain cartilage unique viscoelastic and mechanical properties (Kiani et al., 2002). In addition, due to the proteoglycans molecular characteristics, the resulting network works as a molecular filter, which selectively prevents the passage of certain molecules and facilitates the diffusion of others. This creates an excellent barrier system capable of block the transit of molecules with a molecular weight between 40 and 180 kDa (Kiani et al., 2002).

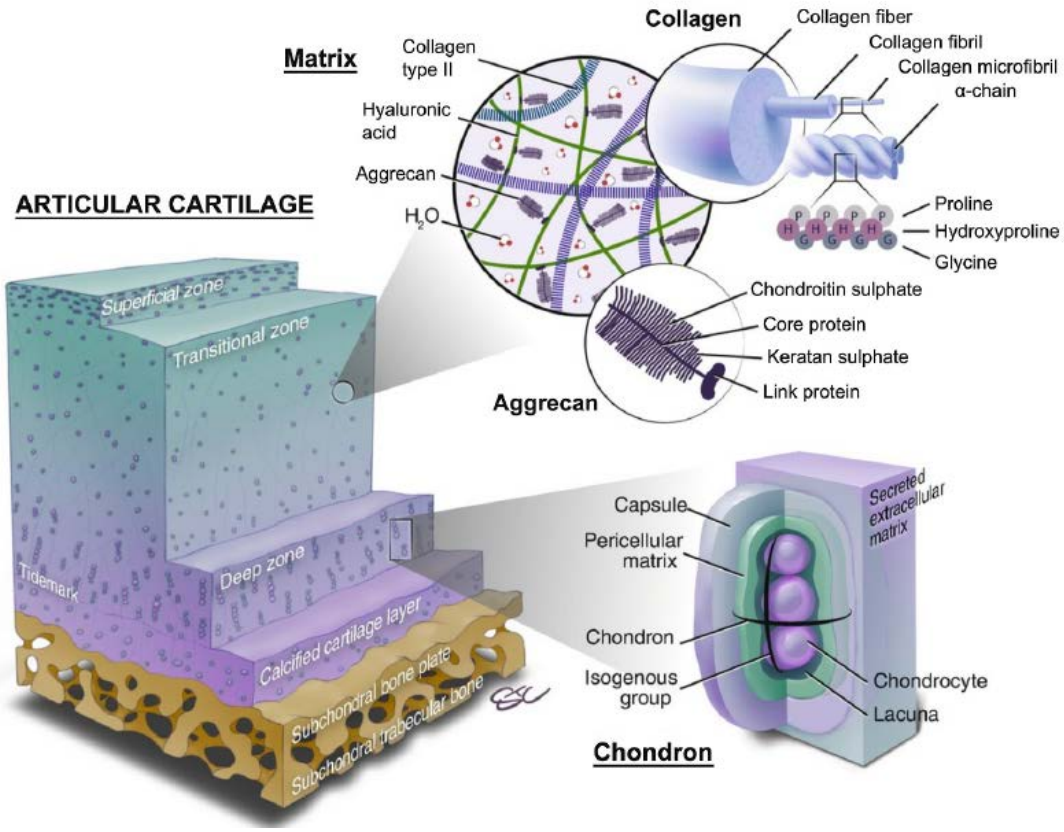

Figure 1.3 Articular cartilage. Schematic representation of the articular cartilage extracellular structure and its main individual components including the collagen type II and aggrecan in matrix, and chondron (Baumann et al., 2019).

Based on orientation and cell density, organisation of collagen fibres, and content and distribution of proteoglycans, articular cartilage can be morphologically distinct in four zones: superficial, transitional (or intermediate), deep (or radial) and calcified zone (Fig. 1.3).

The superficial zone is characterised by high number of flattened chondrocyte oriented in parallel to the surface, which produce high amounts of HA and lubricating proteoglycan lubricin (also known as proteoglycan-4 or PRG4). The collagen fibrils, mainly collagen type II and IX fibres, are tightly packed and also oriented in parallel to the surface. This orientation counteracts osmotic swelling pressure of the tissue below protecting the layers below from biomechanical stress. It is mainly responsible for the viscoelastic ability to resist tensile tangential generated by the flux of the synovial fluid on the surface during rotational movement of the joint (Teshima et al., 1995).

Below the superficial zone is located the transitional zone which represent 40%-60% of articular cartilage. It consists of randomly oriented collagen fibres with a limited number and sparse of spherical chondrocytes. This layer contains more proteoglycans, which maintain the fluids within the tissue and are responsible for the articular cartilage distinctive compression resistance property (Sophia Fox et al., 2009). Beneath the transitional zone is situated the deep zone. In the deep zone the

collagen fibres are aligned perpendicular to the surface, while the chondrocytes are organised in columns oriented parallel to collagen fibres, improving resistance to compressive forces.

A tidemark separates the deep zone from below calcified zone, so named for the presence of calcium salts in the ECM. This zone connects the cartilage to the bone, by implanting the collagen fibrils of the deep zone to the subchondral bone. In this zone there is a small number of hypertrophic chondrocytes which express hypertrophic markers such as collagen type X and alkaline phosphatase (ALP) to calcify the ECM (Poole et al., 2001).

Due to the lack of nerves, blood and lymphatic vessels, and limited cellularity, cartilage shows restricted capabilities for intrinsic healing and repair. For this reasons the maintenance and health of this tissue is essential for joint function, since it is continuously subjected to severe biomechanical load. Specifically, cartilage continuously remodels itself solicited by external stimuli such as daily mechanical forces which induce deformations of the ECM, captured by the mechanoreceptors and voltage-dependent channels located in the cell membrane of the chondrocytes (Mobasheri et al., 2010). This mechanism triggers environmental modification of the pericellular milieu through the increase in concentration of proteoglycans,and changes in ionic concentration and pH. The increase of proteoglycans in the matrix results in an increase in free anion groups which, being hydrophilic, can bind further water molecules allowing a growth in the volume of the amorphous component and therefore inducing a ECM remodelling. However, in the most stressed areas, inappropriate or persistent mechanical stimuli could eventually lead to cartilage injuries (Heijink et al., 2012). In addition, the absence of blood supply, lymphatic drainage and innervation makes cartilage repair more difficult. Chondrocytes synthesise the matrix components but also secrete enzymes that degrade the various ECM components during the physiological turnover process. Pathological imbalance takes place when chondrocytes activate the catabolic enzymes, reduce the production of their inhibitors and therefore leading to the accelerate ECM degradation. If the degradation and damage of the matrix exceed the poor reparative capability of the chondrocytes, the damage becomes permanent, leading to degenerative and pathological processes, such as osteoarthritis, the word most common joint disease.

1.4 Osteoarthritis

Osteoarthritis (OA) is a degenerative disease with various aetiology and complex pathogenesis, characterised by the progressive deterioration of the articular cartilage, that causes structural and functional failure resulting in pain and severe disability of the affected joint (Xia et al., 2014). It can affect small, medium, and large joints, although in terms of a painful disease, the hip and knee are most frequently affected. Evidences have showed that in the United States in up to 10% of men and 13% of women aged above 60 years are affected by OA of the knee (Zhang et al., 2010).

The exact OA aetiology is not yet fully understood although it generally refers to a multifactorial aetiology for the different elements that influence the risk of OA development. In the vast majority of cases, OA appears insidiously, and may develop without apparent initial cause. In this case referring to idiopathic or primary OA where the main risk factor is related to ageing which lead to reduced regenerative capacity of cartilage. In addition, another important determinant is sex with a significant incidence increase in women than men (Sacitharan, 2019). In about 5% of cases, OA appears in younger subjects who present predisposing and genetic conditions, or joint deformity, traumatic injuries or underlying systemic disease that jeopardises the joints, such as diabetes and obesity. In this context, the disease is called secondary OA (Van Spil et al., 2019).

Despite, OA for a long time was considered as an ageing disease and an inevitable process ‘wear and tear’ of articular cartilage, this definition is reductive since the bases of this escalating damage depend on a compromised balance between anabolic and catabolic mechanisms, which can be consequent to several risk factors like ageing, muscle atrophy, metabolic disorders, inflammatory conditions, injuries and mechanical overload, or wrong biomechanics of the joint.

The central OA feature is the progressive deterioration of the articular cartilage. This process is usually divided mainly into three stages. (1) Chondrocyte loss and phenotypic transformation, influenced by genetic and biochemical factors. (2) Early OA, in which chondrocytes proliferate with formation of cell clusters, and increased collagen and proteoglycans production that interact to remodel the cartilage matrix. This initial phase is followed by an increase of catabolic activities with the subsequent proteoglycans loss, and the normal horizontal arrangement of the collagen type II fibres in the surface zone, is disrupted and cracks. Consequently, the water retention inside the matrix diminishes, thereby decreasing the resistance of articular cartilage to compression (Loeser et al., 2012; Mobasheri et al., 2017). The main cartilage matrix-degrading enzymes involved in this process are disintegrin and zinc-dependent metalloproteinases (MMPs) with thrombospondin motifs (ADAMTS) 4 and 5 responsible for aggrecan proteolysis, and MMP-1,3 and 13 collagen type II degradation (Troeberg et al., 2012). (3) Late OA, in which the repeated damage and chronic

inflammation lead to disappearance of the chondrocytes, marked loss of cartilage, full-thickness cartilage fragments detach, and extensive changes in the subchondral bone which becomes exposed. There is therefore hardening and sclerosis (irreversible bone thickening) of the cancellous bone below. Small fractures of the joint bone and the empty spaces created by the fractures allow synovial fluid to penetrate subchondral regions. Osteophytes are formed at the joint margins, and these are covered with fibrocartilage, which gradually ossify (Geyer and Schönfeld, 2017). In addition, remodelling of subchondral bone occurs together with the development of blood vessels located in vascular channels that contain osteoblasts and sensory nerves (Fig 1.4). This vascular channels promote biochemical communication between the bone and cartilage. In response to multiple stimulations, chondrocytes modify further their phenotype and start to express a subset of factors such as cytokines, chemokines, alarmins, damage-associated molecular patterns (DAMPs), and adipokines, which begin a vicious cycle of cartilage breakdown (Jang et al., 2021). These molecular factors through the synovial fluid, reach also the synovial membrane where trigger alterations and involving it, in this process. Synovial membrane became hyperplastic with an increase in the number of synovial macrophages, and hypertrophic, with small villi or folds, infiltration of blood cells and vascularity increase in the subintimal layer. The involvement of synovial membrane and the recruitment of inflammatory cells with the consequent production increase of mediators as cytokines such as Interleukin-1 (IL-1) and Tumor Necrosis Factor (TNF), prostaglandins and nitric oxide accelerates the process of tissue degeneration, promoting chondrocytes injury and apoptosis (Berenbaum et al., 2013).

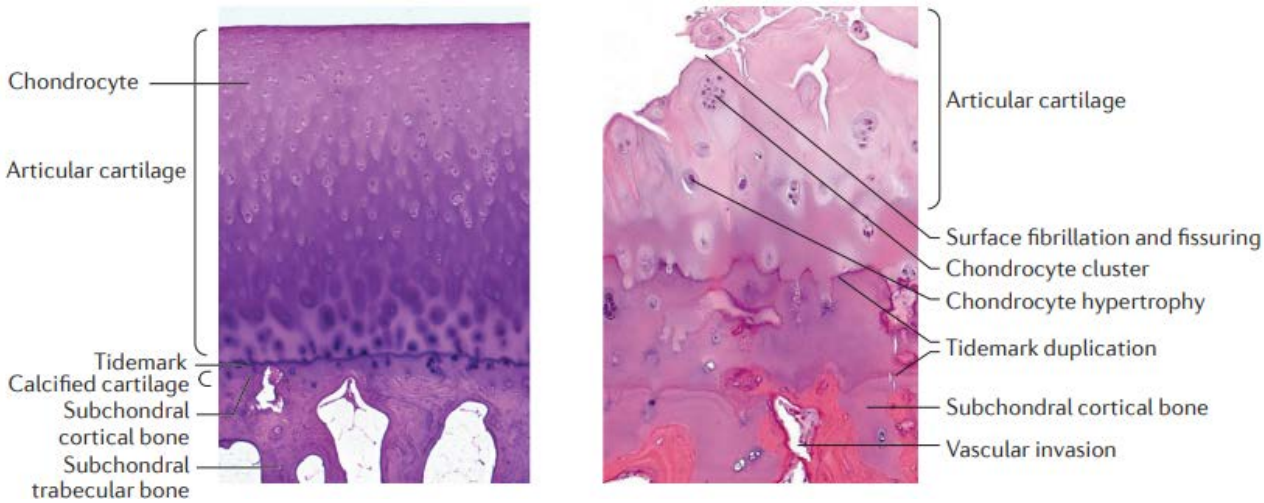

Figure 1.4. Histological comparison between healthy and osteoarthritic articular cartilage. On the left is reported an histological section of human cartilage where are highlighted the main structural elements, including chondrocytes, tidemark (separating the calcified and articular cartilage), calcified cartilage, subchondral cortical and trabecular bone. On the right is reported a histopathological section of the articular cartilage showing advanced osteoarthritic changes, characterised by fissuring and fragmentation of the ECM, chondrocyte proliferation and hypertrophy, duplication and advancement of the tidemark, expansion of the zone of calcified cartilage, thickening of the subchondral cortical plate and vascular invasion of the bone and calcified cartilage (Adapted from Martel-Pelletier et al., 2016).

Since OA can be (especially in early stage) asymptomatic, and there is no correlation between OA symptoms and radiographic determination, the diagnosis of OA is made only when the pathology became symptomatic. At this point the disease is at an advanced stage with potential irreversible structural changes in the affected joint. Classically, the diagnosis is made using conventional radiography with the pertinent image findings, including loss of joint space, osteophyte formation, subchondral sclerosis, and subchondral cysts (Robinson et al., 2018). The severity of disease is determined using the Kellgren-Lawrence severity grade, a semi-quantitative classification system (Kellgren and Lawrence,1957). In recent years, magnetic resonance imaging (MRI) has been used to evaluate knee pain and has helped identify the classical diagnostic signs as well as recognising osteophyte formation in difficult to access areas such as the intercondylar notch (Oo et al., 2017). MRIs can also help to show other associated, soft tissue findings such as synovial hypertrophy, effusion, meniscal tear, and cartilage loss that are not seen on ordinary radiographs (Oo et al., 2017). To date, since the exact pathogenesis is not completely understood, the clinical OA management is focused mainly on symptomatic therapy with pain reduction. Analgesics, oral or topical non-steroidal anti-inflammatory drugs as well as intra-articular corticosteroid injection are all indicated for OA management (Kolasinski et al., 2020). Meanwhile lifestyle changes, including adopting a healthy diet with eight loss and appropriate program of physical exercise, are considerate as preventive approaches and capable of symptom improvement or reduction their development. However, in patients with end-stage disease, the only effective solutions available to relieve the pain and re-establish the joint motility, are based on the use of tissue grafts and prosthetic joints. However, these methods are limited by the poor availability of suitable donor tissue, the risk of infection, and implant failure associated with total joint replacements (Langer and Vacanti, 1993). These limitations are the driving forces behind much research into cell-based methods and tissue engineering approach for effectively treating diseased or damaged cartilage.

1.5 Tissue engineering: an alternative to cartilage repair

As described above, OA disease is characterised by poor regenerative properties of articular cartilage once injured. An attractive alternative strategy for cartilage repair is tissue engineering, which aims to repair, regenerate, and/or improve diseased or injured articular cartilage functionality, presenting great potential to improve articular cartilage therapy. A rapid expanding field in this last two decades, tissue engineering is a discipline that applies the current knowledge of material science, cellular and molecular biology, and bioengineering to design tissue templates with the aim of restore the function and structure of an injured tissue (Danisovic et al., 2012). The modern tissue engineering for cartilage repair, is based on the use of three key elements (also known as triad): 3D scaffolds, progenitor cells and biochemical and biophysical stimuli (Wei and Dai, 2021). In fact, this field relies extensively on the use of 3D scaffolds which are designed to mimic structural and biological cues of the native cartilage unit, supporting both cartilaginous repair and the integration of the newly formed matrix with the surrounding tissues. The scaffolds essentially act as a template for tissue formation and are typically seeded with cells which may be treat with growth factors, or subjected to biophysical stimuli through the use of bioreactors, i.e. devices or systems which apply different types of mechanical stimuli to cells (Martin et al., 2004). The cell-seeded scaffolds are either cultured in vitro to synthesise new tissue which can then subsequently be implanted into an injured site, or are implanted directly into the injured site, where new tissues synthesis is induced directly in vivo.

1.5.1. Scaffolds features

Numerous scaffolds are produced from a variety of biomaterials and manufactured using a plethora of fabrication techniques, but generally several requirements from different perspectives need to be considered for scaffolds suitability:

1) Biocompatibility. The first condition of every scaffold for tissue engineering is that it must be biocompatible; cells need to be able to survive, adhere, function normally, and migrate onto the surface or through the scaffold and begin to proliferate before to produce new matrix. After implantation, the scaffold must no show any immune reaction in order to prevent it causing such a severe inflammatory response that it might reduce healing or cause rejection by the body.
2) Biodegradability. Scaffolds are not intended as permanent implants. For this reason, the scaffold must be biodegradable in order to allow cells to produce their own extracellular

matrix. In addition, the component produced from this degradation should also be non-toxic and without interference with surrounding tissue (Zhang et al., 2009).

3) Scaffold architecture. Usually scaffolds show an interconnected pore structure and high porosity to ensure cell penetration and promote oxygen, nutrients and waste diffusion and exchange within the construct and to the ECM formed by the cells.
4) Mechanical properties. Ideally, the scaffolds should show mechanical properties consistent with native tissue into which it is to be implanted. For this reason, creating scaffolds with adequate mechanical properties is the greatest challenge in attempting to engineer articular cartilage. Because the ideal scaffold should recreate the composition of cartilage in terms of the liquid and solid phases of the tissue and also reproduce its zonal and regional organisation as well as facilitate the integration of the new formed tissue with the adjacent native one (Cao et al., 2014).

In order to obtain the ideal scaffold that better satisfy the characteristics above described for cartilage repair, a lot of polymers have been tested and studied. These polymers, usually presented in the form of hydrogels composed of native ECM-mimicking networks, are usually classify into synthetic and natural polymers, and their corresponding derivatives (Szychlinska et al., 2019).

The most commonly synthetic polymers (aliphatic polyesters) used for the realisation of scaffolds are polyethylene glycol (PEG) (Chu et al., 2020), polylactic acid (PLA) (Singhvi et al., 2019), polyglycolic acid (PGA) (Horbert et al., 2021) poly(lactic acid-co-glycolic acid) (PLGA) (Dhanabalan et al., 2020), and polycaprolactone (PCL) (Zheng et al., 2021) (Fig. 1.5). The advantage of using these synthetic polymers resides in their ease of processing, preserving the sterility of the material, optimal mechanical properties, and the possibility of controlling the degradation times by altering their structure. However, these synthetic polymers show some disadvantages related to their limited bioactivity for cell attachment, inadequate intercellular signal transmission, and common hydrophobic character, as well as their harmful acidic degradation products (Ge et al., 2012; Camarero-Espinosa et al., 2016). The latter may induce a potential increase in local pH, triggering an excessive inflammatory responses and poor clearance and chronic inflammation associated with high molecular weight of polymers products (Stoop, 2008). Most recent research efforts have pursued the combination of different materials, natural and synthetic, with the objective to exploit the best properties of each of them.

Several natural materials, have acquired widespread explorations due to the structural similarity to native cartilage and the consequent biocompatibility, biodegradability and little inflammatory response. Natural polymers mainly investigated, include polysaccharides such as hyaluronic acid

(HA), chondroitin sulfate, alginate, agarose, chitosan, gellan gum, and protein-based materials such as collagen, gelatin, silk, and fibrin (Wei and Dai, 2021) (Fig.1.5).

HA is the most abundant GAG in native cartilage and plays a pivotal role in the structural and functional maintenance of cartilage. For these reasons based HA-scaffolds have been highly studied. However, by itself, HA exhibits low intrinsic biomechanical properties. To improve its mechanical performance, HA has been often combined with stronger polymers in cartilage repair or subjected to chemical modifications at the hydroxyl and carboxyl functional groups using methacrylate, thiol, enzyme and amino acid (Broguiere et al., 2016; Jooybar et al., 2019; Vainieri et al, 2020; Chen et al., 2021). Chondroitin sulphate shows similarities with HA, in fundamental structural and biological processes of cartilage. It presents good cell encapsulation and adhesion properties but is subjected to fast degradation by chondroitinase, and show low mechanical strength. For this reason, it is often combined with other polymers (Jeuken et al., 2016). The other natural polysaccharides alginate, agarose, chitosan and gellan gum exhibit structural similarity with GAGs and for this reason, they have been widely explored in tissue engineering for cartilage repair. Their inferior mechanical strength and low bioactivity are always addressed by combining with other polymers and encapsulating different kind of bioactive molecules inside the constructs (Rennerfeldt et al., 2013; Lee et al., 2021; Saygili et al., 2021; Li et al., 2021).

Among the protein based- materials, collagen is the most characterised and used. Collagen comprises about 25% of the total protein of human body, making it a valid choice for tissue engineering applications. Collagen contains cell binding sites and its natural properties are similar to that of soft tissue (Rezvani Ghomi et al., 2021). Different types of collagen have been studied as matrices for cartilage engineering, of which collagen type I is the most commonly used to form scaffolds . Collagen type I based scaffolds have been shown to promote chondrocyte proliferation and cartilage tissue formation (Camarero-Espinosa et al., 2016). Nevertheless, the mechanical properties of collagen type I are generally not enough to withstand load-bearing in joints. Therefore, collagen type I usually is modified or used in combination with other polymers, to enhance their chemical and mechanical properties, which can be tailored to cartilage (Kilmer et al., 2022). Collagen type I can also be denatured to produce gelatin, which can be modified to produce gelatin methacryloyl (GelMa) (Yue et al., 2015). GelMA hydrogels can be produced by photo-crosslinking and its mechanical and chemical properties are easily tunable.

In conclusion, scaffolds based on natural materials usually show very interesting results in terms of biocompatibility and chondrogenesis support. However, to date, common disadvantages such as the difficulty of processing them into desired shapes or architectures, the difficulty of functionalisation,

and the fast enzymatic degradation of the biopolymers lead often to unreproducible results due to batch-to-batch differences (Camarero-Espinosa et al., 2016).

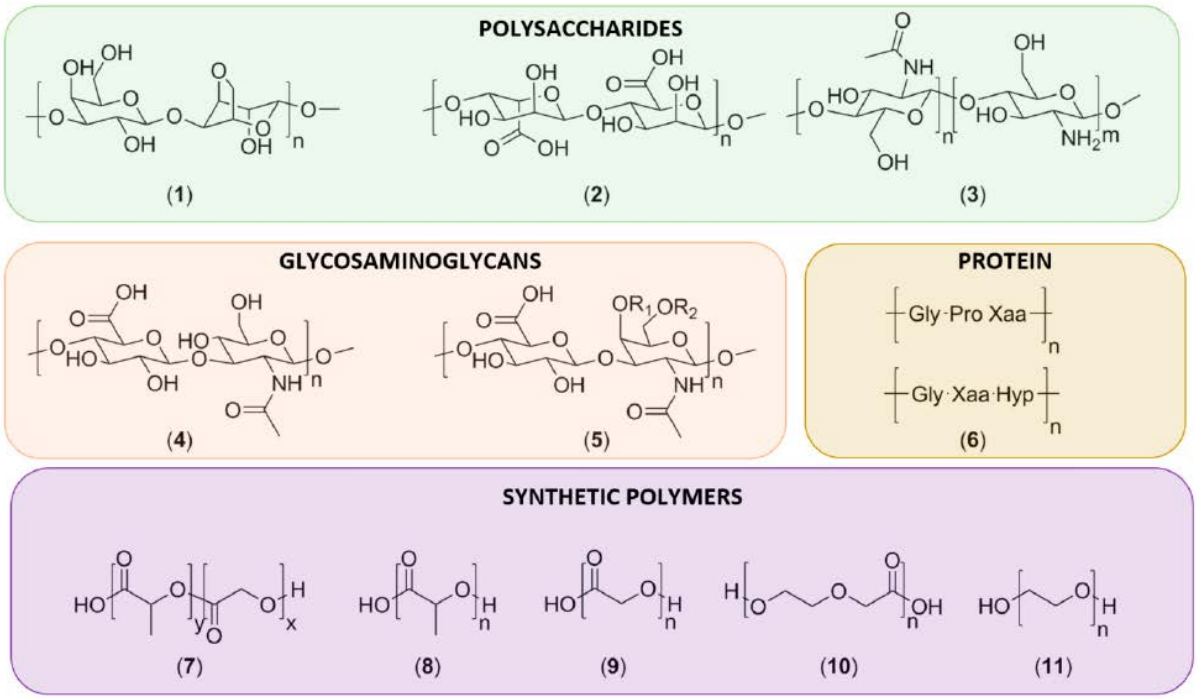

Figure 1.5 Schematic representation of commonly biopolymer structures used in cartilage repair. Displayed are the natural polymers (1) agarose, (2) alginate, (3) chitosan, (4) hyaluronic acid, (5) chondroitin-4- (6) collagen, which show two common tripeptide repeats, where Hyp represents L-4- hydroxyproline and X represents any amino acid other than Gly, Pro or Hyp, and is often a basic or acidic amino acid. Synthetic polymers (7) poly(lactic-co-glycolic acid) (PLGA), (8) poly(lactic acid) (PLA), (9) poly(glycolic acid) (PGA), (10) polydioxanone (PDS) and (11) poly(ethylene glycol) (PEG) (Jeuken et al., 2016).

1.5.2. Progenitor Cells

The use and addition of cells with chondrogenic differentiation potential inside the scaffolds is widespread in tissue engineering for the creation of an engineered cartilage unit. The incorporated cells are universally considered to improve the outcome of ECM deposition and tissue regeneration, influenced also by the interaction between the artificial scaffolds and surrounding native tissue. In contrast to the high number of biomaterials used to build a biomimetic 3D architecture in cartilage tissue engineering, a limited number of cell populations is available, including those existed in the host tissue such as chondrocytes, chondroprogenitor cells and mesenchymal stem cells (MSCs) with multipotency or pluripotency especially bone marrow-derived mesenchymal stem cells (BM-MSCs), adipose stem cells (ASCs), synovial mesenchymal stem cells (SMSCs), embryonic stem cells (ESCs) and induced pluripotent stem cells (iPSCs) (Wei and Dai, 2021).

As the main cell type resident in articular cartilage and responsible for its structural and functional maintenance, chondrocytes are one of the most widely used cell types in cartilage tissue engineering.

It has been observed that chondrocytes embedded in a wide range of biomaterials are able to maintain their morphology and phenotype, and to promote new ECM formation (Li et al., 2019; Camarero-Espinosa et al., 2020; Xu et al., 2022).

The chondrocytes proliferation and differentiation, vary in scaffolds with different compositions, and also can be influenced by the architecture of the scaffolds, including structural form, size and geometry pore, dimensionality and orientation fibres (Nuernberger et al., 2011). Nevertheless, the use of chondrocytes still faces a several of challenges related to the limited number of cells that can be isolated from host tissues, the limited proliferative potential and the phenomenon of dedifferentiation that occur in vitro culture. In fact, in vitro expansion of chondrocytes appears to be complicated, since they show low proliferation capacity and tend to lose their morphology, phenotype and function from the first passage in monolayer. These changes are mainly characterised by the gradually switch from chondrogenic markers expression like SOX9, aggrecan and collagen type II, to increase the expression of hypertrophy markers, such as collagen type I, ALP and Runx2. Therefore, this issue represents one of the biggest limitations in cartilage tissue engineering (Graceffa et al., 2019).

The use of stem cells represents a potential and promising solution to avoid the drawbacks associated with articular chondrocytes. Among the various types of stem cells, MSCs especially those derived from the bone marrow (BM-MSCs) are the most widely studied and characterised in tissue engineering for cartilage repair, due to their benefits like relative easiness of isolation and proliferation, ability to differentiate into multiple cells lineages including chondrocytes, osteoblasts, adipocytes, myocytes and tenocytes (Pittenger et al., 1999). Continuous studies in basic research and preclinical trial based on MSCs use, have achieved promising outcomes in cartilage regeneration and other diseases (Richardson et al., 2016). MSCs are located in various parts of human body and hence, they can be isolated from various sources such as bone marrow, adipose tissue, synovia, dental pulp, placenta, umbilical cord, and other skeletal tissues. Under standard culture conditions, they exhibit plastic-adherent property, show a fibroblastic-like shape and are characterised by specific markers expression such as $CD11b^+$, $CD14^-$, $CD34^-$, $CD45^-$, HLA-DR^-, $CD73^+$, $CD90^+$ and $CD105^+$ (Dominici et al., 2006). Therefore, MSCs can be easily expanded in vitro to create large amounts of cells that retain multipotency, representing one of the biggest advantages compared to chondrocytes use (Pittenger et al., 1999). In vitro MSCs chondrogenesis occurs when the cells are seeded in a three-dimensional environment represented by simple 3D cultures or scaffolds, in order to promote cell–cell and cell–matrix interactions (Sekiya et al., 2002; Le et al., 2020). In addition, this process is supported by the use of specific stimuli such as growth factors like TGFβ, BMPs and IGF and mechanical stimulation (Wei and Dai, 2021). In these conditions MSCs are induced to differentiate

in chondrogenic sense and to express cartilage- specific markers including collagen type II, aggrecan and GAGs (Nurul et al., 2021).

The encapsulation of MSCs inside the scaffolds, and their differentiation efficiency, have been broadly studied in a plenty of materials for cartilage regeneration (Armiento et al., 2018). In fact, a large number of scaffolds have been developed, both of synthetic and natural materials, or in combinations each other, assembled and created by using different kind of techniques, with the aim of creating the artificial microenvironment that best matches the characteristics of the native cartilage. Although considerable progress has been made, unfortunately to date, the MSCs use for cartilage regeneration still presents some limits to be addressed and solved. These limits are due to the differentiation of MSCs in the late weeks of culture, which switchs from the chondrogenic to hypertrophic one. The cells start to produce collagen type I, collagen type X and other hyperthrophic markers, suggesting that the differentiation of MSCs continue towards osteogenic phenotypes (Barry et al., 2001). As a consequence of this event, a fibrous cartilage with different composition, matrix organisation, and lower mechanical properties is obtained, compared to native articular cartilage. A currently investigated explanation for this issue, is the possibility that adult MSCs are intrinsically committed towards terminal, hypertrophic chondrocyte differentiation and cannot stably differentiate into articular chondrocytes (Occhetta et al., 2016).To better understand this tendency of adult MSCs, it is necessary to take a step back.

1.5.2.1 Going back to origin: Cartilage development

During human development, three main germ layers (as all animals with bilateral symmetry) are formed, which are called ectoderm, endoderm, and mesoderm, from which cartilage arise.

MSCs are derived from the mesoderm and form the components of the appendicular skeleton, the limbs, where chondrogenesis occurs. The latter begins when MSCs undergo cell–cell and cell– ECM interactions via gap junctions, leading to the cells proliferation and condensation, resulting in increased cell density within cell condensates called nodules. Mesenchymal condensation is characterised by upregulation of adhesion molecules such as versican, tenascin, syndecan, neural cell adhesion molecule 1 (N-CAM), N-cadherin, etc (Usami et al., 2016).

Here, the MSCs differentiate into chondroprogenitor cells giving rise to the cartilage anlage, and in general to the formation of the joint interzone, which will determine the specific location of the future joint. Subsequently the chondroprogenitor cells differentiate into chondrocytes which starting to produce the ECM rich in collagen type II, IV, IX, XI, and aggrecan. Therefore, differentiated

chondrocytes begin to be isolated from the ECM, whose molecules contribute to give the cells the typical spherical shape.

Basically, the chondrogenesis stop in this development stage, and the chondrocytes may experience two different fates: they can differentiate into transient chondrocytes becoming hypertrophic that will be reabsorbed and replaced by bone tissue (endochondral ossification), or they can remain mature chondrocytes responsible for maintaining the ECM of the cartilage in which they are embedded in the lacunae throughout the life span (Armiento et al., 2018).

Specifically, the chondrocytes located in the nodules centre stop proliferating, increase in volume and become hypertrophic. The latter alter the composition of the ECM at this site by synthesising MMP13, collagen type X and ALP which are involved in the degradation of the ECM and in the regulation of bone mineralisation respectively. They also synthetises the vascular endothelial growth factor (VEGF), to induce neighbouring MSCs differentiate in blood vessels (Camarero-Espinosa et al., 2016). Once the blood vessels infiltrate the cartilage, the hypertrophic chondrocytes undergo apoptosis and the surrounding cells differentiate into osteoblasts, starting the formation of the first ossification centre from which the bone will continue to lengthen. At the other end of the cartilage anlage, a second ossification centre is formed with same process described above, which encloses a portion of cartilage in the interzone where the proliferating chondrocytes are arranged in orderly column to form the growth plate. The latter will be responsible for bone growth until adulthood (Kronenberg et al., 2003) (Fig 1.6).

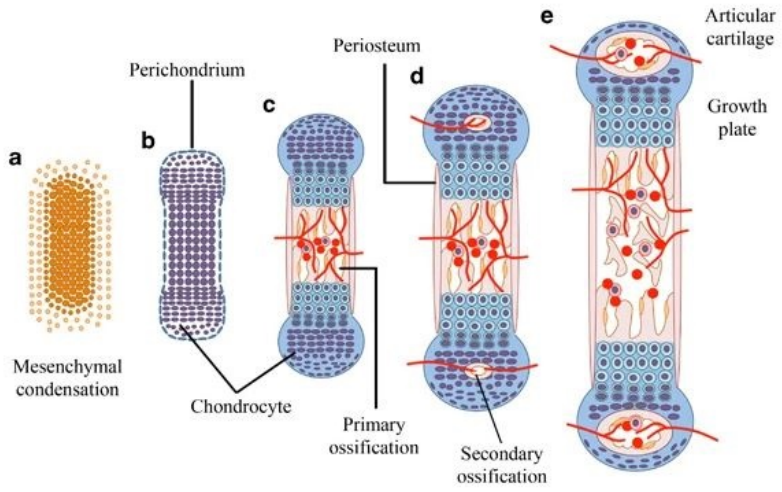

Figure 1.6 Schematic representation of cartilage development and endochondral ossification. (**a**) The process of endochondral ossification begins from mesenchymal condensation of MSCs at prospective skeleton sites. The MSCs undergo chondrogenic differentiation, and makes cartilage primordium. (**b**) The primordial cartilage continues to grow, forming an avascular cartilaginous tissue surrounded by the perichondrium. Chondrocytes in the centre part of the primordium initiate the growth plate, and undergo hypertrophy. (**c**) Hypertrophic chondrocytes are calcified and invaded by micro vessels forming primary ossification. (**d**) Vessels invade the epiphyses and form secondary ossification centre with osteoblasts and bone marrow. (**e**) The growth plate contributes to long bone growth. Articular cartilage provides resilience and smooth movement to the joint (Usami et al., 2016).

In this process the remaining cartilage is reduced to a thin layer above the second ossification centre which constitutes the articular cartilage. In the early stage, chondrocytes proliferate and produce ECM components resulting in a tissue with densely packed cells. Upon maturation, and as a response to the applied mechanical forces, cartilage remodels by varying its composition and structure. Moreover, the initially thick cartilage layer becomes thinner (Williams et al., 2008). The main molecular and structural changes in cartilage are related to the collagen and proteoglycan content and orientation. During the development, wide amounts of collagen are produced that increases in crosslinking density as the cartilage ages (Eyre et al., 1988). Upon maturation, the collagen type II density increases and collagen XI, which is the most abundant collagen form in young cartilage, disappears. Over time, the concentration of proteoglycans decreases as they decompose into GAGs. The molecular weight of aggrecan decreases leading also to a decrease in the concentration of chondroitin sulfate (Wells et al., 2003). At the same time the concentration of other GAGs such as keratan sulfate and HA increases, especially in areas were load is applied. Cartilage maturation is reached together with the maturity of the skeleton. At this point, the proliferative capacity of chondrocytes is extremely low, and cells live in a quiet stage for several years. Overall, at cartilage maturity, the cell density is significantly decreased and due to their lower proliferative and metabolic activity, the healing response of the tissue is also decreased (Williams et al., 2008).

It is important to mention that cartilage development and endochondral ossification are highly regulated by complex processes, which involve a wide range of growth factors, transcription factors, and extracellular matrix proteins. Growth factors include insulin-like growth factors (IGFs), parathyroid hormone-related protein (PTHrP), fibroblast growth factors (FGFs), platelet derived growth factors (PDGFs), transforming growth factors β (TGFβs), bone morphogenetic proteins (BMPs), Indian hedgehog (IHH), and Wingless/In (Wnt)/β-catenin (Usami et al., 2016).

There are also various transcription factors that regulate cartilage development and endochondral ossification. For example, the transcription factors SOX5, 6, and 9 (known as the SOX-trio), also play a key role in promoting chondrogenesis with SOX9, in particular, directly influencing upregulation of pro-chondrogenic genes such as COL2A1 and ACAN. They are essential not only for cartilage formation and but also for postnatal growth plate formation and function. Runx2 is considered the main transcription factor involved in bone formation, and also exerts an indispensable role for stimulation of chondrocyte hypertrophy and induction of matrix calcification (O'Shea et al., 2022).

Ultimately the study of articular cartilage development becomes an essential step because it provides a better guide in understanding and predicting new regeneration mechanisms and in designing new therapeutic strategies for cartilage repair and regeneration. In particular, this knowledge encourages the development of different strategies with the aim of "reprogramming" the fate of MSCs by

exposing them to specific stimuli that can be used to limit or reverse the MSCs tendency to hypertrophic differentiation, and guide them towards differentiation into stable cartilage. From this perspective, defining an effective, and possibly temporally organised, combination of stimuli represents an important challenge for optimising tissue engineering procedures based on the use of MSCs for cartilage repair (Occhetta et al., 2016).

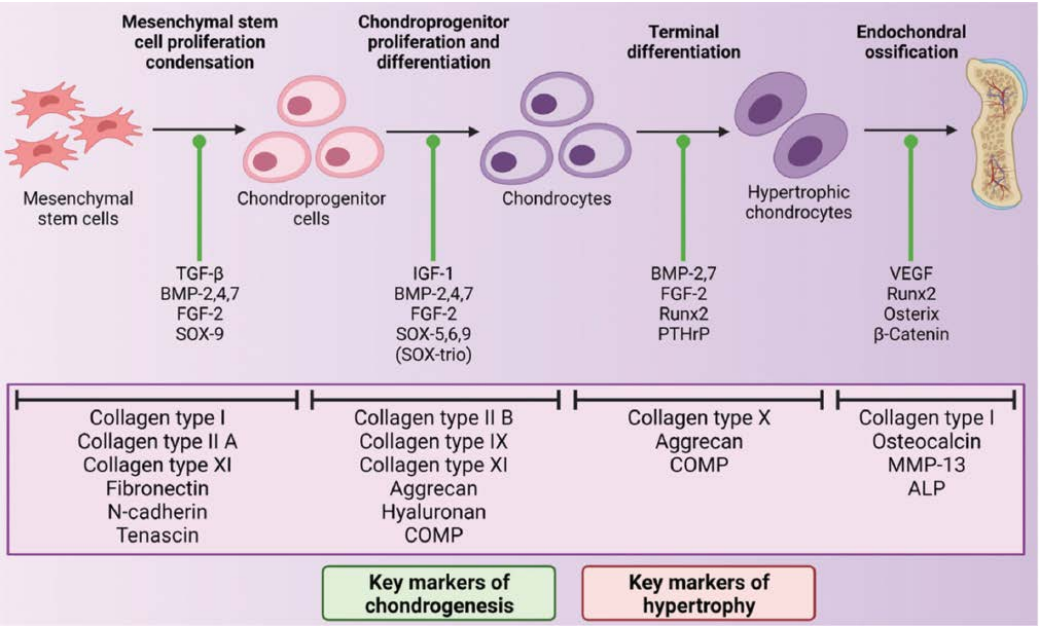

Figure 1.7 Schematic representation of chondrogenesis, starting with MSCs proliferation and condensation, until endochondral ossification. The main factors involved in the transition from one stage of the chondrogenic pathway to the next are highlighted with a green indicator. The characteristic ECM proteins of each stage are highlighted below (O'Shea et al., 2022).

1.5.3. Biochemical and Biophisical Stimuli

Having regard of what said above, apart from the cells encapsulated inside the 3D scaffolds, the inclusion of different stimuli, divided into molecular and physical ones, which play key roles in MSCs differentiation during cartilage development and adult cartilage homeostasis, is also essential to provide an appropriate microenvironment for the cartilage engineered.

1.5.3.1. Biochemical stimuli

The molecular signals used in cartilage repair consist of growth factors naturally occurring in the body and/or small synthetic molecular compounds. They are capable to mediate the growth, proliferation and differentiation of progenitor cells by activating specific pathways and stimulating the expression of the most important chondrogenic markers. IGFs, FGFs, TGFβs and BMPs, are among the most characterised growth factors, while dexamethasone (DEX) and kartogenin (KGN) are the typical synthetic molecules used in cartilage tissue engineering (Wei and Dai, 2021).

IGFs are single chain polypeptide with similar amino acid sequence to insulin. IGF-1 represents the isoform that promote the chondrocytes survival and proliferation, and is of involved in articular cartilage repair (Schmidt et al., 2006). Indeed, IGF-1 is a mediator of cartilage homeostasis by balancing the proteoglycan synthesis and breakdown through chondrocytes (Schmidt et al., 2006). In aged and degenerate articular cartilage, there is a progressive decrease of chondrocyte responsiveness to IGF-1, with diminishing capability to maintain structural and functional integrity. In recent years, the IGF-1 incorporation and delivery has gained wide application in designing osteochondral scaffolds for osteochondral tissue engineering, since it is also involved in osteoblastic differentiation (Kim et al.,2013).

FGF family is composed by 22 protein members in human (FGF1-14, 16–23). Each FGF factor can activate one of the four FGF receptors located on the cell surface to regulate the cells proliferation, migration and differentiation. Among them, FGF2 and FGF18 are known to be the most important ones in chondrogenesis and skeletal development (Ornitz and Marie, 2015). FGF2 is also known as basic fibroblast growth factor (bFGF) that stimulates the matrix synthesis in articular cartilage and acts as a chondrocyte mitogen (Yang et al., 2018). FGF18 (also known as Sprifermin, the recombinant human FGF18 form, rhFGF18) is required in skeletal growth to coordinate the chondrogenesis and osteogenesis. In a monolayer culture, the supplementation of FGF18 promotes the round cell morphology and proliferation of chondrocytes, as well as the expression decrease of collagen type I, while in 3D cultures increases the number chondrocytes and enabled human OA chondrocytes to produce ECM (Gigout et al., 2018). Interestingly, the intra-articular injection of sprifermin markedly promotes the proliferation of articular chondrocytes and the ECM synthesis, increasing cartilage thickness in a dose-dependent manner in patient with OA (Eckstein et al., 2021). It is also able to efficiently inhibit MMPs activity and not activates hypertrophic pathways, reducing articular cartilage degeneration. Sprifermin is currently in phase III clinical trial, and no local or systemic safety concerns have been reported (Song et al., 2021).

TGFβ is a large superfamily of cell regulatory proteins consists over 30 members including TGFβs, BMPs, activins, growth and differentiation factors (GDFs) and Nodal. All this factors share a quaternary dimer structure and signal via formation of heteromeric complex between two types of serine threonine-protein kinase receptors, known as TGFβ receptor type I and type II (TGFβR1 and TGFβR2). Specifically, there are seven type I (activin-receptor like kinases, ALK1-7) and five type II (TGFβRII, ACVR2A, ACVR2B, BMPRII, AMHRII) receptors (Schmierer and Hill, 2007). Since every growth factor recruits a specific, but not unique, receptor complex, this choice in receptor allows for differences in growth factor sensitivity. After formation of functional receptor complexes, TGFβ family members activate multiple intracellular signalling pathways, which generally are

divided into SMAD- dependent or –independent, but SMAD-dependent signalling is regarded as the canonical signalling pathway of TGFβ family members (Thielen et al., 2019).

Among all TGFβ family members, the three TGFβ isoforms (TGFβ1, 2, and 3) play central role in chondrocyte maturation, endochondral ossification, and are able to promote the synthesis of proteoglycans and collagen type II in chondrocytes (Grimaud et al., 2002). In addition, they promote the chondrogenic and osteogenic (hypertrophic) differentiation of MSCs, in dose-dependent manner (van der Kraan et al., 2009). All three isoforms are produced by cells in inactive form as homodimers, consist of latency-associated peptide (LAP) and latent TGFβ binding protein (LTBP) that remain bound together until the mature ligand is liberated. The non-covalent linkage of LAP to the mature ligand prevents the binding with receptor (van der Kraan, 2017). This production in the inactive form separates secretion from activity, represent an important concept in TGFβ biology. All three forms of TGFβ are produced by chondrocytes, and a large quantity of inactive TGFβ is secreted in the cartilage ECM. TGFβ is activated when the noncovalent bond between LAP and TGFβ is disrupted. This can occur enzymatically by degradation of LAP by MMP3, and other serine proteases, or by chemical modification of LAP by reactive oxygen species, or mechanically (Zhang et al., 2017).

The main signalling pathway starts when activated TGFβ binds TGFβRII, forming a complex that recruits ALK5 and successively, the signal is transduced inside the cells by the phosphorylation of SMAD2/3 which form a complex with SMAD4 that translocate in the nucleus where activates several transcription factors including SOX9 with the consequent synthesis of cartilage ECM components (van der Kraan, 2017). TGFβ can activate another signalling pathway, binding the receptor type I, ALK1 which phosphorylates SMAD1/5/9 involved in hypertrophic differentiation. Indeed, a complex with SMAD4 is formed, translocate in the nucleus were activated RUNX2 transcription factor (Szychlinska et al., 2017; Thielen et al., 2019) (Fig.1.8).

Which pathway is activated by TGFβ depends on receptor level expression, co-receptor expression and concentration of TGFβ. Specifically, a low dose of TGFβ predominantly signals via SMAD2/3, whereas at high consentrations, SMAD1/5/9 signalling becomes more pronounced. Importantly, both pathways have been described to antagonise each other in chondrocytes (van der Kraan, 2017). TGFβ signalling is associated with cartilage ECM production and maintenance, and an imbalance between SMAD2/3 and SMAD1/5/9 pathways has also been observed during OA progression and ageing (Graceffa et al., 2019). It is important to mentioned that TGFβ isoforms also activate the MAP kinase mitogen-activated kinases (MAPK) cascade, involving TGFβ-activated kinase 1 (TAK1) or extracellular signal-regulated kinase 1 and 2 (ERK1/2) which contribute to chondrogenic differentiation of MSCs, and chondrocytes phenotype maintenance. TGFβ isoforms are considered the growth factors with the most powerfull chondrogenic potential, and for this reason they are widely

used in tissue engineering for cartilage repair in order to optimise the chondrogenesis and new ECM production of progenitor cells insede the scaffolds (Thielen et al., 2019).

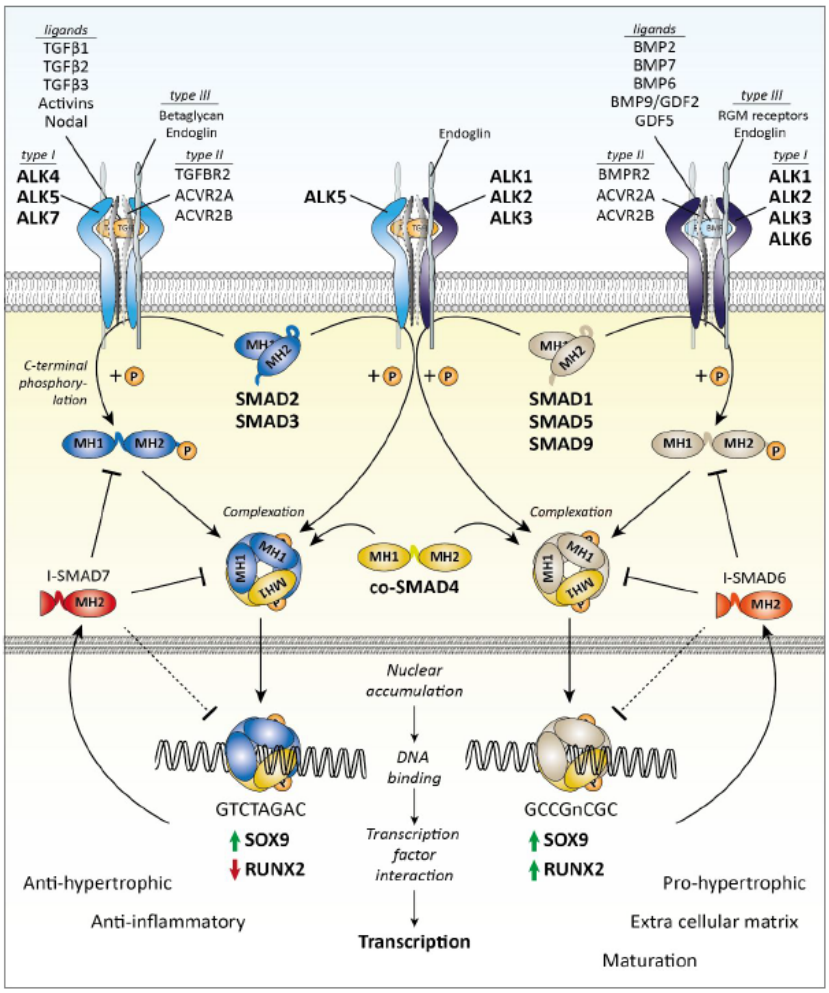

Figure 1.8 Schematic representation of TGFβ family SMAD-dependent signalling pathway. Ligands binding induces the formation of a receptor complex containing a type I and type II receptors. Type III receptors stabilise and facilitate the binding of TGFβ to the receptor complex, which recruits a receptor SMAD (R-SMAD). The R-SMAD is subsequently phosphorylated on its C-terminal domain, and a complex is formed with the common SMAD4 (co-SMAD4). This complex translocates to the nucleus where it can bind transcription factors, like SOX9 and RUNX2, and activates transcription of specific DNA sequences. The activation of SMAD2/3 signalling results in anti-hypertrophic and anti-inflammatory function, whereas activation of SMAD1/5/9 signaling is associated with pro-hypertrophic regulation of ECM and maturation of the cartilage. Other important factorsare the inhibitory SMADs, SMAD6 and SMAD7, whose expression provides the cell with a negative feedback mechanism. (Thielen et al., 2019).

Also BMPs, the other members group of TGFβ superfamily, have been shown to be effective tissue engineering growth factors for cartilage regeneration, among which BMP2, 4, 6, and 9 are the most extensively studied ones (Wei and Dai, 2021). BMP2 alone or combined with other growth factors has been vastly utilised for the MSCs chondrogenic differentiation and ECM production and proliferation of chondrocytes to regenerate cartilage or osteochondral tissues both in vitro and in vivo (Blaney et al., 2007; Deng et al., 2018).

BMP4 notably is involved in bone formation and bone healing, but also is able to accelerate the chondrogenesis of MSCs and the regeneration of hyaline cartilage (Chubinskaya et al., 2008). In the same line, BMP6 drive both chondrogenic and osteogenic differentiation of adult MSCs from

different tissues and it endogenous expression is detected in the cartilage of both healthy and osteoarthritic joint (Dvořáková et al., 2013). BMP9 was considered a potent inducer of mesenchymal progenitor cells chondrogenesis, but is accompanied by pronounced hypertrophy, providing to be potentially the most osteogenic BMP during endochondral ossification (Deng et al., 2018).
BMPs bind type II receptor (BMPR2, ACVR2A, and ACVR2B), which recruits a type I receptor (ALK1, 2,3,6) leading to the activation of SMAD 1/5/9 pathway (Thielen et al., 2019). However, since BMPs direct cells towards a more hypertrophic and osteogenic differentiation compred to TGFβ isoforms, the use of these growth factors for cartilage tissue engineering is controversial while are widely used for osteochondral and bone tissue engineering.
Finally, among the synthetic molecules used in cartilage tissue engineering, is important to mentioned DEX for its wide use. The latter is a synthetic glucocorticoid that has been frequently applied clinically to treat inflammatory diseases (Hartmann et al., 2016). DEX has been found to potentiate the chondrogenic differentiation of MSCs in vitro, particularly when used in combination with growth factors such as TGFβs and BMPs (Shintani and Hunziker, 2011). DEX dosage and exposure stage during differentiation were considered to be depending elements in deciding the differentiation lineage of MSCs (Hartmann et al., 2016).

1.5.3.2. Biophisical Stimuli

In addition to molecular signalling, mechanical signals represent another elements to consider for tissue engineering, as they can largely influence cell fate and the biological processes involved in chondrogenesis and in the formation of new ECM, essential in the construction of artificial cartilage. In this context, the fundamental role played by mechanical signals was highlighted starting from the cartilage formation during embryonic development. In fact, active foetal movements such as whole-body movements, kicking, and stretching subject the developing skeleton to stresses, which exert positive effects on correct musculoskeletal development (Shea et al., 2015). Specifically, to cartilage, animal studies based on mouse and chick embryo models of immobilisation have shown that the absence of movements causes shorter cartilaginous elements with poorly defined condyles due to reduced cell proliferation at the terminal condyle, disruption of the chondrocytes organisation into columns, and abnormal joint cavitation (Roddy et al., 2011; Armiento et al., 2018; Khatib et al., 2021). In addition to playing a vital role in cartilage development, mechanical forces are essential for maintaining cartilage homeostasis within a healthy joint. As described in the previous sections, articular cartilage is designed to withstand significant complex load and deformation during locomotion and physical activity. Mechanical loading applied on cartilage is vital important for the

diffusion of nutrients within the tissue and the waste of catabolites, and stimulate chondrocytes to produce ECM component essential for the remodelling and turnover of ECM. On the other hand, is well known that inactivity of the joint leads to the cartilage degradation (Sanchez-Adams. et al., 2014).

Although the macroscopic effects of mechanical loading in vivo are well established, the molecular mechanisms still remain unclear. Different studied have shown that, part of mechanotrasduction in vivo chondrocytes, is mediated through mechanoreptors, principally integrins, associated with stretch-activated ion channels and voltage-gated calcium channels, like TRPV4 (O'Connor et al., 2014). Integrins are binding proteins to the pericellular matrix mainly located in immotile primary cilia on chondrocytes, MSCs and chondroprogenitor cells. The cilia are able to transduce mechanical loading inside the cells, and activated several pathways such as WNT, Hedgehog, and TGF/BMPs (Panadero et al., 2016).

Therefore, mechanical loading is an important signalling factor in articular cartilage biology. It is consequently crucial to insert mechanical signals in vitro systems for tissue engineering, since they could contribute to obtaining in vitro tissues with characteristics more similar to the native one. To investigate their effects in vitro, external mechanical signals are usually applied through bioreactors or loading devices that allow to expose scaffolds with cells to different forms of mechanical loads (Monaco et al., 2020). The latter in the cartilage are a complex combination of tensile, shear, and compressive stresses and strains. In vitro, the ways of providing mechanical signals are based in the reduction to single mechanical components such as uniaxial compression, direct shear stress, perfusion (shear stress) and hydrostatic pressure. Each one of this mechanical solicitations can be applied individually or combined, simulating one or some of the different components recapitulating the complex motion of in vivo condition by reproducing the so-called complex multi-axil load (O'Connor et al., 2013).

Spinner flasks, laminar flow bioreactors, and flow perfusion bioreactors, for example, are the most used devices to apply the hydrostatic pressure exerted by culture medium movements on constructs, which instead in vivo is produced by the liquid environment of the articular cartilage including the synovial fluid and the interstitial fluid, while the fluid shear generates with the liquid flow (Monaco et al., 2020). Chondrocytes encapsulated in 3D hydrogels subjected to this kind of forces were able to synthesise new ECM, while the application of intermittent hydrostatic pressure together with TGFβ3 supplementation, has been reported to increase Sox9, collagen type II, and aggrecan gene expression levels by human MSCs in pellet cultures (Miyanishi et al., 2006; Xia et al., 2017). Mechanical stimuli can be also applied directly to constructs in form of static or dynamic compression, and shear. Many research groups have designed and built different bioreactors that can

apply compression or shear, ranging from uncontrolled to fully defined computer-controlled shear application, which allows for regulated frequency and amplitude (Grad et al., 2011).

Among this mechanical forces, dynamic compressive loading represents the most widely studied and used mechanical signal, in MSCs-based cartilage regeneration. Several studies have shown that this kind of mechanical stimulus is able to enhance chondrogenic differentiation of MSCs, despite being less strong than growth factor treatment in initiating MSCs differentiation. However, MSCs differentiation can be enhanced, and increase of collagen type II, aggrecan, TGFβ1, and Sox9 gene expression levels following dynamic compressive loading were observed (Fahy et al., 2018). The cells response can be also influenced by different factors, such as pre-differentiation period and some specific loading parameters, including optimal load cycle and frequency, as well as the scaffold biomaterial, are provided (Szychlinska et al., 2017).

Also shear stress is an important mechanical signal with similar effects. However, when compression and shear are applied individually in the constructs, limited effects have been observed, or as in the case of BM-MSCs, compression and shear alone are not able to induce chondrogenic differentiation (Schätti et al., 2011). Different results are observed when compression and shear are applied together with multiaxial stimulation. The latter results are more effective than a single loading at inducing ECM biosynthesis in MSC-derived chondrocytes. Multiaxial load is able to enhance collagen type II and aggrecan expression, to increase their deposition, and to increase GAGs production, without supplementation of exogenous growth factors. This occurs since multiaxial signals activated the TGFβ pathway, as observed on BM-MSCs embedded in poly-urethane (PU) scaffolds which stimulated by compressive load and surface shear stress, upregulated gene expression and protein synthesis of TGFβ1 and TGFβ3 (Li et al., 2010; Gardner et al., 2016). This evidence is also reinforced by other studies on BM-MSCs and articular cartilage explant, in which dynamic compression upregulated Smad2/3 phosphorylation (Mouw et al., 2007; Madej et al., 2014).

Despite the great advances that have been made in the field of biomechanics in providing appropriate mechanical stimulus through bioreactors for engineered tissue construction, several limitations involved in the design and fabrication of bioreactors remain to be resolved, for example, lack of universal standards and discrepancy in design parameters, as well as limitations related to the different biomaterials used which by themselves may differently transmit mechanical signals to embedded cells (Li et al., 2017).

1.6 Physical Activity as a prevention for OA management

The management of OA focuses on alleviating its secondary effects since there is currently no resolutive cure. Nonsteroidal anti-inflammatory drugs, opioid and non-opioid analgesics, intra-articular injections of steroids and hyaluronic acid are generally prescribed to patients to reduce pain and improve joint function, but they fail in modifying disease progression in terms of prevention and chondroprotection (Zhang et al., 2007; Cheng and Visco, 2012). The chronic nature of OA encourages the use of pharmacological approaches that can be considered safe for long term use and, at the same time, might be able to slow its progression. To date, however, there is no effective drug capable of acting on the pathophysiology of OA, and their use is limited due to the side effects in patients by over usage (Zhang et al., 2007).

This has led to consider non-pharmacological, regenerative and behavioural treatments (Musumeci et al., 2014). Among these, exercise represents a useful tool to alleviate symptoms of OA and slow its progression (Musumeci et al., 2015; Castrogiovanni et al., 2019; Di Rosa et al., 2019). It was demonstrated that physical exercise exerts short-term benefits in reducing pain, improving physical function, balance, muscle strength and flexibility (Uthman et al., 2013). Training tailored to improve OA includes anaerobic, aerobic, flexibility workouts and aquatic exercise (Castrogiovanni and Musumeci, 2016). It is essential to plan a protocol of movement whose type, duration and intensity represents the best approach to induce positive changes within the joint, but does not worsen the pathological condition by excessive load bearing or exhausting exercise (Musumeci et al., 2013). It seems that a combination of aerobic fitness training and strengthening exercises could be optimal to address the spectrum of impairments associated with OA (Bennell and Hinman 2011).

The most important effect of exercise on articular cartilage is that it keeps the joints lubricated and facilitates cycles of catabolism and anabolism within the tissue. Mechanical stresses, derived from exercise, facilitate diffusion of nutrients and stimulates the ECM remodelling by promoting the synthesis of the molecular components of ECM. Sedentary and immobilisation eventually compromise the lubricant properties of joint, although this can be reversed with activity. Joint lubrication is largely determined by the lubricin, one of the major joint lubricants, which expression and levels are influenced by exercise.

Lubricin is expressed by chondrocytes located in the superficial zone of articular cartilage and by synoviocytes type B from synovia and it has received considerable attention as a chondroprotective molecule (Elsaid et al., 2012). Several studies on healthy and OA rat models, have shown that moderate physical exercise as normal joint loading, and mechanical stimulation promote an expression increase of lubricin from chondrocytes and synoviocytes, resulting also in high levels in

synovial fluid. These leads to an improve joint lubrication and prevent cartilage degeneration with enhanced lubrication of articular cartilage surface and increase joint mobility (Musumeci et al., 2015; Castrogiovanni et al., 2019).

Moreover, exercise may delay the progression of OA by inhibiting the degradation of ECM and promoting cartilage synthesis (Kong et al., 2022). For example, exercise is able to reduce the activity of MMP2 in the tendons around the knee joint and in quadriceps tendons of OA rats (subjected to resistance training for eight weeks), and greatly relieve the adverse effects of OA on the knee joint. Therefore, exercise may reduce the degradation of the ECM by inhibiting the activity of MM-2 from achieving the purpose of treating OA (Vasilceac et al. 2021). As described in the paragraphs above, collagen type II and MMP 13 are essential components related to a good balance between synthesis and degradation of cartilage ECM. It was demonstrated in OA rat model, that swimming training applied in the early stage of OA, increase production and deposition of new collagen type II fibres, while the levels of MMP13 were reduced, strengthening the hypothesis in which exercise training in the early stage of OA contributes to maintain a balance between the degradation and anabolism of ECM preventing cartilage damage (Hsieh and Yang, 2018).

Exercise relieves the pathological changes of OA by affecting other mechanisms related to the disease such as, apoptosis, autophagy, and inflammatory response (Kong et al., 2022).

Otherwise, after long periods of immobility, the joints become stiff and lose some of their range of movement, also not supported by the muscle who can incur in atrophy. Efficacy of exercise is also extended to other components of the joints such as the synovium, muscle, ligaments, tendons, and bone (Gahunia et al., 2012). Synovial fluid produced by the synovial membrane within the joints has a short-term response to exercise, thus requiring regular exercise to stay lubricated, nourished, and healthy. In response to physical activity, osteoblasts are engaged in remodelling and building new bone tissue and in improving density, being more able to withstand mechanical loads. In addition, muscles respond rapidly to exercise by synthesising proteins and increasing in size. The integrity of tendons and ligaments is critical for joint function, which become stronger and more resistant to injury when exercised (Gahunia et al., 2012).

1.7 References

Armiento AR, Stoddart MJ, Alini M, Eglin D. Biomaterials for articular cartilage tissue engineering: Learning from biology. Acta Biomater. 2018 Jan; 65:1-20. doi: 10.1016/j.actbio.2017.11.021. Epub 2017 Nov 8. PMID: 29128537.

Barry F, Boynton RE, Liu B, Murphy JM. Chondrogenic differentiation of mesenchymal stem cells from bone marrow: differentiation-dependent gene expression of matrix components. Exp Cell Res. 2001 Aug 15;268(2):189-200. doi: 10.1006/excr.2001.5278. PMID: 11478845.

Baumann, C.A., Hinckel, B.B., Bozynski, C.C., Farr, J. (2019). Articular Cartilage: Structure and Restoration. In: Yanke, A., Cole, B. (eds) Joint Preservation of the Knee. Springer, Cham. https://doi.org/10.1007/978-3-030-01491-9_1.

Bennell KL, Hinman RS. A review of the clinical evidence for exercise in osteoarthritis of the hip and knee. J Sci Med Sport. 2011 Jan;14(1):4-9. doi: 10.1016/j.jsams.2010.08.002. Epub 2010 Sep 17. PMID: 20851051.

Berenbaum F. Osteoarthritis as an inflammatory disease (osteoarthritis is not osteoarthrosis!). Osteoarthritis Cartilage. 2013 Jan;21(1):16-21. doi: 10.1016/j.joca.2012.11.012. Epub 2012 Nov 27. PMID: 23194896.

Blaney Davidson EN, Vitters EL, van Lent PL, van de Loo FA, van den Berg WB, van der Kraan PM. Elevated extracellular matrix production and degradation upon bone morphogenetic protein-2 (BMP-2) stimulation point toward a role for BMP-2 in cartilage repair and remodeling. Arthritis Res Ther. 2007;9(5):R102. doi: 10.1186/ar2305. PMID: 17922907.

Brendan FB, Zuscik MJ, Xing L. Chapter 11 - Biology of Bone and Cartilage. Genetics of Bone Biology and Skeletal Disease (Second Edition). 2018; Pages 173-195.https://doi.org/10.1016/B978-0-12-804182-6.00011-3.

Broguiere N, Isenmann L, Zenobi-Wong M. Novel enzymatically cross-linked hyaluronan hydrogels support the formation of 3D neuronal networks. Biomaterials. 2016 Aug;99:47-55. doi: 10.1016/j.biomaterials.2016.04.036. Epub 2016 May 10. PMID: 27209262.

Bruckner P, van der Rest M. Structure and function of cartilage collagens. Microsc Res Tech. 1994 Aug 1;28(5):378-84. doi: 10.1002/jemt.1070280504. PMID: 7919525.

Camarero-Espinosa S, Calore A, Wilbers A, Harings J, Moroni L. Additive manufacturing of an elastic poly(ester)urethane for cartilage tissue engineering. Acta Biomater. 2020 Jan 15;102:192-204. doi: 10.1016/j.actbio.2019.11.041. Epub 2019 Nov 26. PMID: 31778830.

Camarero-Espinosa S, Rothen-Rutishauser B, Foster EJ, Weder C. Articular cartilage: from formation to tissue engineering. Biomater Sci. 2016 May 26;4(5):734-67. doi: 10.1039/c6bm00068a. Epub 2016 Feb 29. PMID: 26923076.

Cao Z, Dou C, Dong S. Scaffolding Biomaterials for Cartilage Regeneration. Journal of Nanomaterials, 2014, 1–8. doi:10.1155/2014/489128

Castrogiovanni P, Di Rosa M, Ravalli S, Castorina A, Guglielmino C, Imbesi R, Vecchio M, Drago F, Szychlinska MA, Musumeci G. Moderate Physical Activity as a Prevention Method for Knee Osteoarthritis and the Role of Synoviocytes as Biological Key. Int J Mol Sci. 2019 Jan 25;20(3):511. doi: 10.3390/ijms20030511. PMID: 30691048.

Castrogiovanni, P.; Musumeci, G. Which is the Best Physical Treatment for Osteoarthritis? J. Funct. Morphol. Kinesiol. 2016, *1*(1), 54-68; https://doi.org/10.3390/jfmk101005.

Chen J, Yang J, Wang L, Zhang X, Heng BC, Wang DA, Ge Z. Modified hyaluronic acid hydrogels with chemical groups that facilitate adhesion to host tissues enhance cartilage regeneration. Bioact Mater. 2020 Nov 29;6(6):1689-1698. doi: 10.1016/j.bioactmat.2020.11.020. PMID: 33313448;

Cheng DS, Visco CJ. Pharmaceutical therapy for osteoarthritis. PM R. 2012 May;4(5 Suppl):S82-8. doi: 10.1016/j.pmrj.2012.02.009. PMID: 22632707.

Chu S, Maples MM, Bryant SJ. Cell encapsulation spatially alters crosslink density of poly(ethylene glycol) hydrogels formed from free-radical polymerizations. Acta Biomater. 2020 Jun;109:37-50. doi: 10.1016/j.actbio.2020.03.033. Epub 2020 Apr 5. PMID: 32268243.

Chubinskaya S, Segalite D, Pikovsky D, Hakimiyan AA, Rueger DC. Effects induced by BMPS in cultures of human articular chondrocytes: comparative studies. Growth Factors. 2008 Oct;26(5):275-83. doi: 10.1080/08977190802291733. PMID: 18651287.

Danisovic L, Varga I, Zamborsky R, Böhmer D. The tissue engineering of articular cartilage: cells, scaffolds and stimulating factors. Exp Biol Med (Maywood). 2012 Jan;237(1):10-7. doi: 10.1258/ebm.2011.011229. Epub 2011 Dec 7. PMID: 22156044.

Deng ZH, Li YS, Gao X, Lei GH, Huard J. Bone morphogenetic proteins for articular cartilage regeneration. Osteoarthritis Cartilage. 2018 Sep;26(9):1153-1161. doi: 10.1016/j.joca.2018.03.007. Epub 2018 Mar 24. PMID: 29580979.

Dhanabalan KM , Gupta VK , Agarwal R . Rapamycin-PLGA microparticles prevent senescence, sustain cartilage matrix production under stress and exhibit prolonged retention in mouse joints. Biomater Sci. 2020 Aug 7;8(15):4308-4321. doi: 10.1039/d0bm00596g. Epub 2020 Jun 29. PMID: 32597443.

Di Rosa M, Castrogiovanni P, Musumeci G. The Synovium Theory: Can Exercise Prevent Knee Osteoarthritis? The Role of "Mechanokines", A Possible Biological Key. J Funct Morphol Kinesiol. 2019 Jan 23;4(1):11. doi: 10.3390/jfmk4010011. PMID: 33467326.

Dominici M, Le Blanc K, Mueller I, Slaper-Cortenbach I, Marini F, Krause D, Deans R, Keating A, Prockop Dj, Horwitz E. Minimal criteria for defining multipotent mesenchymal stromal cells. The International Society for Cellular Therapy position statement. Cytotherapy. 2006;8(4):315-7. doi: 10.1080/14653240600855905. PMID: 16923606.

Dvořáková J, Kučera L, Kučera J, Švík K, Foglarová M, Muthný T, Pravda M, Němcová M, Velebný V, Kubala L. Chondrogenic differentiation of mesenchymal stem cells in a hydrogel system based on an enzymatically crosslinked tyramine derivative of hyaluronan. J Biomed Mater Res A. 2014 Oct;102(10):3523-30. doi: 10.1002/jbm.a.35033. Epub 2013 Nov 15. PMID: 24243864.

Eckstein F, Hochberg MC, Guehring H, Moreau F, Ona V, Bihlet AR, Byrjalsen I, Andersen JR, Daelken B, Guenther O, Ladel C, Michaelis M, Conaghan PG. Long-term structural and symptomatic effects of intra-articular sprifermin in patients with knee osteoarthritis: 5-year results from the FORWARD study. Ann Rheum Dis. 2021 Aug;80(8):1062-1069. doi: 10.1136/annrheumdis-2020-219181. Epub 2021 May 7. PMID: 33962962.

Elsaid KA, Zhang L, Waller K, Tofte J, Teeple E, Fleming BC, Jay GD. The impact of forced joint exercise on lubricin biosynthesis from articular cartilage following ACL transection and intra-articular lubricin's effect in exercised joints following ACL transection. Osteoarthritis Cartilage. 2012 Aug;20(8):940-8. doi: 10.1016/j.joca.2012.04.021. Epub 2012 May 8. PMID: 22579916.

Eyre DR, Dickson IR, Van Ness K. Collagen cross-linking in human bone and articular cartilage. Age-related changes in the content of mature hydroxypyridinium residues. Biochem J. 1988 Jun 1;252(2):495-500. doi: 10.1042/bj2520495. PMID: 3415669.

Fahy N, Alini M, Stoddart MJ. Mechanical stimulation of mesenchymal stem cells: Implications for cartilage tissue engineering. J Orthop Res. 2018 Jan;36(1):52-63. doi: 10.1002/jor.23670. Epub 2017 Aug 11. PMID: 28763118.

Fraser JR, Laurent TC, Laurent UB. Hyaluronan: its nature, distribution, functions and turnover. J Intern Med. 1997 Jul;242(1):27-33. doi: 10.1046/j.1365-2796.1997.00170.x. PMID: 9260563.

Gahunia HK, Pritzker KP. Effect of exercise on articular cartilage. Orthop Clin North Am. 2012 Apr;43(2):187-99, v. doi: 10.1016/j.ocl.2012.03.001. PMID: 22480468.

Gardner OFW, Fahy N, Alini M, Stoddart MJ. Joint mimicking mechanical load activates TGFβ1 in fibrin-poly(ester-urethane) scaffolds seeded with mesenchymal stem cells. J Tissue Eng Regen Med. 2017 Sep;11(9):2663-2666. doi: 10.1002/term.2210. Epub 2016 Jul 22. PMID: 27445107

Ge Z, Li C, Heng BC, Cao G, Yang Z. Functional biomaterials for cartilage regeneration. J Biomed Mater Res A. 2012 Sep;100(9):2526-36. doi: 10.1002/jbm.a.34147. Epub 2012 Apr 10. PMID: 22492677.

Geyer M, Schönfeld C. Novel Insights into the Pathogenesis of Osteoarthritis. Curr Rheumatol Rev. 2018;14(2):98-107. doi: 10.2174/1573397113666170807122312. PMID: 28782470.

Gigout A, Guehring H, Froemel D, Meurer A, Ladel C, Reker D, Bay-Jensen AC, Karsdal MA, Lindemann S. Sprifermin (rhFGF18) enables proliferation of chondrocytes producing a hyaline cartilage matrix. Osteoarthritis Cartilage. 2017 Nov;25(11):1858-1867. doi: 10.1016/j.joca.2017.08.004. Epub 2017 Aug 18. PMID: 28823647.

Graceffa V, Vinatier C, Guicheux J, Stoddart M, Alini M, Zeugolis DI. Chasing Chimeras - The elusive stable chondrogenic phenotype. Biomaterials. 2019 Feb;192:199-225. doi: 10.1016/j.biomaterials.2018.11.014. Epub 2018 Nov 9. PMID: 30453216.

Grad S, Eglin D, Alini M, Stoddart MJ. Physical stimulation of chondrogenic cells in vitro: a review. Clin Orthop Relat Res. 2011 Oct;469(10):2764-72. doi: 10.1007/s11999-011-1819-9. PMID: 21344272

Grimaud E, Heymann D, Rédini F. Recent advances in TGF-beta effects on chondrocyte metabolism. Potential therapeutic roles of TGF-beta in cartilage disorders. Cytokine Growth Factor Rev. 2002 Jun;13(3):241-57. doi: 10.1016/s1359-6101(02)00004-7. PMID: 12486877.

Hartmann K, Koenen M, Schauer S, Wittig-Blaich S, Ahmad M, Baschant U, Tuckermann JP. Molecular Actions of Glucocorticoids in Cartilage and Bone During Health, Disease, and Steroid Therapy. Physiol Rev. 2016 Apr;96(2):409-47. doi: 10.1152/physrev.00011.2015. PMID: 26842265.

Heijink A, Gomoll AH, Madry H, Drobnič M, Filardo G, Espregueira-Mendes J, Van Dijk CN. Biomechanical considerations in the pathogenesis of osteoarthritis of the knee. Knee Surg Sports Traumatol Arthrosc. 2012 Mar;20(3):423-35. doi: 10.1007/s00167-011-1818-0. Epub 2011 Dec 16. PMID: 22173730.

Horbert V, Xin L, Föhr P, Huber R, Burgkart RH, Kinne RW. In Vitro Cartilage Regeneration with a Three-Dimensional Polyglycolic Acid (PGA) Implant in a Bovine Cartilage Punch Model. Int J Mol Sci. 2021 Oct 29;22(21):11769. doi: 10.3390/ijms222111769. PMID: 34769199.

Hsieh YL, Yang CC. Early intervention of swimming exercises attenuate articular cartilage destruction in a rat model of anterior cruciate ligament and meniscus knee injuries. Life Sci. 2018 Nov 1;212:267-274. doi: 10.1016/j.lfs.2018.10.013. Epub 2018 Oct 7. PMID: 30304692.

Jang S, Lee K, Ju JH. Recent Updates of Diagnosis, Pathophysiology, and Treatment on Osteoarthritis of the Knee. Int J Mol Sci. 2021 Mar 5;22(5):2619. doi: 10.3390/ijms22052619. PMID: 33807695.

Jeuken RM, Roth AK, Peters RJRW, Van Donkelaar CC, Thies JC, Van Rhijn LW, Emans PJ. Polymers in Cartilage Defect Repair of the Knee: Current Status and Future Prospects. Polymers (Basel). 2016 Jun 4;8(6):219. doi: 10.3390/polym8060219. PMID: 30979313.

Jooybar E, Abdekhodaie MJ, Alvi M, Mousavi A, Karperien M, Dijkstra PJ. An injectable platelet lysate-hyaluronic acid hydrogel supports cellular activities and induces chondrogenesis of encapsulated mesenchymal stem cells. Acta Biomater. 2019 Jan 1;83:233-244. doi: 10.1016/j.actbio.2018.10.031. Epub 2018 Oct 24. PMID: 30366137.

KELLGREN JH, LAWRENCE JS. Radiological assessment of osteo-arthrosis. Ann Rheum Dis. 1957 Dec;16(4):494-502. doi: 10.1136/ard.16.4.494. PMID: 13498604;

Khatib N, Parisi C, Nowlan NC. Differential effect of frequency and duration of mechanical loading on fetal chick cartilage and bone development. Eur Cell Mater. 2021 May 25;41:531-545. doi: 10.22203/eCM.v041a34. PMID: 34033115.

Kiani C, Chen L, Wu YJ, Yee AJ, Yang BB. Structure and function of aggrecan. Cell Res. 2002 Mar;12(1):19-32. doi: 10.1038/sj.cr.7290106. PMID: 11942407.

Kilmer CE, Walimbe T, Panitch A, Liu JC. Incorporation of a Collagen-Binding Chondroitin Sulfate Molecule to a Collagen Type I and II Blend Hydrogel for Cartilage Tissue Engineering. ACS Biomater Sci Eng. 2022 Mar 14;8(3):1247-1257. doi: 10.1021/acsbiomaterials.1c01248. Epub 2022 Feb 8. PMID: 35133126;

Kim K, Lam J, Lu S, Spicer PP, Lueckgen A, Tabata Y, Wong ME, Jansen JA, Mikos AG, Kasper FK. Osteochondral tissue regeneration using a bilayered composite hydrogel with modulating dual growth factor release kinetics in a rabbit model. J Control Release. 2013 Jun 10;168(2):166-78. doi: 10.1016/j.jconrel.2013.03.013. Epub 2013 Mar 28. PMID: 23541928.

Knudson CB, Knudson W. Cartilage proteoglycans. Semin Cell Dev Biol. 2001 Apr;12(2):69-78. doi: 10.1006/scdb.2000.0243. PMID: 11292372.

Kolasinski SL, Neogi T, Hochberg MC, Oatis C, Guyatt G, Block J, Callahan L, Copenhaver C, Dodge C, Felson D, Gellar K, Harvey WF, Hawker G, Herzig E, Kwoh CK, Nelson AE, Samuels J, Scanzello C, White D, Wise B, Altman RD, DiRenzo D, Fontanarosa J, Giradi G, Ishimori M, Misra D, Shah AA, Shmagel AK, Thoma LM, Turgunbaev M, Turner AS, Reston J. 2019 American College of Rheumatology/Arthritis Foundation Guideline for the Management of Osteoarthritis of the Hand, Hip, and Knee. Arthritis Care Res (Hoboken). 2020 Feb;72(2):149-162. doi: 10.1002/acr.24131. Epub 2020 Jan 6. Erratum in: Arthritis Care Res (Hoboken). 2021 May;73(5):764. PMID: 31908149.

Kolasinski SL, Neogi T, Hochberg MC, Oatis C, Guyatt G, Block J, Callahan L, Copenhaver C, Dodge C, Felson D, Gellar K, Harvey WF, Hawker G, Herzig E, Kwoh CK, Nelson AE, Samuels J, Scanzello C, White D, Wise B, Altman RD, DiRenzo D, Fontanarosa J, Giradi G, Ishimori M, Misra D, Shah AA, Shmagel AK, Thoma LM, Turgunbaev M,

Turner AS, Reston J. 2019 American College of Rheumatology/Arthritis Foundation Guideline for the Management of Osteoarthritis of the Hand, Hip, and Knee. Arthritis Care Res (Hoboken). 2020 Feb;72(2):149-162. doi: 10.1002/acr.24131. Epub 2020 Jan 6. Erratum in: Arthritis Care Res (Hoboken). 2021 May;73(5):764. PMID: 31908149.

Kong H, Wang XQ, Zhang XA. Exercise for Osteoarthritis: A Literature Review of Pathology and Mechanism. Front Aging Neurosci. 2022 May 3;14:854026. doi: 10.3389/fnagi.2022.854026. PMID: 35592699.

Kronenberg HM. Developmental regulation of the growth plate. Nature. 2003 May 15;423(6937):332-6. doi: 10.1038/nature01657. PMID: 12748651.

Langer R, Vacanti JP. Tissue engineering. Science. 1993 May 14;260(5110):920-6. doi: 10.1126/science.8493529. PMID: 8493529.

Le H, Xu W, Zhuang X, Chang F, Wang Y, Ding J. Mesenchymal stem cells for cartilage regeneration. J Tissue Eng. 2020 Aug 26;11:2041731420943839. doi: 10.1177/2041731420943839. PMID: 32922718

Lee S, Choi J, Youn J, Lee Y, Kim W, Choe S, Song J, Reis RL, Khang G. Development and Evaluation of Gellan Gum/Silk Fibroin/Chondroitin Sulfate Ternary Injectable Hydrogel for Cartilage Tissue Engineering. Biomolecules. 2021 Aug 11;11(8):1184. doi: 10.3390/biom11081184. PMID: 34439850.

Li K, Zhang C, Qiu L, Gao L, Zhang X. Advances in Application of Mechanical Stimuli in Bioreactors for Cartilage Tissue Engineering. Tissue Eng Part B Rev. 2017 Aug;23(4):399-411. doi: 10.1089/ten.TEB.2016.0427. Epub 2017 May 24. PMID: 28463576.

Li P, Fu L, Liao Z, Peng Y, Ning C, Gao C, Zhang D, Sui X, Lin Y, Liu S, Hao C, Guo Q. Chitosan hydrogel/3D-printed poly(ε-caprolactone) hybrid scaffold containing synovial mesenchymal stem cells for cartilage regeneration based on tetrahedral framework nucleic acid recruitment. Biomaterials. 2021 Nov; 278: 121131. doi: 10.1016/j .biomaterials.2021.121131. Epub 2021 Sep 15. PMID: 34543785.

Li Y, Liu Y, Xun X, Zhang W, Xu Y, Gu D. Three-Dimensional Porous Scaffolds with Biomimetic Microarchitecture and Bioactivity for Cartilage Tissue Engineering. ACS Appl Mater Interfaces. 2019 Oct 9;11(40):36359-36370. doi: 10.1021/acsami.9b12206. Epub 2019 Sep 24. PMID: 31509372.

Li Z, Kupcsik L, Yao SJ, Alini M, Stoddart MJ. Mechanical load modulates chondrogenesis of human mesenchymal stem cells through the TGF-beta pathway. J Cell Mol Med. 2010 Jun;14(6A):1338-46. doi: 10.1111/j.1582-4934.2009.00780.x. Epub 2009 May 11. PMID: 19432813.

Loeser RF, Goldring SR, Scanzello CR, Goldring MB. Osteoarthritis: a disease of the joint as an organ. Arthritis Rheum. 2012 Jun;64(6):1697-707. doi: 10.1002/art.34453. Epub 2012 Mar 5. PMID: 22392533.

Madej W, van Caam A, Blaney Davidson EN, van der Kraan PM, Buma P. Physiological and excessive mechanical compression of articular cartilage activates Smad2/3P signaling. Osteoarthritis Cartilage. 2014 Jul;22(7):1018-25. doi: 10.1016/j.joca.2014.04.024. Epub 2014 May 2. PMID: 24795273.

Martel-Pelletier J, Barr AJ, Cicuttini FM, Conaghan PG, Cooper C, Goldring MB, Goldring SR, Jones G, Teichtahl AJ, Pelletier JP. Osteoarthritis. Nat Rev Dis Primers. 2016 Oct 13;2:16072. doi: 10.1038/nrdp.2016.72. PMID: 27734845.

Martin I, Wendt D, Heberer M. The role of bioreactors in tissue engineering. Trends Biotechnol. 2004 Feb;22(2):80-6. doi: 10.1016/j.tibtech.2003.12.001. PMID: 14757042.

Miyanishi K, Trindade MC, Lindsey DP, Beaupré GS, Carter DR, Goodman SB, Schurman DJ, Smith RL. Effects of hydrostatic pressure and transforming growth factor-beta 3 on adult human mesenchymal stem cell chondrogenesis in vitro. Tissue Eng. 2006 Jun;12(6):1419-28. doi: 10.1089/ten.2006.12.1419. PMID: 16846340.

Mobasheri A, Lewis R, Maxwell JE, Hill C, Womack M, Barrett-Jolley R. Characterization of a stretch-activated potassium channel in chondrocytes. J Cell Physiol. 2010 May;223(2):511-8. doi: 10.1002/jcp.22075. PMID: 20162564

Mobasheri A, Rayman MP, Gualillo O, Sellam J, van der Kraan P, Fearon U. The role of metabolism in the pathogenesis of osteoarthritis. Nat Rev Rheumatol. 2017 May;13(5):302-311. doi: 10.1038/nrrheum.2017.50. Epub 2017 Apr 6. PMID: 28381830.

Monaco G, El Haj AJ, Alini M, Stoddart MJ. Ex Vivo Systems to Study Chondrogenic Differentiation and Cartilage Integration. J Funct Morphol Kinesiol. 2021 Jan 5;6(1):6. doi: 10.3390/jfmk6010006. PMID: 33466400.

Mouw JK, Connelly JT, Wilson CG, Michael KE, Levenston ME. Dynamic compression regulates the expression and synthesis of chondrocyte-specific matrix molecules in bone marrow stromal cells. Stem Cells. 2007 Mar;25(3):655-63. doi: 10.1634/stemcells.2006-0435. Epub 2006 Nov 22. PMID: 17124008.

Musumeci G, Castrogiovanni P, Trovato FM, Imbesi R, Giunta S, Szychlinska MA, Loreto C, Castorina S, Mobasheri A. Physical activity ameliorates cartilage degeneration in a rat model of aging: a study on lubricin expression. Scand J Med Sci Sports. 2015 Apr;25(2):e222-30. doi: 10.1111/sms.12290. Epub 2014 Jul 9. PMID: 25039883.

Musumeci G, Loreto C, Imbesi R, Trovato FM, Di Giunta A, Lombardo C, Castorina S, Castrogiovanni P. Advantages of exercise in rehabilitation, treatment and prevention of altered morphological features in knee osteoarthritis. A narrative review. Histol Histopathol. 2014 Jun;29(6):707-19. doi: 10.14670/HH-29.707. Epub 2014 Jan 22. PMID: 24452819.

Musumeci G, Maria Trovato F, Imbesi R, Castrogiovanni P. Effects of dietary extra-virgin olive oil on oxidative stress resulting from exhaustive exercise in rat skeletal muscle: a morphological study. Acta Histochem. 2014 Jan;116(1):61-9. doi: 10.1016/j.acthis.2013.05.006. Epub 2013 Jul 1. PMID: 23810034.

Nuernberger S, Cyran N, Albrecht C, Redl H, Vécsei V, Marlovits S. The influence of scaffold architecture on chondrocyte distribution and behavior in matrix-associated chondrocyte transplantation grafts. Biomaterials. 2011 Feb;32(4):1032-40. doi: 10.1016/j.biomaterials.2010.08.100. Epub 2010 Nov 11. PMID: 21074264.

Nurul AA, Azlan M, Ahmad Mohd Zain MR, Sebastian AA, Fan YZ, Fauzi MB. Mesenchymal Stem Cells: Current Concepts in the Management of Inflammation in Osteoarthritis. Biomedicines. 2021 Jul 7;9(7):785. doi: 10.3390/biomedicines9070785. PMID: 34356849.

Occhetta P, Stüdle C, Barbero A, Martin I. Learn, simplify and implement: developmental re-engineering strategies for cartilage repai. Swiss Med Wkly. 2016 Aug 21;146:w14346. doi: 10.4414/smw.2016.14346. PMID: 27544431.

O'Conor CJ, Case N, Guilak F. Mechanical regulation of chondrogenesis. Stem Cell Res Ther. 2013 Jul 1;4(4):61. doi: 10.1186/scrt211. PMID: 23809493

O'Conor CJ, Leddy HA, Benefield HC, Liedtke WB, Guilak F. TRPV4-mediated mechanotransduction regulates the metabolic response of chondrocytes to dynamic loading. Proc Natl Acad Sci U S A. 2014 Jan 28;111(4):1316-21. doi: 10.1073/pnas.1319569111. Epub 2014 Jan 13. PMID: 24474754;

Oo WM, Linklater JM, Hunter DJ. Imaging in knee osteoarthritis. Curr Opin Rheumatol. 2017 Jan;29(1):86-95. doi: 10.1097/BOR.0000000000000350. PMID: 27755179.

Ornitz DM, Marie PJ. Fibroblast growth factor signaling in skeletal development and disease. Genes Dev. 2015 Jul 15;29(14):1463-86. doi: 10.1101/gad.266551.115. PMID: 26220993.

O'Shea DG, Curtin CM, O'Brien FJ. Articulation inspired by nature: a review of biomimetic and biologically active 3D printed scaffolds for cartilage tissue engineering. Biomater Sci. 2022 May 17;10(10):2462-2483. doi: 10.1039/d1bm01540k. PMID: 35355029

Panadero JA, Lanceros-Mendez S, Ribelles JL. Differentiation of mesenchymal stem cells for cartilage tissue engineering: Individual and synergetic effects of three-dimensional environment and mechanical loading. Acta Biomater. 2016 Mar;33:1-12. doi: 10.1016/j.actbio.2016.01.037. Epub 2016 Jan 27. PMID: 26826532.

Pittenger MF, Mackay AM, Beck SC, Jaiswal RK, Douglas R, Mosca JD, Moorman MA, Simonetti DW, Craig S, Marshak DR. Multilineage potential of adult human mesenchymal stem cells. Science. 1999 Apr 2;284(5411):143-7. doi: 10.1126/science.284.5411.143. PMID: 10102814.

Poole AR, Kojima T, Yasuda T, Mwale F, Kobayashi M, Laverty S. Composition and structure of articular cartilage: a template for tissue repair. Clin Orthop Relat Res. 2001 Oct;(391 Suppl):S26-33. doi: 10.1097/00003086-200110001-00004. PMID: 11603710.

Qi H, Chen Q, Ren H, Wu X, Liu X, Lu T. Electrophoretic deposition of dexamethasone-loaded gelatin nanospheres/chitosan coating and its dual function in anti-inflammation and osteogenesis. Colloids Surf B Biointerfaces. 2018 Sep 1;169:249-256. doi: 10.1016/j.colsurfb.2018.05.029. Epub 2018 May 18. PMID: 29783150.

Rennerfeldt DA, Renth AN, Talata Z, Gehrke SH, Detamore MS. Tuning mechanical performance of poly(ethylene glycol) and agarose interpenetrating network hydrogels for cartilage tissue engineering. Biomaterials. 2013 Nov;34(33):8241-57. doi: 10.1016/j.biomaterials.2013.07.052. Epub 2013 Aug 6. PMID: 23932504;

Rezvani Ghomi E, Nourbakhsh N, Akbari Kenari M, Zare M, Ramakrishna S. Collagen-based biomaterials for biomedical applications. J Biomed Mater Res B Appl Biomater. 2021 Dec;109(12):1986-1999. doi: 10.1002/jbm.b.34881. Epub 2021 May 24. PMID: 34028179.

Richardson SM, Kalamegam G, Pushparaj PN, Matta C, Memic A, Khademhosseini A, Mobasheri R, Poletti FL, Hoyland JA, Mobasheri A. Mesenchymal stem cells in regenerative medicine: Focus on articular cartilage and intervertebral disc regeneration. Methods. 2016 Apr 15;99:69-80. doi: 10.1016/j.ymeth.2015.09.015. Epub 2015 Sep 15. PMID: 26384579.

Robinson PD, McEwan J, Adukia V, Prabhakar M. Osteoarthritis and arthroplasty of the hip and knee. Br J Hosp Med (Lond). 2018 Apr 2;79(4):C54-C59. doi: 10.12968/hmed.2018.79.4.C54. PMID: 29620976.

Roddy KA, Kelly GM, van Es MH, Murphy P, Prendergast PJ. Dynamic patterns of mechanical stimulation co-localise with growth and cell proliferation during morphogenesis in the avian embryonic knee joint. J Biomech. 2011 Jan 4;44(1):143-9. doi: 10.1016/j.jbiomech.2010.08.039. Epub 2010 Sep 29. PMID: 20883996.

Sacitharan PK. Ageing and Osteoarthritis. Subcell Biochem. 2019;91:123-159. doi: 10.1007/978-981-13-3681-2_6. PMID: 30888652.

Sanchez-Adams J, Leddy HA, McNulty AL, O'Conor CJ, Guilak F. The mechanobiology of articular cartilage: bearing the burden of osteoarthritis. Curr Rheumatol Rep. 2014 Oct;16(10):451. doi: 10.1007/s11926-014-0451-6. PMID: 25182679.

Saygili E, Kaya E, Ilhan-Ayisigi E, Saglam-Metiner P, Alarcin E, Kazan A, Girgic E, Kim YW, Gunes K, Eren-Ozcan GG, Akakin D, Sun JY, Yesil-Celiktas O. An alginate-poly(acrylamide) hydrogel with TGF-β3 loaded nanoparticles for cartilage repair: Biodegradability, biocompatibility and protein adsorption. Int J Biol Macromol. 2021 Mar 1;172:381-393. doi: 10.1016/j.ijbiomac.2021.01.069. Epub 2021 Jan 18. PMID: 33476613.

Schätti O, Grad S, Goldhahn J, Salzmann G, Li Z, Alini M, Stoddart MJ. A combination of shear and dynamic compression leads to mechanically induced chondrogenesis of human mesenchymal stem cells. Eur Cell Mater. 2011 Oct 11;22:214-25. doi: 10.22203/ecm.v022a17. PMID: 22048899.

Schmidt MB, Chen EH, Lynch SE. A review of the effects of insulin-like growth factor and platelet derived growth factor on in vivo cartilage healing and repair. Osteoarthritis Cartilage. 2006 May;14(5):403-12. doi: 10.1016/j.joca.2005.10.011. Epub 2006 Jan 18. PMID: 16413799.

Schmierer B, Hill CS. TGFbeta-SMAD signal transduction: molecular specificity and functional flexibility. Nat Rev Mol Cell Biol. 2007 Dec;8(12):970-82. doi: 10.1038/nrm2297. PMID: 18000526.

Schunke M, Schulte E, Schumacher U, Voll M, Wesker K, Ross L. Thieme atlas of anatomy. General anatomy and musculoskeletal system. 2014; 2nd ed. New York: Thieme Medical Publishers, Inc.

Sekiya I, Vuoristo JT, Larson BL, Prockop DJ. In vitro cartilage formation by human adult stem cells from bone marrow stroma defines the sequence of cellular and molecular events during chondrogenesis. Proc Natl Acad Sci U S A. 2002 Apr 2;99(7):4397-402. doi: 10.1073/pnas.052716199. Epub 2002 Mar 26. PMID: 11917104

Shea CA, Rolfe RA, Murphy P. The importance of foetal movement for co-ordinated cartilage and bone development in utero: clinical consequences and potential for therapy. Bone Joint Res. 2015 Jul;4(7):105-16. doi: 10.1302/2046-3758.47.2000387. PMID: 26142413

Shintani N, Hunziker EB. Differential effects of dexamethasone on the chondrogenesis of mesenchymal stromal cells: influence of microenvironment, tissue origin and growth factor. Eur Cell Mater. 2011 Nov 24;22:302-19; discussion 319-20. doi: 10.22203/ecm.v022a23. PMID: 22116649.

Singhvi MS, Zinjarde SS, Gokhale DV. Polylactic acid: synthesis and biomedical applications. J Appl Microbiol. 2019 Dec;127(6):1612-1626. doi: 10.1111/jam.14290. Epub 2019 Jun 17. PMID: 31021482.

Song Z, Li Y, Shang C, Shang G, Kou H, Li J, Chen S, Liu H. Sprifermin: Effects on Cartilage Homeostasis and Therapeutic Prospects in Cartilage-Related Diseases. Front Cell Dev Biol. 2021 Dec 14;9:786546. doi: 10.3389/fcell.2021.786546. PMID: 34970547.

Sophia Fox AJ, Bedi A, Rodeo SA. The basic science of articular cartilage: structure, composition, and function. Sports Health. 2009 Nov;1(6):461-8. doi: 10.1177/1941738109350438. PMID: 23015907.

Stoop R. Smart biomaterials for tissue engineering of cartilage. Injury. 2008 Apr;39 Suppl 1:S77-87. doi: 10.1016/j.injury.2008.01.036. PMID: 18313475.

Szychlinska MA, D'Amora U, Ravalli S, Ambrosio L, Di Rosa M, Musumeci G. Functional Biomolecule Delivery Systems and Bioengineering in Cartilage Regeneration. Curr Pharm Biotechnol. 2019;20(1):32-46. doi: 10.2174/1389201020666190206202048. PMID: 30727886.

Szychlinska MA, Stoddart MJ, D'Amora U, Ambrosio L, Alini M, Musumeci G. Mesenchymal Stem Cell-Based Cartilage Regeneration Approach and Cell Senescence: Can We Manipulate Cell Aging and Function? Tissue Eng Part B Rev. 2017 Dec;23(6):529-539. doi: 10.1089/ten.TEB.2017.0083. Epub 2017 Jun 22. PMID: 28514935.

Teshima R, Otsuka T, Takasu N, Yamagata N, Yamamoto K. Structure of the most superficial layer of articular cartilage. J Bone Joint Surg Br. 1995 May;77(3):460-4. PMID: 7744937.

Thielen NGM, van der Kraan PM, van Caam APM. TGFβ/BMP Signaling Pathway in Cartilage Homeostasis. Cells. 2019 Aug 24;8(9):969. doi: 10.3390/cells8090969. PMID: 31450621

Troeberg L, Nagase H. Proteases involved in cartilage matrix degradation in osteoarthritis. Biochim Biophys Acta. 2012 Jan;1824(1):133-45. doi: 10.1016/j.bbapap.2011.06.020. Epub 2011 Jul 8. PMID: 21777704

Usami Y, Gunawardena AT, Iwamoto M, Enomoto-Iwamoto M. Wnt signaling in cartilage development and diseases: lessons from animal studies. Lab Invest. 2016 Feb;96(2):186-96. doi: 10.1038/labinvest.2015.142. Epub 2015 Dec 7. PMID: 26641070

Uthman OA, van der Windt DA, Jordan JL, Dziedzic KS, Healey EL, Peat GM, Foster NE. Exercise for lower limb osteoarthritis: systematic review incorporating trial sequential analysis and network meta-analysis. BMJ. 2013 Sep 20;347:f5555. doi: 10.1136/bmj.f5555. PMID: 24055922.

Vainieri ML, Lolli A, Kops N, D'Atri D, Eglin D, Yayon A, Alini M, Grad S, Sivasubramaniyan K, van Osch GJVM. Evaluation of biomimetic hyaluronic-based hydrogels with enhanced endogenous cell recruitment and cartilage matrix formation. Acta Biomater. 2020 Jan 1;101:293-303. doi: 10.1016/j.actbio.2019.11.015. Epub 2019 Nov 11. PMID: 31726249.

van der Kraan PM, Blaney Davidson EN, Blom A, van den Berg WB. TGF-beta signaling in chondrocyte terminal differentiation and osteoarthritis: modulation and integration of signaling pathways through receptor-Smads. Osteoarthritis Cartilage. 2009 Dec;17(12):1539-45. doi: 10.1016/j.joca.2009.06.008. Epub 2009 Jun 26. PMID: 19583961.

van der Kraan PM. The changing role of TGFβ in healthy, ageing and osteoarthritic joints. Nat Rev Rheumatol. 2017 Mar;13(3):155-163. doi: 10.1038/nrrheum.2016.219. Epub 2017 Feb 2. PMID: 28148919.

Van Spil WE, Kubassova O, Boesen M, Bay-Jensen AC, Mobasheri A. Osteoarthritis phenotypes and novel therapeutic targets. Biochem Pharmacol. 2019 Jul;165:41-48. doi: 10.1016/j.bcp.2019.02.037. Epub 2019 Mar 1. PMID: 30831073.

Vasilceac FA, Marqueti RC, Neto IVS, Nascimento DDC, Souza MC, Durigan JLQ, Mattiello SM. Resistance training decreases matrix metalloproteinase-2 activity in quadriceps tendon in a rat model of osteoarthritis. Braz J Phys Ther. 2021 Mar-Apr;25(2):147-155. doi: 10.1016/j.bjpt.2020.03.002. Epub 2020 Mar 12. PMID: 32276877

Wei W, Dai H. Articular cartilage and osteochondral tissue engineering techniques: Recent advances and challenges. Bioact Mater. 2021 May 28;6(12):4830-4855. doi: 10.1016/j.bioactmat.2021.05.011. PMID: 34136726

Wells T, Davidson C, Mörgelin M, Bird JL, Bayliss MT, Dudhia J. Age-related changes in the composition, the molecular stoichiometry and the stability of proteoglycan aggregates extracted from human articular cartilage. Biochem J. 2003 Feb 15;370(Pt 1):69-79. doi: 10.1042/BJ20020968. PMID: 12431185.

Williams GM, Klisch SM, Sah RL. Bioengineering cartilage growth, maturation, and form. Pediatr Res. 2008 May;63(5):527-34. doi: 10.1203/PDR.0b013e31816b4fe5. PMID: 18427298.

Xia B, Di Chen, Zhang J, Hu S, Jin H, Tong P. Osteoarthritis pathogenesis: a review of molecular mechanisms. Calcif Tissue Int. 2014 Dec;95(6):495-505. doi: 10.1007/s00223-014-9917-9. Epub 2014 Oct 14. PMID: 25311420

Xia H, Liu H, Zhang Z, Zhang W, Liu W, Cao Y, Zhou G. Improvement of In Vitro Three-Dimensional Cartilage Regeneration by a Novel Hydrostatic Pressure Bioreactor. Stem Cells Transl Med. 2017 Mar;6(3):982-991. doi: 10.5966/sctm.2016-0118. Epub 2016 Nov 7. PMID: 28297584

Xu W, Zhu J, Hu J, Xiao L. Engineering the biomechanical microenvironment of chondrocytes towards articular cartilage tissue engineering. Life Sci. 2022 Oct 4;309:121043. doi: 10.1016/j.lfs.2022.121043. Epub ahead of print. PMID: 36206835.

Yang W, Cao Y, Zhang Z, Du F, Shi Y, Li X, Zhang Q. Targeted delivery of FGF2 to subchondral bone enhanced the repair of articular cartilage defect. Acta Biomater. 2018 Mar 15;69:170-182. doi: 10.1016/j.actbio.2018.01.039. Epub 2018 Feb 2. PMID: 29408545.

Yue K, Trujillo-de Santiago G, Alvarez MM, Tamayol A, Annabi N, Khademhosseini A. Synthesis, properties, and biomedical applications of gelatin methacryloyl (GelMA) hydrogels. Biomaterials. 2015 Dec;73:254-71. doi: 10.1016/j.biomaterials.2015.08.045. Epub 2015 Aug 28. PMID: 26414409

Zhang L, Hu J, Athanasiou KA. The role of tissue engineering in articular cartilage repair and regeneration. Crit Rev Biomed Eng. 2009;37(1-2):1-57. doi: 10.1615/critrevbiomedeng.v37.i1-2.10. PMID: 20201770.

Zhang W, Moskowitz RW, Nuki G, Abramson S, Altman RD, Arden N, Bierma-Zeinstra S, Brandt KD, Croft P, Doherty M, Dougados M, Hochberg M, Hunter DJ, Kwoh K, Lohmander LS, Tugwell P. OARSI recommendations for the management of hip and knee osteoarthritis, part I: critical appraisal of existing treatment guidelines and systematic review of current research evidence. Osteoarthritis Cartilage. 2007 Sep;15(9):981-1000. doi: 10.1016/j.joca.2007.06.014. Epub 2007 Aug 27. PMID: 17719803.

Zhang Y, Alexander PB, Wang XF. TGF-β Family Signaling in the Control of Cell Proliferation and Survival. Cold Spring Harb Perspect Biol. 2017 Apr 3;9(4):a022145. doi: 10.1101/cshperspect.a022145. PMID: 27920038.

Zhang Y, Jordan JM. Epidemiology of osteoarthritis. Clin Geriatr Med. 2010 Aug;26(3):355-69. doi: 10.1016/j.cger.2010.03.001. Erratum in: Clin Geriatr Med. 2013 May;29(2):ix. PMID: 20699159.

Zheng R, Wang X, Xue J, Yao L, Wu G, Yi B, Hou M, Xu H, Zhang R, Chen J, Shen Z, Liu Y, Zhou G. Regeneration of Subcutaneous Cartilage in a Swine Model Using Autologous Auricular Chondrocytes and Electrospun Nanofiber Membranes Under Conditions of Varying Gelatin/PCL Ratios. Front Bioeng Biotechnol. 2021 Dec 21;9:752677. doi: 10.3389/fbioe.2021.752677. PMID: 34993184.

2 The purpose and design of the present research

Having regard of what said above and considering a numerous aspects and multifactorial nature of the OA disease, the aim of this research was to improve the knowledge of the morpho-molecular mechanisms occurring in the osteoarthritic and normal cartilage and to find the possible therapeutic solutions for this complicated and multifactorial disease.

The aims of the first couple of two research work (the first is a preliminary study, while the second is already published) were to contribute to the field of tissue engineering with new insights about the chondrogenic differentiation of hBM-MSCs in two different 3D in vitro culture models represented by pellets and GelMA/HA hydrogels exposed to TGFβ1 priming and mechanical stimulation and the efficacy of a cell –free collagen type I- based scaffold in repairing cartilage tissue in a vivo rat model for OA.

Thereafter**,** the aims of the other two research articles were to contribute to the field of prevention of OA with new insights about the role of Autotaxin (ATX), Lubricin and physical exercise in OA progression, and the consequence of atrophy in a population of stem cells in healthy muscle.

2.1 Aims of the single researches

In vitro study of hBM-MSCs chondrogenic differentiation in pellet cultures and GelMA/HA hydrogels exposed to TGFβ1 priming and multiaxial loading:

The treatment of osteochondral defects in clinical practice is hindered by the poor self-healing ability of cartilage. Tissue engineering, combining the use of progenitor cells, biocompatible scaffolds, biochemical and biophysical stimuli, emerges as a promising strategy for joint regeneration. The developed in vitro models aim to recapitulate the in vivo situation. To more closely mimic the knee environment, current in vitro models need improvements to reflect the complexity of the native tissue. The aim of this preliminary study was to evaluate the chondrogenic differentiation of primary human bone-marrow- derived mesenchymal stromal cells (hBM-MSCs) from two different donors, in two different in vitro models: in the first part of the study pellet cultures exposed to TGFβ1 at different times were used, while in the second part chondrogenesis was investigated by encapsulating hBM-MSCs in hydrogels consisting of Gelatin Methacryloyl (GelMA) and hyaluronic acid (HA), exposed to multiaxial loading alone and after one week of TGFβ1 priming.

hBM-MSCs chondrogenic differentiation was evaluated over 21 days at the gene expression level and total DNA, sulphated glycosaminoglycan, H&E and safranin O staining and immunohistochemistry were evaluated. After 21 days of culture, pellets showed a chondrogenic and

partly hypertrophic phenotype, related to the TGFβ1 exposure times, while without the growth factor showed a very low differentiation capacity. In the second in vitro model, hBM-MSCs seeded inside hydrogels were able to chondrogenically differentiate only by the combined use of priming and mechanical stimulation, producing a more stable cartilage-like ECM, corroborating with high levels of chondrogenic markers and low levels of hypertrophic markers.
Although this study needs to be extended by other evaluations and subjected to appropriate optimisations, the developed in vitro model appears to be a good candidate for cartilage tissue engineering.

Evaluation of a cell –free collagen type I- based scaffold for articular cartilage regeneration in an orthotopic rat model:

The management of chondral defects represents a big challenge because of the limited self-healing capacity of cartilage. Many approaches in this field obtained partial satisfactory results. Cartilage tissue engineering, combining innovative scaffolds and stem cells from different sources, emerges as a promising strategy for cartilage regeneration. The aim of this study was to evaluate the capability of a cell-free collagen I-based scaffold to promote cartilaginous repair after orthotopic implantation in vivo. Articular cartilage lesions (ACL) were created at the femoropatellar groove in rat knees and cell free collagen I-based scaffolds (S) were then implanted into right knee defect for the ACL-S group. No scaffold was implanted for the ACL group. At 4-, 8- and 16-weeks post-transplantation, degrees of cartilage repair were evaluated by morphological, histochemical and gene expression analyses. Histological analysis shows the formation of fibrous tissue, at 4-weeks replaced by a tissue resembling the calcified one at 16-weeks in the ACL group. In the ACL-S group, progressive replacement of the scaffold with the newly formed cartilage-like tissue is shown, as confirmed by Alcian Blue staining. Immunohistochemical and quantitative real-time PCR(qRT-PCR) analyses display the expression of typical cartilage markers, such as collagen type I and II (*ColI* and *ColII*), *Aggrecan* and *Sox9*. The results of this study display that the collagen I-based scaffold is highly biocompatible and able to recruit host cells from the surrounding joint tissues to promote cartilaginous repair of articular defects, suggesting its use as a potential approach for cartilage tissue regeneration.

Immunohistochemical evaluation of autotaxin and lubricin in mild osteoarthritic rat model performing moderate physical activity.

Levels of the enzyme autotaxin (ATX) are elevated in synovial fluid and plasma of osteoarthritic patients, correlating positively with radiographic and symptomatic severity of the disease. Therefore, ATX is studied as potential marker for the progression of osteoarthritis (OA), whereas the

chondrocyte-secreted glycoprotein Lubricin has chondroprotective properties. The aim of this study was to evaluate the expression of ATX and Lubricin in healthy and mild OA rat articular cartilage of femur, tibia and patella, and to analyse the effect of a protocol of moderate physical activity on their expressions. Mild OA resulted from anterior cruciate ligament transection and rats exercised on a treadmill for 12 weeks. Computerized staining intensity of immunostaining was used to evaluate ATX and Lubricin expressions. Higher expressions of ATX were found in femur and tibia of OA rats, suggesting that this molecule could participate in the progression of the disease, although not involved in the patella. In the femur, physical activity performed by OA rats was able to lower ATX expression, encouraging the evidence that joint movement is beneficial for the cartilage, although no significant differences in Lubricin expression were detected in femur, tibia and patella. This evidence might shade some light about the role of ATX, Lubricin and physical exercise in OA progression.

Morphological Evidence of Telocytes in Skeletal Muscle Interstitium of Exercised and Sedentary Rodents

Skeletal muscle atrophy, resulting from states of hypokinesis or immobilization, leads to morphological, metabolic, and functional changes within the muscle tissue, a large variety of which are supported by the stromal cells populating the interstitium. Telocytes represent a recently discovered population of stromal cells, which has been increasingly identified in several human organs and appears to participate in sustaining cross-talk, promoting regenerative mechanisms and supporting differentiation of local stem cell niche. The aim of this morphologic study was to investigate the presence of Telocytes in the tibialis anterior muscle of healthy rats undergoing an endurance training protocol for either 4 weeks or 16 weeks compared to sedentary rats. Histomorphometric analysis of muscle fibers diameter revealed muscle atrophy in sedentary rats. Telocytes were identified by double-positive immunofluorescence staining for CD34/CD117 and CD34/vimentin. The results showed that Telocytes were significantly reduced in sedentary rats at 16 weeks, while rats subjected to regular exercise maintained a stable Telocytes population after 16 weeks. Understanding of the relationship between Telocytes and exercise offers new chances in the field of regenerative medicine, suggesting possible triggers for Telocytes in sarcopenia and other musculoskeletal disorders, promoting adapted physical activity and rehabilitation programmes in clinical practice.

3 In vitro study of hBM-MSCs chondrogenic differentiation in pellet cultures and GelMA/HA hydrogels exposed to TGFβ1 priming and multiaxial loading

3.1 Introduction

Osteoarthritis, injuries and osteochondritis are the most common causes of cartilage damage and deterioration, resulting in pain and severe disability of the affected joint. The resulting social and economic implications, which importance correlates with the great number of people globally affected, legitimise the strong and imperative interest, on the part of the scientific community, to study the phenomenon in depth (Safiri et al., 2020). However, current therapies have significant limitations, prompting the development of new cartilage tissue engineering approaches. Currently, autologous chondrocytes implantation (ACI) and matrix-assisted autologous chondrocytes implantation (MACI), remain the advanced- therapy medicinal product approved by the FDA (Food and Drug Administration) and EMA (European Medicines Agency) (Makris et al., 2015). Nevertheless, both treatment show some limitations, related to donor site morbidity due to the required cartilage biopsy, as well as to the small size of harvestable cartilage associated with a low chondrocyte yield and limited in vitro expansion potential (Erggelet et al., 2003; Brittberg, 2010). Due to the limited source of autologous chondrocytes for transplantation procedures, much attention has focused on MSCs, multipotent progenitor cells, isolated from many adult organs, that possess self-renewal capability and can differentiate into multiple lineages including adipocytes, osteoblasts and chondrocytes (Pittenger et al.,1999). Particularly, hBM-MSCs represent an attractive alternative cell source to autologous chondrocytes since they can be easily isolated from bone marrow aspirates with limited donor site morbidity and, following expansion, they continue to maintain multilineage potential (Gardner et al., 2013). Indeed, hBM-MSCs are well investigated in the clinical setting, are the best characterised, and many studies describe how they are useful in cartilage repair after injury or disease such as OA (De Bari and Roelofs, 2018). However, to date, the main challenge related to in vitro hBM-MSC chondrogenic differentiation is the lack of an appropriate cultural environment capable of reproduce in vivo physiological conditions and prevent or reduce the progression of MSC-derived chondrocytes hypertrophic differentiation which lead to produce an ECM rich in collagens type I and X markers of fibrocartilage responsible of endochondral ossification of the newly formed

cartilage (Wei et al., 2012; Somoza et al., 2014). In the last years several studies have been conducted, and different in vitro models have been developed to investigate in depth the chondrogenic differentiation of MSCs and its advantages and limitations for their use in tissue engineering.

For the first time in 1998 Johnstone et al. introduced the pellet culture, which has become the gold standard for differentiating BM-MSCs into chondrocyte-like cells in vitro (Johnstone et al., 1998). In this model, in order to form pellet culture, 2×10^5 BM-MSCs were pelleted in induction medium with the TGFβ1 supplementation, providing to be effective in achieving MSCs chondrogenic differentiation, by creating a three-dimensional environment that allows a close contact among the cells similar to those that occur during embryonic development in pre-cartilage condensation (Johnstone et al., 1998).

Since then, a large number of research groups have used pellet cultures with the aim of characterise and optimise the chondrogenic capacity of BM-MSCs or stromal cells from other tissue. Not much has changed since the introduction of culture pellets and many studies continue to use this in vitro model, with the same or similar number of cells to form the pellets, and different weeks of culture in induction medium with different compounds, supplemented with one of the TGFβ isoforms (TGFβ1, 2, or 3) (Freyria et al., 2012; Goldberg et al., 2017). Although the chondrogenic effects of different growth factors have been investigated, TGFβ remains the most important and most frequently used chondrogenic induction factor (Puetzer et al., 2010; Jakobsen et al., 2014).

TGFβ induces the cells within the pellets to acquire a chondrocyte-like phenotype which begin to secrete a cartilage-like matrix rich in aggrecan, collagen II and GAGs, defining large pellets (1-3mm). However, a limitation of this model, is that TGFβ-induced chondrogenesis over time leads to hypertrophy of MSCs, similarity observed during osteochondral ossification (Mueller and Tuan, 2008). In fact, hypertrophic markers such as collagen type I and X, MMP13 and RUNX2, start to be upregulated (Barry et al., 2001; Futrega et al., 2015). Recently, it was demonstrated by using micropellets model that only one day of TGFβ1 exposure is enough to enhance chondrogenic and hypertrophic differentiation pathways of hBM-MSCs (Futrega et al., 2021). Therefore, in this in vitro model, the problem related to hypertrophic differentiation persist.

In parallel, considerable investments have been made by tissue engineering in order to develop an in vitro model capable of mimicking the physiological characteristics of articular cartilage as much as possible, combining the use of progenitor cells, biocompatible 3D scaffolds and biochemical and physical factors.

In this context, attention has been given to the use of hydrogels, stable water-swollen polymeric networks, which are a suitable platform for maintaining the cellular phenotype and promoting the formation of cartilage-like neotissue by homogeneously distributing the cells, and acting as a scaffold

for the accumulation of ECM components (Zhu and Marchant, 2011). In particular, hydrogels based on natural biopolymers show many advantages over synthetic polymers, such as excellent biocompatibility and low immunoresponse.

Gelatin Methacryloyl (GelMA) is a photocrosslinkable gelatin that has caught the attention of tissue engineers due to its excellent biocompatibility (Van Den Bulcke et al., 2000). GelMA undergoes photoinitiated radical polymerisation (i.e. under UV light exposure with the presence of a photoinitiator) to form covalently crosslinked hydrogels. As the hydrolysis product of collagen I, the main component of ECM in most tissues, gelatin contains many arginine-glycine-aspartic acid (RGD) sequences that promote cell attachment, as well as the target sequences for MMPs that are suitable for cell remodelling, while its functionalisation with Methacryloyl allows tunability of the mechanical characteristics (Van Hoorick et al., 2017; Agten et al., 2022). In addition, GelMA is biodegradable, non- cytotoxic and show limited immunogeniticy (Yue et al., 2015).

Recent studies have shown that encapsulation of progenitor cells in GelMA, is able to maintain the cell chondrogenic potential and can lead to cartilage-like matrix formation also after an in vitro culture period of 3 to 8 weeks (Levato et al., 2017; Mouser et al., 2018; Hölzl et al., 2022; Agten et al., 2022). It has also been demonstrated in several in vivo models that after different weeks of implantation in the defect sites, functionalised GelMA scaffolds promote the recruitment of endogenous MSCs, and chondrogenic differentiation (Qiao et al., 2021; Ding et al., 2022; Huang et al., 2022).

Furthermore, GelMA functionalised with HA shows better viscoelastic properties and constitutes a beneficial microenvironment for chondrogenesis, since HA is highly present in native cartilage, has anabolic effects on matrix synthesis, and is also implicated in a wide range of biological processes such as cell proliferation, attachment, migration, differentiation, and tissue homeostasis (Callahan et al., 2012; Levett et al., 2014). HA incorporation into GelMA hydrogels promotes chondrogenesis and chondrocyte phenotype, increasing matrix accumulation, and enhancing matrix distribution in several promising studies (Levett et al., 2014; Meinert et al., 2017; Pahoff et al., 2019; Nedunchezian et al., 2022).

To further improve the current in vitro models, other elements that would help to improve the cartilage engineered characteristics have been introduced into the culture system such as mechanical stimuli. As described in general introduction, mechanical stimuli largely influence cell fate and the biological processes in vivo, involved in chondrogenesis and in the formation of new ECM, resulting essential for cartilage development. In this regard, the introduction of bioreactor or loading devices use, in 3D cell cultures, allow to reproduce the knee environment in vitro and to apply a range of different forces, both alone or combined, recapitulating the complex motion found in vivo condition by reproducing the complex multi-axial load (Grad et al., 2011).

Several studies have shown that MSCs can be directed towards chondrogenic differentiation and stimulated to produce cartilage-like ECM in the absence of any growth factors through exposure to multi-axial loading (a combination of shear and compression load). Specifically, the application of multi-axial load leads to the endogenous production of TGFβ1 by MSCs within the loaded scaffolds, which then drives the differentiation and deposition of cartilage-like matrix, suggesting that mechanical stimulation is a key determinant of MSCs differentiation. In this context the used biomaterials play an essential role, which provide mechanical support but also help to transmit the mechanical forces within cell bodies (Li et al., 2010; Schätti et al., 2011; Delaine-Smi and Reilly, 2012).

The aim of the present study was to investigate the chondrogenic differentiation of hBM-MSCs, isolated from the bone marrow of two donors by using two different in vitro models.

As first step the investigation was carried out using the pellet culture model, which, as explained above, represents the gold standard method. The pellets were cultured for 21 days with or without TGFβ1supplementation in order to evaluate the effects, and if the primary cells used, responded in the same manner to the TGFβ1 chondrogenic stimuli. In addition, the hBM-MSCs response at only one week of TGFβ1exposure, was also investigated.

In the second part of the study, chondrogenic differentiation of the same hBM-MSCs, was evaluated in a more complex in vitro model, combining a series of different elements in order to apply the principles of tissue engineering and try to recreate an in vitro model that could more faithfully mimic the physiological characteristics. The hBM-MSCs were seeded in hydrogels consisting of GelMA and HA, as based on recent data in the literature, it appears to be a promising combination for the in vitro chondrogenesis study. These hydrogels were subjected to multiaxial loading by using a custom-made joint-simulating bioreactor housed at AO Reserch Institute (ARI) in Davos, in order to evaluate how the hBM-MSCs seeded in this kind of construct were able to respond to mechanical stimulation in the chondrogenic sense without the use of growth factors. Furthermore, it was also investigated how a TGFβ1 priming (pre-incubation) of one week prior to apply the loading, was able to alter the hBM-MSCs response to mechanical stimulation.

3.2 Materials and Methods

3.2.1 hBM-MSCs isolation and expansion

Bone marrow aspirate from human vertebral bodies was obtained with full ethical approval (Freiburg, EK-326/08) and the written consent from patients undergoing routine surgical procedure.

MSCs were isolated from the bone marrow of two independent donors (Table 1) using Ficoll density separation (Sigma-Aldrich, Buchs, Switzerland). Mononuclear cells were collected from the interphase and the adherent cell fraction was seeded at a density of 50,000 cells/cm^2 and left to attach for 4 days in alpha minimum essential medium (αMEM) (Gibco, Carlsbad, CA, United States), supplemented with 10% Sera Plus fetal bovine serum (FBS) (Pan Biotech, Aidenbach, Germany), 100U/mL penicillin, 100µg/mL streptomycin (Gibco), and 5-ng/mL recombinant human fibroblast growth factor basic protein (bFGF) (Fitzgerald Industries International). Cells were maintained at 37ºC in a humidified atmosphere of 5% CO_2 and the culture medium was exchanged every second day. After 4 days, non-adhering hematopoietic cells were removed to select the MSC cells. Thereafter, hBM-MSCs were cultured from passage 1 up to passage 4, with a seeding density of 3,000 cells/cm² in T300 tissue culture flasks (TPP, Trasadingen, Switzerland), in the same conditions described above. Upon reaching 80% confluency, the cells were detached by using Trypsin- EDTA (0.5%) (ThermoFisher, UK) for 5 min at 37ºC. For the deactivation of trypsin, 1:2 growth medium containing 10% FBS was used, and then cells were centrifuged at 400 x *g* for 5min. The obtained cells were used for further expansion, 3D cultures or for RNA isolation. hBM-MSCs obtained from each donor were used separately in two independent experiments.

Donor	Age	Sex
1	53	Male
2	55	Male

Table 1. Details of the used donors.

3.2.2 Chondrogenic differentiation in pellet culture

Chondrogenic potential of hBM-MSCs from each donor was performed in pellet culture.

A total of 250,000 cells per pellet were seeded in V-bottom 96-well plates (Corning, NY, USA) and centrifuged for 5 min at 500 x *g* in order to form the pellets. After 24h overnight (ON) incubation in chondropermissive medium (CpM) contained Dulbecco's Modified Eagle Medium (DMEM) high glucose (Gibco, UK), 1% ITS+ (Corning, NY, USA), 1% non-essential amino acids (ThermoFisher,

UK), 50µg/ml ascorbic acid- 2 phosphate (Sigma-Aldrich, Germany), 100 nM dexamethasone (Sigma-Aldrich, Germany) and 100 U/mL plus 100 µg/mL penicillin and streptomycin respectively to allow complete aggregation, pellets were divided in two groups: i) pellets cultured in CpM. ii) pellets cultured in chondrogenic medium (CgM) consisting of CpM supplemented with 10-ng/ml TGF-β1(Fitzgerald Industries International, Acton, MA, USA) (standard chondrogenic medium). The first media change was defined as day 0 and the pellet cultures were maintained for 21 days, with media change three times per week. All the cultures were performed with two independent donors, with two replicates for each experimental group. Cells were maintained under standard cell culture conditions (37ºC and 5% CO_2 in a humidified atmosphere). Pellets were harvested for further analyses after 7, 14 and 21 days of culture.

3.2.3 Preparation of Gelatin-Methacryloyl (GelMA)/ Hyaluronic acid (HA) Hydrogels

Lyophilised and sterile GelMA from bovine bone, (Gelomics PTY LTD, AU) was dissolved at 20% (w/v) in sterile phosphate buffered saline (PBS) at 37ºC in a humidified atmosphere of 5% CO_2 ON. Lithium phenyl-2,4,6-trimethylbenzoylphosphinate (LAP, Sigma-Aldrich, Germany) was used as photocrosslinker for GelMA polymerisation. LAP powder was prepared at 4% (w/v) in PBS under sterile conditions and protected from the light, let to completely dissolved for 20 min at 37ºC and then stored at 4ºC until use.

HA (1MDa, ALB Technology) prepared at 0.04%(w/v) in PBS was left to dissolve under oscillation at 4ºC ON. Subsequently, in order to reduce the number of solutions to be used during the preparation of the hydrogels, HA and LAP solutions were mixed together to obtain a solution 1:10 consisting of 0.04% (w/v) 1MDa HA and 0.4% (w/v) LAP and after was kept at 37ºC until use.

hBM-MSCs (p4) were trypsinized, suspended at a density of $15x10^6$ cells/ml in a 100µl of 20%(w/v) GelMA. Then 100 µl of 0.04% (w/v) 1MDa HA and 0.4% (w/v) LAP solution was added in order to obtain a total volume of 200 µl of cell/hydrogel suspension per hydrogel at final concentration of 10%(w/v) GelMA, 0.2%(w/v) LAP and 0.02%(w/v) HA. The cell-laden hydrogel precursor was pipetted in custom-made polydimethylsiloxane (PDMS) moulds crosslinked for 7 min in a Visible Light Crosslinking System (LunaCrosslinker™, Gelomics PTY LTD, AU) to obtain cylindrical hydrogels with a thickness of 4 mm and a diameter of 8 mm. The hydrogels were taken from the moulds with a spoon and placed in 4% (w/v) agarose rings in order to keep the fixed position of the hydrogels inside the custom-made holders where the cell-laden hydrogel were kept in culture. The custom-made holders were used to place the samples inside the bioreactor for mechanical loading.

All samples were cultured for 21 days, with half of the samples maintained under free-swelling conditions, while the remaining samples were exposed to mechanical loading. Specifically, cell-laden hydrogels were divided in four groups of which: two groups, one maintained in static condition and the other exposed to mechanical stimulation, were cultured in CpM for 21 days. The other two groups were cultured in CgM and maintained in static conditions for 7 days. After that, one group was kept in static condition for 21 days and cultured in CpM while the other group was subjected to mechanical stimulation and cultured also in CpM for 21 days. The culture conditions were kept constant at 37°C and 5% CO2. The culture medium was changed every second day and the conditioned medium was collected and then stored at −20°C for later analysis.

3.2.4 Multiaxial loading of GelMA/HA Hydrogels

A custom-made joint-simulating bioreactor based on tribological principles was used to apply the multi-axial loading on the surface of the hydrogels. The latter were exposed to 15 loading cycles, with dynamic compression at 1 Hz and shear of ±25º for 1 hour a day, five times a week. The application of multi-axial mechanical load to GelMA/HA Hydrogels in this system has been widely described previously for fibrin-poly(ester-urethane) (PU) scaffolds (Wimmer at al., 2004; Schätti et al., 2011; Zahedmanesh et al., 2014; Gardner et al., 2017; Ladner et al., 2022).

3.2.5 RNA Isolation

After 0, 7,14 and 21 days of culture, 3D pellets and GelMA/HA Hydrogels were harvested for total RNA isolation, while total RNA from monolayers at day 0 was isolated to assess basal gene expression levels.

Cells from monolayer cultures were washed in PBS and then collected in Tri Reagent (Molecular Research Center, Inc., Cincinnati, OH, USA) supplemented with 0.5% (*v*/*v*) Polyacryl Carrier (Molecular Research Center, Inc., Cincinnati, OH, USA) at room temperature, then stored at −80 °C until use. On the day of the RNA extraction, the samples were thawed at room temperature and then 100 µl of 1-Bromo-3-chloropropane (BCP) (Sigma-Aldrich, Germany) per 1 mL Tri Reagent was added to each sample. After incubation at room temperature for 15 min and centrifugation at 12,000 x *g* at 4°C for 15 min a phase separation was obtained and approximately 80 % of aqueous phase containing RNA was transferred into a new tube. RNA was precipitated by using 500µl of isopropanol (Sigma-Aldrich, Germany) at room temperature with gentle agitation for 10 min. Samples were then centrifuged at 12,000 x *g* at 4°C for 8 min, the supernatant removed, and the resultant RNA pellets were washed and centrifuged three times with 1 ml of ice-cold 75% ethanol. The ethanol was

removed, the pellet left to air-dry for 5 min and was then resuspended in 20 µL of DEPC-treated water and stored at −80°C until use.

Pellets were harvested (two pellets were pooled for one sample), washed in PBS and incubated with Tri Reagent supplemented with 0.5% (*v*/*v*) Polyacryl Carrier at room temperature. Subsequently the samples were homogenised with Tissue Lyser (Qiagen, Venlo, The Netherlands) at 30Hz for 3 min and then centrifuged at 12.000 x *g* for 10 min. The supernatant was transferred in a new tube and stored at -80°C until use. On the day of the RNA extraction, the samples were thawed, and aqueous phase containing RNA was obtained for each sample, as described above for the monolayer culture and then mixed 1:1 with 70% ethanol. RNA was isolated using RNeasy Mini Kit (Qiagen Venlo, The Netherlands), according to the manufacturer's protocol. RNA was eluted in a 30 µl total volume of RNase-free water with two consecutive steps of elution performed in the same collection tube.

GelMA/HA hydrogels were harvested, washed in PBS, transferred to Eppendorf tubes (Eppendorf, Hamburg, Germany), snap frozen in liquid nitrogen, and stored at -80°C until use. For RNA extraction each hydrogel was pulverised using a custom-made mortar and pastel, followed by another pulverisation step using a pellet pastel to crush the hydrogel while keeping the samples frozen. Subsequently Tri Reagent with 0.5% (*v*/*v*) Polyacryl Carrier was added to each sample followed by an incubation of 10 min at 4ºC. Samples were then added to QIAShredder columns (Qiagen, Venlo, The Netherlands), centrifuged at 20,000 x g for 5 min and the supernatants were collected and transferred in new tubes (Hasler et al., 2020). Phase separation and RNA precipitation were performed as previously described for monolayer culture.

3.2.6 RNA assessment and cDNA synthesis

The quantity and purity of the isolated RNA, were quantify by absorbance measurements with NanoDrop™ One/One^{C} spectrophotometer (Thermo Scientific, Waltham, MA, USA). The obtained A260/A280 and A260/A230 ratios were used to assess the purity of the RNA samples.

Total RNA (500 ng in 40 µl for each samples) was retrotranscribed by using SuperScript™ VILO™ (Invitrogen, Waltham, MA, USA), according to the manufacturer's instructions. cDNA was diluted 1 to 5 with 1X Tris-EDTA buffer (Sigma-Aldrich, Germany) and stored at −20°C until use.

3.2.7 qRT-PCR

Real-time PCR was performed by using TaqMan Universal Master Mix with 5 ng of cDNA in a total reaction volume of 10 µl and each PCR reaction was run in technical triplicates for 40 cycles using a QuantStudio^{TM} 6 Pro Real-Time PCR System (Applied Biosystems^{TM}, Foster City, CA, USA).

A panel of human chondrogenic markers (*SOX9*, *COL2A1*, *ACAN* and *PRG4*), hypertrophic markers (*COL10A1*, *COL1A1* and *MMP13*), osteogenic markers (*RUNX2* and *ALPL*) and the transforming growth factor receptors 1 and 2 (*TGFβ-R1* and *TGFβ-R2*) were analysed. Monolayers at day 0 were used to assess basal gene expression and used to normalise the data, while *RPLP0* and *PPIA* were used as endogenous control genes. Primers for *SOX9*, *ALP*, *PRG4*, *PPIA*, *TGFβ-R1* and *TGFβ-R2* were purchased from Applied Biosystems (Warrington, United Kingdom) (Table 2), while primers for *RPLP0*, *COL2A1*, *COL10A1*, *COL1A1*, *ACAN*, *RUNX2* and *MMP13* were synthesised by Microsynth AG (Balgach, Switzerland) (Table 3).

Relative expression levels of target mRNA were performed according to the comparative Ct method using the geometric mean of the housekeeper genes RPLP0 and PPIA. The gene expression levels for each marker was determined relative to day 0 monolayer culture according to $2^{-\Delta\Delta Ct}$ method.

Gene	TaqMan Gene Expression Assays
SOX9	Hs00165814_m1
ALP	Hs00758162_m1
PPIA	Hs99999904_m1
PRG4	Hs00981633_m1
TGFβ-R1	Hs00610320_m1
TGFβ-R2	Hs00234253_m1
MMP13	Hs00942584_m1

Table 2. TaqMan Gene Expression Assays used for qRT-PCR

Gene	Primer forward (5'-3')	Primer reverse (5'-3')	Probe (5' FAM- 3' TAMRA
RPLP0	5'-TGG GCA AGA ACA CCA TGA TG-3'	5'-CGG ATA TGA GGC AGC AGT TTC-3'	5'-AGG GCA CCT GGA AAA CAA CCC AGC-3'
COL2A1	5'-GGC AAT AGC AGG TTC ACG TAC A-3'	5'-GAT AAC AGT CTT GCC CCA CTT ACC-3'	5'-CCT GAA GGA TGG CTG CAC GAA ACA TAC-3'
ACAN	5'-AGT CCT CAA GCC TCC TGT ACT CA-3'	5'-CGG GAA GTG GCG GTA ACA-3'	5'-CCG GAA TGG AAA CGT GAA TCA GAA TCA ACT-3'
COL1A1	5'-CCC TGG AAA GAA TGG AGA TGA T-3'	5'-ACT GAA ACC TCT GTG TCC CTT CA-3'	5'-CGG GCA ATC CTC GAG CAC CC-3'
COL10A1	5'-ACG CTG AAC GAT ACC AAA TG-3'	5'-TGC TAT ACC TTT ACT CTT TAT GGT GTA-3'	5'-ACT ACC CAA CAC CAA GAC ACA GTT CTT CAT TCC-3'
RUNX2	5'-AGC AAG GTT CAA CGA TCT GAG AT-3'	5'-TTT GTG AAG ACG GTT ATG GTC AA-3'	5'-TGA AAC TCT TGC CTC GTC CAC TCC G-3'

Table 3. Human oligonucleotide primers and probes used for qRT-PCR

3.2.8 DNAquantification

After day 0 and 21 days of culture, pellets and GelMA/HA hydrogels were digested for 16h at 56ºC in 0.5 ml proteinase K (0.5 mg/ml). To determinate the total amount of DNA, a fluorescence assay using DNA intercalating Bisbenzimide Hoechst 33258 dye (Polysciences Inc., Warrington, PA, United States) was performed. Fluorescence was measured using Tecan Micro Plate Reader (excitation: 360 nm, emission: 460 nm) and purified calf thymus DNA was used as a standard (Lubio Science, Luzern, Switzerland) (Labarca and Paigen, 1980).

3.2.9 Sulfated Glycosaminoglycans (sGAG) quantification

To determine the amount sulphated glycosaminoglycan (GAG) produced by each sample, the dimethyl-methylenblue (DMMB) assay (pH 3) (Sigma-Aldrich, Buchs, Switzerland) was performed. The samples were digested with the same procedure described for DNA assay. Absorbance was measured using Tecan Micro Plate Reader at 525 nm, and bovine chondroitin 4-sulphate sodium salt from bovine trachea (Fluka, St. Louis, MO, United States) was used as a standard (Farndale et al., 1986). GelMA/HA Hydrogels were blanked with cell-free hydrogel to eliminate the background caused by the hyaluronan already present in the constructs.
GAGs released by hydrogels in culture media were also measured to analyse the release of matrix molecules from the construct.

3.2.10 Histological Analysis

After 21 days of culture, the 3D pellets and the hydrogels were collected and fixed with 4% fomaldehyde/ 10% neutral buffered formalin solution (Sigma-Aldrich, Buchs, Switzerland) for 24h at room temperature. The specimens were then washed in tap water, dehydrated in graded ethanol, and paraffin embedded. The histological analysis was performed on 5 µm sections obtained using Microm HM 325 rotary microtome (Thermo Fischer Scientific, Waltham, MA, USA).
Sections were dewaxed in xylene, hydrated in graded ethanol, and stained with Haematoxylin & Eosin (H&E) to evaluate tissue structure and cell morphology, and with Safranin O (counterstained with fast green) to detect proteoglycans and proteoglycan-depleted collagen-rich areas. The sections were examined using a Zeiss Axioplan light microscope (Carl Zeiss, Oberkochen, Germany) and the pictures were acquired with a digital camera AxioCam MRc5 (Carl Zeiss, Oberkochen, Germany).

3.2.11 Immunohistochemistry (IHC)

For IHC, 3D pellets and the hydrogels were processed as previously described for histological analysis. Subsequently, the slides were dewaxed in xylene, hydrated using graded ethanol, and incubated for 10 min in 3% H_2O_2 solution to quench endogenous peroxidase activity. The sections were then placed in a thermoregulated bath (80°C for 30 min) with Universal heat-induced epitope retrieval (HIER) antigen reagent (Abcam, Cambridge, UK) to unmask antigenic sites. To reduce the non-specific binding of the antibody, the sections were then treated with a protein block solution (Abcam, Cambridge, UK) for 1 h, then the sections were incubated overnight at 4ºC with specific primary antibodies at the appropriate dilutions with antibody diluent solution (Abcam, Cambridge, UK). Details on primary antibodies sources and dilutions are shown in Table 4. Immune complexes were then treated with biotinylated link antibodies (horseradish peroxidase polymer (HRP)-conjugated anti-rabbit and anti-mouse were used as secondary antibodies) and then detected with peroxidase-labelled streptavidin, both incubated for 10 min at room temperature (mouse and rabbit specific HRP Plus (ABC) detection IHC kit, Abcam, Cambridge, UK). Immunoreactivity was then visualised by incubating the sections for 1-10 min in a 3,3' -diaminobenzidine (DAB) solution (DAB substrate kit, Abcam, Cambridge, UK). The sections were lightly counterstained with haematoxylin, mounted in Glycerol Vinyl Alcohol (GVA) (Zymed Laboratories, San Francisco, CA, USA), observed with the Axioplan Zeiss light microscope (Carl Zeiss, Oberkochen, Germany), and photographed with the digital camera (AxioCam MRc5, Carl Zeiss, Oberkochen, Germany).

Primary Antibody	Host Species	Producer	Dilution
Anti-Aggrecan	Mouse	Abcam	1:100
Anti-Collagen type II	Rabbit	Abcam	1:100
Anti- Collagen type I	Rabbit	Sigma-Aldrich	1:100
Anti-Collagen type X	Rabbit	Abcam	1:200
Anti-SOX9	Rabbit	Abcam	1:500

Table 4. Primary antibody used for the IHC and their diluitions.

3.2.12 Statistical analysis

Data were generated from two independent experiments, each carried out using the hBM-MSCs from a different donor. All experiments were performed in duplicate for each group at different timepoints to reduce methodological variability. Each measurement was performed in technicaltriplicate . Analyses were performed between the appropriate control group and treatment groups as well as between different treatment groups, using one-way or two-ways ANOVA with Tukey's or Sidak's

post-hoc testing as required. A significance level of $p < 0.05$ was applied and data are presented as Mean and Standard Deviation (SD). Analyses were performed using GraphPad Instat® Biostatistics version 9.0 software (GraphPad Software, Inc., La Jolla, CA, USA).

3.3 Results

3.3.1Chondrogenic potential evaluation of hBM-MSCs in pellets culture

As a first experimental phase, the chondrogenic potential of hBM-MSCs from each donor was evaluated by using pellets cultured in two different media for 21 days: chondropermissive medium (CpM) and chondropermissive medium supplemented with TGFβ1, also called chondrogenic medium (CgM) in order to evaluate the responsiveness of the donors to the growth factor. In addition, in order to investigate if the cells are responsive to 7 days (1 week) of TGFβ1 exposure, one group of pellets was cultured for 1 week with CgM, followed by 2 weeks with CpM (without TGFβ1 exposure). Molecular analysis (Gene expression analysis, Sulfated Glycsaminaglicans (sGAGs) and DNA quantification) were carried out after 7, 14, and 21 days of culture, while Histological analysis and Immuhistochemistry were carried out after 21 days of culture.

3.3.1.1 Gene expression analysis

Firstly, a panel of human chondrogenic markers (*SOX9*, *COL2A1*, *ACAN* and *PRG4*) was analysed. The two donors displayed the same trends of varying degrees of magnitude. Specifically, was observed an overall upregulation in the pellets cultured in CgM. In fact, *SOX9*, *COL2A1* and *ACAN* showed a higher expression in all timepoints in pellets cultured in CgM compared to the other two groups (Fig.3.1A-C, Fig.3.2A-C).

Specificanly, after 7 days of culture in CgM, *SOX9* expression was increased compared with the pellets cultured in CpM. The expression reached a peak at day 14 and remaining roughly the same at day 21. However, with a culture of only one week in CgM, the expression of *SOX9* showed the same expression level of the CpM group, tending to decrease at day 21 and overall *SOX9* followed the same trend in both donors (Fig.3.1A, Fig.3.2A).

Also the expression of *COL2A1* and *ACAN* showed the same tendency in both donors. The expression of both genes was increased in the pellets cultured in CgM compared with CpM group at all timepoints, reaching a peak at day 14 and reaming the same levels at day 21 (Fig.3.1B-C, Fig.3.2B-C). On the other hand, with a cultured of only one week in CgM, the expression of both genes was stable at day 14 and day 21 and comparable with the expression at day 7 in CgM group (Fig.3.1B-C, Fig.3.2B-C).

However, the expression of *PRG4* appear to respond in the opposite way to TGFβ1 exposure in both donors. *PRG4* was more expressed in CpM group compared with CgM group in all timepoints,

although the *PRG4* expression was constant in CpM group in all timepoint. In CgM group, the expression of *PRG4* started to decrease at day 7 reaching lower levels at day 21 (Fig.3.1D, Fig.3.2D).

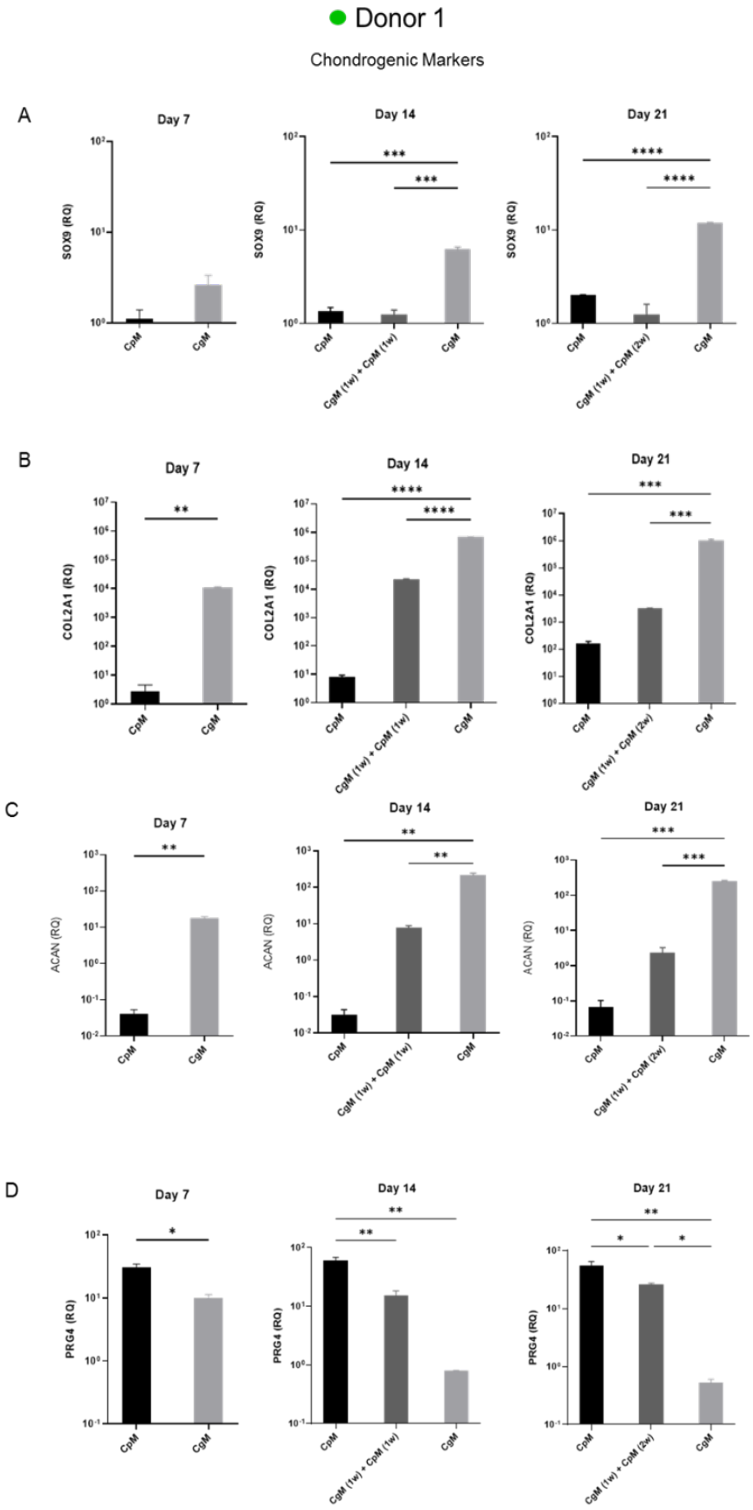

Figure 3.1 Gene expression measured by qRT-PCR of chondrogenic markers *SOX9* (A), *COL2A1* (B), *ACAN* (C) and *PRG4* (D) in pellets culture obtained with hBM-MSCs from donor 1. The pellets were cultured with standard chondropermissive medium (CpM), standard chondropermissive medium supplemented with TGFβ1 (CgM), and CgM for 1 week and CpM for the followed 2 weeks. The samples were harvested at days 7,14, and 21. Relative quantification of target mRNA was performed according to $2^{-\Delta\Delta Ct}$ method. Value represent means ± SD of one donor in experimental duplicate. Statistical significance was defined as * $p< 0.05$, ** $p< 0.01$, *** $p<0.001$ and **** $p<0.0001$.

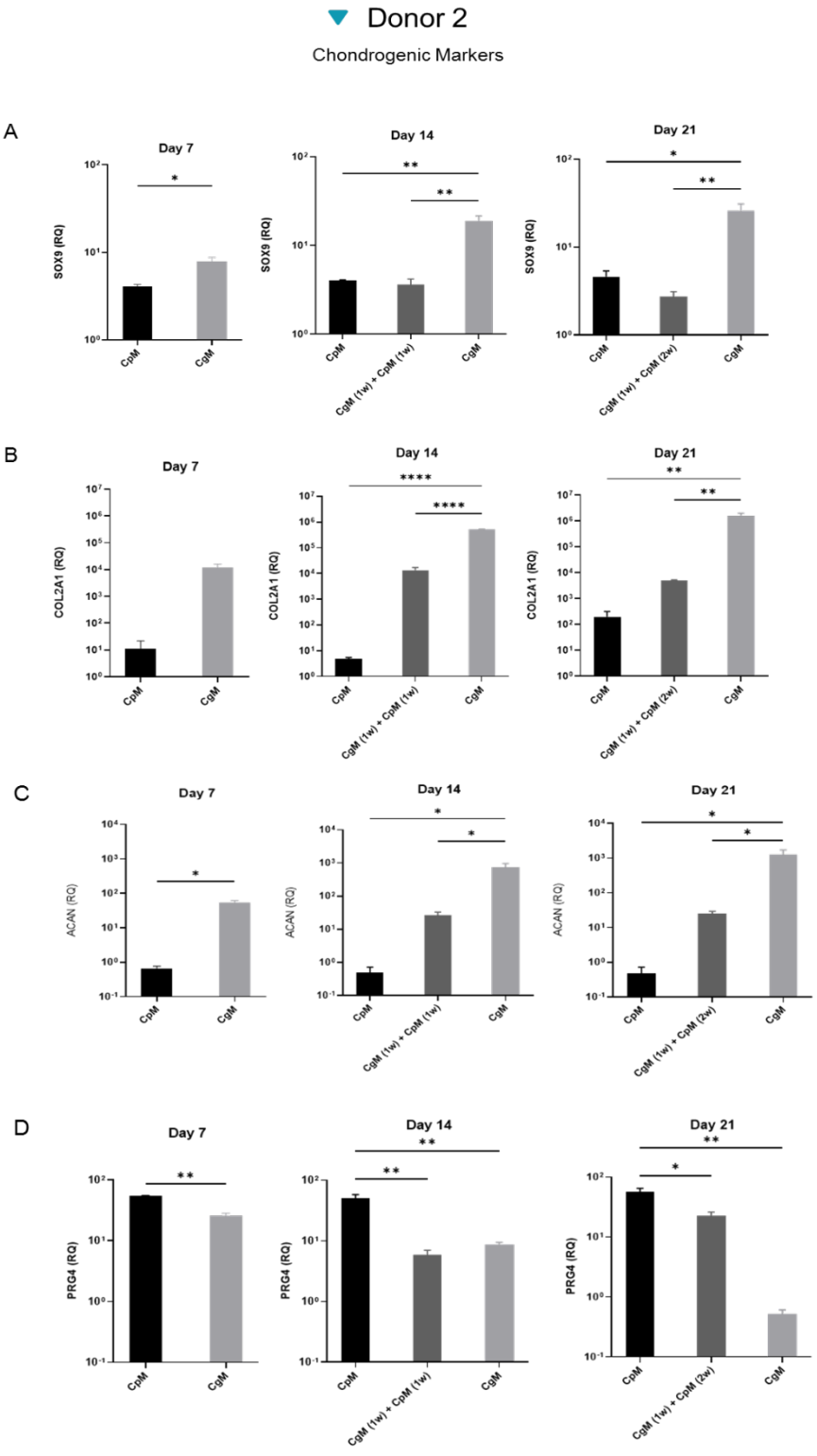

Figure 3.2 Gene expression measured by qRT-PCR of chondrogenic markers SOX9 (A), COL2A1 (B), ACAN (C) and PRG4 (D) in pellets culture with hBM-MSCs from donor 2. The pellets were cultured with standard chondropermissive medium (CpM), standard chondropermissive medium supplemented with TGFβ1 (CgM), and CgM for 1 week and CpM for the followed weeks. The samples were harvested at days 7,14 and 21. Relative quantification of target mRNA was performed according to $2^{-\Delta\Delta Ct}$ method. Value represent means ± SD of one donor in experimental duplicate. Statistical significance was defined as * $p< 0.05$, ** $p< 0.01$, *** $p<0.001$ and **** $p<0.0001$.

A panel of genes associated with hBM-MSCs hypertrophic differentiation (*COL10A1*, *COL1A1* and *MMP13*) was investigated. Also for this genes, an overall upregulation when the pellets were cultured with CgM was observed in both donors. The expression of *COL10A1* was similar in both donors with a trend comparable to *ACAN* and *COL2A1* expression (Fig.3.3A, Fig.3.4A). However, *COL1A1* and *MMP13* showed an expression patterns different in both donors. In particular *COL1A1* expression in donor 1 was increased only with TGFβ1 supplementation with no differences between the two groups(Fig.3.3B). In donor 2, the expression of *COL1A1* was increased in the pellets cultured in CgM compared with CpM group, but the expression was higher after 21 days of CgM compared to only one week of CgM (Fig.3.4B).

The *MMP13* expression in donor1 followed the other genes trend with the expression higher in CgM group but the expression peak was reached at day 21 rather than day 14. Meanwhile with an only week of CgM the expression of *MMP13* was stable in all timepoint(Fig.3.3C). However, in donor 2 very low expression levels in CpM group compared to CgM groups were observed, but no differences between a continuous exposure of CgM at 21 days, and the exposure with only one week of CgM, were detected (Fig.3.4C).

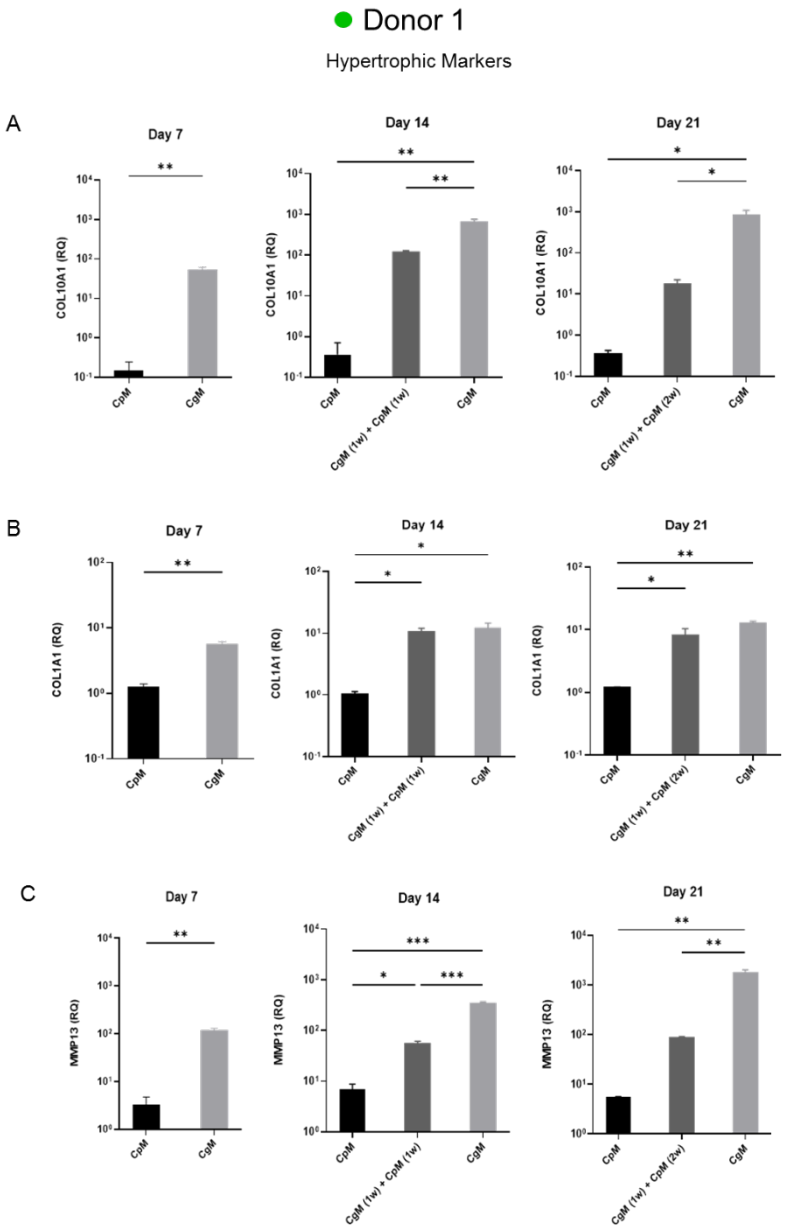

Figure 3.3 Gene expression measured by qRT-PCR of hypertrophic markers as *COL10A1* (A), *COL1A1* (B), *MMP13* (C) in pellets culture obtained with hBM-MSCs from donor 1. The pellets were cultured with standard chondropermissive medium (CpM), standard chondropermissive medium supplemented with TGFβ1 (CgM), and CgM for 1 week and CpM for the followed weeks. The samples were harvested at days 7,14 and 21. Relative quantification of target mRNA was performed according to $2^{-\Delta\Delta Ct}$ method. Value represent means ± SD of one donor in experimental duplicate. Statistical significance was defined as * p< 0.05, ** p< 0.01, *** p<0.001 and **** p<0.0001.

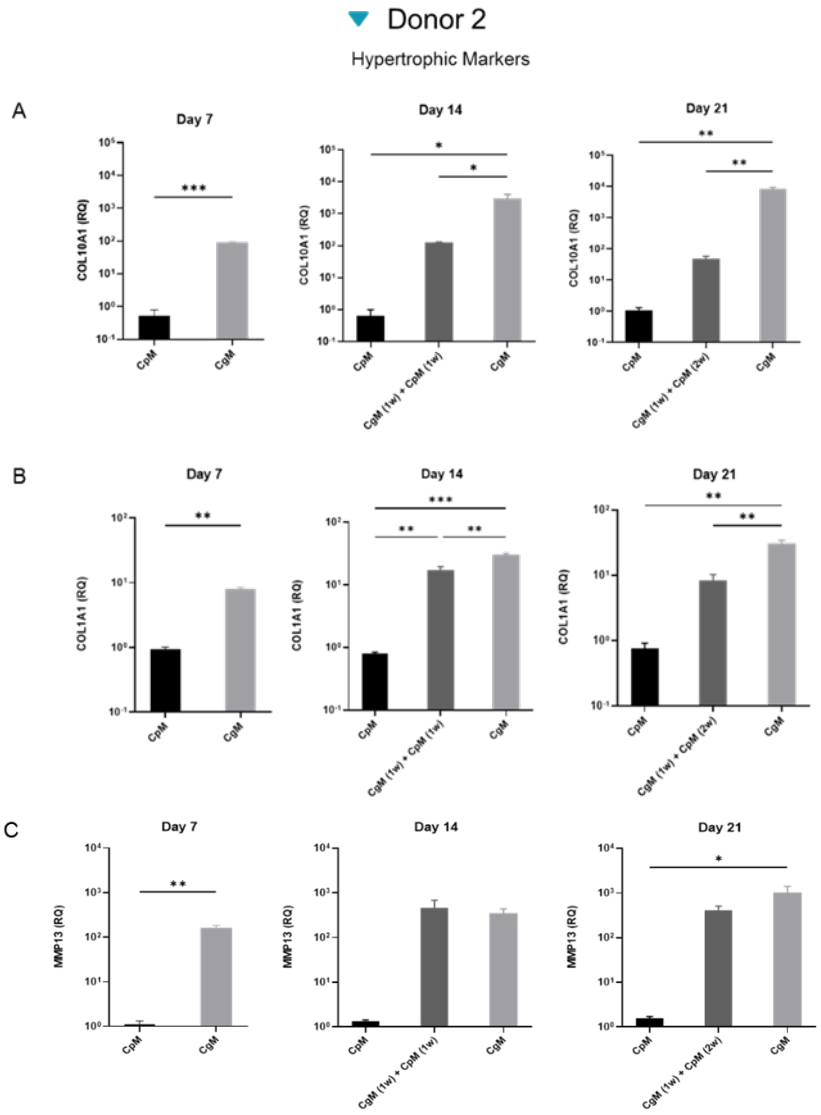

Figure 3.4. Gene expression measured by qRT-PCR of hypertrophic markers as COL10A1 (A), COL1A1 (B), MMP13 (C) in pellets culture obtained with hBM-MSCs from donor 2. The pellets were cultured with standard chondropermissive medium (CpM), standard chondropermissive medium supplemented with TGFβ1 (CgM), and CgM for 1 week and CpM for the followed weeks. The samples were harvested at days 7,14 and 21. Relative quantification of target mRNA was performed according to $2^{-\Delta\Delta Ct}$ method. Value represent means ± SD of one donor in experimental duplicate. Statistical significance was defined as * p< 0.05, ** p< 0.01, *** p<0.001 and **** p<0.0001.

3.3.1.2 Sulfated Glycsaminaglicans (sGAGs) and DNA quantification

After 7 of culture, no differences were observed in DNA content among different groups and both donors. At day 14 an increase of DNA content was observed in pellets cultured in CgM, while at day 21 pellets with only one week of CgM maintained the same amount of DNA and the group in CgM showed a further increase. (Fig.3.5A).

However, an overall increase in sGAGs amount was observed in the in pellet cultured in CgM in both donors starting at day 14, with a further significant increase at day 21 (Fig.3.5B). On the other hand

after only one week of CgM culturing, pellets showed the same sGAGs amount at days 14 and where the levels were comparable to CpM group (Fig.3.5B).

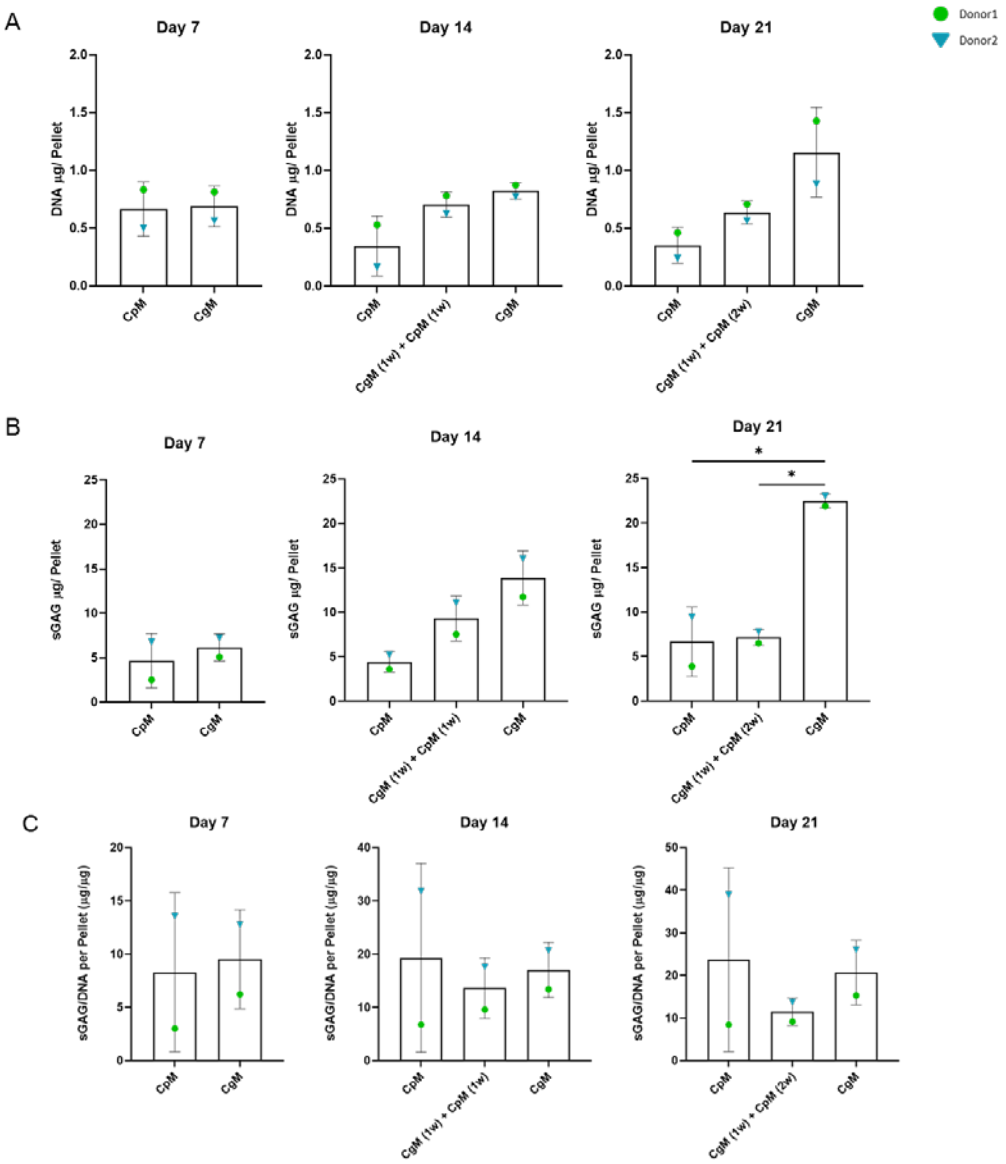

Figure 3.5 DNA (A) and sGAGs produces (retained) (B) in the pellets culture. The pellets were cultured with standard chondropermissive medium (CpM), standard chondropermissive medium supplemented with TGFβ1 (CgM), and CgM for 1 week and CpM for the followed weeks. The samples were harvested at days 7,14 and 21. Values represent mean ± SD of the two hBM-MSCs independent donors in experimental duplicated. Statistical significance was defined as * $p < 0.05$.

3.3.1.3 Histological analysis

After 21 days of chondrogenic differentiation in CpM, CgM, and only 1 week of CgM cultures, pellets were stained with Haematoxylin and Eosin (H&E) in order to investigate their histological assestment and cell morphology. Pellets cultured in CpM of both donors showed small sizes; the cells exbihted fibroblast-like shape were and were randomly distributed throughout the pellets area, surrounded by few ECM deposition.However, with the TGFβ1 exposure a different pellets morphology was observed. After only 1 week of CgM culturing, pellets grew larger compared with CpM group, showing undifferentiated and differentiated regions, differently organised in the two donors: in donor 1 the differentiated region appeared as an external capsule, with parallel fibers to the pellet surface, that embedded an inner less differentiated region. In donor 2 small differentiated regions were identified peripheral part of pellet (Fig.3.6).

Nevertheless, after 21 days of CgM culture, pellets showed bigger sizes compared with the other two groups. The cells were uniformly distributed in pellet area with a chondrocyte-like rounded morphology and surrounded in abundant dense ECM. No differences were observed between the pellets cultured for 21 days in CgM of the two donors (Fig.3.6).

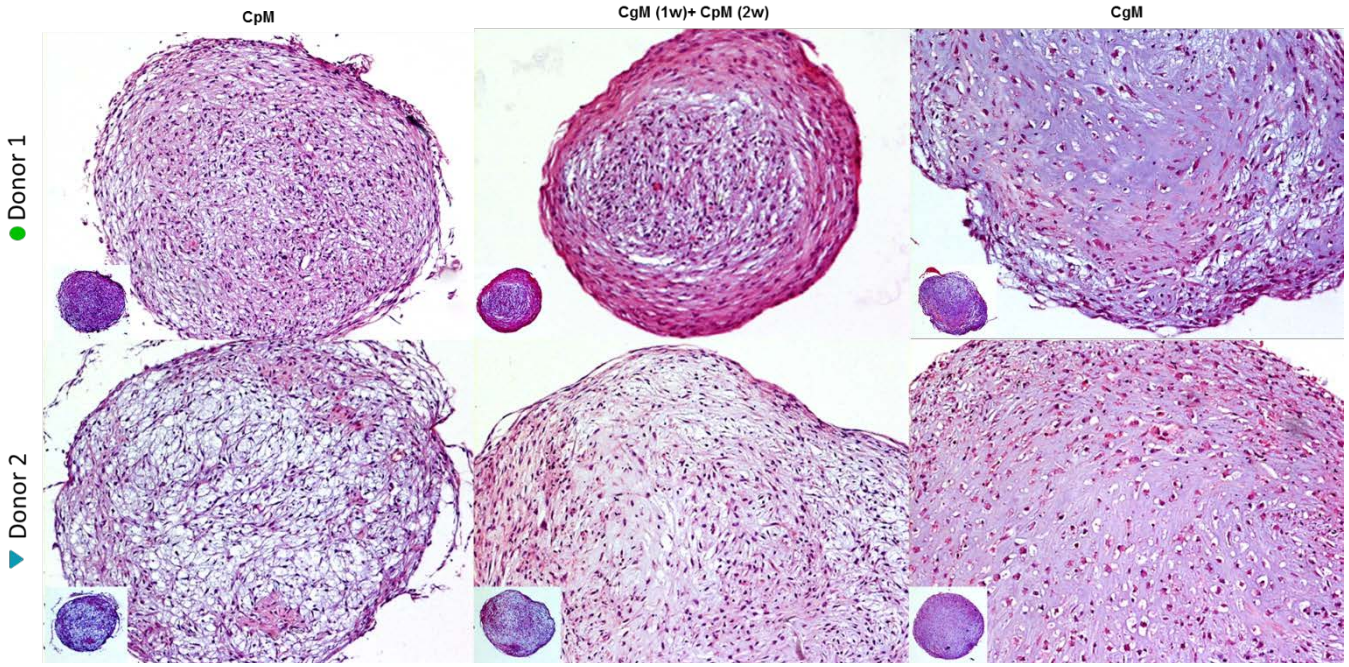

Figure 3.6. Histological assessment of pellets obtained by hBM-MSCs from donor 1 and 2 after 21 days of chondrogenic cultures. From left to right, haematoxylin and eosin (H&E) staining of pellets cultured in CpM, 1 week in CgM followed by 2 weeks of CpM and CgM. Images showing longitudinal sections of pellets at magnification 10X. Insert: images showing the full sections of the pellets at magnification of 2.5X.

To evaluate the production of cartilaginous matrix deposition and sGAGs content, the pellet sections were stained with Safranin O and counterstained with Fast green after 21 days of culture. Overall the staining confirmed the observations done with the H&E. After 21 days of culture a positive Safranin O staining was observed in all pellets of both donors. In pellets cultured in CpM the staining was very low compared with the pellets cultured for 21 days in CgM, where was observed a stronger positive staining, suggesting the cartilage-like ECM presence characterised by high GAGs content. With only 1 week of CgM culture, pellets showed roughly the sGAGs amount comparable with CpM pellet group. However, in these pellets the chondrogenic differentiate areas (observed also with H&E) were highlighted by the green staining which indicated collagen fibers presence and deposition (Fig. 3.7).

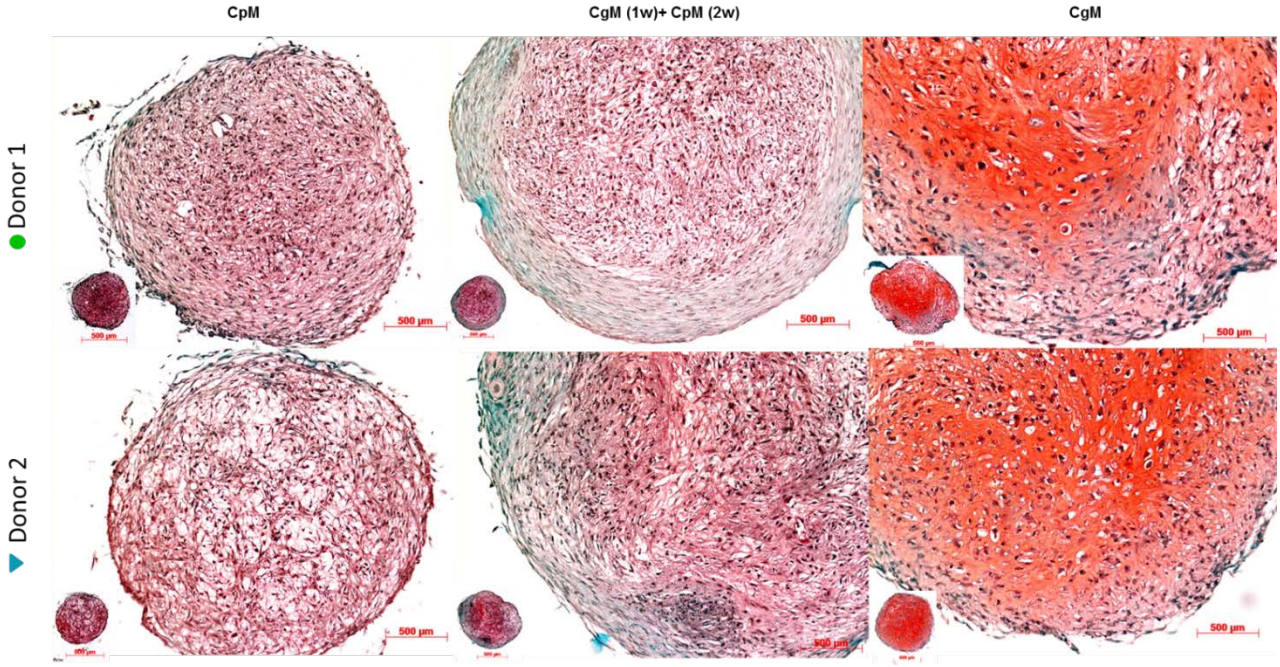

Figure 3.7. Histological evaluation of sGAGs content by Safranin O counterstained with Fast green, in pellets obtained by hBM-MSCs from donor 1 and 2 after 21 days of chondrogenic cultures. Images showing the longitudinal sections of pellets at magnification of 10X and small inserts with full sections at magnification of 2.5X. Scale bar: 500 µm.

3.3.1.4 Immunohistochemical Analysis of SOX9, Aggrecan, Col II, Col X and Col I in Pellet Cultures

Immunohistochemistry (IHC) was performed in pellet sections in order to evaluate the expression and the distribution inside the pelletsof main biomarker of chondrogenesis (SOX9, Aggrecan and COL.2) and hypertrophy (COL.X and COL.1).

Immunohistochemical analysis for SOX9 expression confirmed the results observed for gene expression. SOX9 expression was increased in pellets grown in CgM for 21 days, compared to the other groups. In fact, SOX9 presence was detected in most of the nuclei of the differentiated cells which were homogeneously distributed along the whole pellets area. In contrast to the pellets grown in CpM for 21 days, showed a much lower number of immunoreactive nuclei, suggesting a low differentiation activity. Interestingly, the pellets cultured in CgM for only one week showed low levels of SOX9, but the cells with higher levels of SOX9 levels inside the nuclei were mainly localised in the differentiation areas highlighted by H&E and Safranin O stains (Fig.3.8).

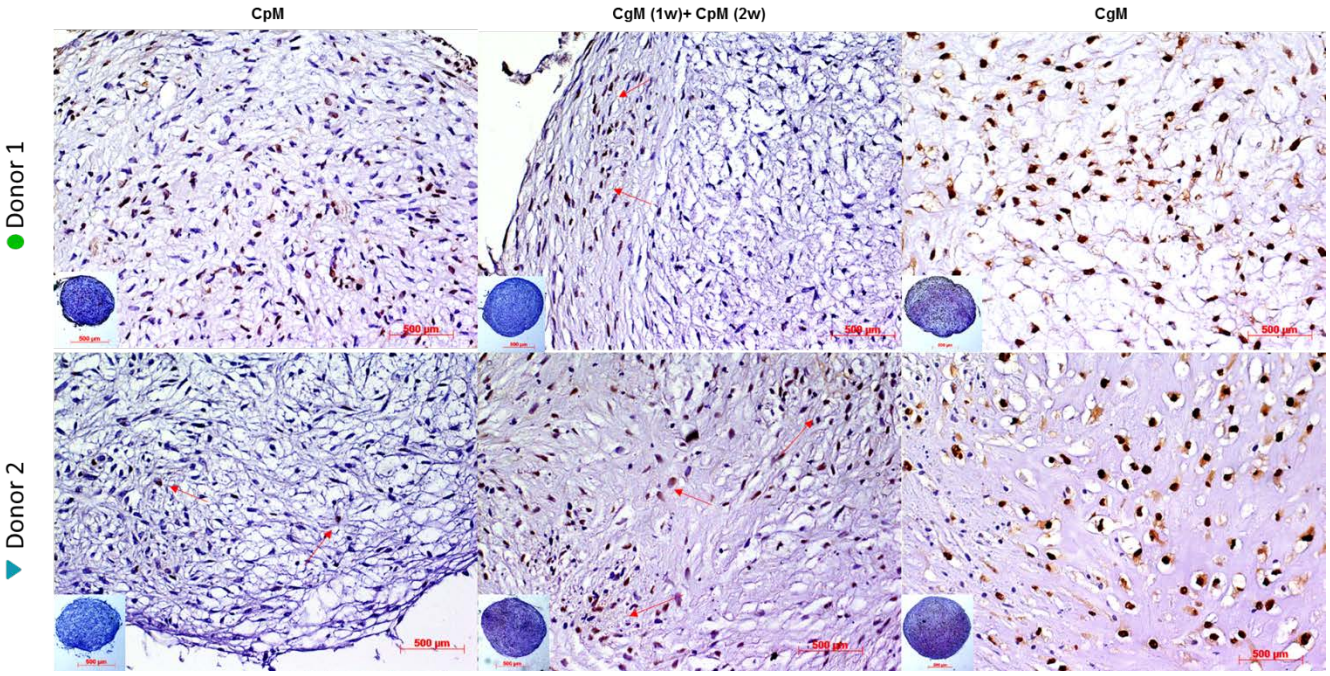

Figure 3.8 SOX9 immunohistochemical evaluation in pellets obtained by hBM-MSCs from donor 1 and 2 after 21 days of chondrogenic cultures. Images showing the longitudinal sections of pellets at magnification of 20X and small inserts with full sections at magnification of 2.5X. Scale bar: 500 µm.

Similarly, the other biomarker analysed by IHC, followed the trend observed with corresponding gene expression.

Aggrecan staining was almost completely absent in pellets cultured in CpM while in pellets cultured for only 1 week with in CgM, aggrecan deposition mainly located in differentiation zones was observed. Otherwise in the pellets grown in CgM a different distribution was observed in the two donors: in donor 1 the aggrecan was located in a specific areas of the pellet, while aggrecan in donor 2 showed a distribution throughout the pellet but mainly localized in the pericellular space (Fig.3.9-3.10). IHC showed highly content of Collagen II and homogeneously distributed throughout the pellets cultured in CgM, while lower quantity in the pellets cultured in CpM were observed. After 1 week of CgM culture, donor 1 showed high content of collagen II mainly in the differentiation zone, while donor 2 showed a homogeneous distribution in all pellet

area. Collagen X in both donors showed an immunoreactivity almost absence in CpM group, while with 1 week of CgM culturing, collagen X content was higher and located in the differentiation zones. On the other hand, after 21 days of CgM culture, pellets of donor 1 showed collagen X located in only one portion of the sample, while donor 2 showed homogeneous distribution throughout the sample. Collagen I exhibited less immmunoreactivity in all groups pellets of both donors, compared to the other biomarkers but with similar pattern. In donor 1, collagen I followed mainly the same distribution of collagen x, while in donor 2, followed the same distribution of aggrecan (Fig.3.9-3.10).

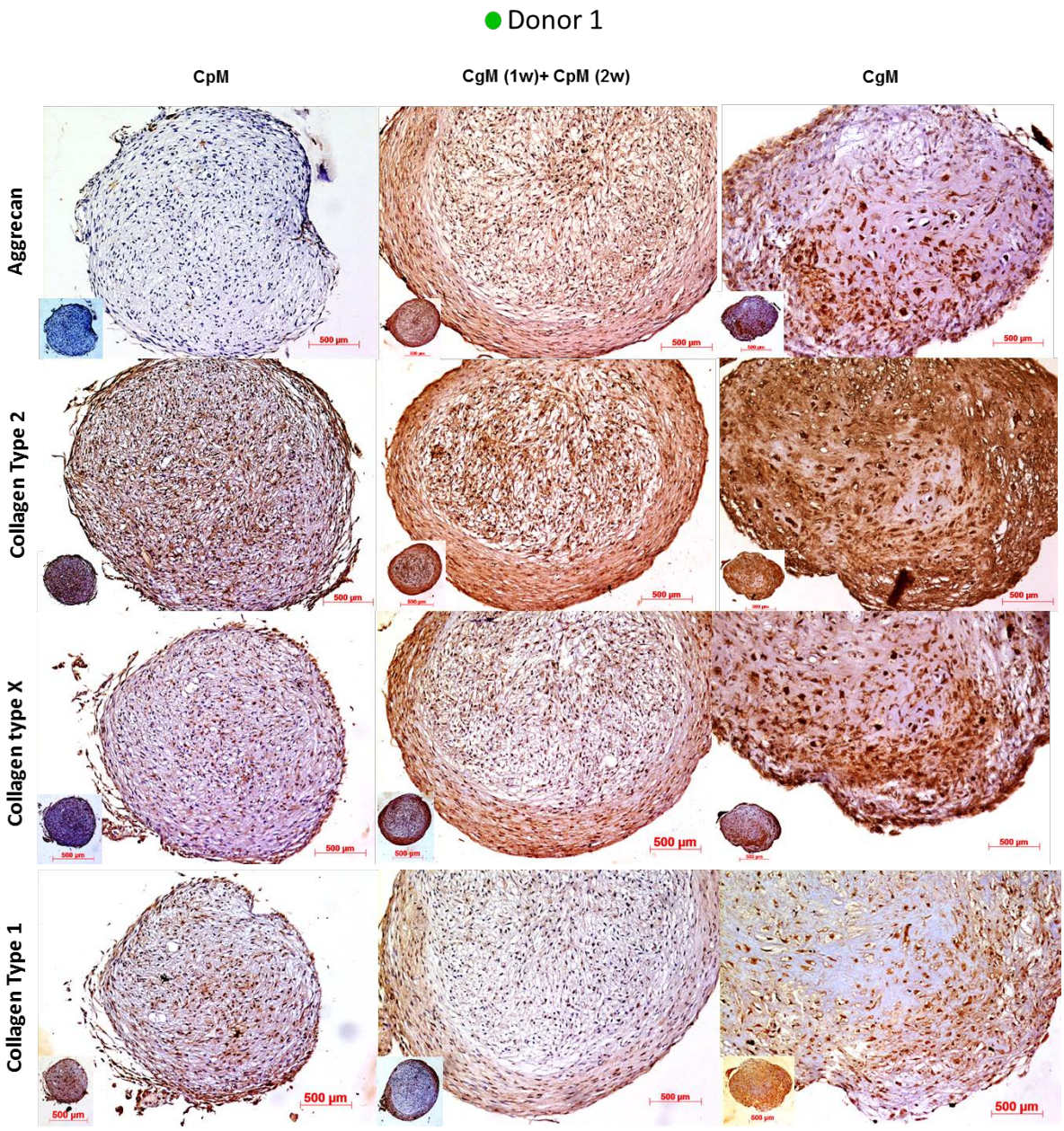

Figure 3.9 Aggrecan, Collagen type II, Collagen type X and Collagen type I immunohistochemical evaluation in pellets obtained by hBM-MSCs from donor 1 after 21 days of chondrogenic cultures. Images showing the longitudinal sections of pellets at magnification of 10X and small inserts with full sections at magnification of 2.5X. Scale bar: 500 µm.

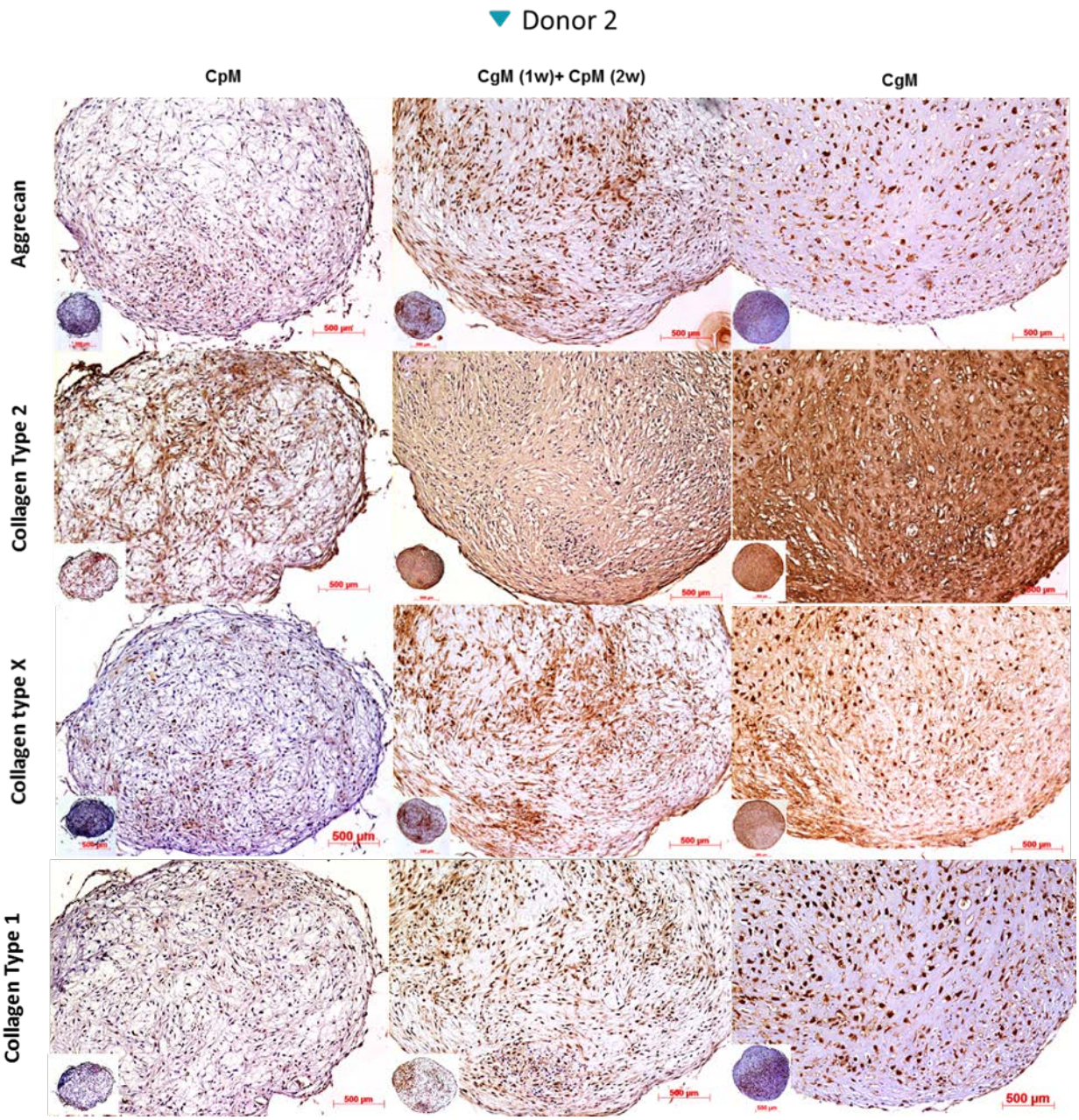

Figure 3.10 Immunohistochemical evaluation of Aggrecan, Collagen type II, Collagen type X and Collagen type I in pellets obtained by hBM-MSCs from donor 2 after 21 days of chondrogenic cultures. Images showing the longitudinal sections of pellets at magnification of 10X and small inserts with full sections at magnification of 2.5X. Scale bar: 500 µm.

3.3.2 Effects of TGFβ1 priming and mechanical loading on hBM-MSCs within GelMA/HA Hydrogels.

The purpose of this second part of the study, was to determinate if the hBM-MSCs, from both donors, seeded in GelMA/HA hydrogels were able to respond to multiaxial loading with chondrogenic differentiation. In addition. since the potential interaction between the cells differentiation state and the timing of mechanical loading initiation in poorly investigated, the other aim was to examine the effects of chondrogenic priming on the cells, and on their capability to response to mechanical loading. To achieve this, cell-laden hydrogels were primed for 1 week with TGFβ1prior to apply multiaxial loading for three addition weeks. Loaded samples were compared to time-matched free swelling samples (as control). The hydrogels were harvested at the end of their loading cycle for the analysis.

3.3.2.1 Gene expression analysis

Genes associated with chondrogenic differentiation (*SOX9*, *COL2A1*, *ACAN*, and *PRG4*), hypertrophy (*COL10A1*, *COL1A1*, and *MMP13*), osteogenic differentiation (*RUNX2* and *ALP*), and TGFβ1 receptors (*TGFβ1-R1*and *TGFβ1-R2*) were investigated.

The two donors displayed the same trends to a varying degree of magnitude. Among the majority of markers analysed, an overall upregulation was observed with TGFβ1 priming.

Firstly, the expression of the main transcription factors involved in chondrogenic differentiation (*SOX9*) and osteogenic differentiation (*RUNX2*) were investigated. No differences of the expression of both genes were observed between loaded and static group without priming of both donors. After priming, *SOX9* showed an increased expression in both groups (static and loaded), with higher levels observed in priming plus loading group. Specifically, *SOX9* reached an expression peak at day 14 in both donor, which dropped at day 21, where in donor 1 the levels of *SOX9* were maintained high in priming plus static group, while in donor 2 the *SOX9* levels were almost uniform in all groups (Fig.3.11A, Fig.3.12A). Donor 1 showed expression levels of *RUNX2* comparable in all groups, while donor 2 showed increased levels after priming, with a peak at day 21only in priming plus static group (Fig.3.11B, Fig.3.12B). The *SOX9/RUNX2* chondrogenic ratio showed increased levels at day 7 and 14 after priming and loading in donor 1, while no differences were observed between priming groups at day 21, but the differences were high compared with the groups without priming. Donor 2 showed a peak in *SOX9*/*RUNX2* ratio at day 14 compared with the other groups, while at day 7 and day 21 no differences between all groups were observed. (Fig.3.11C, Fig.3.12C).

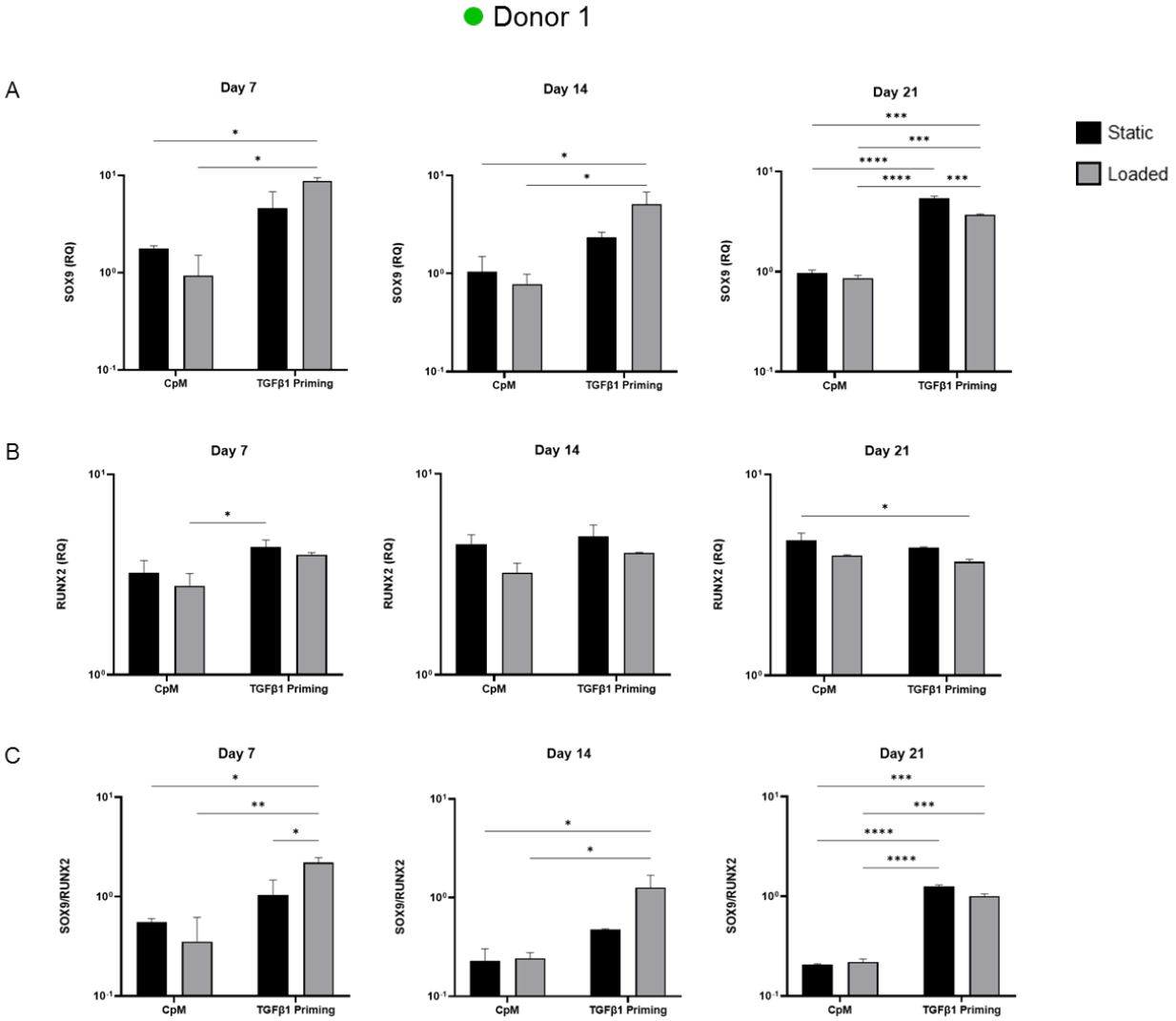

Figure 3.11 Gene expression measured by qRT-PCR of *SOX9* (A), *RUNX2* (B) and *SOX9/RUNX2* ratio (C) in GelMa/HA hydrogels seeded with hBM-MSCs from donor 1. Hydrogels were organised in 4 group as previously described in materials & methods section. The samples were harvested at day 7, 14 and 21 days after loading. Relative quantification of target mRNA was performed according to $2^{-\Delta\Delta Ct}$ method. Value represent means ± SD in experimental duplicate. Statistical significance was defined as * $p< 0.05$, ** $p< 0.01$, *** $p<0.001$ and **** $p<0.0001$.

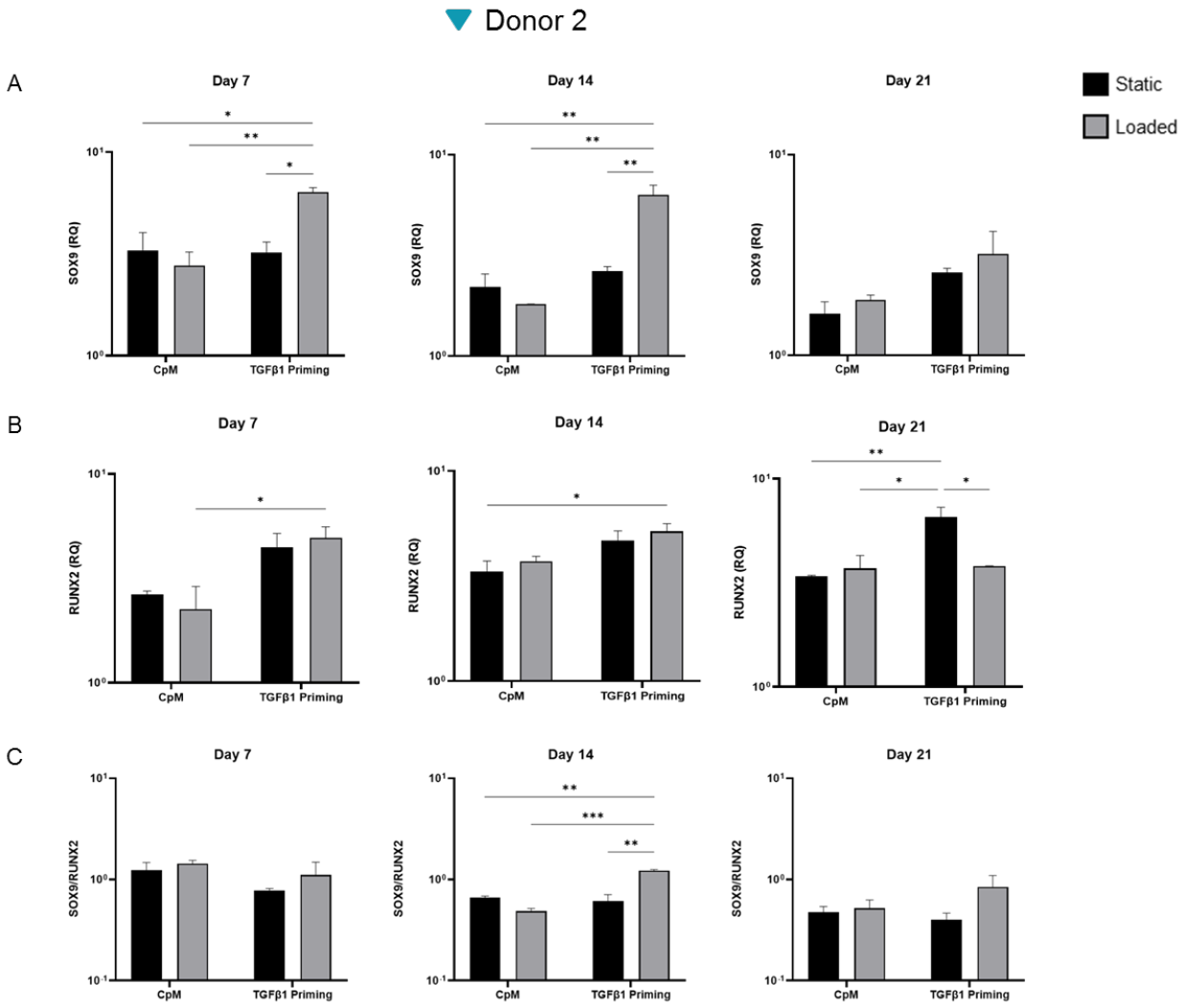

Figure 3.12. Gene expression measured by qRT-PCR of *SOX9* (A), *RUNX2* (B) and *SOX9/RUNX2* ratio (C) in GelMa/HA hydrogels seeded with hBM-MSCs from donor 2. Hydrogels were organised in 4 group as previously described in materials & methods section. The samples were harvested at day 7, 14 and 21 days after loading. Relative quantification of target mRNA was performed according to $2^{-\Delta\Delta Ct}$ method. Value represent means ± SD in experimental duplicate. Statistical significance was defined as * p< 0.05, ** p< 0.01, *** p<0.001 and **** p<0.0001.

Successively, the expression of the main chondrogenic markers *ACAN*, *COL2A1* and *PRG4* were investigated.

COL2A1 and *ACAN* showed the same trend in both donors. Low expression levels and no significant differences were observed between the hydrogels stimulated with only mechanical loading and their matched static group in all timepoints and in both donors (Fig.3.13A-B Fig.3.14A-B). On the other hands, an increased expression of both genes was observed after 1 week of priming. In addiction mechanical loading applied after priming, led to a significant *COL2A1* upregulation at day 21 and a significant *ACAN* upregulation at day 14 and 21 compared with primed static group in both donors (Fig.3.13A-B Fig.3.14A-B). Conversely, *PRG4* showed an opposite trend (as observed also in pellets culture) compared to ACAN and COL2A1. In fact, *PRG4* showed higher expression levels in

unprimed groups at day 21 in donor 1 and atday14 and day 21 in donor 2, but no differences were observed between loading groups and matched static groups. (Fig.3.313C, Fig.3.14C).

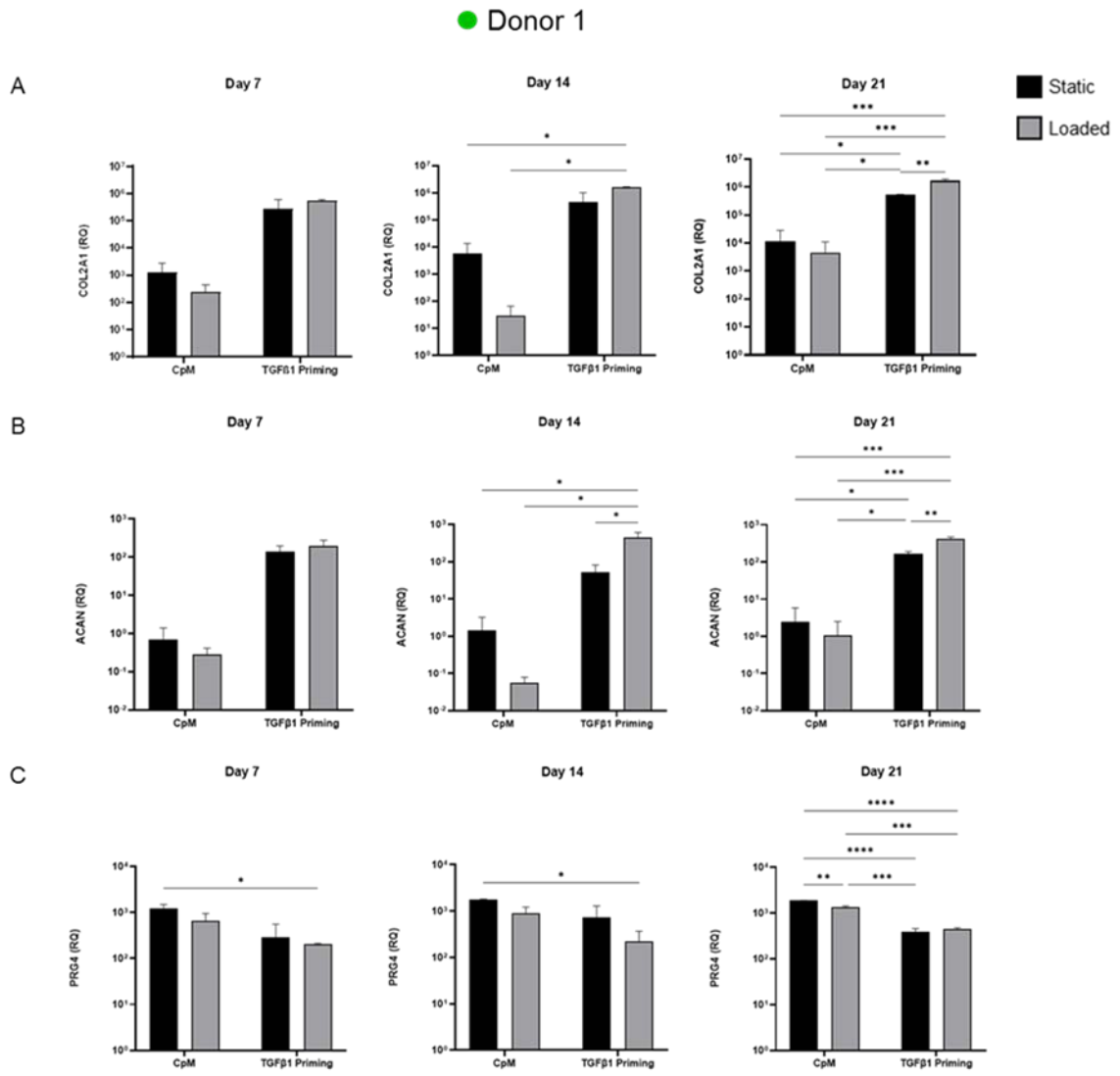

Figure 3.13. Gene expression measured by qRT-PCR of *COL2A1* (A), *ACAN* (B) and *PRG4* (C) in GelMa/HA hydrogels seeded with hBM-MSCs from donor 1. Hydrogels were organised in 4 group as previously described in materials & methods section. The samples were harvested at day 7, 14 and 21 days after loading. Relative quantification of target mRNA was performed according to $2^{-\Delta\Delta Ct}$ method. Value represent means ± SD in experimental duplicate. Statistical significance was defined as * p< 0.05, ** p< 0.01, *** p<0.001 and **** p<0.0001.

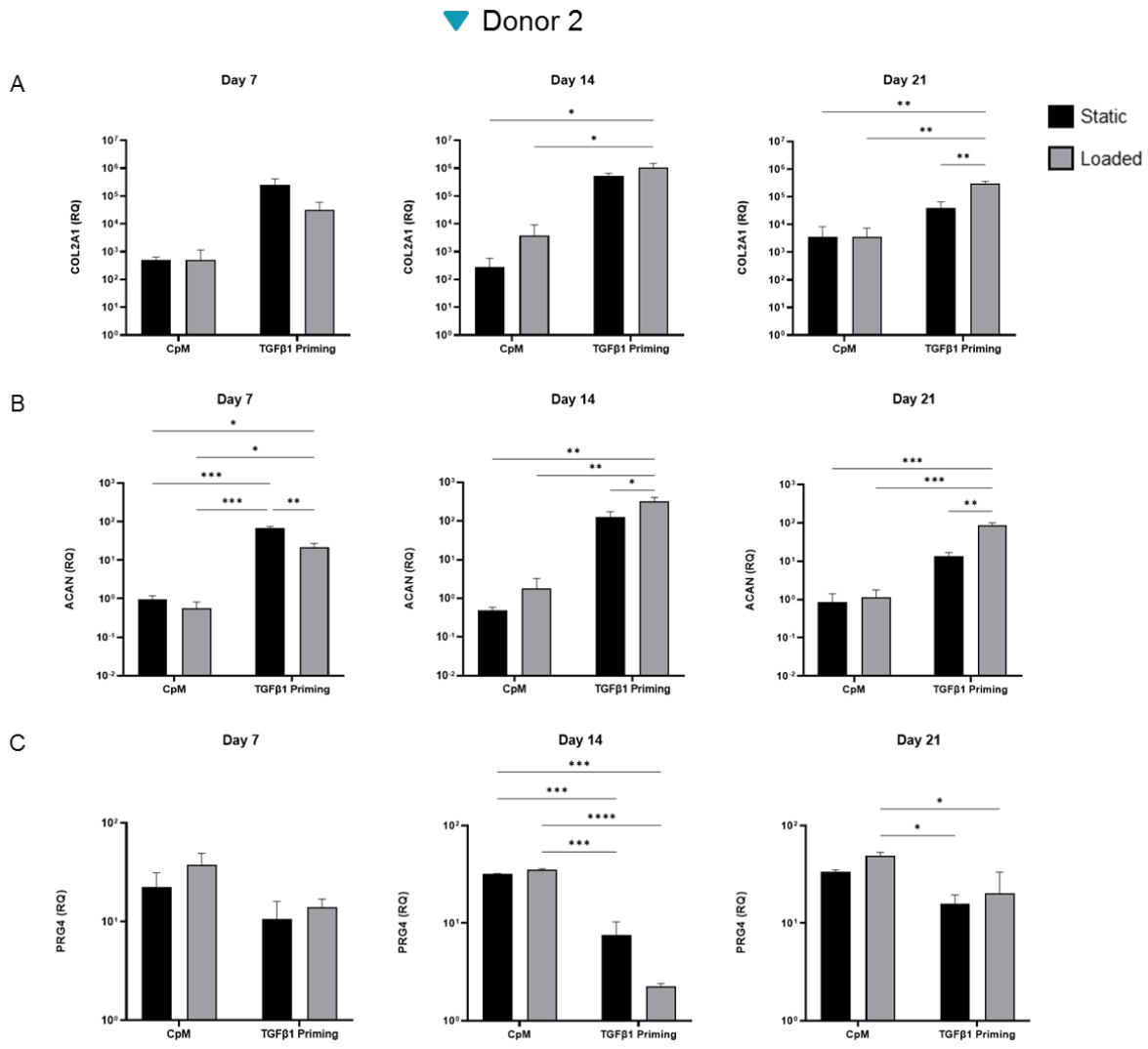

Figure 3.14 Gene expression measured by qRT-PCR of *COL2A1* (A), *ACAN* (B) and *PRG4* (C) in GelMa/HA hydrogels seeded with hBM-MSCs from donor 2. Hydrogels were organised in 4 group as previously described in materials & methods section. The samples were harvested at day 7, 14 and 21 days after loading. Relative quantification of target mRNA was performed according to $2^{-\Delta\Delta Ct}$ method. Value represent means ± SD in experimental duplicate. Statistical significance was defined as * p< 0.05, ** p< 0.01, *** p<0.001 and **** p<0.0001.

Then, the expression of hypertrophic markers *COL10A1*, *COL1A1* and *MMP13* was analysed.

The three genes showed the same trend of chondrogenic markers which is low expression in the unprimed groups with no significant differences between loaded and matched static group, while TGFβ1 priming exerted an expression increase of these genes in both donors. Overall the hypertrophic markers showed the same expression pattern in both donors. Interestingly, mechanical loading did not promote any increase of *COL10A1* after priming in both donors where no difference between loaded and static primed groups were observed (Fig.3.15A, Fig.3.16A). Also *COL1A1* followed this trend, but only donor 1 showed an increase at day 21 in priming plus loading group compared with the matched static group (Fig.3.15B, Fig.3.16B). In addition, mechanical stimulation applied after

priming did not promote any upregulation of MMP13 in both donors, on the contrary the levels were slightly lower compared to matched static group (Fig.3.15C, Fig.3.16C).

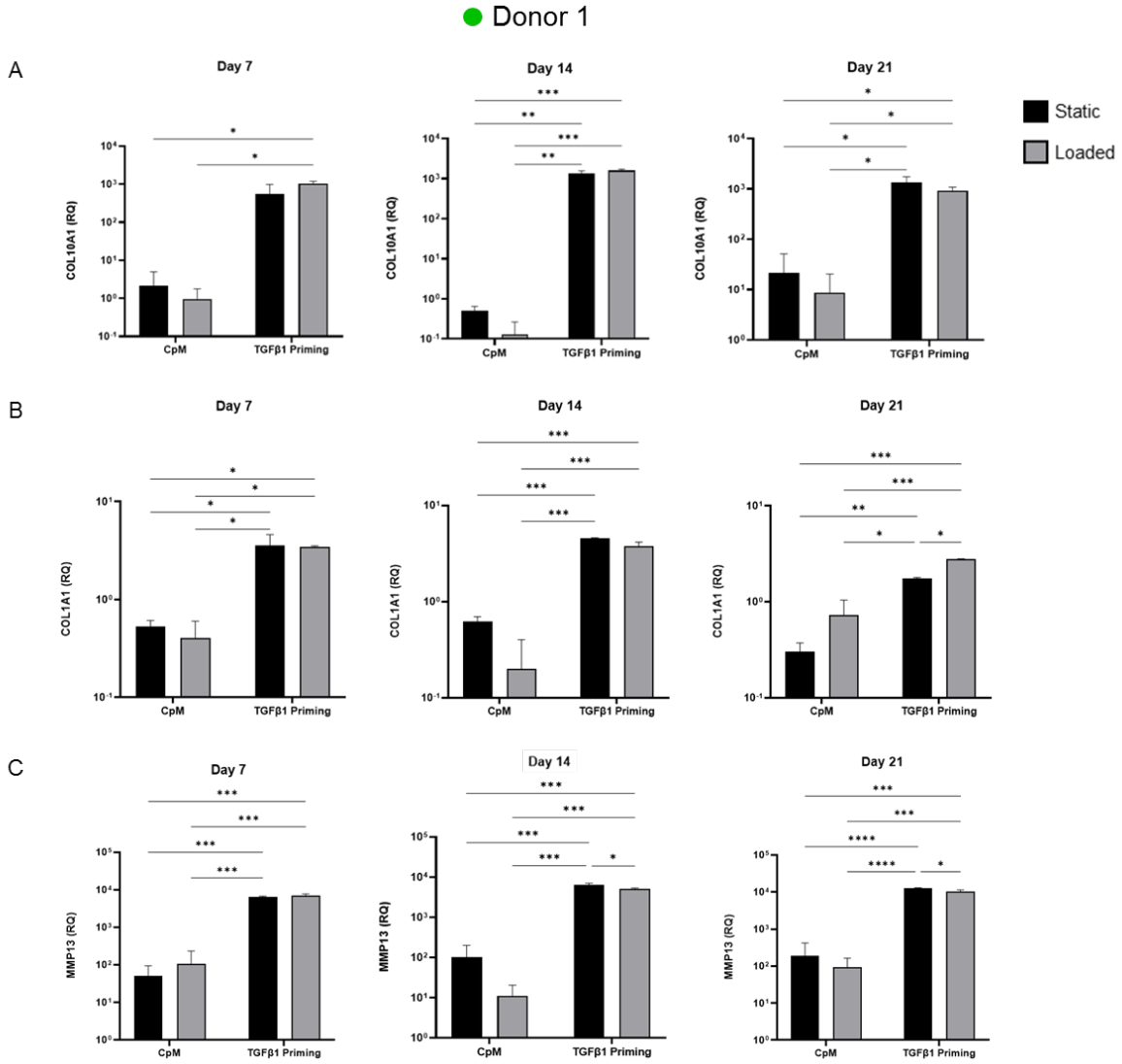

Figure 3.15 Gene expression measured by qRT-PCR of *COL10A1* (A), *COL1A1* (B) and *MMP13* (C) in GelMa/HA hydrogels seeded with hBM-MSCs from donor 1. Hydrogels were organised in 4 group as previously described in materials & methods section. The samples were harvested at day 7, 14 and 21 days after loading. Relative quantification of target mRNA was performed according to $2^{-\Delta\Delta Ct}$ method. Value represent means ± SD in experimental duplicate. Statistical significance was defined as * p< 0.05, ** p< 0.01, *** p<0.001 and **** p<0.0001.

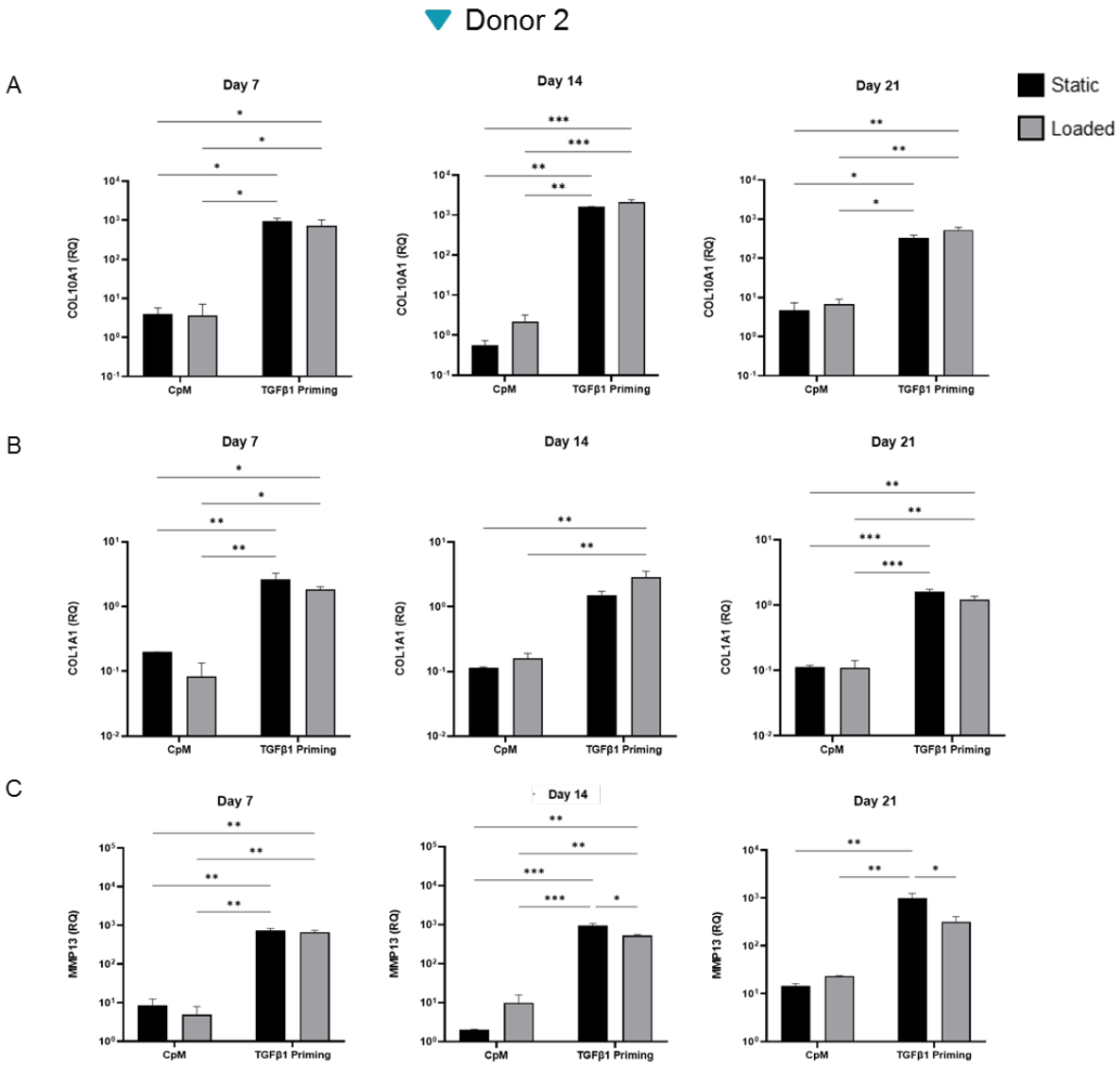

Figure 3.16. **Gene expression measured by qRT-PCR of *COL10A1* (A), *COL1A1* (B) and *MMP13* (C) in GelMa/HA hydrogels seeded with hBM-MSCs from donor 2.** Hydrogels were organised in 4 group as previously described in materials & methods section. The samples were harvested at day 7, 14 and 21 days after loading. Relative quantification of target mRNA was performed according to $2^{-\Delta\Delta Ct}$ method. Value represent means ± SD in experimental duplicate. Statistical significance was defined as * p< 0.05, ** p< 0.01, *** p<0.001 and **** p<0.0001.

In order to investigated if the osteogenesis was also activated by laoding and the combitation of priming and loading, the expression of ALP was analysed. No significant differenceswere observed in the groups no primed while after priming increased levels of ALP were observed in static group compared with loading group at day 21 in donor 1, and at day 7 and day 14 in donor 2 (Fig.3.17).

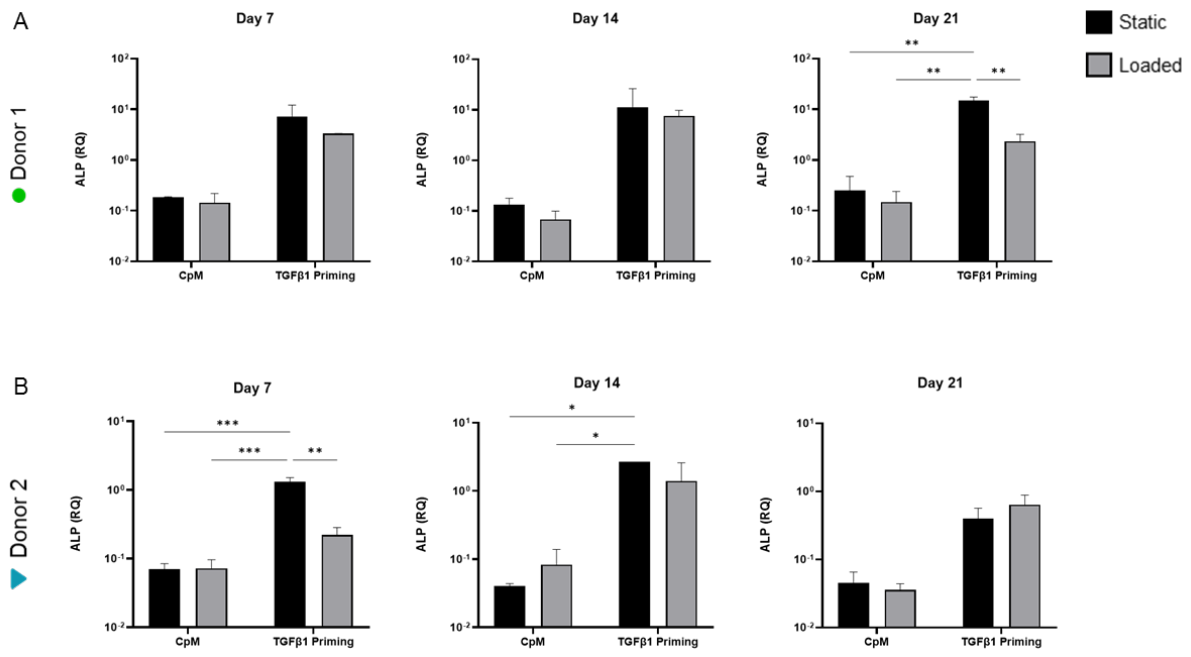

Figure 3.17. Gene expression measured by qRT-PCR of *ALP* (A) in GelMa/HA hydrogels seeded with hBM-MSCs from donor 1 (A) and 2 (B). Hydrogels were organised in 4 group as previously described in materials & methods section. The samples were harvested at day 7, 14 and 21 days after loading. Relative quantification of target mRNA was performed according to $2^{-\Delta\Delta Ct}$ method. Value represent means ± SD in experimental duplicate. Statistical significance was defined as * p< 0.05, ** p< 0.01, *** p<0.001 and **** p<0.0001.

Finally, the expression of TGFβ1 receptors, *TGFβ1-R1* and *TGFβ1-R2*, were also investigated.

The *TGFβ1-R2* expression was homogeneous in all groups and in both donors while *TGFβ1-R1* expression appeared to be slightly increased in the primed groups with higher levels in priming group plus static, at day 21 in donor 1 and day 7 and day 21 in donor 2 (Fig 3.18-3.19).

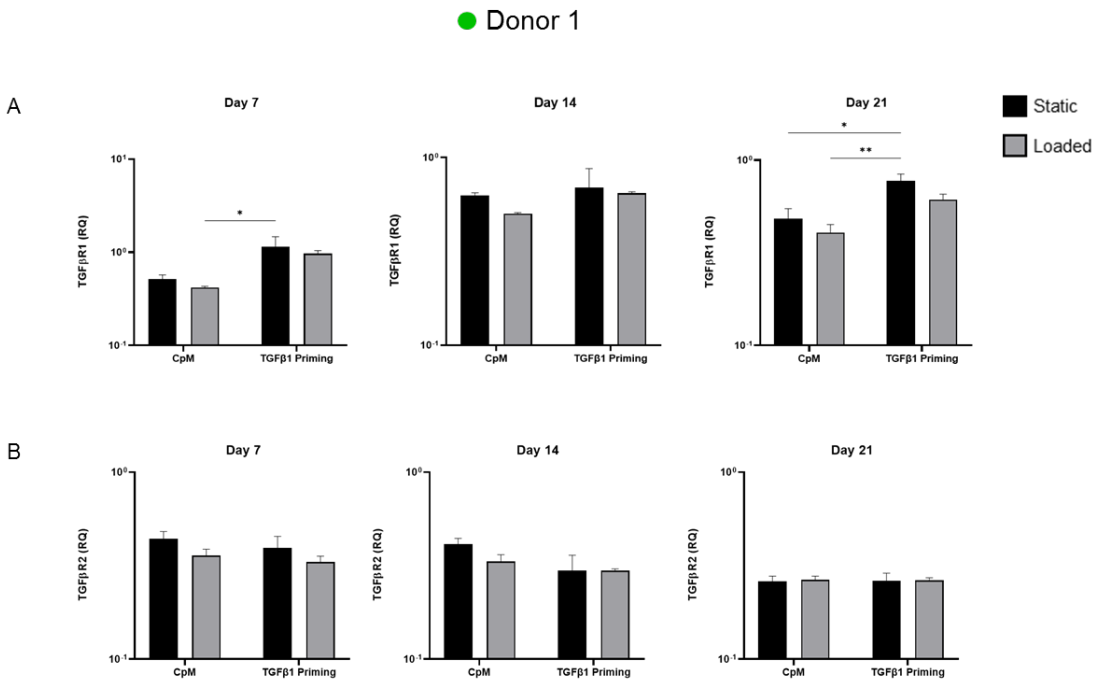

Figure 3.18. **Gene expression measured by qRT-PCR of *TGFβ1-R1* (A) and *TGFβ1-R2* (B) in GelMa/HA hydrogels seeded with hBM-MSCs from donor 1.** Hydrogels were organised in 4 group as previously described in materials & methods section. The samples were harvested at day 7, 14 and 21 days after loading. Relative quantification of target mRNA was performed according to $2^{-\Delta\Delta Ct}$ method. Value represent means ± SD in experimental duplicate. Statistical significance was defined as * $p< 0.05$, ** $p< 0.01$, *** $p<0.001$ and **** $p<0.0001$.

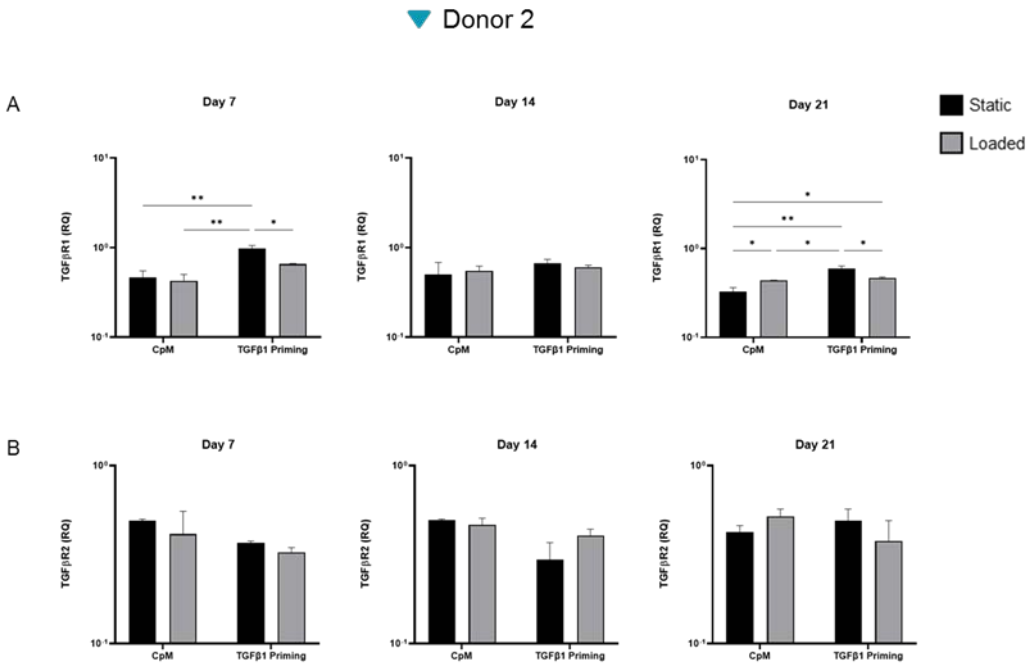

Figure 3.19. Gene expression measured by qRT-PCR of *TGFβ1-R1* (A) and *TGFβ1-R2* (B) in GelMa/HA hydrogels seeded with hBM-MSCs from donor 2. Hydrogels were organised in 4 groups as previously described in materials & methods section. The samples were harvested at day 7, 14 and 21 days after loading. Relative quantification of target mRNA was performed according to $2^{-\Delta\Delta Ct}$ method. Value represent means ± SD in experimental duplicate. Statistical significance was defined as * p< 0.05, ** p< 0.01, *** p<0.001 and **** p<0.0001.

3.3.2.2 Sulfated Glycosaminaglicans and DNA quantification

After 21 days of loading and culture, no statistical significant differences were observed in DNA content among the different groups and in both donors (Fig.3.20A).

GAGs deposited inside the hydrogels after 21 days of culture were significantly more in the priming plus loading group, compared with other groups, while no differences were observed between no primed groups (Fig.3.20B). These data were confirmed also by GAGs per scaffold/DNA ratio at day 21, where was significantly higher in priming plus loading group, confirming a synergistic effect of priming and loading in inducing a notable of the cartilage- like matrix production and deposition by hBM-MSCs inside the GelMa/HA hydrogels (Fig.3.20C).

GAGs in the medium were also monitored and analysed at each medium change to investigate the trend of GAGs release over the 21 days of loading and culture (Fig. 3.21A). Starting from day 2, an important difference of GAGs released, was observed between the groups, in which the GAGs released were higher in the groups with priming (static and loaded), also due to TGFβ1 pre-treatment which stimulated an increase of GAGs production. Despite this, priming plus loading group showed more amount of GAGs released compared not only with the non-primed groups, but also between with matched static group, suggesting that just two days of loading were enough to trigger more

GAGs production. Overall this trend was maintained for all three weeks of loading where the combination of priming and loading favoured a more GAGs release into the medium, while loaded alone promoted only a slightly increase of GAGs releasing compared with the corresponding static group (Fig. 3.21A), but basically without priming the GAGs released were low. Importantly, with the progress of time, statistical significance was lost due to donor-dependent response to mechanical loading for which the amount of GAGs produces was different between the two donors. Specifically, donor 1 showed an overall lower GAG production, compared to the donor 2, and this difference was gradually more evident with time. Nevertheless, both donors maintained the same trend over time (Fig.3.21B).

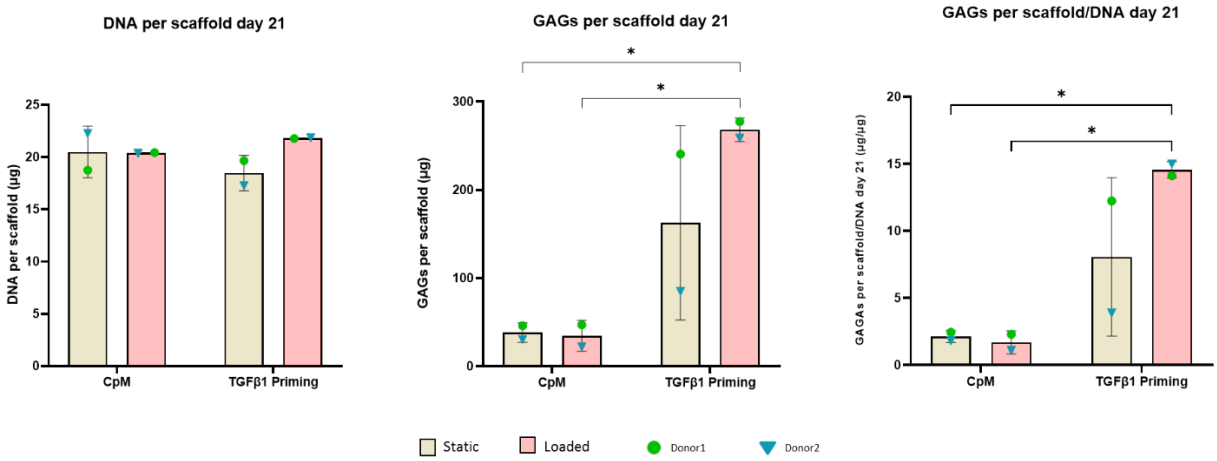

Figure 3.20. DNA assessment (A), GAGs produces (retained) (B), and GAGs normalised to the DNA (C), in GelMa/HA hydrogels seeded with hBM-MSCs from donor 1 and 2 after 21 days of culture and loading. Hydrogels were organised in 4 groups as previously described in materials & methods section. The samples were harvested after 21 days after loading and culture. All samples (that contained HA) were blanked with cell-free hydrogels in order to delete the background caused by HA already inside the hydrogels. Values represent mean ± SD of the two hBM-MSCs independent donors in experimental duplicated/triplicated. Statistical significance was defined as * $p < 0.05$

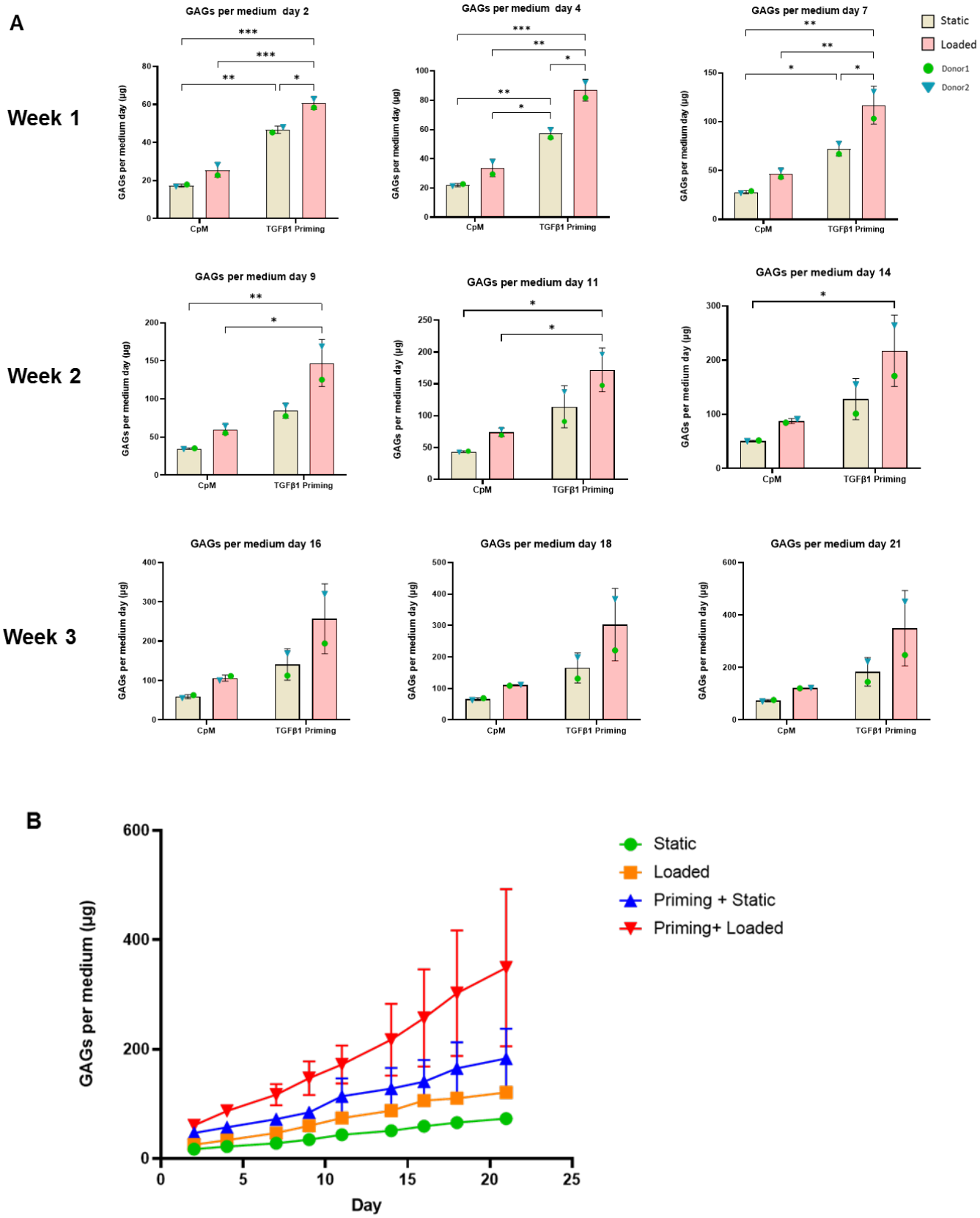

Figure 3.21. GAGs level produced and released into culture medium from GelMa/HA hydrogels seeded with hBM-MSCs from donor 1 and 2 over 21 days of culture and loading (A) and cumulative representation GAGs produces and released over time (B). Hydrogels were organised in 4 groups as previously described in materials & methods section. The medium was collected every medium change day. Values represent mean ± SD of the two hBM-MSCs independent donors in experimental triplicated. Statistical significance was defined as * $p< 0.05$, ** $p< 0.01$, *** $p<0.001$.

3.3.2.3 Histological analysis of GelMa/HA hydrogels

After 21 days of mechanical stimulation and culture, hydrogels were stained with H&E, in order to analyse the cell morphology and distribution inside the constructs. As shown in Fig. 3.22, both the static and loaded hydrogels without priming of both donors, exhibited similar cellular organisation. The cells were homogeneously distributed within the hydrogels, organised in small groups, in which it was possible to observe a scarce or absent deposit of extracellular matrix around the cells. Overall donor 2 showed a slightly higher number of cells but in both donors there was no difference between loaded and static hydrogels. However, the hydrogels subjected to one week of TGFβ1 priming, showed differentpeculiarities. Donor 1 with priming and loading showed evident chondrogenic differentiation, in which the high number of chondrocytes were located mainly in the upper part of the hydrogels, with a chondron-like organisation, where the cells were surrounded by a dense extracellular matrix. In the primed and static hydrogels of donor 1 instead it was possible to identify only a few groups of cells organised in a similar manner, but the number was considerably lower and located only in the hydrogels corners and the matrix surrounding the cells was more heterogeneous. The primed and loaded hydrogels of donor 2 also showed the same donor 1 cells organatation , but in smaller numbers. The matched static hydrogels showed a different cell morphology. The most number of cells were located in the hydrogels upper corners, where exhibited a flatted shape and embedded by a less dense and compact matrix (Fig.3.22).

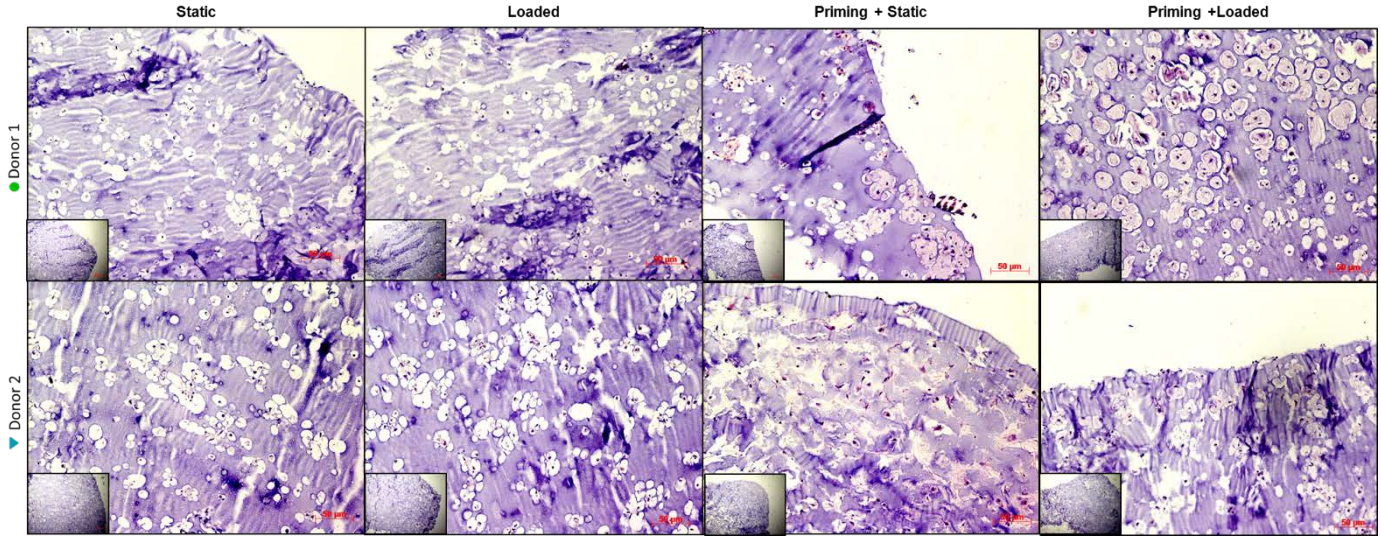

Figure 3.22. Histological assessment of GelMa/HA hydrogels seeded with hBM-MSCs from donor 1 and 2 after 21 days of culture and loading. Images showing longitudinal sections of hydrogels stained by haematoxylin and eosin (H&E) at magnification 10X. Insert: images showing the full sections at magnification of 2.5X. Scale bar: 50 µm.

In order to evaluate the deposition of sulphated GAGs after 21 days of culture and mechanical stimulation, hydrogels were stained with Safranin O counterstained with Fast green (Fig.3.23). The staining confirmed the histological assessment of H&E. Non-primed static hydrogels showed low positive stained compared with non-primed loaded hydrogel, where more red staining was observed, suggesting a more GAGs deposition inside the GelMa. However, no positive staining was observed in the scarce matrix surrounding the cells. Interestingly, a stronger positive staining was observed in the primed and loaded hydrogels of both donors where the chondron-like structure showed a very high GAGs deposition confirming that in this hydrogel areas, the chondrogenic differentiation of the hBM-MSCs was occurred (Fig.3.23). Diversely, the primed and static hydrogel of both donors showed very lower red staining compared with matched loaded hydrogel suggesting a lower levels of GAGs and a different matrix composition that surrounded the cells (Fig.3.23).

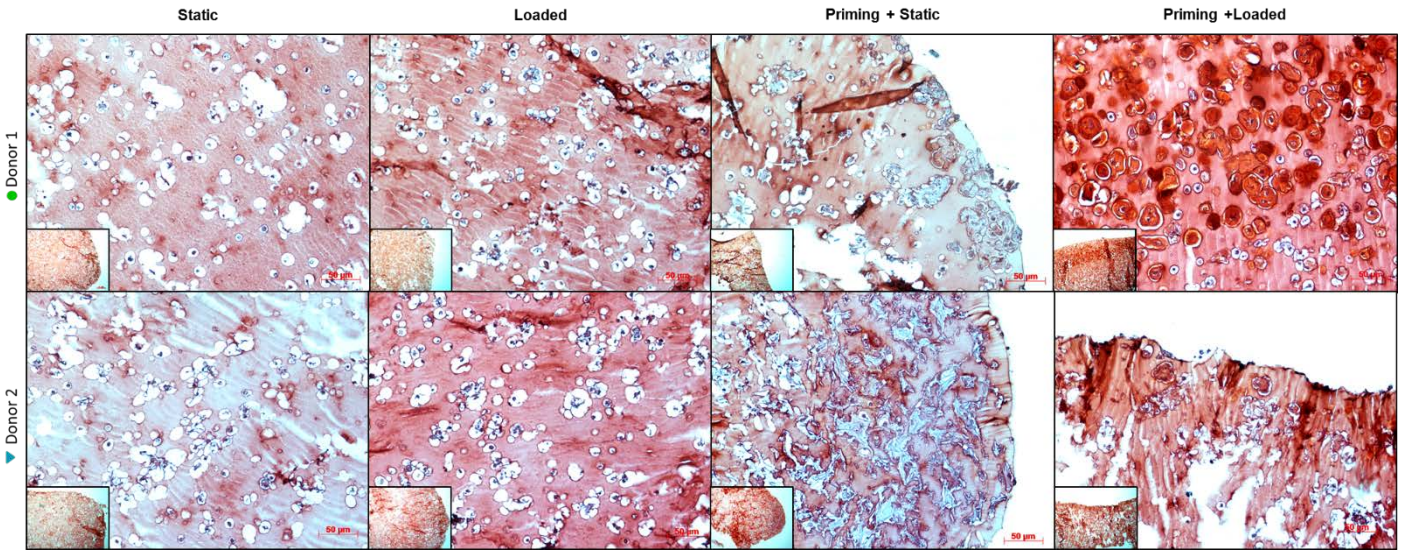

Figure 3.23. Histological evaluation of sulphated GAGs content by Safranin O counterstained with Fast green in GelMa/HA hydrogels seeded with hBM-MSCs from donor 1 and 2 after 21 days of culture and loading. Images showing longitudinal sections of hydrogels at magnification 10X. Insert: images showing the full sections at magnification of 2.5X. Scale bar: 50 µm.

3.3.2.4 Immunohistochemical Analysis of Aggrecan, Collagen II and Collagen X in GelMa/HA hydrogels

Finally, IHC was performed in the hydrogels sections, in order to investigate the deposition and distribution of the main chondrogenic markers such as aggrecan and collagen II, and Collagen X as hypertrophic marker. Unprimed static and loaded hydrogels of both donors showed low deposition of aggrecan, collagen II and collagen X located in the poor matrix surrounded the cells and no differences between static and loaded hydrogels were observed, although donor 2 showed more immunoreactivity compared to donor 1 (Fig.3.24-25). However, primed hydrogels displayed higher deposition of three markers compared to the non-primed hydrogels. The combination of TGFβ1 priming and loading led to high deposition of aggrecan, collagen II and Collage X in both donors, located in the chondron-like structure while a high immureactivity of collagen II were observed also in all hydrogels suggesting that a high production of collagen such as to be deposited also inside hydrogel matrix (Fig.3.24-25). Primed and static hydrogel showed a modest deposition of aggrecan, collagen II and Collagen X but only in the upper corners while few deposition, comparable to unprimed hydrogel were observed (Fig.3.24-25).

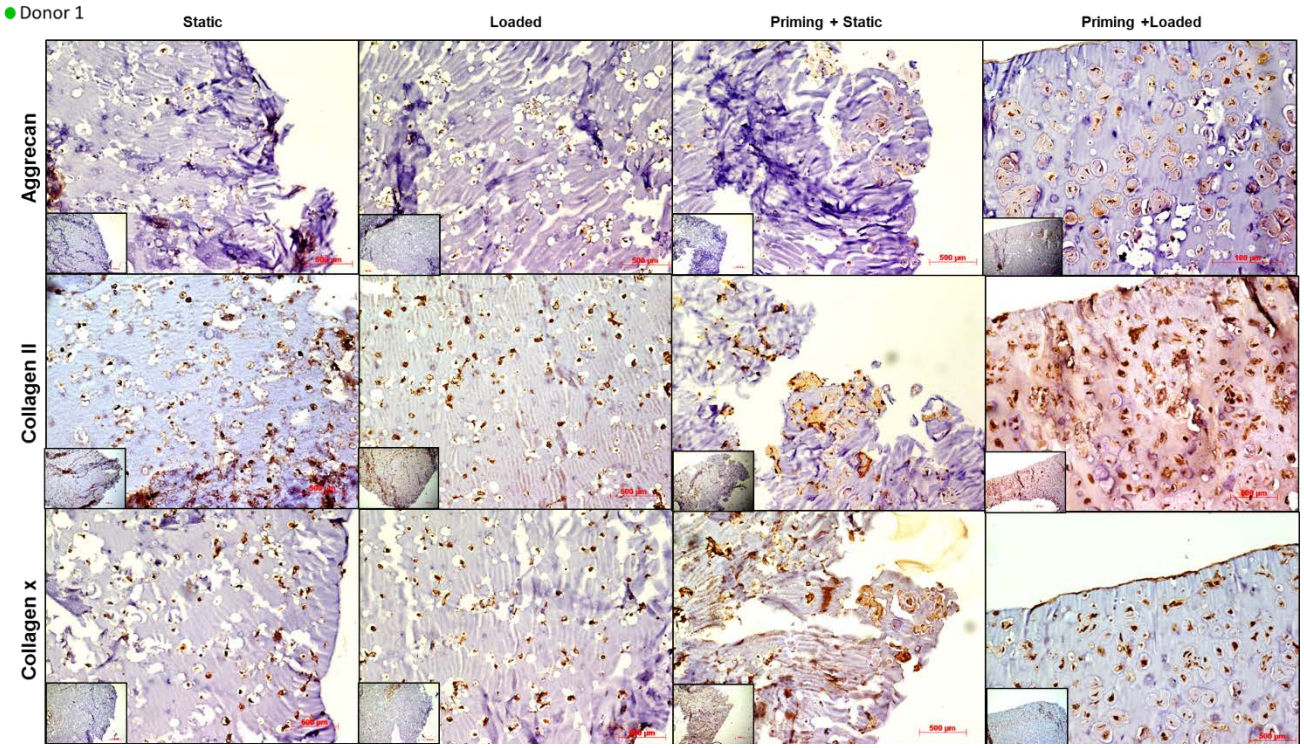

Figure 3.24. Immunohistochemical evaluation of Aggrecan, Collagen type II and Collagen type X in GelMa/HA hydrogels seeded with hBM-MSCs from donor 1 after 21 days of culture and loading. Images showing longitudinal sections of hydrogels at magnification 10X. Insert: images showing the full sections at magnification of 2.5X. Scale bar: 500 µm.

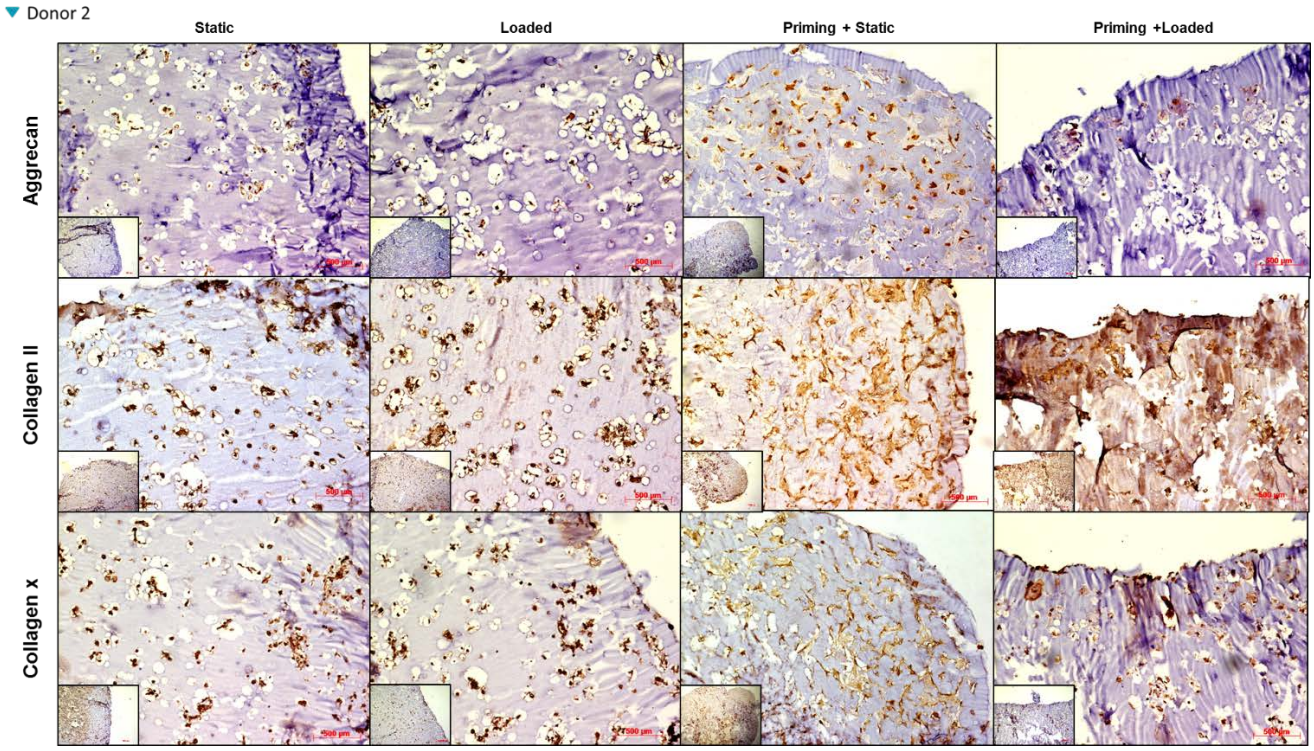

Figure 3.25 Immunohistochemical evaluation of Aggrecan, Collagen type II and Collagen type X in GelMa/HA hydrogels seeded with hBM-MSCs from donor 2 after 21 days of culture and loading. Images showing longitudinal sections of hydrogels at magnification 10X. Insert: images showing the full sections at magnification of 2.5X. Scale bar: 500 µm

3.4 Discussion and Conclusions

The aim of this preliminary study was to investigate the in vitro chondrogenic differentiation of primary hBM-MSCs from two different donors by using two different 3D culture models, and their capability to form new cartilagineous tissue.

In the first part of the study the analysis was carried out in pellet cultures, which represents the gold standard method and the simplest one, to study the chondrogenesis of progenitor cells in vitro since 1990s (Johnstone et al., 1998). In this model BM-MSCs are pelleted and cultured with a condition medium supplemented with one of TGFβ isoforms. Pelleted BMSCs are a logical starting point into the chondrogenic differentiation process, since during development MSCs condensation is an essential step for cartilage formation (Hall et al., 1995). In vitro, TGFβ1 promotes BMSC differentiation in part through the indirect downregulation of N-cadherin, causing relaxation of cytoskeletal tension, leading to reduced RhoA/ROCK signalling and upregulation of chondrogenic signalling such as SMAD2/3 – dependent pathway (Tuli et al., 2003). After an extended TGFβ1 exposure (2-5 weeks), pellets show big size with a cartilage-like ECM rich in collagen II, aggrecan and GAGs content (Futrega et al., 2015). However, the advantage of TGFβ1 use also hides the biggest limitation of this in vitro model. In fact, the extensive TGFβ1 exposure, leads to the activation of the signals that regulate the hypertrophic condition, including the SMAD1/5/9 -dependent pathway. Therefore, in the end, the obtained pellets show an ECM that is also characterised by the presence of collagen X and other markers of hypertrophy, with characteristics more similar to fibrocartilage ECM and different from the native articular cartilage (Mueller and Tuan, 2008; Narcisi et al., 2015; Occhetta et al., 2018).

In this first experimental part, however, it was intended to use pellets to evaluate the chondrogenic differentiation capacity of the primary hBM-MSCs used in this study, and if the cells from two different donors responded in the same way to TGFβ1. To achieve this, the pellets were cultured for three weeks divided in three different experimental groups: without TGFβ1, subjected to a single week and to continuous exposure of TGFβ1 for three weeks. On the whole, the results obtained were in line and consistent with the results currently existent in the literature. In fact, the pellets exposed to TGFβ1 for 21 days showed bigger sizes than the other two groups of pellets and a uniformly distributed ECM rich in GAGs, as evidenced by histological analyses. Gene expression analysis confirmed that continuous TGFβ1 exposure has led to upregulation of both chondrogenesis (*SOX9*, *COL2A1*, and *ACAN*) and hypertrophic (*COL10A1*, *COL1A1* and *MMP13*) markers and these results were also confirmed by IHC analysis. On the other hand, pellets, cultured without TGFβ1 supplementation, demonstrated a very low differentiation condition, characterised by small sizes, low

presence of GAGs and low levels of gene expression of both chondrogenic and hypertrophic markers. However, pellets exposed to the TGFβ1 only during the first week of culture, showed a trend which was places in the middle between the other two conditions. In fact, with only one week of TGFβ1 supplementation, differentiation processes is increased, but from when the TGFβ1supplementation was suspended, the differentiation appears to stop. This is easily understood by comparing the expression levels of the chondrogenic and hypertrophic markers of these pellets, with the gene expression of the same markers at day 7 of the pellets exposed to TGFβ1 continuously for three weeks, as they appear to not have significant differences. Finally, histological analysis highlighted a low GAGs content and a heterogeneous ECM which underlines a differentiation process incomplete without TGFβ1.

Overall, this first group of results demonstrates that hBM-MSCs pelleted from two different donor differentiate in chondrogenic sense only in presence of TGFβ1. However, in this in vitro model, chondrogenesis is accompanied by an elevated expression of hypertrophic markers

Pellet culture also in this preliminary study represented a valid in vitro model to evaluate the chondrogenic potential of MSCs.

In the second part of this study, was developed a more complex in vitro model based on current knowledge of tissue engineering by combining use of 3D scaffolds, mechanical stimulation and growth factors, with the aim of improving the quality of hBM- MSCs chondrogenic differentiation and trying to limit hypertrophy with the consequence to obtain an ECM with characteristics more similar to articular cartilage.

It was chosen to encapsulate the hBM- MSCs in hydrogels consisting of GelMA and HA, as based on various recent studies, it appears to be an optimal combination of natural biopolymers due to its excellent biocompatibility, biological and mechanical properties that are able to promote vitality, proliferation and cell differentiation. In static cultures for example, human chondrocytes inside GelMA/HA maintain stable their phenotype and produce abundant cartilage-like ECM (Levett et al., 2014b; Nedunchezian et al., 2022), while MSCs and iPCs are able to differentiate into chondrogenic sense, and produce ECM rich in GAGs and collagen II, with or without growth factors pre-incubation (Levett et al., 2014; Meinert et al., 2017; Agten et al., 2022). In addition, after 3-4 weeks of culture, GelMA/HA hydrogels show mechanical properties, such as compressive strength, similar that of native articular cartilage suggesting the potential application of in vitro mechanical stimuli, by using bioreactor system, on this kind of construct in order to improve hBM- MSCs chondrogenesis (Levett et al., 2014b; Pahoff et al., 2019). To date only Meinet and collegues demonstrated that human articular chondrocytes encapsulated in GelMA and hyaluronic acid methacrylate (HAMA) hydrogels were able to respond to uni- and biaxial mechanical stimuli by upregulation of hyaline cartilage-

specific marker genes (Meinet et al., 2017). Therefore, on the basis of these evidences one of the objectives of this study was to investigate if multiaxial loading applied on GelMA/HA hydrogels, is able to induce hBM- MSCs chondrogenesis in the absence of any exogenous growth factors, as widely demonstrate in fibrin- PU scaffolds (Wimmer at al., 2004; Schätti et al., 2011; Zahedmanesh et al., 2014; Gardner et al., 2017; Ladner et al., 2022). The hydrogels were exposed to multiaxial loading 1h per day for three weeks. To evaluate mechanical stimulation effects, analysis of the gene expression at each time point, quantification of the GAGs and histological analysis were performed, and each result obtained was compared with matched static group of hydrogels. From the analysis carried out it emerged that the hBM- MSCs of both donors were not able to respond to the mechanical stimulation with chondrogenic differentiation. This is demonstrated by the very strong results obtained in which all analysed genes both chondrogenic and hypertrophic markers showed low expression levels. GelMA/HA hydrogels also showed a low production of GAGs as evidenced by quantification at each medium change after loading, and by the GAGAs quantified within the scaffolds after three weeks of loading. All these evidences were also confirmed by the histological and Immunohistochemical analysis in which it is possible to notice that the cells produced poor ECM after three weeks of loading and no significant differences were observed compared to the hydrogels maintained in static conditions. Overall all these data are consistent with the fact that the only mechanical stimulation applied in these constructs is not able to activate the chondrogenic differentiation, but the exact reasons why hBM- MSCs in this type of construct do not respond to mechanical stimulation remain unknown in this preliminary results. Therefore, it was considered to introduce TGFβ1 as chondrogenic stimulating factor in support of mechanical stimulation. It was hypothesised that a TGFβ1priming was able to give an extra stimulus to the hBM- MSCs in order to direct their differentiation in a chondrogenic direction before applying the multiaxial loading. The idea of priming comes from a recent study by McDermott et al., in which are investigated the effects of chondrogenic priming duration on the response of engineered constructs to dynamic mechanical compression (McDermott et al., 2021). Specifically, they chondrogenically (pre-incubation with TGFβ3) primed fibrin hydrogel-encapsulated hBM-MSCs to various stages of chondrogenic maturation (0, 2, 4, or 6 weeks of priming) prior to applying dynamic compression for two additional weeks. Their results showed that after two-weeks of priming, compression supports chondrogenesis for the duration of mechanical stimulation by increasing the expression of chondrogenic markers (McDermott et al., 2021). On the basis of these results, in this study we wanted to investigate the effects of priming in this case with TGFβ1one week on GelMA/HA hydrogels prior to apply three weeks of multiaxial loading. It was selected only one week of priming based also on the results obtained in the first part with pellets, in which one week of exposure to TGFβ1was able to activate

chondrogenesis even if the differentiation process stops once the growth factor is not added. Instead in this in vitro model it was hypothesised that after the priming week, the multiaxial loading could be able to carry out the differentiation process.

The data obtained strongly demonstrated that the hBM-MSCs of both donors encapsulated inside GelMA/HA hydrogels primed with TGFβ1b were able to respond to mechanical stimulation with chondrogenic differentiation. Hydrogels subjected to priming and loading showed increased expression levels of *SOX9*, *COL2A1*, and *ACAN* (with expression peaks reached at different timepoints) compared to the other experimental groups. The combined application of the two stimuli also promoted the increase GAGs production both within the hydrogels and released in the culture medium. Interesting results were also obtained from histological analyses in which the groups subjected to priming and loading the hBM-MSCs differentiate showed a chondron-like organisation uniformly distributed inside hydrogel, in which the differentiated cells are surrounded by an intense ECM. Safranin O staining confirmed a high deposition of GAGs inside these areas. IHC also showed high levels of aggrecan and collagen II in these sites. In contrast, the cells inside GelMA/HA hydrogels primed and kept in static conditions t produced an ECM not uniformly distributed and was mainly concentrated at the hydrogel corners. This suggests that most probably the multiaxial loading as it occurs in the native cartilage, promote s the diffusion of nutrients and oxygen inside the matrix and facilitate the cellular organisation and the ECM remodelling inside the hydrogels. Other interesting results obtained are related to hypertrophic markers.

Hydrogels subjected to TGFβ1 priming, as expected, also showed increased expression levels of hypertrophic factors (*COL10A*, *COL1A1* and *MMP13*) but interestingly no expression differences were found between the loaded scaffolds and statistics on (except COL1A1at day 21 for donor 1which was higher in loaded group, and MMP13 at day 21 for donor 2, which was lower in loaded group). From these results it can be deduced that multiaxial loading did not activate hypertrophy differentiation despite the multiaxial loading stimulate chondrogenic differentiation of hBM-MSCs by activating the TGFβ1 pathway (Li et al., 2010). This evidences also confirmed by the collagen X IHC in which the levels of collagen X detected were lower than in collagen II. probably the levels of hypertrophy are kept lower thanks to the presence of HA which, as previously demonstrated, the addition of HA in fibrin -PU scaffold subjected to multiaxial load is able to stabilise the BM-MSCs derived chondrocyte phenotype through the reduced upregulation of collagen X (Monaco et al., 2020; Monaco et al.; 2021).

In conclusion, the second part of this preliminary study demonstrated that the hBM-MSCs seeded in GelMA/HA hydrogels are able to differentiate in chondrogenic sense thanks to the combination of one week of TGFβ1 priming and three weeks of multiaxial loading. This combination of stimuli

together with the use of GelMA and HA as hydrogels components, proves to be an optimal in vitro model for hBM-MSCs chondrogenesis. Another important results are related to hypertrophic differentiation that seems to be limited and no activated by mechanical stimulation. However, several questions remain to be addressed such as why the hBM-MSCs were unable to respond to the mechanical loading only after a TGFβ1 priming. Future analysis will be performed to investigate in depth this phenomenon. In addition, the analysis will be extended with other hBM-MSCs from other donors in order to evaluate and improve reproducibility and will be also investigate if by reducing TGFβ1 priming time and increasing HA concentration, a more hypertrophy reduction can be achieved.

3.5 References

Agten H, Van Hoven I, Viseu SR, Van Hoorick J, Van Vlierberghe S, Luyten FP, Bloemen V. In vitro and in vivo evaluation of 3D constructs engineered with human iPSC-derived chondrocytes in gelatin methacryloyl hydrogel. Biotechnol Bioeng. 2022 Oct;119(10):2950-2963. doi: 10.1002/bit.28168. Epub 2022 Jul 9. PMID: 35781799.

Barry F, Boynton RE, Liu B, Murphy JM. Chondrogenic differentiation of mesenchymal stem cells from bone marrow: differentiation-dependent gene expression of matrix components. Exp Cell Res. 2001 Aug 15;268(2):189-200. doi: 10.1006/excr.2001.5278. PMID: 11478845.

Brittberg M. Cell carriers as the next generation of cell therapy for cartilage repair: a review of the matrix-induced autologous chondrocyte implantation procedure. Am J Sports Med. 2010 Jun;38(6):1259-71. doi: 10.1177/0363546509346395. Epub 2009 Dec 4. PMID: 19966108.

Callahan LA, Ganios AM, McBurney DL, Dilisio MF, Weiner SD, Horton WE Jr, Becker ML. ECM production of primary human and bovine chondrocytes in hybrid PEG hydrogels containing type I collagen and hyaluronic acid. Biomacromolecules. 2012 May 14;13(5):1625-31. doi: 10.1021/bm3003336. Epub 2012 May 4. PMID: 22559049

De Bari C, Roelofs AJ. Stem cell-based therapeutic strategies for cartilage defects and osteoarthritis. Curr Opin Pharmacol. 2018 Jun;40:74-80. doi: 10.1016/j.coph.2018.03.009. Epub 2018 Apr 3. PMID: 29625333.

Delaine-Smith RM, Reilly GC. Mesenchymal stem cell responses to mechanical stimuli. Muscles Ligaments Tendons J. 2012 Oct 16;2(3):169-80. PMID: 23738294

Ding X, Gao J, Yu X, Shi J, Chen J, Yu L, Chen S, Ding J. 3D-Printed Porous Scaffolds of Hydrogels Modified with TGF-β1 Binding Peptides to Promote *In Vivo* Cartilage Regeneration and Animal Gait Restoration. ACS Appl Mater Interfaces. 2022 Apr 13;14(14):15982-15995. doi: 10.1021/acsami.2c00761. Epub 2022 Apr 1. PMID: 35363484.

Erggelet C, Sittinger M, Lahm A. The arthroscopic implantation of autologous chondrocytes for the treatment of full-thickness cartilage defects of the knee joint. Arthroscopy. 2003 Jan;19(1):108-10. doi: 10.1053/jars.2003.50025. PMID: 12522411.

Farndale RW, Buttle DJ, Barrett AJ. Improved quantitation and discrimination of sulphated glycosaminoglycans by use of dimethylmethylene blue. Biochim Biophys Acta. 1986 Sep 4;883(2):173-7. doi: 10.1016/0304-4165(86)90306-5.

Freyria AM, Mallein-Gerin F. Chondrocytes or adult stem cells for cartilage repair: the indisputable role of growth factors. Injury. 2012 Mar;43(3):259-65. doi: 10.1016/j.injury.2011.05.035. Epub 2011 Jun 21. PMID: 21696723.

Futrega K, Palmer JS, Kinney M, Lott WB, Ungrin MD, Zandstra PW, Doran MR. The microwell-mesh: A novel device and protocol for the high throughput manufacturing of cartilage microtissues. Biomaterials. 2015 Sep;62:1-12. doi: 10.1016/j.biomaterials.2015.05.013. Epub 2015 May 20. PMID: 26010218.

Futrega K, Robey PG, Klein TJ, Crawford RW, Doran MR. A single day of TGF-β1 exposure activates chondrogenic and hypertrophic differentiation pathways in bone marrow-derived stromal cells. Commun Biol. 2021 Jan 4;4(1):29. doi: 10.1038/s42003-020-01520-0. PMID: 33398032

Gardner OF, Archer CW, Alini M, Stoddart MJ. Chondrogenesis of mesenchymal stem cells for cartilage tissue engineering. Histol Histopathol. 2013 Jan;28(1):23-42. doi: 10.14670/HH-28.23. PMID: 23233057.

Gardner OFW, Musumeci G, Neumann AJ, Eglin D, Archer CW, Alini M, Stoddart MJ. Asymmetrical seeding of MSCs into fibrin-poly(ester-urethane) scaffolds and its effect on mechanically induced chondrogenesis. J Tissue Eng Regen Med. 2017 Oct;11(10):2912-2921. doi: 10.1002/term.2194. Epub 2016 Jul 13.

Goldberg A, Mitchell K, Soans J, Kim L, Zaidi R. The use of mesenchymal stem cells for cartilage repair and regeneration: a systematic review. J Orthop Surg Res. 2017 Mar 9;12(1):39. doi: 10.1186/s13018-017-0534-y. PMID: 28279182.

Grad S, Eglin D, Alini M, Stoddart MJ. Physical stimulation of chondrogenic cells in vitro: a review. Clin Orthop Relat Res. 2011 Oct;469(10):2764-72. doi: 10.1007/s11999-011-1819-9. PMID: 21344272.

Hall BK, Miyake T. Divide, accumulate, differentiate: cell condensation in skeletal development revisited. Int J Dev Biol. 1995 Dec;39(6):881-93. PMID: 8901191.

Hasler J, Hatt LP, Stoddart MJ, Armiento AR. Stable Reference Genes for qPCR Analysis in BM-MSCs Undergoing Osteogenic Differentiation within 3D Hyaluronan-Based Hydrogels. Int J Mol Sci. 2020 Dec 2;21(23):9195. doi: 10.3390/ijms21239195.

Hölzl K, Fürsatz M, Göcerler H, Schädl B, Žigon-Branc S, Markovic M, Gahleitner C, Hoorick JV, Van Vlierberghe S, Kleiner A, Baudis S, Pauschitz A, Redl H, Ovsianikov A, Nürnberger S. Gelatin methacryloyl as environment for chondrocytes and cell delivery to superficial cartilage defects. J Tissue Eng Regen Med. 2022 Feb;16(2):207-222. doi: 10.1002/term.3273. Epub 2021 Dec 15. PMID: 34861104;

Huang B, Li P, Chen M, Peng L, Luo X, Tian G, Wang H, Wu L, Tian Q, Li H, Yang Y, Jiang S, Yang Z, Zha K, Sui X, Liu S, Guo Q. Hydrogel composite scaffolds achieve recruitment and chondrogenesis in cartilage tissue engineering applications. J Nanobiotechnology. 2022 Jan 6;20(1):25. doi: 10.1186/s12951-021-01230-7. PMID: 34991615;

Jakobsen RB, Østrup E, Zhang X, Mikkelsen TS, Brinchmann JE. Analysis of the effects of five factors relevant to in vitro chondrogenesis of human mesenchymal stem cells using factorial design and high throughput mRNA-profiling. PLoS One. 2014 May 9;9(5):e96615. doi: 10.1371/journal.pone.0096615. PMID: 24816923

Johnstone B, Hering TM, Caplan AI, Goldberg VM, Yoo JU. In vitro chondrogenesis of bone marrow-derived mesenchymal progenitor cells. Exp Cell Res. 1998 Jan 10;238(1):265-72. doi: 10.1006/excr.1997.3858. PMID: 9457080.

Labarca C, Paigen K. A simple, rapid, and sensitive DNA assay procedure. Anal Biochem. 1980 Mar 1;102(2):344-52. doi: 10.1016/0003-2697(80)90165-7.

Ladner YD, Armiento AR, Kubosch EJ, Snedeker JG, Stoddart MJ. Optimization of loading protocols for tissue engineering experiments. Sci Rep. 2022 Mar 24;12(1):5094. doi: 10.1038/s41598-022-08849-y.

Levato R, Webb WR, Otto IA, Mensinga A, Zhang Y, van Rijen M, van Weeren R, Khan IM, Malda J. The bio in the ink: cartilage regeneration with bioprintable hydrogels and articular cartilage-derived progenitor cells. Acta Biomater. 2017 Oct 1;61:41-53. doi: 10.1016/j.actbio.2017.08.005. Epub 2017 Aug 4. PMID: 287827.

Levett PA, Hutmacher DW, Malda J, Klein TJ. Hyaluronic acid enhances the mechanical properties of tissue-engineered cartilage constructs. PLoS One. 2014 Dec 1;9(12):e113216. doi: 10.1371/journal.pone.0113216. PMID: 25438040.

Levett PA, Melchels FP, Schrobback K, Hutmacher DW, Malda J, Klein TJ. A biomimetic extracellular matrix for cartilage tissue engineering centered on photocurable gelatin, hyaluronic acid and chondroitin sulfate. Acta Biomater. 2014 Jan;10(1):214-23. doi: 10.1016/j.actbio.2013.10.005. Epub 2013 Oct 16. PMID: 24140603.

Li Z, Kupcsik L, Yao SJ, Alini M, Stoddart MJ. Mechanical load modulates chondrogenesis of human mesenchymal stem cells through the TGF-beta pathway. J Cell Mol Med. 2010 Jun;14(6A):1338-46. doi: 10.1111/j.1582-4934.2009.00780.x. Epub 2009 May 11. PMID: 19432813.

Makris EA, Gomoll AH, Malizos KN, Hu JC, Athanasiou KA. Repair and tissue engineering techniques for articular cartilage. Nat Rev Rheumatol. 2015 Jan;11(1):21-34. doi: 10.1038/nrrheum.2014.157. Epub 2014 Sep 23. PMID: 25247412.

McDermott AM, Eastburn EA, Kelly DJ, Boerckel JD. Effects of chondrogenic priming duration on mechanoregulation of engineered cartilage. J Biomech. 2021 Aug 26;125:110580. doi: 10.1016/j.jbiomech.2021.110580. Epub 2021 Jun 17. PMID: 34198021.

Meinert C, Schrobback K, Hutmacher DW, Klein TJ. A novel bioreactor system for biaxial mechanical loading enhances the properties of tissue-engineered human cartilage. Sci Rep. 2017 Dec 5;7(1):16997. doi: 10.1038/s41598-017-16523-x. PMID: 29208903.

Monaco G, El Haj AJ, Alini M, Stoddart MJ. Sodium hyaluronate supplemented culture medium combined with joint-simulating mechanical loading improves chondrogenic differentiation of human mesenchymal stem cells. Eur Cell Mater. 2021 Jun 6;41:616-632. doi: 10.22203/eCM.v041a40. PMID: 34091884.

Monaco G, El Haj AJ, Alini M, Stoddart MJ. Sodium Hyaluronate Supplemented Culture Media as a New hMSC Chondrogenic Differentiation Media-Model for in vitro/ex vivo Screening of Potential Cartilage Repair Therapies. Front Bioeng Biotechnol. 2020 Mar 31;8:243. doi: 10.3389/fbioe.2020.00243. PMID: 32296689.

Mouser VHM, Dautzenberg NMM, Levato R, van Rijen MHP, Dhert WJA, Malda J, Gawlitta D. Ex vivo model unravelling cell distribution effect in hydrogels for cartilage repair. ALTEX. 2018;35(1):65-76. doi: 10.14573/altex.1704171. Epub 2017 Sep 8. PMID: 28884783.

Mueller MB, Tuan RS. Functional characterization of hypertrophy in chondrogenesis of human mesenchymal stem cells. Arthritis Rheum. 2008 May;58(5):1377-88. doi: 10.1002/art.23370. PMID: 18438858.

Narcisi R, Cleary MA, Brama PA, Hoogduijn MJ, Tüysüz N, ten Berge D, van Osch GJ. Long-term expansion, enhanced chondrogenic potential, and suppression of endochondral ossification of adult human MSCs via WNT signaling

modulation. Stem Cell Reports. 2015 Mar 10;4(3):459-72. doi: 10.1016/j.stemcr.2015.01.017. Epub 2015 Feb 26. PMID: 25733021.

Nedunchezian S, Wu CW, Wu SC, Chen CH, Chang JK, Wang CK. Characteristic and Chondrogenic Differentiation Analysis of Hybrid Hydrogels Comprised of Hyaluronic Acid Methacryloyl (HAMA), Gelatin Methacryloyl (GelMA), and the Acrylate-Functionalized Nano-Silica Crosslinker. Polymers (Basel). 2022 May 13;14(10):2003. doi: 10.3390/polym14102003. PMID: 35631885

Occhetta P, Pigeot S, Rasponi M, Dasen B, Mehrkens A, Ullrich T, Kramer I, Guth-Gundel S, Barbero A, Martin I. Developmentally inspired programming of adult human mesenchymal stromal cells toward stable chondrogenesis. Proc Natl Acad Sci U S A. 2018 May 1;115(18):4625-4630. doi: 10.1073/pnas.1720658115. Epub 2018 Apr 16. PMID: 29666250.

Pahoff S, Meinert C, Bas O, Nguyen L, Klein TJ, Hutmacher DW. Effect of gelatin source and photoinitiator type on chondrocyte redifferentiation in gelatin methacryloyl-based tissue-engineered cartilage constructs. J Mater Chem B. 2019 Mar 14;7(10):1761-1772. doi: 10.1039/c8tb02607f. Epub 2019 Jan 8. PMID: 32254918.

Pittenger MF, Mackay AM, Beck SC, Jaiswal RK, Douglas R, Mosca JD, Moorman MA, Simonetti DW, Craig S, Marshak DR. Multilineage potential of adult human mesenchymal stem cells. Science. 1999 Apr 2;284(5411):143-7. doi: 10.1126/science.284.5411.143. PMID: 10102814.

Puetzer JL, Petitte JN, Loboa EG. Comparative review of growth factors for induction of three-dimensional in vitro chondrogenesis in human mesenchymal stem cells isolated from bone marrow and adipose tissue. Tissue Eng Part B Rev. 2010 Aug;16(4):435-44. doi: 10.1089/ten.TEB.2009.0705. PMID: 20196646.

Qiao Z, Lian M, Han Y, Sun B, Zhang X, Jiang W, Li H, Hao Y, Dai K. Bioinspired stratified electrowritten fiber-reinforced hydrogel constructs with layer-specific induction capacity for functional osteochondral regeneration. Biomaterials. 2021 Jan;266:120385. doi: 10.1016/j.biomaterials.2020.120385. Epub 2020 Oct 17. PMID: 33120203.

Safiri S, Kolahi AA, Smith E, Hill C, Bettampadi D, Mansournia MA, Hoy D, Ashrafi-Asgarabad A, Sepidarkish M, Almasi-Hashiani A, Collins G, Kaufman J, Qorbani M, Moradi-Lakeh M, Woolf AD, Guillemin F, March L, Cross M. Global, regional and national burden of osteoarthritis 1990-2017: a systematic analysis of the Global Burden of Disease Study 2017. Ann Rheum Dis. 2020 Jun;79(6):819-828. doi: 10.1136/annrheumdis-2019-216515. Epub 2020 May 12. PMID: 32398285.

Schätti O, Grad S, Goldhahn J, Salzmann G, Li Z, Alini M, Stoddart MJ. A combination of shear and dynamic compression leads to mechanically induced chondrogenesis of human mesenchymal stem cells. Eur Cell Mater. 2011 Oct 11;22:214-25. doi: 10.22203/ecm.v022a17.

Somoza RA, Welter JF, Correa D, Caplan AI. Chondrogenic differentiation of mesenchymal stem cells: challenges and unfulfilled expectations. Tissue Eng Part B Rev. 2014 Dec;20(6):596-608. doi: 10.1089/ten.TEB.2013.0771. Epub 2014 May 27. PMID: 24749845.

Tuli R, Tuli S, Nandi S, Huang X, Manner PA, Hozack WJ, Danielson KG, Hall DJ, Tuan RS. Transforming growth factor-beta-mediated chondrogenesis of human mesenchymal progenitor cells involves N-cadherin and mitogen-activated protein kinase and Wnt signaling cross-talk. J Biol Chem. 2003 Oct 17;278(42):41227-36. doi: 10.1074/jbc.M305312200. Epub 2003 Jul 31. PMID: 12893825.

Van Den Bulcke AI, Bogdanov B, De Rooze N, Schacht EH, Cornelissen M, Berghmans H. Structural and rheological properties of methacrylamide modified gelatin hydrogels. Biomacromolecules. 2000 Spring;1(1):31-8. doi: 10.1021/bm990017d. PMID: 11709840.

Van Hoorick J, Gruber P, Markovic M, Tromayer M, Van Erps J, Thienpont H, Liska R, Ovsianikov A, Dubruel P, Van Vlierberghe S. Cross-Linkable Gelatins with Superior Mechanical Properties Through Carboxylic Acid Modification: Increasing the Two-Photon Polymerization Potential. Biomacromolecules. 2017 Oct 9;18(10):3260-3272. doi: 10.1021/acs.biomac.7b00905. Epub 2017 Sep 15. PMID: 28850786

Wei F, Zhou J, Wei X, Zhang J, Fleming BC, Terek R, Pei M, Chen Q, Liu T, Wei L. 2012. Activation of Indian hedgehog promotes chondrocyte hypertrophy and upregulation of MMP-13 in human osteoarthritic cartilage. Osteoarthritis Cartilage 20(7):755-763.

Wimmer MA, Grad S, Kaup T, Hänni M, Schneider E, Gogolewski S, Alini M. Tribology approach to the engineering and study of articular cartilage. Tissue Eng. 2004 Sep-Oct;10(9-10):1436-45. doi: 10.1089/ten.2004.10.1436.

Yue K, Trujillo-de Santiago G, Alvarez MM, Tamayol A, Annabi N, Khademhosseini A. Synthesis, properties, and biomedical applications of gelatin methacryloyl (GelMA) hydrogels. Biomaterials. 2015 Dec; 73:254-71. doi: 10.1016/j.biomaterials.2015.08.045. Epub 2015 Aug 28. PMID: 26414409

Zahedmanesh H, Stoddart M, Lezuo P, Forkmann C, Wimmmer MA, Alini M, Van Oosterwyck H. Deciphering mechanical regulation of chondrogenesis in fibrin-polyurethane composite scaffolds enriched with human mesenchymal stem cells: a dual computational and experimental approach. Tissue Eng Part A. 2014 Apr;20(7-8):1197-212. doi: 10.1089/ten.TEA.2013.0145. Epub 2014 Jan 11.

Zhu J, Marchant RE. Design properties of hydrogel tissue-engineering scaffolds. Expert Rev Med Devices. 2011 Sep;8(5):607-26. doi: 10.1586/erd.11.27. PMID: 22026626;

4 Evaluation of a Cell-Free Collagen Type I-Based Scaffold for Articular Cartilage Regeneration in an Orthotopic Rat Model

Marta Anna Szychlinska[1,†], Giovanna Calabrese[2,†], Silvia Ravalli[1], Anna Dolcimascolo[2], Paola Castrogiovanni[1], Claudia Fabbi[3], Caterina Puglisi[4], Giovanni Lauretta[1], Michelino Di Rosa[1], Alessandro Castorina[5,6], Rosalba Parenti[2] and Giuseppe Musumeci[1,7,8,]*

[1]Department of Biomedical and Biotechnological Sciences, Anatomy, Histology and Movement Sciences Section, School of Medicine, University of Catania, 95123 Catania, Italy;

[2]Department of Biomedical and Biotechnological Sciences, Physiology Section, School of Medicine, University of Catania, 95123 Catania, Italy;

[3]Fin-Ceramica Faenza, 48018 Faenza, Italy;

[4]Istituto Oncologico del Mediterraneo (IOM), 95029 Viagrande, 95123 Catania, Italy;

[5]School of Life Science, Faculty of Science, University of Technology Sydney, Sydney, NSW 123, Australia;

[6]Discipline of Anatomy & Histology, School of Medical Sciences, The University of Sydney, Sydney, NSW 123, Australia

[7]Research Center on Motor Activities (CRAM), University of Catania, 95123 Catania, Italy

[8]Department of Biology, Sbarro Institute for Cancer Research and Molecular Medicine, College of Science and Technology, Temple University, Philadelphia, PA 19122, USA

Correspondence: g.musumeci@unict.it; Tel.: +095-378-2036

[†]These authors have contributed equally to this work.

Materials 2020, 13(10), 2369; DOI: 10.3390/ma13102369

4.1 Introduction

The repair and healing capacity of articular cartilage after injury is complicated due to its avascular, hypo-cellular and aneural nature [1]. For this reason, even a minor lesion may lead to progressive damage and cartilage degeneration, determining osteoarthritis (OA) development. OA is a common progressively degenerative disease involving primarily articular cartilage and further all joint tissues and leading to severe pain and joint disability [2,3]. Several therapeutic approaches have been developed for the treatment of articular cartilage defects, including autografts and osteochondral allografts, microfracture, autologous chondrocyte and mesenchymal stem cell-based therapies [4,5]. However, the results reported in this field showed limited satisfactory results and the management of chondral defects remains a big challenge. This is mostly due to the biochemical and mechanical properties of the obtained engineered cartilage, which often do not match those of the native tissue [6].

Tissue engineering for regenerative approaches emerges as one of the most promising biomedical applications for cartilage tissue regeneration. The latter is based on the use of innovative biomaterials, which act as scaffolds, mimicking a three-dimensional (3D) extracellular matrix (ECM) microenvironment, with or without the use of chondrocytes or mesenchymal stem cells from different sources [7–10]. Over the past decades, several advances in this field have arisen, based on the innovative techniques used for biomaterial characterization, design and functionalization [11,12].

The biomaterials used in cartilage engineering approaches should provide mechanical support, shape, and cell-scale architecture for neo-tissue formation as cells expand and organize. In addition to defining the 3D architecture for the neo-tissue, the scaffold provides the microenvironment (synthetic temporary ECM) for regenerative cell recruitment, support, proliferation, differentiation and, finally, neo-tissue formation [13]. The most commonly used degradable biomaterials nowadays include some synthetic polyesters such as poly(l-glycolic acid) (PLGA) and poly(l-lactic acid) (PLLA) and natural biopolymers such as collagen, alginate, fibrin and chitosan [14,15]. The natural polymers show better biological properties that are more suitable for the native cartilage microenvironment, promoting required biocompatibility, cellular responses and biodegradability [16]. Among them, collagen type I is widely used for scaffold construction and cartilage tissue engineering approaches, due to its high biocompatibility and widespread clinical usage [17–20]. Although there are many scaffolds based on collagen, its long-term performance still shows an inferior mechanical property and limited chondrogenic capacity. For this reason, improvements of the physical and structural properties of collagen I-based scaffolds are still required, as stated and highlighted by Irawan et al., in the recently published review [21]. Recently, the biocompatibility and the chondrogenic potential of a new 3D

collagen type I-based scaffold has been evaluated by our research group both in vitro and in vivo (etherotopic implantation) [22,23]. Our in vitro results performed using this scaffold in combination with human adipose-tissue derived mesenchymal stem cells (hADMSCs) showed that the scaffold is able to promote the early stages of chondrogenic cell differentiation and that the addiction of specific inductive factors induces complete differentiation as highlighted both by specific cartilage markers expression and typical chondrocyte morphology [22]. The most important cartilage markers are represented by glycosaminoglycans (GAGs), collagen type II and aggrecan, which are typical ECM components of hyaline cartilage that characterise the articular cartilage of diarthrodial joints. Collagen type I, instead represents the main constituent of the fibrocartilage matrix, which possesses completely different mechanical properties compared to hyaline cartilage [1,6]. Another important chondrogenic marker is represented by SOX9, a transcription factor expressed by chondrocytes, which are the only cell type present within the cartilage tissue. It has been identified as a regulator of the chondrocyte lineage, essential for chondrocyte differentiation and cartilage formation. It is associated with the enhancement of collagen II and aggrecan synthesis within the cartilage matrix [24]. In vivo data obtained by subcutaneous implantation (heterotopic model) of a cell free scaffold showed that it is biocompatible and able to recruit host cells and to guide them towards the chondrogenic differentiation [22]. Furthermore, the cartilage-like microstructural properties of this biomaterial, in terms of density and elasticity, were combined in a simple production process [25], which makes this scaffold even very interesting to be evaluated for cartilage regenerative approaches. For this reason, to further evaluate and emphasize the data obtained in our previous studies, the aim of the present work was to continue the validation of this cell-free collagen I-based scaffold in an articular cartilage lesion (ACL) orthotopic model in terms of host cells recruitment, ECM deposition and cartilaginous repair promotion. The results of the present study complete the multi-step evaluation process of the 3D collagen I-based scaffold and may pave the way to the use of the latter in the cartilage regeneration approaches.

4.2 Materials & Methods

4.2.1 Scaffold Features

Collagen I-based scaffolds used in the present study were manufactured by Fin-Ceramica Faenza SpA (Faenza, Italy). The characterization and process of manufacturing were already widely defined in our previous study [22] and summarised below. These supports present a cylindrical form (8 mm diameter and 5 mm height) and are made up of equine type I collagen gel (1wt%) furnished in aqueous acetic buffer solution (pH = 3.5) (Opocrin SpA, Modena, Italy). The development process and physical and chemical features have been explained previously [22,23]. In Brief, collagen gel was diluted in water and supplied by 0.1 M NaOH solution, up to the isoelectric point (pH = 5.5), in which it precipitated in fibres. Subsequently, it was crosslinked at 37 °C by 48 h long immersion of the fibres in $NaHCO_3$/Na_2CO_3 (Sigma Aldrich, Milan, Italy) and Merck Millipore, aqueous solution with a 1,4-butanediol-diglycidyl-ether (BDDGE) and freeze-dried for 25 h under vacuum conditions (P = 0.29 mbar) to obtain a porous 3D structure. Finally, the collagen constructs were treated with gamma-rays at a minimum of 25 kGy.

The characterisation of 3D collagen scaffolds from a morphological and microstructural point of view was performed by scanning electron microscopy (SEM) by using an SEM-LEO 438 VP (Carl Zeiss AG, Oberkochen, Germany). Before the analysis, 3D scaffolds were sputter-coated with gold. SEM images were assessed by image J software by calculating the mean pore diameter (mean value of 67 ± 31 microns on a total of 327 pores) (Figure 1). The swelling ability of the material was estimated on 20 cartilaginous cylindrical constructs (ø = 10 mm, h = 4 mm) and determined by evaluating the weight increase and the percent increase in both dimensions [35], as already reported in our previous study [22]. The data analysis did not include the outlier values (Huber test). The porosity and density of collagen constructs were assessed with a glass pycnometer full of highly purified water on n. 20 scaffolds (d = 18 mm; h = 4 30mm) [36]. Pore diameter was then calculated using the geometric volume of the scaffolds and the mean value of the achieved densities [22].

4.2.2 Breeding and Housing of Animals, Experimental Design and Surgery Procedure

Twenty-seven 2-month-old healthy female Wistar outbred rats (Charles River Laboratories, Milan, Italy), with a bodyweight of 300 ± 20 g, were used in the present study. The animals were kept in polycarbonate cages (10.25”W × 18.75”D × 8”H) at controlled humidity and temperature (20–23 °C) throughout the whole period of the experiment, with free access to food and water and a 12 h

light/dark photoperiod. The 27 animals were divided into three groups at three different time points as shown in Table 1. The ACL groups consisted of rats submitted to surgical treatment to create defects inducing the ACL model. In the CTRL group, only 4-week samples were taken into account for the analysis.

Study Groups	Time Points	Number of Rats
CTRL	4, 8, 16 weeks	n. 9 (3 × each time point)
ACL (only lesion)	4, 8, 16 weeks	n. 9 (3 × each time point)
ACL-S (lesion + scaffold)	4, 8, 16 weeks	n. 9 (3 × each time point)

Table 2.1. Experimental groups.

Total anaesthesia (30 mg/kg Zoletil 100 + altadol 5 mg/kg + maintenance mixture of O_2 and isoflurane 2%–2.5%, Vibrac, Milan, Italy) was used for the surgery procedure. The electric clipper was used to shave the right limb anterior portion, which was then cleaned with povidone iodine (Sceptre Medical, New Delhi, India). The vertical incision was made through the medial border of the skin around the knee cap and, subsequently, through the articular capsule. Afterwards, the patella was moved laterally to expose the right limb femorotibial joint. By flexing the knee, the femoral condyles were exposed and a 1 mm × 1.5 mm sharp surgical forceps and needles were used to make a hole within the articular cartilage at the level of the femoropatellar groove of the right limb. Each rat from the ACL-S group received the same treatment, i.e., the collagen scaffolds were sterilely cut into 1 mm × 1.5 mm pieces and implanted into the femoral condyle hole on the right leg while no material was implanted in rats from the ACL group. The implantation was made using press-fit fixation, without supplementary fixation devices. The patella was then removed back, and the articular capsule and skin were sutured by using a 3–0 polydioxanone suture (Figure 6). Post-surgery, one dose of antibiotic Convenia® 0.1 mL/kg, (Vibrac, Milan, Italy), anti-inflammatory (Meloxicam 1 mg/kg) and analgesic (Tramadol 5 mg/kg) drugs, was administered for 3 days. After surgery, the animals were free to move in the cages without joint immobilization. During all the experimental period the suffering of animals was monitored through their observation (weight, lameness, fur appearance, consumption of food and water), performed once a day. The animals from all groups (CTRL, ACL and ACL-S) and all the sub-groups (4-, 8- and 16-weeks) after the surgical procedures were sacrificed by carbon dioxide (CO_2) overdose. After euthanasia, femurs were explanted, cleaned of soft tissues and the samples were

processed for histological, immunohistochemical and gene expression analyses. All the procedures were carried out at the Center for Advanced Preclinical In Vivo Research (CAPIR), University of Catania, conformed to the guidelines of the Institutional Animal Care and Use Committee (I.A.C.U.C.) of the University of Catania (Protocol n. 2112015-PR of the 14.01.2015, Italian Ministry of Health).

The experiments were conducted in accordance with the Italian Animal Protection Law (116/1992) and the European Community Council Directive (86/609/EEC).

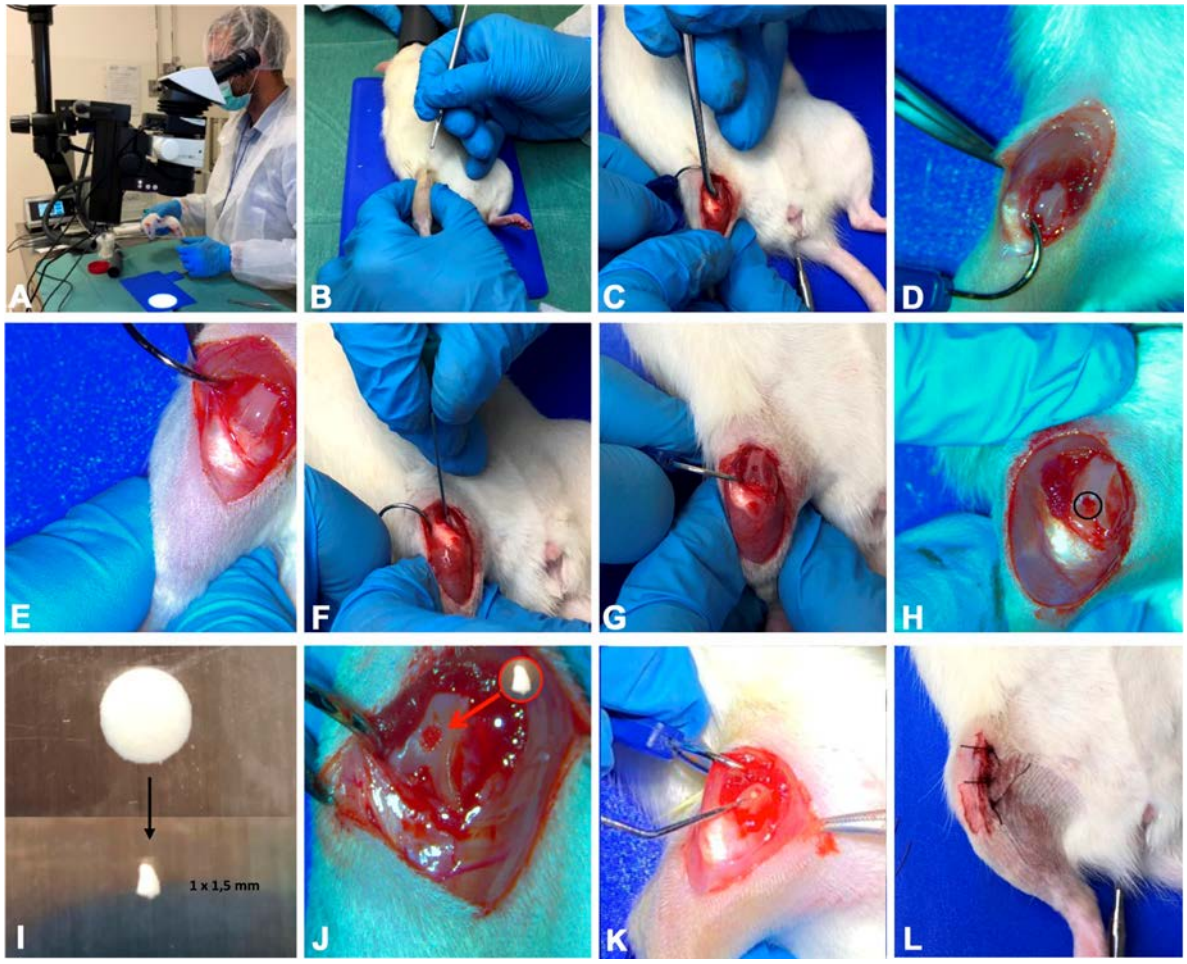

Figure 2.1 The photographs representing the surgical procedure performed to create defects (ACL induction) and to implant a collagen I-based scaffold. (**A**) total anaesthesia induction; (**B**) knee joint preparation for the incision; (**C–E**) vertical incision through the skin and articular capsule along the medial border and lateral displacement of the patella; (**F–H**) hole formation at the level of the femoropatellar groove in both ACL and ACL-S groups; (**I**) collagen I-based scaffold preparation and cutting; (**J**) collagen I-based scaffold implantation into the hole in the ACL-S group only; (**K**,**L**) patella replacement and the articular capsule and skin suture.

4.2.3 Histology Analysis

Cartilage samples were washed in phosphate-buffered saline (PBS, Bio-Optica, Milano, Italy), fixed in 10% buffered-formalin (Bio-Optica, Milan, Italy) for 24 h at room temperature. Afterwards, the samples were dehydrated in graded ethanol (Bio-Optica, Milan, Italy), cleaned in xylene (Bio-Optica,

Milan, Italy) and paraffin-embedded (Bio-Optica, Milan, Italy), being careful to preserve the desired anatomical orientation. For the general evaluation of the morphological structure of the cartilage, the slides of 4–5 µm thickness were cut from the obtained paraffin blocks and haematoxylin and eosin-stained (H&E; Bio-Optica, Milan, Italy) as previously described [33]. The samples were then examined with a Zeiss Axioplan light microscope (Carl Zeiss, Oberkochen, Germany) and by a digital camera (AxioCam MRc5, Carl Zeiss), used to take images. For qualitative histological analysis the following parameters were analysed:

- The type of repaired tissue on the lesion surface (cartilaginous, fibrous or calcified);
- Capability of the collagen I-based scaffold to recruit host cells and promote cartilaginous matrix deposition;
- The scaffold biocompatibility and reabsorption of the collagen I-based scaffold.

4.2.4 Analysis of sGAGs by Histochemistry

The samples were obtained as described above. Alcian Blue staining (Bio-Optica, Milan, Italy) was used to evaluate the expression of glycosaminoglycans (GAGs). The evaluation was made by computerised densitometric measurements. The samples were observed with a Zeiss Axioplan light microscope (Carl Zeiss, Oberkochen, Germany) and the images were taken using a digital camera (AxioCam MRc5, Carl Zeiss, Oberkochen, Germany).

4.2.5 Immunohistochemistry (IHC) Analysis

Articular cartilage samples were processed for immunohistochemical analysis as previously described [37]. In brief, the sections were de-waxed in xylene, hydrated in graded ethanol scale and incubated in 0.3% H_2O_2/PBS to stop endogenous peroxidase activity for 30 min. Afterwards, the slides were cleaned for 20 min with PBS (Bio-Optica, Milan, Italy). The slides were heated in a microwave oven (5min×3, 750W, LG Electronics Italia S.p.A., Milan, Italy) in Tris-EDTA buffer (pH 8.0; Bio-Optica, Milan, Italy) or in citrate buffer–pH 6 (pH 6.0; Bio-Optica, Milan, Italy), for the antigenic retrieval [38]. Afterwards, the slides were incubated overnight at 4 °C with diluted rabbit polyclonal antibodies against types I collagen (ab34710; Abcam, Cambridge, UK) and type II collagen (ab34712; Abcam, Cambridge, UK); rabbit monoclonal anti-SOX9 (ab185966; Abcam, Cambridge, UK) and anti-aggrecan (ab3778; Abcam, Cambridge, UK) antibodies, diluted 1:100 in PBS (Sigma-Aldrich, Milan, Italy). Immune-complexes were then incubated with biotinylated link antibodies (HRP-conjugated anti-rabbit and anti-mouse were used as secondary antibodies) and detected with peroxidase-labelled streptavidin

(LSAB + System-HRP, K0690, Dako, Glostrup, Denmark). Immunoreactivity was labelled using 0.1% $3,3^0$-diaminobenzidine (DAB) (DAB substrate Chromogen System; Dako, Glostrup, Denmark). The Mayer's hematoxylin (Histolab Products AB, Göteborg, Sweden) was used for the counterstain and then the sections were mounted in GVA (Zymed Laboratories, San Francisco, CA, USA), observed with an Axioplan Zeiss light microscope (Carl Zeiss, Oberkochen, Germany) and captured with a digital camera (AxioCam MRc5, Carl Zeiss, Oberkochen, Germany).

4.2.6 Computerized Morphometric Measurements and Image Analysis

One field of about 550,000 μm^2, corresponding to the defect area, carefully selected from each section (three sections for each time point), was analysed for histochemical assessment of Alcian Blue staining, detecting GAGs expression, and to quantify the level of positive anti-Collagen I, anti-Collagen II, anti-Aggrecan and anti-SOX9 antibodies immunoexpression. The image analysis software (AxioVision Release 4.8.2-SP2 Software, Carl Zeiss Microscopy GmbH, Jena, Germany), which quantifies the staining level as the densitometric count ($pixel^2$) normalized to the defect area of each sample, was used. The samples were analysed by using the Zeiss Axioplan light microscope (Carl Zeiss, Oberkochen, Germany) and the pictures were taken with a digital camera (AxioCam MRc5, Carl Zeiss, Oberkochen, Germany). Two investigators (one anatomical morphologist and one histologist) made the morphological assessment. If disputes occurred, a unanimous agreement was reached after section re-evaluation and before proceeding with data interpretation.

4.2.7 Quantitative Real-Time Polymerase Chain Reaction (q-PCR)

Total RNA was isolated from paraffin-embedded tissue sections by using the RNeasy FFPE Kit (Qiagen, Germantown, MD, USA). cDNA was synthesised from 1 µg of total RNA using a High-Capacity cDNA Reverse Transcription Kit (Applied Biosystems). Quantitative RT-PCR was performed using the SYBR Green method on a 7900HT Real Time PCR (Applied Biosystems). Specific primers for chondral genes, including *COL1A1*, *COL2A1*, *aggrecan* and *SOX9*, were designed using Primer Blast [39] and selecting exon-exon junctions on mRNA as a target region for annealing. Gene expression was assessed using the $2^{-\Delta\Delta Ct}$ method [40]. Oligonucleotide sequences are reported in Table 2. Results were normalised to the levels of Beta-Tubulin (TUBB), used as an endogenous control.

Target Gene	Forward	Reverse
COL1A1	CCGGAAACAGACAAGCAACCCAAA	AAAGGAGCAGAAAGGGCAGCATTG
COL2A1	TGGTCTTGGTGGAAACTTTGCTGC	AGGTTCACCAGGTTCACCAGGATT
Aggrecan	TGTGGTGATGATCTGGCACGAGAA	CGGCGGACAAATTAGATGCGGTT
Sox9	AACAACCCGTCTACACACAGCTCA	TGGGTAATGCGCTTGGATAGGTCA
TuBB4a	GACGTGAGTACTGCTCCGC	CTTGCAGGTGCACGATTTCC

Table 2.2. Primer sequences.

4.2.8 Statistical Analysis

The statistical evaluation was carried out by using GraphPad Instat® Biostatistics version 3.0 software (GraphPad Software, Inc., La Jolla, CA, USA), as previously described [41]. Differences between experimental groups were evaluated by using a two-way ANOVA followed by Tukey's multiple comparison post hoc test. Datasets were tested for normal distribution with the Kolmogorov–Smirnov test. All variables were normally distributed. For all experiments, *p*-values of less than 0.05 were considered statistically significant (*$p< 0.05$; **$p< 0.01$; ***$p< 0.001$; ****$p< 0.0001$ and ns, not significant). The data are presented as the mean value ± SD, as previously described [42].

4.3 Results

4.3.1 3D Scaffold Characterization before Implantation

The microstructural and morphological properties of the 3D ColI-based scaffold were evaluated by SEM analysis as previously indicated [22,23]. Briefly, Figure 1 shows SEM images of the 3D scaffold at different magnifications, displaying a high porosity of the scaffold with 3D intersected pores without any defined alignment of the collagen fibers. Pore distribution analysis indicated a frequency (> 65%) of pores between 40 and 100 μm in size. The swelling test was performed to assess the change of material structure clearly demonstrating that the collagen I-based scaffold is highly hydrophilic and reaches a steady-state in less than 1 min. The volume of absorbed PBS was quantified to evaluate the capability of the collagen scaffold to maintain the liquid assigned to the support of the 3D structure. After swelling, both diameter (6 ± 1%) and thickness (27 ± 9%) of the scaffold appeared significantly increased.

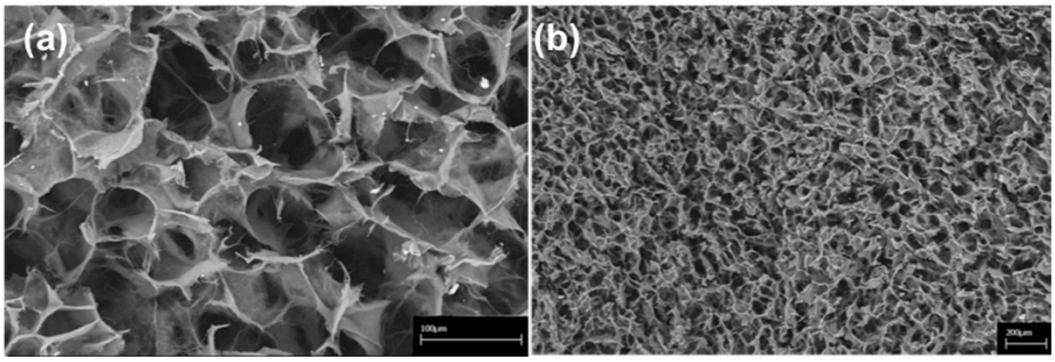

Figure 2.2. Scanning Electron Microscopy (SEM) images of the collagen-based scaffold. At higher magnification, interconnected collagen fibres are detectable within the scaffold. Scale bars: 100 μm in (a); 200 μm in (b).

4.3.2 Morphological Evaluation of Explanted Femurs

To assess the capability of the collagen I-based scaffold to promote cartilage restoration we performed macroscopic (Figure 2A) and microscopic (Figure 2B) evaluation on the explanted femurs at 4-, 8-, and 16-weeks post-surgery and orthotopic implantation. The hematoxylin and eosin (H&E) staining was used to study the microscopic morphology of the femoral articular cartilage in both groups (femurs with implanted collagen I-scaffolds: ACL-S group, and femurs without scaffolds: ACL group) in order to detect alterations. In the control group, articular cartilage showed a normal cytoarchitecture. In the superficial zone, cells appeared flat and small; in the middle and deep zone, chondrocytes were organised in columns; the tidemark was very strong and evident (Figure 2Ba).

In the articular cartilage of the ACL group, the general tissue organization was completely altered due to the defect induction. The superficial, middle and deep zones, as well as the tidemark, were not observable anymore at all the time points (Figure 2Bb–d). At 4 weeks post-surgery, the H&E staining

revealed a newly formed fibrous tissue (scar tissue) in the superficial zone at the surface of the subchondral bone, corresponding to the defect repair (Figure 2Bb). At 8- and 16-weeks the scar tissue tended to be progressively replaced by a tissue that appeared to be calcified, suggested by the morphological aspect of the tissue and poor proteoglycans deposit, further evidenced by Alcian Blue staining (Figure 3). The peri-native cartilage features appeared totally altered (Figure 2Bc,d). In the articular cartilage of the implanted group (ACL-S), at 4-weeks post-surgery, the H&E staining showed the presence of newly formed tissue at the interface between the subchondral bone and collagen scaffold, which presented morphological features resembling a prechondrogenic mesenchymal-like tissue, characterised by the spindle-shaped cells growing without any apparent internal organisation (Figure 2Be). However, this observation has not been validated by specific stainings and would need to be confirmed. Afterwards, the samples revealed the capacity of the biomaterial to recruit host cells that infiltrated, adhered and grown within the scaffold (8-weeks, Figure 2Bf). A progressive integration and replacement of the degradable collagen scaffold with the reparative newly formed cartilage-like tissue were shown (16-weeks, Figure 2Bg).

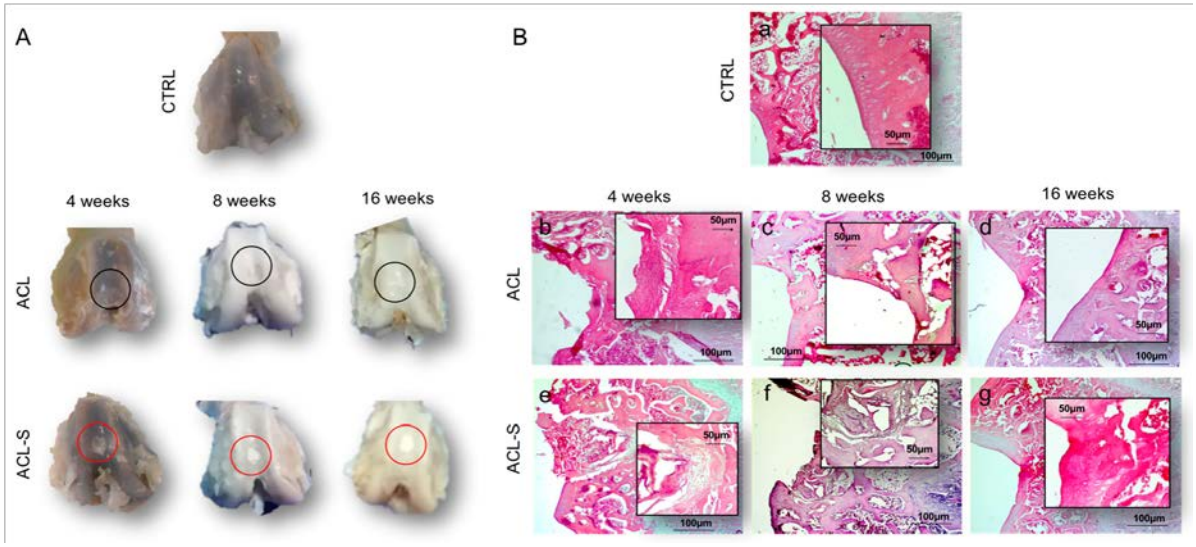

Figure 2.3. **Cartilage repair evaluation through macroscopic and microscopic evaluation.** (**A**) Macroscopic evaluation of repair capacity of femoral articular cartilage explants after defect creation indicated with black circles (ACL group) and in vivo scaffold implantation indicated with red circles (ACL-S group) at 4-, 8- and 16-weeks; (**B**) Histological evaluation by H&E staining of femoral articular cartilage samples after defect creation (ACL group) and in vivo scaffold implantation (ACL-S group) at 4-, 8- and 16-weeks: (a) control sample presenting a normal cartilage cytoarchitecture; (b) ACL group sample at 4-weeks presenting fibrocartilage formation at the defect area level; (c,d) ACL group sample at 8- and 16-weeks presenting cartilage calcification corresponding to the defect area level; (e) ACL-S group sample at 4-weeks presenting a prechondrogenic mesenchyme-like tissue features at the interface between scaffold and the peri-native tissue; (f) ACL-S group sample at 8-weeks presenting matrix deposition within the scaffold, suggesting host cell recruitment and their chondrogenic differentiation; (g) ACL-S group sample at 16-weeks presenting a total scaffold reabsorption and replacement with a newly formed cartilage-like tissue. Scale bar: 100 µm. The inserts represent the image magnifications (scale bar: 50 µm) to evidence the morphology changes observed in a time-dependent manner.

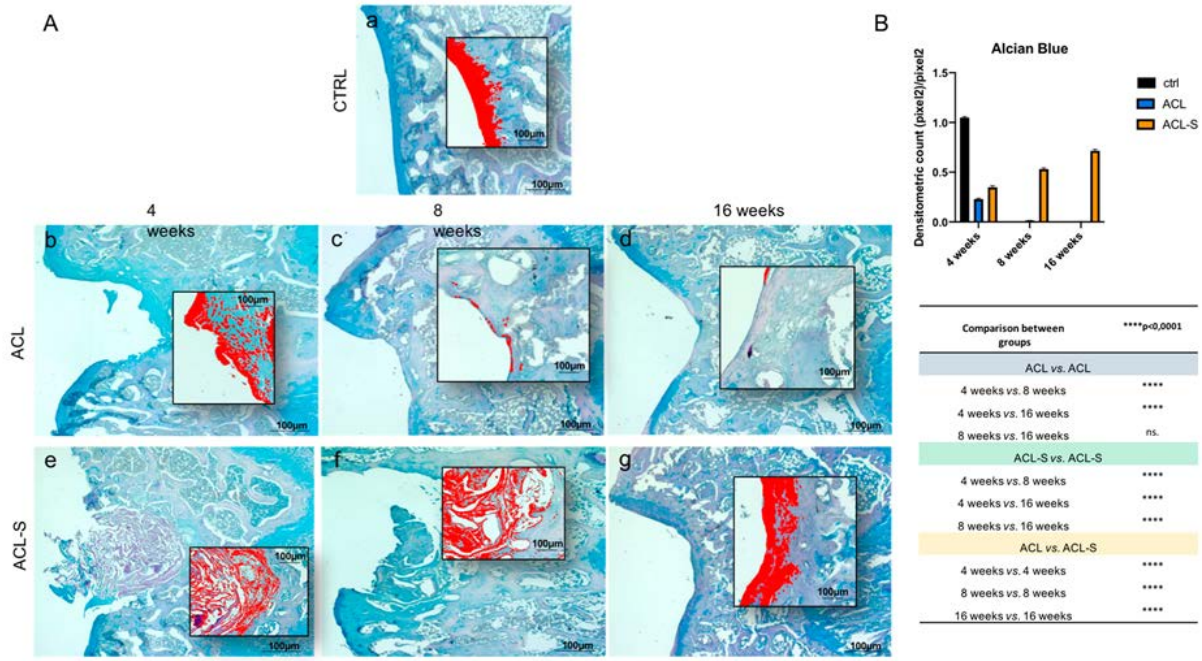

Figure 2.4. Histochemical evaluation of the deposition of sGAGs in femoral articular cartilage samples at 4-, 8- and 16-weeks post-surgery revealed by the intensity of Alcian Blue staining through computerised densitometric measurements and image analysis. (**A**) The inserts represent the image magnifications (scale bar: 100 µm) analysed by the software: the red colour corresponds to high intensity Alcian Blue staining. (a) control sample of articular cartilage; (b–d) ACL group samples at 4-, 8- and 16-weeks; (e–g) ACL-S group samples at 4-, 8- and 16-weeks. Scale bars: 100 µm. (**B**) Graph representing staining level expressed as densitometric count (pixel^2) normalized to the area of each section expressed in pixel^2. Results are presented as the mean ± SD. Two-way ANOVA test followed by Tukey's multiple comparison test reported that all pairwise comparisons were significantly different (p-value < 0.0001) except for ACL 8-weeks vs. ACL 16-weeks, which was not significant (ns.).

The evaluation of cartilage repair was also assessed by the deposition of sulfated glycosaminoglycans (sGAGs) revealed by the intensity of Alcian Blue staining (Figure 3). In the ACL group at 4-weeks, the newly formed fibrous tissue showed a low-intensity blue staining (Figure 3Ab), which diminished progressively and in a significant way with the supposed calcification of the cartilage tissue through the time points and, especially, at 16-weeks (p-value < 0.0001, Figure 3Ad, B). In the ACL-S group (Figure 3Ae–g), the Alcian Blue staining was much stronger than in the defect control group (ACL group). The internal repair integrity was underlined by the higher ECM deposition within the scaffolds due to the recruitment of host cells, moreover, it appeared progressive through the time points, especially at 16-weeks post-implantation (p-value < 0.0001, Figure 3Af, B).

4.3.3 Ex Vivo Evaluation of Cartilage Regeneration

Immunohistochemical staining with statistical analysis was carried out in all groups to evaluate cartilage repair through the expression level of SOX9 (Figure 4A), a pivotal transcription factor for cartilage formation and ECM cartilaginous structural molecules, Aggrecan (Figure 4A'), Collagen type I (Figure 5A), and Collagen type II (Figure 5A'). A very strong expression of SOX9 was seen at 4-weeks post-surgery, especially in the ACL group (Figure 4Ab). It decreased significantly at 8-

weeks in both ACL (p-value < 0.0001, Figure 4Ac, B) and ACL-S (p-value < 0.0001, Figure 4Af, B) groups, to increase again at 16-weeks especially in ACL-S group (p-value < 0.001, Figure 4Ag, B). Overall, the SOX9 expression was significantly higher in ACL-S group when compared to defect control group (ACL group), both at 8- (p-value < 0.05, Figure 4Af, B) and 16-weeks (p-value < 0.0001, Figure 4Ag, B). The expression profile of aggrecan showed a progressive increase through the time points, with the highest peak at 16-weeks in the ACL-S group (Figure 4A'g). Overall, aggrecan expression was always higher in the ACL-S group when compared to the defect control group and it was significant at 8- (p-value < 0.05, Figure 4A'f, B') and 16-weeks (p-value < 0.001, Figure 4A'g, B'). Collagen type I expression was strong at 4-weeks (Figure 5Ae) and 8-weeks (Figure 5Af), in the ACL-S group, decreasing significantly at 16-weeks post-surgery (p-value < 0.0001, Figure 5Ag,B). However, the collagen I expression resulted significantly higher in the ACL-S group when compared to the defect control (ACL group) at all time points: 4-weeks (p-value < 0.0001, Figure 5Ae,B), 8-weeks (p-value < 0.0001, Figure 5Af,B), 16-weeks (p-value < 0.001, Figure 5Ag,B). A very strong expression of collagen type II was seen at 4-weeks post-surgery, especially in the ACL-S group in which it was significantly higher when compared to the defect control group (ACL group) (p-value < 0.0001, Figure 5A'e,B') and it decreased progressively through the time points (Figure 5A'f,g). The expression profile of collagen II demonstrated a significant difference

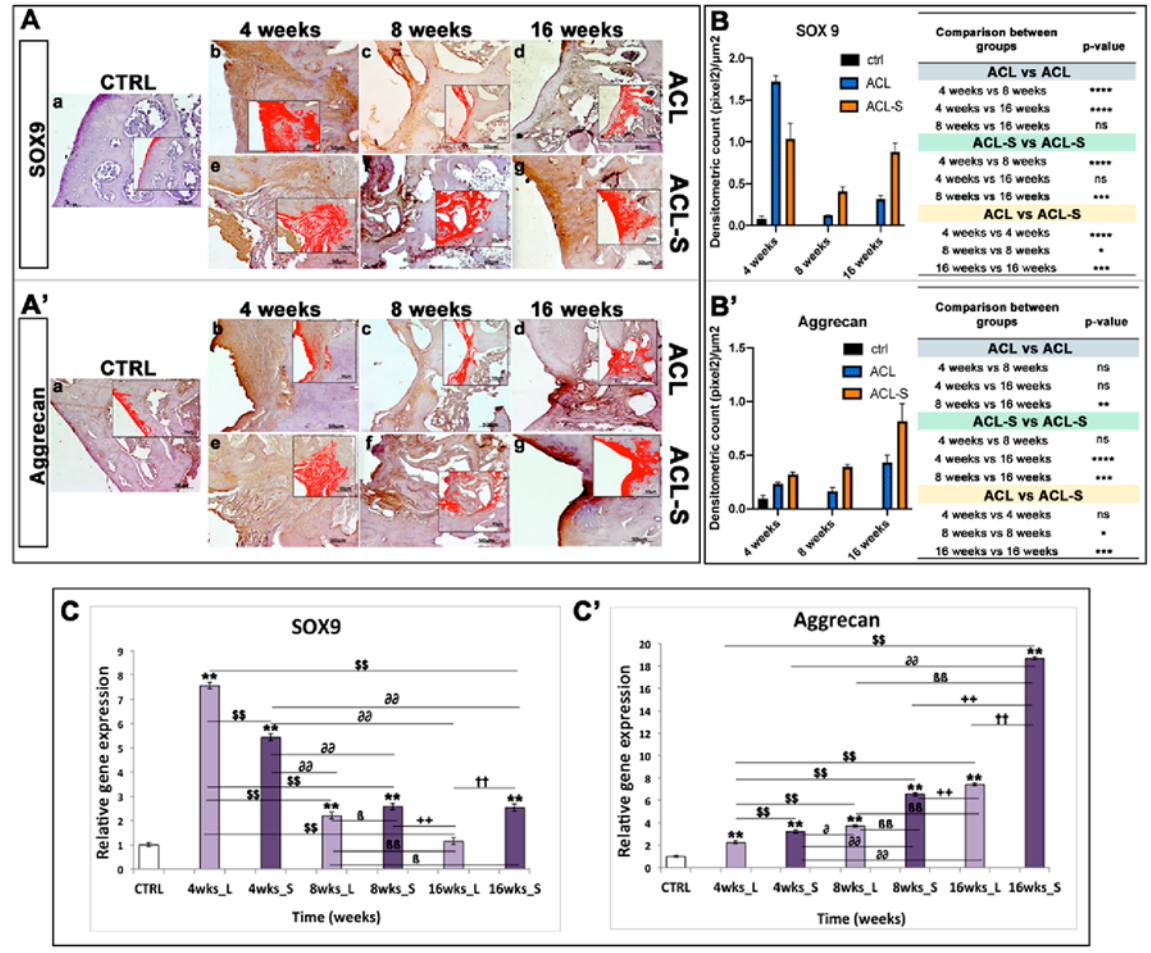

Figure 2.5. Sox9 and aggrecan evaluation in femoral articular cartilage samples at 4-, 8- and 16-weeks post-surgery. (**A–A'**) Immunohistochemical analyses: (a) control sample of articular cartilage; (b–d) ACL group samples at 4-, 8- and 16-weeks; (e–g) ACL-S group samples at 4-, 8- and 16-weeks. In the inserts, the red colour corresponds to brown staining (immune complexes labelled with chromogen); scale bars 50 µm. (**B–B'**) Graph representing staining level expressed as densitometric count (pixel^2) normalized to the area of each section expressed in µm^2. (**C–C'**) Relative quantitation (RQ) of gene expression showing the time-course of Sox9 and Aggrecan in ACL (L) and ACL-S (S) groups, after 4-, 8-, and 16-weeks from surgery. TUBB4a has been used as endogenous controls. Results are presented as the mean ± SD. Differences between groups were evaluated by using a two-way ANOVA followed by Tukey's multiple comparison post-hoc test (* $p < 0.05$; ** $p < 0.01$; *** $p < 0.001$; **** $p < 0.0001$; ns, not significant). * CTRL vs 4-, 8-, 16-wks_L and 4-, 8-, 16-wks_S; $ 4-wks_L vs 8-, 16-wks_L and 4-,8-, 16-wks_S; ∂ 4-wks_S vs 8-, 16-wks_L and 8-, 16-wks_S; β 8-wks_L vs 16-wks_L and 8-, 16-wks_S; + 8-wks_S vs 16-wks_L and 16-wks_S; † 16-wks_L vs 16-wks_S.

between the ACL and ACL-S groups at 4-weeks (*p*-value < 0.0001, Figure 5A'b,e,B') but not at 8- and 16-weeks (*p*-value < 0.05, Figure 5A'c,d,f,g,B').

A qRT-PCR analysis was performed on total RNA isolated from explanted scaffolds to evaluate the expression of specific genes correlated to cartilage phenotype. The expression profiles of cartilaginous genes, including *ColI*, *ColII*, *Aggrecan* and *Sox9* at 4-, 8-, and 16-weeks were compared to control mRNA levels. Logarithmic RQ values are reported in Figures 4 and 5.

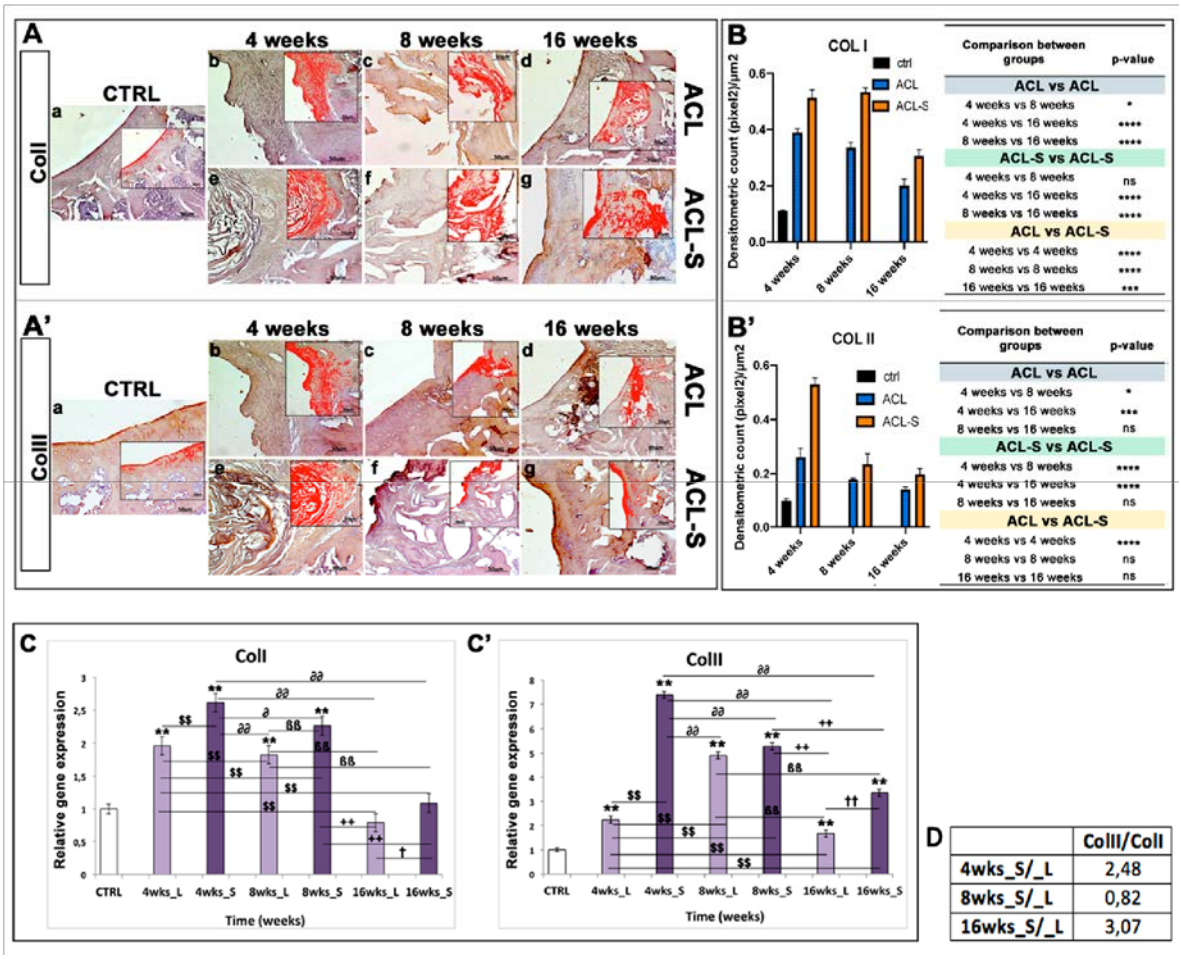

Figure 2.6. **Collagen type I and collagen type II evaluation in femoral articular cartilage samples at 4-, 8- and 16-weeks post-surgery.** (**A–A'**) Immunohistochemical analyses: (a) control sample of articular cartilage; (b–d) ACL group samples at 4-, 8- and 16-weeks; (e–g) ACL-S group samples at 4-, 8- and 16-weeks. In the inserts, the red colour corresponds to brown staining (immune complexes labelled with chromogen); scale bars 50 µm. (**B–B'**) Graph representing staining level expressed as densitometric count (pixel^2) normalized to the area of each section expressed in µm^2. (**C–C'**) Relative quantitation (RQ) of gene expression showing the time-course of ColI and ColII in ACL (L) and ACL-S (S) groups, after 4-, 8-, and 16-weeks from surgery. TUBB4a has been used as endogenous controls. Results are presented as the mean ± SD. Differences between groups were evaluated by using a two-way ANOVA followed by Tukey's multiple comparison post-hoc test (*p < 0.05; **p < 0.01; ***p < 0.001; ****p < 0.0001; ns, not significant). (**D**) Table showing the ratio of collagen II/collagen I (ColII/ColI). * CTRL vs 4-, 8-, 16-wks_L and 4-, 8-, 16-wks_S; $ 4-wks_L vs 8-, 16-wks_L and 4-, 8-, 16-wks_S; ∂ 4-wks_S vs 8-, 16-wks_L and 8-, 16-wks_S; β 8-wks_L vs 16-wks_L and 8-, 16-wks_S; + 8-wks_S vs 16-wks_L and 16-wks_S; † 16-wks_L vs 16-wks_S.

Sox9 displayed a characteristic peak of expression at 4-weeks both in the ACL (RQ = 7.563) and in ACL-S groups (RQ = 5.432) that decreased progressively over time (ACL group: 8-weeks, RQ = 2.199 and 16-weeks RQ = 1.143; ACL-S group: 8-weeks RQ = 2.580, 16-weeks RQ = 2.528), even if the ACL-S group maintained a higher expression of *Sox9* when compared to the ACL group (Figure 4C).

Aggrecan exhibited a lower expression until the 8th week with a peak of expression at the 16th week in both groups, although the ACL-S group (RQ = 18.687) displayed a more pronounced expression than the ACL group (RQ = 7.433) (Figure 4C').

ColI showed an increased expression during the fourth week in both groups, RQ = 1.965 in the ACL group and RQ = 2.612 in the ACL-S group, that decreased down to 0.792 and 1.085 at 16-weeks, respectively for the ACL and ACL-S groups (Figure 5C).

Finally, *ColII* showed a distinctive peak of expression at 4-weeks for ACL-S (RQ = 7.388) with a subsequent decrease and reduced modulation (3.355 orders of magnitude) until week 16; in contrast, the ACL group showed a higher *ColII* expression at 8-weeks (RQ = 4.905) that subsequently decreased to 1.671 orders of magnitude at week 16 (Figure 5C'). Moreover, the gene expression profile data showed a ratio of *ColII*/*ColI* for ACL-S/ACL groups of 2.48 fold at 4-weeks, 0.82 at 8-weeks and 3.07 at 16-weeks post-surgery (Figure 5D).

4.4 Discussion

The aim of the present study was to evaluate the extent to which the cell-free collagen I-based 3D scaffold might support hyaline cartilage repair of femoral articular cartilage defects, created to reproduce the ACL model, at 16-weeks post-surgery. The concept of using cell-free scaffolds in tissue engineering is widely accepted and has been advanced by Omori et al., in 2008, in an interesting study on laryngeal cartilage reconstruction in a canine model [26], where the authors suggested the successful cartilage reconstruction by the in situ tissue engineering approach.

In the present study, the collagen I-based scaffolds were confirmed to be biocompatible, as already demonstrated in our previous study [23] and as evidenced by the histological analysis of the present study, showing total biodegradation and replacement of the biomaterial with the newly formed cartilage-like tissue at 16-weeks post-implantation (Figure 2B). Moreover, as previously revealed [22,27,28], the scaffolds showed good immune tolerance by the animals, as suggested by the absence of scar-like tissue formation and inflammatory cell infiltration at the interface between the scaffold and peri-native cartilage tissue (Figure 2B). Furthermore, the H&E and Alcian Blue staining demonstrated that the collagen-based scaffold allowed the formation of an articular cartilage-like tissue corresponding to the defect area at the femoropatellar groove level. It was underlined by the significantly higher deposition of sGAGs at 16-weeks post-implantation (Figure 3g) when compared to the defect control group (Figure 3d). The latter showed, instead, newly formed tissue resembling calcified tissue in the area corresponding to the defect, at the same time point. These data were confirmed by immunohistochemical analysis, which showed a higher expression of cartilage markers in ACL-S group samples, when compared to the ACL group samples (Figures 4 and 5), at all the time points. The only exception regards the SOX9 expression, which at its highest peak, corresponded to the ACL group sample at 4-weeks post-surgery (Figure 4Ab). The latter was probably due to the fact

that, at 4-weeks, we expected that the formation of fibrous tissue might be preceded by mesenchymal tissue formation, characterized by a high SOX9 expression [29,30]. Afterwards, along with the probably observed calcification-unlike process (8- and 16-weeks post-surgery) in the ACL group, a significant decrease of SOX9 expression was observed (Figure 4Ac,d,B). It probably happened because the recruited host cells were not supported by any 3D structure, like that given by the collagen I-based scaffold (ACL-S group, Figure 4Ae–g). Indeed, it has been widely shown that the 3D architectural support enhances and improves the cartilaginous matrix formation and stability [31–33]. SOX9 is a transcription factor that plays a key role in chondrogenesis, both by driving the collagen type II and aggrecan expression and by supporting the survival of chondrocyte [29,34]. Apart from the exception of week 4, the results of immunohistochemistry demonstrated that SOX9 expression was maintained always higher in the ACL-S group, especially at 16-weeks post-implantation. These results were observed also in the expression profiles of collagen II (Figure 5) and, especially, of aggrecan, which the highest peak corresponded to the the ACL-S group at 16-weeks (Figure 4A'g). Another important observation regards the expression profiles of collagen type I and II, which the highest peaks corresponded to the ACL-S group at week 4, as seen in Figure 5Ae,A'e. This was probably due to the fact that at this time point, the collagen I-based scaffolds still conserved their integrity, and have not yet undergone the biodegradation process, which was observable at 8- and, even more, at 16-weeks after implantation (Figures 2 and 3). However, the scaffold has not been specifically labelled and this observation would need to be further confirmed. The collagen II high expression was also justified by the infiltrated cells within the scaffolds, already synthesising this cartilage marker, and occupying a bigger area when compared to the cartilage repair tissue at 8- and 16-weeks (Figure 2). The immunohistochemistry results were further confirmed by the gene expression analysis, which presented the same expression profiles of all the chondrogenic markers, as seen in Figures 4C and 5C. Overall, the results of histological, histochemical, immunohistochemical and gene expression analysis confirmed that implantation of collagen I-based scaffold within the cartilage defects of rats, improved the cartilage tissue regeneration
when compared to the group without the scaffolds.

4.5 Conclusions

In conclusion, our data support the high biocompatibility of the collagen I-based scaffold, which is able to efficaciously integrate into the host articular cartilage and to promote the development of new cartilage-like tissue by recruiting the host cells and driving them towards the chondrogenic differentiation. Moreover, thanks to the good biodegradability over time (up to 16-weeks), this scaffold represents a promising tool for cartilage tissue engineering and repair approaches.

4.6 References

1. Karuppal, R. Current concepts in the articular cartilage repair and regeneration. *J. Orthop.* **2017**, *14*, A1–A3. [CrossRef] [PubMed]
2. Di Rosa, M.; Szychlinska, M.; Tibullo, D.; Malaguarnera, M.; Musumeci, G. Expression of CHI3L1 and CHIT1 in Osteoarthritic Rat Cartilage Model. A Morphological Study. *Eur. J. Histochem.* **2014**, *58*, 2423. [CrossRef] [PubMed]
3. Szychlinska, M.A.; Trovato, F.M.; Di Rosa, M.; Malaguarnera, L.; Puzzo, L.; Leonardi, R.; Castrogiovanni, P.; Musumeci, G. Co-Expression and Co-Localization of Cartilage Glycoproteins CHI3L1 and Lubricin in Osteoarthritic Cartilage: Morphological, Immunohistochemical and Gene Expression Profiles. *Int. J. Mol. Sci.* **2016**, *17*, 359. [CrossRef] [PubMed]
4. Redondo, M.; Beer, A.; Yanke, A. Cartilage Restoration: Microfracture and Osteochondral Autograft Transplantation. *J. Knee Surg.* **2018**, *31*, 231–238. [CrossRef]
5. Richter, D.; Schenck, R.C.; Wascher, D.C.; Treme, G. Knee Articular Cartilage Repair and Restoration Techniques: A Review of the Literature. *Sports Health* **2015**, *8*, 153–160. [CrossRef]
6. Armiento, A.R.; Stoddart, M.; Alini, M.; Eglin, D. Biomaterials for articular cartilage tissue engineering: Learning from biology. *Acta Biomater.* **2018**, *65*, 1–20. [CrossRef]
7. Sharma, P.; Kumar, P.; Sharma, R.; Bhatt, V.D.; Dhot, P.S. Tissue Engineering; Current Status & Futuristic Scope. *J. Med. Life* **2019**, *12*, 225–229. [CrossRef]
8. Eftekharid, A.; Dizaj, S.M.; Sharifi, S.; Salatin, S.; Saadat, Y.R.; Vahed, S.Z.; Samiei, M.; Ardalan, M.R.; Rameshrad, M.; Ahmadian, E.; et al. The Use of Nanomaterials in Tissue Engineering for Cartilage Regeneration; Current Approaches and Future Perspectives. *Int. J. Mol. Sci.* **2020**, *21*, 536. [CrossRef]
9. Huang, B.J.; Hu, J.C.; Athanasiou, K.A. Cell-based tissue engineering strategies used in the clinical repair of articular cartilage. *Biomaterials* **2016**, *98*, 1–22. [CrossRef]
10. Kwan, H.; Chisari, E.; Khan, W.S. Cell-Free Scaffolds as a Monotherapy for Focal Chondral Knee Defects. *Materials* **2020**, *13*, 306. [CrossRef]
11. Campos, Y.; Almirall, A.; Fuentes, G.; Bloem, H.L.; Kaijzel, E.L.; Cruz, L.J. Tissue Engineering: An Alternative to Repair Cartilage. *Tissue Eng. Part B Rev.* **2019**, *25*, 357–373. [CrossRef] [PubMed]
12. Szychlinska, M.A.; D'Amora, U.; Ravalli, S.; Ambrosio, L.; Di Rosa, M.; Musumeci, G. Functional Biomolecule
    Delivery Systems and Bioengineering in Cartilage Regeneration. *Curr. Pharm. Biotechnol.* **2019**, *20*, 32–46. [CrossRef] [PubMed]
13. Im, G. Biomaterials in orthopaedics: The past and future with immune modulation. *Biomater. Res.* **2020**, *24*,7. [CrossRef] [PubMed]
14. Dai, Y.; Shen, T.; Ma, L.; Wang, D.-A.; Gaoa, C. Regeneration of osteochondral defects in vivo by a cell-free cylindrical poly(lactide-co-glycolide) scaffold with a radially oriented microstructure.
    J. Tissue Eng. Regen. Med. **2017**, *12*, 1647–1661. [CrossRef] [PubMed]
15. Szychlinska, M.; Castrogiovanni, P.; Nsir, H.; Di Rosa, M.; Guglielmino, C.; Parenti, R.; Calabrese, G.; Pricoco, E.; Salvatorelli, L.; Magro, G.; et al. Engineered cartilage regeneration from adipose tissue derived-mesenchymal stem cells: A morphomolecular study on osteoblast, chondrocyte and apoptosis evaluation. *Exp. Cell Res.* **2017**, *357*, 222–235. [CrossRef]

16. Dang, J.; Leong, K.W. Natural polymers for gene delivery and tissue engineering. *Adv. Drug Deliv. Rev.* **2006**, *58*, 487–499. [CrossRef]
17. Gavenis, K.; Schneider, U.; Maus, U.; Mumme, T.; Muller-Rath, R.; Schmidt-Rohlfing, B.; Andereya, S.Cell-free repair of small cartilage defects in the Goettinger minipig: Which defect size is possible? *Knee Surg. Sports Traumatol. Arthrosc.* **2011**, *20*, 2307–2314. [CrossRef]
18. Efe, T.; Theisen, C.; Fuchs-Winkelmann, S.; Stein, T.; Getgood, A.; Rominger, M.B.; Paletta, J.R.J.; Schofer, M.D. Cell-free collagen type I matrix for repair of cartilage defects—Clinical and magnetic resonance imaging results. *Knee Surg. Sports Traumatol. Arthrosc.* **2011**, *20*, 1915–1922. [CrossRef]
19. Schüttler, K.F.; Schenker,H.; Theisen, C.; Schofer,M.D.; Getgood, A.; Roessler, P.P.; Struewer, J.; Rominger, M.B.; Efe, T. Use of cell-free collagen type I matrix implants for the treatment of small cartilage defects in the knee: Clinical and magnetic resonance imaging evaluation. *Knee Surg. Sports Traumatol. Arthrosc.* **2013**, *22*, 1270–1276. [CrossRef]
20. Roessler, P.P.; Pfister, B.; Gesslein, M.; Figiel, J.; Heyse, T.J.; Colcuc, C.; Lorbach, O.; Efe, T.; Schüttler, K.F. Short-term follow up after implantation of a cell-free collagen type I matrix for the treatment of large cartilage defects of the knee. *Int. Orthop.* **2015**, *39*, 2473–2479. [CrossRef]
21. Irawan, V.; Sung, T.-C.; Higuchi, A.; Ikoma, T. Collagen Scaffolds in Cartilage Tissue Engineering and Relevant Approaches for Future Development. *Tissue Eng. Regen. Med.* **2018**, *15*, 673–697. [CrossRef] [PubMed]
22. Calabrese, G.; Forte, S.; Gulino, R.; Cefalì, F.; Figallo, E.; Salvatorelli, L.; Maniscalchi, E.T.; Angelico, G.; Parenti, R.; Gulisano, M.; et al. Combination of Collagen-Based Scaffold and Bioactive Factors InducesAdipose-Derived Mesenchymal Stem Cells Chondrogenic Differentiation In vitro. *Front. Physiol.* **2017**, *8*, 50. [CrossRef] [PubMed]
23. Calabrese, G.; Gulino, R.; Giuffrida, R.; Forte, S.; Figallo, E.; Fabbi, C.; Salvatorelli, L.; Memeo, L.; Gulisano, M.;
Parenti, R. In Vivo Evaluation of Biocompatibility and Chondrogenic Potential of a Cell-Free Collagen-Based Scaffold. *Front. Physiol.* **2017**, *8*, 984. [CrossRef]
24. Lefebvre, V.; Dvir-Ginzberg, M. SOX9 and the many facets of its regulation in the chondrocyte lineage. *Connect. Tissue Res.* **2016**, *58*, 2–14. [CrossRef] [PubMed]
25. Deponti, D.; Di Giancamillo, A.; Gervaso, F.; Domenicucci, M.; Domeneghini, C.; Sannino, A.; Peretti, G.M. Collagen Scaffold for Cartilage Tissue Engineering: The Benefit of Fibrin Glue and the Proper Culture Time in an Infant Cartilage Model. *Tissue Eng. Part A* **2014**, *20*, 1113–1126. [CrossRef] [PubMed]
26. Omori, K.; Nakamura, T.; Kanemaru, S.; Magrufov, A.; Yamashita, M.; Shimizu, Y. In Situ Tissue Engineering of the Cricoid and Trachea in a Canine Model. *Ann. Otol. Rhinol. Laryngol.* **2008**, *117*, 609–613. [CrossRef] [PubMed]
27. Calabrese, G.; Giuffrida, R.; Forte, S.; Salvatorelli, L.; Fabbi, C.; Figallo, E.; Gulisano, M.; Parenti, R.; Magro, G.; Colarossi, C.; et al. Bone augmentation after ectopic implantation of a cell-free collagen-hydroxyapatite scaffold in the mouse. *Sci. Rep.* **2016**, *6*, 36399. [CrossRef]
28. Calabrese, G.; Giuffrida, R.; Forte, S.; Fabbi, C.; Figallo, E.; Salvatorelli, L.; Memeo, L.; Parenti, R.; Gulisano, M.; Gulino, R. Human adipose-derived mesenchymal stem cells seeded into a collagen-hydroxyapatite scaffold promote bone augmentation after implantation in the mouse. *Sci. Rep.* **2017**, *7*, 7110. [CrossRef]
29. Lefebvre, V.; Angelozzi, M.; Haseeb, A. SOX9 in cartilage development and disease. *Curr. Opin. Cell Biol.* **2019**, *61*, 39–47. [CrossRef]

30. Akiyama, H.; Kim, J.E.; Nakashima, K.; Balmes, G.; Iwai, N.; Deng, J.M.; Zhang, Z.; Martin, J.F.; Behringer, R.R.; Nakamura, T.; et al. Osteo-chondroprogenitor cells are derived from Sox9 expressing precursors. *Proc. Natl. Acad. Sci. USA* **2005**, *102*, 14665–14670. [CrossRef]
31. Jin, G.Z.; Kim, H.W. Chondrogenic Potential of Dedifferentiated Rat Chondrocytes Reevaluated in Two- and Three-Dimensional Culture Conditions. *Tissue Eng. Regen. Med.* **2017**, *15*, 163–172. [CrossRef] [PubMed]
32. Ng, J.; Wei, Y.; Zhou, B.; Burapachaisri, A.; Guo, X.E.; Vunjak-Novakovic, G. Extracellular matrix components and culture regimen selectively regulate cartilage formation by self-assembling human mesenchymal stem cells in vitro and in vivo. *Stem Cell Res. Ther.* **2016**, *7*, 183. [CrossRef] [PubMed]
33. Estes, B.; Guilak, F. Three-Dimensional Culture Systems to Induce Chondrogenesis of Adipose-Derived Stem Cells. *Breast Cancer* **2011**, *702*, 201–217. [CrossRef]
34. Liu, C.F.; Angelozzi, M.; Haseeb, A.; Lefebvre, V. SOX9 is dispensable for the initiation of epigenetic remodeling and the activation of marker genes at the onset of chondrogenesis. *Development* **2018**, *145*, 164459. [CrossRef] [PubMed]
35. Ma, L.; Gao, C.; Mao, Z.; Zhou, J.; Shen, J.; Hu, X.; Han, C. Collagen/chitosan porous scaffolds with improved biostability for skin tissue engineering. *Biomaterials* **2003**, *24*, 4833–4841. [CrossRef]
36. She, H.; Xiao, X.; Liu, R. Preparation and characterization of polycaprolactone-chitosan composites for tissue engineering applications. *J. Mater. Sci.* **2007**, *42*, 8113–8119. [CrossRef]
37. Szychlinska, M.A.; Castrogiovanni, P.; Trovato, F.M.; Nsir, H.; Zarrouk, M.; Furno, D.L.; Di Rosa, M.; Imbesi, R.; Musumeci, G. Physical activity and Mediterranean diet based on olive tree phenolic compounds from two different geographical areas have protective effects on early osteoarthritis, muscle atrophy and hepatic steatosis. *Eur. J. Nutr.* **2018**, *58*, 565–581. [CrossRef]
38. Szychlinska, M.; Imbesi, R.; Castrogiovanni, P.; Guglielmino, C.; Ravalli, S.; Di Rosa, M.; Musumeci, G. Assessment of Vitamin D Supplementation on Articular Cartilage Morphology in a Young Healthy Sedentary Rat Model. *Nutrients* **2019**, *11*, 1260. [CrossRef]
39. Ye, J.; Coulouris, G.; Zaretskaya, I.; Cutcutache, I.; Rozen, S.G.; Madden, T. Primer-BLAST: A tool to design target-specific primers for polymerase chain reaction. *BMC Bioinform.* **2012**, *13*, 134. [CrossRef]
40. Livak, K.J.; Schmittgen, T.D. Analysis of relative gene expression data using real-time quantitative PCR and the 2(-Delta Delta C(T)) Method. *Methods* **2001**, *25*, 402–408. [CrossRef]
41. Szychlinska, M.A.; Calabrese, G.; Ravalli, S.; Parrinello, N.L.; Forte, S.; Castrogiovanni, P.; Pricoco, E.; Imbesi, R.; Castorina, S.; Leonardi, R.; et al. Cycloastragenol as an Exogenous Enhancer of ChondrogenicDifferentiation of Human Adipose-Derived Mesenchymal Stem Cells. A Morphological Study. *Cells* **2020**, *9*, 347. [CrossRef] [PubMed].
42. Castrogiovanni, P.; Di Rosa, M.; Ravalli, S.; Castorina, A.; Guglielmino, C.; Imbesi, R.; Vecchio, M.; Drago, F.; Szychlinska, M.A.; Musumeci, G. Moderate Physical Activity as a Prevention Method for Knee Osteoarthritis and the Role of Synoviocytes as Biological Key. *Int. J. Mol. Sci.* **2019**, *20*, 511. [CrossRef] [PubMed].

5 Immunohistochemical evaluation of autotaxin and lubricin in mild osteoarthritic rat model performing moderate physical activity

Silvia Ravalli [a], Federico Roggio [a], Benedetta Magrì [a], Giovanni Lauretta [a], Giuseppe Broggi [b] Rosario Caltabiano [b], Giada Maria Vecchio [b], Gaetano Magro [b], Carla Loreto [a], Alessandro Castorina [c,d], Giuseppe Musumeci [a,e,]*

[a]Department of Biomedical and Biotechnological Sciences, Anatomy, Histology and Movement Sciences Section, School of Medicine, University of Catania, 95123 Catania, Italy;

[b] Department "G.F. Ingrassia," Section of Anatomic Pathology, University of Catania, Catania, Italy

[c] Laboratory of Cellular and Molecular Neuroscience (LCMN), School of Life Sciences, Faculty of Science, University of Technology Sydney, Sydney, NSW 2007, Australia

[d] Laboratory of Neural Structure and Function, School of Medical Science (Neuroscience), University of Sydney, Sydney, NSW 2006, Australia

[e]Research Center on Motor Activities (CRAM), University of Catania, 95123 Catania, Italy

*Correspondence: g.musumeci@unict.it; Tel.: +095-378-2036

Acta Histochem. 2022;124(6):151936. doi: 10.1016/j.acthis.2022.

5.1 Introduction

Molecular homeostasis of the cartilage tissue is based on structural integrity of chondrocytes and their milieu, which are subjected to biomechanical and biochemical stresses (Martínez-Moreno et al., 2019). Imbalances in the physiological anabolic and metabolic processes within the tissue could lead to loss of cytoarchitecture and biomechanical properties of the cartilage that could, in turn, eventually degenerate in osteoarthritis (OA) (Man and Mologhianu, 2014; Musumeci et al., 2012). This latter is a widely common pathology, which is a serious reason for disability among older people and that represents a high burden for worldwide society in terms of healthcare cost (Neogi, 2013). OA is a progressive joint disease that induces several changes in all joint structures prompt by a contribution of biomechanical, genetic and ageing factors (Chen et al., 2017). Although the etiology of OA is still uncertain, inflammation and apoptosis are two main key elements which have been linked to extracellular matrix (ECM) disrupting which will eventually result in the weaking and degradation of articular tissue, remodeling of subchondral bone, followed by the typical pathological signs which include articular pain, swelling, early morning stiffness, and ultimately impairment (Mora et al., 2018; Loreto et al., 2009). Since no specific resolutive treatment is currently available, a progressively higher number of researches has recently posed the attention on molecules that could potentially be used in clinical practice. Disease- modifying osteoarthritis drugs (DMOADs) are a class of agents which are presumed to act on the key mechanisms involved in OA to prevent further structural damages and therefore improve its symptoms (Zhang et al., 2021b). DMOADs can be more target-specific than current drugs for OA, aiming specifically at the cartilage, synovium or subchondral bone. Since their administration can occur through local injection, efficacy and reduction of side effects would be improved (Oo et al., 2021). Some examples can be found in the use of injectable small molecules as inhibitors of the WNT pathway and matrix metalloproteinases (MMPs), human platelet rich plasma (PRP), Sprifermin (recombinant human fibroblast growth factor 18, rhFGF-18) and bone morphogenic protein 7 (BMP-7) (Chen et al., 2021; Schulze-Tanzil, 2021). At present, regulatory agencies have not yet licensed DMOADs for clinical use but several potential molecules are under clinical investigation, e.g. in advanced phase of trial (phase II/III) (Makarczyk et al., 2021). Considerable evidence suggests that plasma and synovial fluid levels of enzyme ATX (ENPP2) are increased in OA patients (Mabey et al., 2015, Chou et al., 2021). ATX is a glycoprotein with lyosophosopholipase D activity, able to convert lysophosphatidylcholine (LPC) to lysophosphatidic acid (LPA). This latter activates multiple signaling pathways, including proinflammatory signaling (Jones et al., 2016; Zhang et al., 2021a; Hayashi et al., 2013). This enzyme is a 125 kDa protein with two N-terminal somatomedin B-like domains, a central phosphodiesterase domain, and a catalytically

inactive nuclease-like domain on the C-terminal region (Yuelling, Fuss, 2008.). Five main isoforms (ATXα– ε) are described and distributed in different tissues, according to different alternative splicing forms of the gene. All the five ATX isoforms have the lyosophosopholipase D activity, although ATXβ and ATXδ are the most distributed and stable isoforms. ATXβ presents the deletion of exons 12 and 21 enriched in human peripheral tissues, ATXγ the deletion of exon 12 and is widely expressed in the central nervous system. ATXα, in which exon 21 is deleted, is expressed in the nervous system and peripheral tissues. ATXδ and ATXε show four amino acid deletions in the L2 linker region of ATXβ and ATXα, respectively. (Zhang et al., 2021a). In the catalytic domain, two zinc ions coordinate with residues of aspartic acid and histidine where a threonine alcohol represents the nucleophile. The lipophilic structures are accommodated in a large hydrophobic pocket (Jones et al., 2016). ATX inhibitors, like cyclic phosphatidic acid (cPA) and its analog carbacyclic phosphatidic acid (ccPA), were able to reduce pain in vivo in acute and chronic models, by inhibiting the cleavage of LPC in loco (Kakiuchi et al., 2011). Mice lacking LPA receptors (LPA1, LPA3 and LPA5) were observed to resist to neuropathic pain following injury in the peripheral nerve (Thirunavukkarasu et al., 2017). Therefore, ATX has been considered to be able to upregulate inflammatory molecules and MMPs, involved in OA progression and participate in neuropathic pain (Thirunavukkarasu et al., 2017; Datta et al., 2019; Abdel-Magid, 2014).

In the present research, we conducted morphological analysis of three regions of interest in rats with surgically-induced mild OA, i.e. articular cartilage in femur, tibia and patella, to evaluate the presence and expression of ATX. In addition, we also aimed to understand the effect of moderate physical exercise on the expression levels of ATX and Lubricin. This latter is a glycoprotein able to lubricate the articular surfaces, protecting the tissue and reducing inflammation in damaged articular cartilage (Ravalli et al., 2020; Musumeci et al., 2013; Leonardi et al., 2012; Iqbal et al., 2016). During OA, reduction in lubricin expression has been linked to the inflammatory processes following degeneration and trauma of cartilage. As a matter of fact, lubricin expression shows an inverse relationship to inflammation. This has been investigated in chondrocyte cell culture and cartilage explant systems suggesting that pro-inflammatory cytokines (e.g. TNF-α and IL-1β), proteolytic enzymes, like procathepsin-B, neutrophil-derived enzymes and MMPs concur to its downregulation. The mechanism by which these factors regulate lubricin and the relationship between lubricin and inflammation remains to be identified. On the other hand, it has been observed that as lubricin levels decrease, inflammation increases suggesting that lubricin may play an indirect role in inhibiting inflammation within the joint. (Musumeci et al., 2014; Iqbal et al., 2016). For this reason, we considered these two molecules as indicative, respectively, of the damage and the health of the cartilage. Our aim is to provide new insights about the involvement of ATX and Lubricin in the

homeostasis of cartilage integrity and pathogenesis of OA, as potential therapeutic targets and biomarkers, and investigate the role of exercise on their expressions.

5.2 Materials and methods

5.2.1 Ethical approval

Animal care and handling were conducted at the Center for Advanced Preclinical In Vivo Research (CAPIR), University of Catania. The guidelines of the Institutional Animal Care and Use Committee (I.A. C.U.C.) of the University of Catania (Approved protocol n. 2112015-PR of the 14.01.2015, Italian Ministry of Health) have been strictly followed. All the procedures were carried out in accordance with the EU Directive 2010/63/EU, as well as the Italian law (D.Lgs. 26/2014).

5.2.2 Animals: housing and breeding

3-month-old healthy male Wistar outbred rats, purchased from Charles River Laboratories, Milan, Italy, with a bodyweight of 250 ± 20 g, were used in the experiment. Rats were housed in polycarbonate cages (10.25″ W X 18.75″ D X 8″H) in stable hygrometric and thermic conditions (20-23 °C) on 12 h light/dark cycle. Water and food could be accessed ad libitum, during the entire period of the study. The rats were fed standard chow: carbohydrates (40%), proteins providing the essential amino acids (30%), and lipids (30%). Lipids consisted in neutral, saturated, and unsaturated fatty acids. The chow was purchased from the Laboratorio Dottori Piccioni, Gessate (Milan), Italy. Twenty-four rats were involved, equally and randomly distributed into four groups: control rats (CTRL), rats developing surgical-induced osteoarthritis (OA), rats developing surgical-induced osteoarthritis and subjected to physical exercise for 12 weeks after the surgery (OAPA), healthy rats subjected to physical exercise for 12 weeks (PA). The number of the rats was calculated in accordance with the 3Rs principles and the resource equation approach. Each procedure was conducted with respect of their suffering (Castrogiovanni et al., 2019). Movement in the cages was free and their health was monitored through objective observation and daily controls (weight, claudication, fur and eyes appearance, consumption of food and water, lethargy) (Castrogiovanni et al., 2019). When 5-month-old, anterior cruciate ligament transection (ACLT) was surgically performed in accordance with a previously adopted protocol in order to induce mild OA (Castrogiovanni et al., 2019) (Table 1). Multiple measurements of cartilage thickness in different points of cartilage were detected in all groups and the semi-quantitative grading criteria of macroscopic Kraus' modified Mankin score (Ostergaard et al., 1997) and microscopic histopathology OARSI system (Gerwin et al., 2010) were

used. The Kraus' modified Mankin score provides grades from 0 to 4: Grade 0, normal cartilage; Grade 1, minimal articular damage; Grade 2, articular cartilage damage affecting up to 30% of the articular surface; Grade 3, loss of up to 50% of the articular cartilage; Grade 4, severe loss of cartilage affecting more than 50% of the articular surface. The Histopathology OARSI system provides grades from 0 to 6: Grade 0, normal articular cartilage; Grade 1, intact surface; Grade 2, surface discontinuity; Grade 3, vertical fissures extending into mid zone; Grade 4, erosion; Grade 5, denudation; Grade 6, deformation. After the surgery, rats were free to move in their cages without operating joint immobilization. After 12 weeks of the in vivo phase of the study, the rats were sacrificed by lethal injection of anesthetic overdose using a mixture of Zoletil 100 (Virbac, Milan, Italy) at a dose of 80 mg/kg and Dexdomitor (Virbac, Milan, Italy) at a dose of 50 mg/kg. Femurs, tibia and patellae were therefore explanted, cleaned of soft tissues and used to proceed with immunohistochemical analysis.

Groups	H&E histological evaluation	Kraus' Modified Mankin Score	Histopathology OARSI System Score
CTRL	Articular cartilage showed normal cytoarchitecture. Cells appeared flat and small in the superficial zone; chondrocytes displayed a columnar organization in the middle and deep zone; the tidemark was evident; cartilage thickness measured 383.0 ± 76.76.	0.76 ± 0.87	0.82 ± 0.76
OA	Articular cartilage presented structural alterations in the superficial and middle zones and chondrocytes were poorly organized in columns in the intermediate and deep zones; a reduction of thickness was observed (260.7 ± 62.34 µm) and the difference was statistically significant when compared with both Group CTRL and PA ($p < 0.0001$).	2.5 ± 0.83	3.25 ± 0.71
OAPA	Better general tissue preservation was observed in comparison with Group OA, where the articular cartilage showed a slight but not statistically significant reduction in thickness (357.9 ± 61.88 µm) when compared with CTRL ($p \geq 0.05$, ns). The cartilage also showed a reduced number of cells.	1.32 ± 0.76	1.32 ± 0.78
PA	Articular cartilage showed normal cytoarchitecture. Cells appeared flat and small in the superficial zone; chondrocytes displayed a columnar organization in the middle and deep zone; the tidemark was evident; cartilage thickness measured 396.5 ± 61.68 µm.	0.85 ± 0.90	0.83 ± 0.73.

Table.1. Hematoxylin & Eosin (H&E) staining in articular cartilage samples, histomorphometric analysis, Kraus' Modified Mankin Score and Histopathology OARSI System Score were used to verify the onset of experimentally induced early OA and have been published in detail in our previous work on the same colony of rats (Castrogiovanni et al., 2019).

5.2.3 Treadmill training

Rats belonging to OAPA and PA groups were subjected to moderate physical activity by the use of a treadmill for 12 weeks (2Biological instrument, Varese, Italy). Rats became familiar with the treadmill by running for 5 days prior to surgery at a speed of 10 m/min. The following protocol was administered to stimulate the movement of flexion-extension of the limbs. The rats performed in the treadmill 3 days a week and, to adapt the exercise to the time-dependent ability of the animals, the speeds and the durations were progressively augmented from 5 m/minute for 5 min in week 1–20 m/min for 25 min in week 12 (Castrogiovanni et al., 2019). The treadmill was gradually inclined between 2° and 6° degrees (type of exercise: interval training, between mild and moderate). A minimal electric shock (0.2 mA) was employed to train and encourage the running. All-electric shock bouts were monitored in real-time and stored by the built-in data acquisition software (2Biological instrument). A maximum of five electric bouts in one session was considered the limit amount for the rat prior to be suspended from the physical activity for their safety.

5.2.4 Immunohistochemistry

Bone samples were explanted, cleaned from soft tissues in phosphate-buffered saline (PBS, Bio-Optica, Milano, Italy), fixed in 10% buffered-formalin (Bio-Optica, Milan, Italy) for 24 h at room temperature and decalcified in TBD-2 decalcifier (ThermoShandon, Pittsburg, PA, USA) according to the manufacturing protocol. After an overnight wash, procedures of dehydration in graded ethanol (Bio-Optica, Milan, Italy), cleaning in xylene (Bio-Optica, Milan, Italy) and paraffin- embedded (Bio-Optica, Milan, Italy) followed, while preserving the desired anatomical orientation. Slides of 5 μm thickness were obtained by the microtome from the paraffin blocks and processed for immunohistochemical analysis. The slides were dewaxed in xylene, hydrated through graded ethanol solutions, and heated (5 min × 3) in polypropylene case with citrate buffer—pH 6 (pH 6.0; Bio-Optica, Milan, Italy), by a microwave oven (750 W, LG Electronics Italia S.p.A., Milan, Italy) to unmask antigenic sites. Therefore, slides underwent incubation for 30 min in 0.3% H2O2/PBS to quench endogenous peroxidase activity and washing for 20 min in PBS (Bio-Optica, Milan, Italy). After blocking, the sections were incubated overnight at + 4 °C with rabbit monoclonal anti-ATX antibody (1:100; Invitrogen, Thermo Fisher Scientific) and rabbit polyclonal anti-Lubricin antibody (1:100; Abcam). After immune complex formation, biotinylated link antibodies were added (horseradish peroxidase polymer (HRP)-conjugated anti-rabbit and anti-mouse were used as secondary antibodies) and therefore conjugated with peroxidase-labeled streptavidin, via incubation for 10 min at room temperature (LSAB + System-HRP, K0690, Dako, Glostrup, Denmark). Immunoreactivity was

obtained by treating the sections for 2 min in 0.1% 3,3′-diaminobenzidine (DAB) (DAB substrate Chromogen System; Dako, Glostrup, Denmark). The slides were counterstained with Mayer's hematoxylin (Histolab Products AB, Goteborg, Sweden) and mounted in ¨ Glycerol Vinyl Alcohol (GVA) (Zymed Laboratories, San Francisco, CA, USA). An Axioplan Zeiss light microscope (Carl Zeiss, Oberkochen, Germany) and a digital camera (AxioCam MRc5, Carl Zeiss, Oberkochen, Germany) were used to observe and photograph the slides.

5.2.5 Computerized densitometric measurements and image analysis

A software of digital image analysis (AxioVision Release 4.8.2-SP2 Software, Carl Zeiss Microscopy GmbH, Jena, Germany) was used to quantify positive staining of anti-ATX and anti-Lubricin. Five representative fields, 20x magnification, scattered in the preparation were selected from each section on the basis of tissue integrity, cleanliness and area of interest. Staining segmentation phase was based on automatic brown detection in the entire image and, where present, the artifacts were manually excluded by the four blinded investigators (two anatomical morphologists, one histopathologist and one histologist) which evaluated the images. Statistical results were expressed as staining intensity ($pixel^2$)/($pixel^2$) of immunostaining on cartilage tissue. The staining intensity of the DAB was normalized by total tissue area. Four blinded investigators (two anatomical morphologists, one histopathologist and one histologist) evaluated the images.

5.2.6 Statistical analysis

Statistical analysis was performed by GraphPad Instat® Biostatistics version 8.0 software (GraphPad Software, Inc. La Jolla, CA, USA). The sample size calculation was reached through the resource equation approach, including minimum and maximum sample sizes, because it was not possible to assume standard deviation and effect size. Based on this approach, the acceptable range of degrees of freedom (DF) for the error term in an analysis of variance (ANOVA) is between 10 and 20. For one-way ANOVA, the between-subject error DF (that is, the within- subject DF) is calculated as: DF = N – k = kn – k = k(n – 1), where N = total number of subjects, k = number of groups, and n = number of subjects per group (Arifin and Zahiruddin, 2017). In this study the sample sizes per group are Minimum n = 10/4 + 1 = 3.5 = rounded up to 4 animals/group Maximum n = 20/4 + 1 = 6 animals/group. The total sample sizes are: Minimum N = Minimum n x 4 = 4 × 4 = 16 animals, Maximum N = Maximum n x 4 = 6 × 4 = 24 animals, therefore 6 animals/group were used for a total of 24 animals. Data were tested for normality with the Kolmogorov–Smirnov and Shapiro-Wilk test. All variables were normally distributed. Differences between experimental groups were evaluated by

using one-way ANOVA followed by Tukey's multiple comparison post hoc test. P-values lower than 0.05 ($p < 0.05$) were statistically significant; p-values lower than 0.01 ($p < 0.01$) were highly statistically significant. Data are showed as mean±SD. Cohen's κ was used to evaluate the agreement between the blinded researchers.

5.3 Results

5.3.1 Histochemistry of ATX

In this work, positive immunostainings for ATX were compared between the four groups: CTRL, OA, OAPA, PA, in the three tissue samples (femur, tibia, and patella). Statistical results are presented as mean±SD of the staining intensity (pixel^2)/(pixel^2) of ATX immunostaining on the total area of the cartilaginous tissues. In the femur, ATX labeling analysis shows a statistically significant increase in its expression in OA ($5{,}2 \times 10^{-3} \pm 2{,}2 \times 10^{-3}$ (pixel^2)/(pixel^2)) vs. CTRL ($2{,}1 \times 10^{-3} \pm 1{,}9 \times 10^{-4}$ (pixel^2)/(pixel^2)) (* $p < 0.05$), vs. OAPA ($2{,}2 \times 10^{-3} \pm 2{,}4 \times 10^{-3}$ (pixel^2)/(pixel^2)) (* $p < 0.05$) and PA ($2{,}3 \times 10^{-3} \pm 1{,}1 \times 10^{-3}$ (pixel^2)/ (pixel^2)) (* $p < 0.05$). No other differences considered significant were highlighted between groups (Fig. 1O). In the tibia, ATX labeling analysis indicates a statistically significant increase in its expression in OA ($4{,}1 \times 10^{-3} \pm 2{,}5 \times 10^{-3}$ (pixel^2)/(pixel^2)) vs. CTRL ($1 \times 10^{-3} \pm 0{,}28 \times 10^{-3}$ (pixel^2)/(pixel^2)) (* $p < 0.05$) and vs. PA ($1{,}1 \times 10^{-3} \pm 0{,}5 \times 10^{-3}$(pixel^2)/(pixel^2)) (* $p < 0.05$). Densitometric values for ATX in OAPA, in the tibia, was $2{,}3 \times 10^{-3} \pm 0{,}72 \times 10^{-3}$ (pixel^2)/(pixel^2). No other statistically significant differences were highlighted between groups (Fig. 1P). In the patella, densitometric values for ATX were CTRL ($0{,}85 \times 10^{-3} \pm 0{,}66 \times 10^{-3}$ (pixel^2)/(pixel^2)), OA ($1{,}6 \times 10^{-3} \pm 1 \times 10^{-3}$ (pixel^2)/(pixel^2)), OAPA ($1{,}6 \times 10^{-3} \pm 0{,}54 \times 10^{-3}$ (pixel^2)/(pixel^2)) and PA ($0{,}51 \times 10^{-3} \pm 0{,}18 \times 10^{-3}$ (pixel^2)/(pixel^2)) (Fig. 1Q). No statistically significant differences were highlighted between groups.

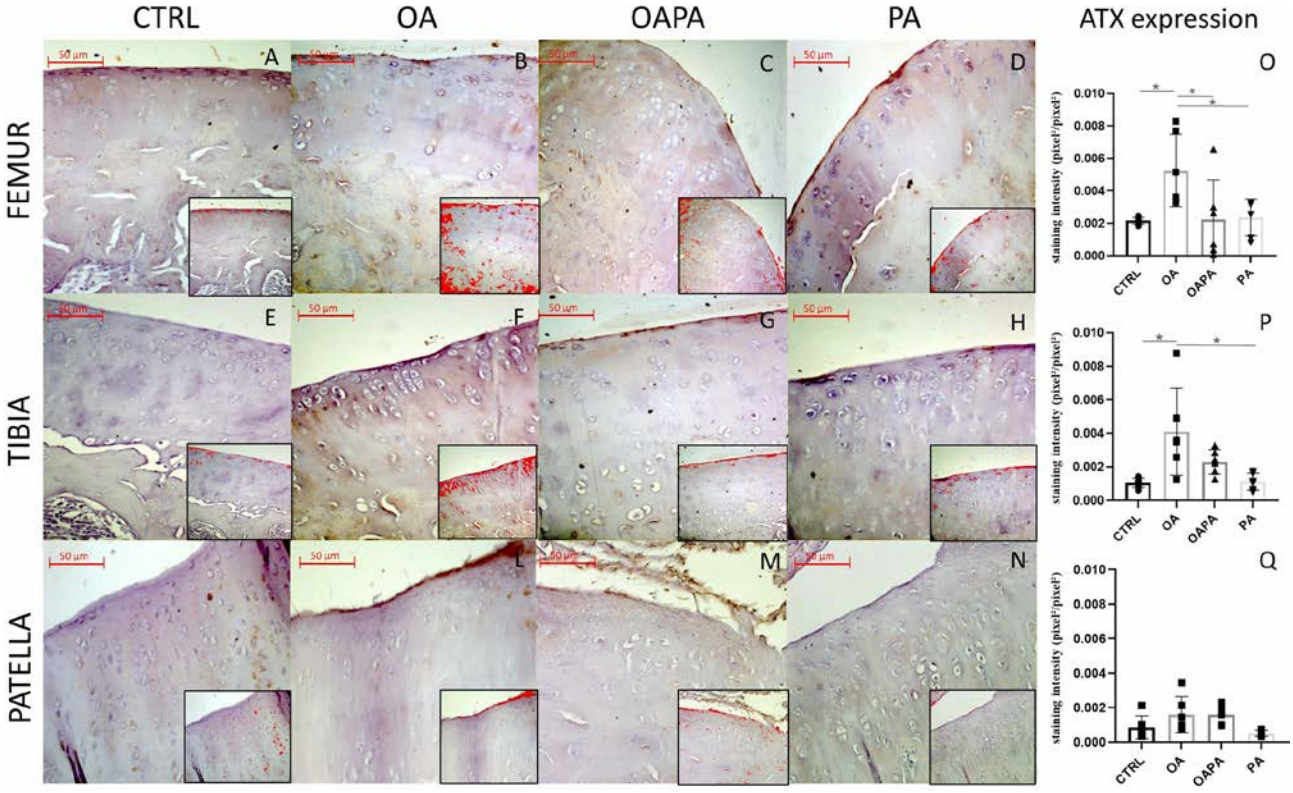

Figure.1. ATX immunostaining (A-N). Representative images of ATX immunostaining for cartilaginous tissue in femur condyles (**A-D**), tibia (**E-H**) and patella (**I-N**) in CTRL (**A, E, I**), OA (**B, F, L**), OAPA (**C, G, M**) and PA (**D, H, N**). (**O-Q**) Statistical analysis of ATX expression and comparison between groups in femur (**O**), tibia (**P**) and patella (**Q**). Each point on the graphs represents a different animal. Five representative fields scattered in the preparation were selected from three different slides for each animal. 20x magnification, scale bars: 50 µm.

5.3.2 Histochemistry of lubricin

In this work, positive immunostainings for Lubricin were compared between the four groups (CTRL, OA, OAPA, PA) in the three tissue samples (femur, tibia, and patella). Statistical results are presented as mean±SD of the staining intensity (pixel^2)/(pixel^2) of Lubricin immunostaining on the total area of the cartilaginous tissues. In the femur, Lubricin labeling analysis shows a statistically significant decrease in its expression in OA ($14 \times 10^{-3} \pm 4{,}8 \times 10^{-3}$ (pixel^2)/(pixel^2)) vs. CTRL ($34 \times 10^{-3} \pm 8{,}7 \times 10^{-3}$ (pixel^2)/(pixel^2)) (* $p < 0.05$) and vs. PA ($34 \times 10^{-3} \pm 17 \times 10^{-3}$ (pixel^2)/(pixel^2)) (* $p < 0.05$). Densitometric values for Lubricin in OAPA, in the femur, was $20 \times 10^{-3} \pm 1{,}9 \times 10^{-3}$ (pixel^2)/(pixel^2). No other differences considered significant were highlighted between groups (Fig. 2O). In the tibia, Lubricin labeling analysis indicates a statistically significant decrease in its expression in OA ($8{,}3 \times 10^{-3} \pm 5{,}1 \times 10^{-3}$ (pixel^2)/(pixel^2)) vs. CTRL ($21 \times 10^{-3} \pm 11 \times 10^{-3}$ (pixel^2)/(pixel^2)) (* $p < 0.05$) and in OAPA ($8{,}2 \times 10^{-3} \pm 2 \times 10^{-3}$ (pixel^2)/(pixel^2)) vs. CTRL ($21 \times 10^{-3} \pm 11 \times 10^{-3}$ (pixel^2)/ (pixel^2)) (* $p < 0.05$). Densitometric values for Lubricin in PA, in the tibia, was $11 \times 10^{-3} \pm 4{,}2 \times 10^{-3}$ (pixel^2)/(pixel^2). No other statistically significant differences were highlighted between groups (Fig. 2P). In the patella, Lubricin labeling analysis indicates a statistically significant decrease in its expression in OA ($4{,}5 \times 10^{-3} \pm 2{,}1$

$\times 10^{-3}$ (pixel^2)/ (pixel^2)) vs. CTRL (26 $\times 10^{-3} \pm 10 \times 10^{-3}$ (pixel^2)/(pixel^2)) (* $p < 0.05$). Densitometric values for Lubricin in OAPA was $22 \times 10^{-3} \pm 15 \times 10^{-3}$ (pixel^2)/(pixel^2) and in PA was $20 \times 10^{-3} \pm 14 \times 10^{-3}$ (pixel^2)/(pixel^2). No other statistically significant differences were highlighted between groups (Fig. 2Q). Negative controls were used to determine the baseline for the analysis and to further validate staining specificity (Fig. 3).

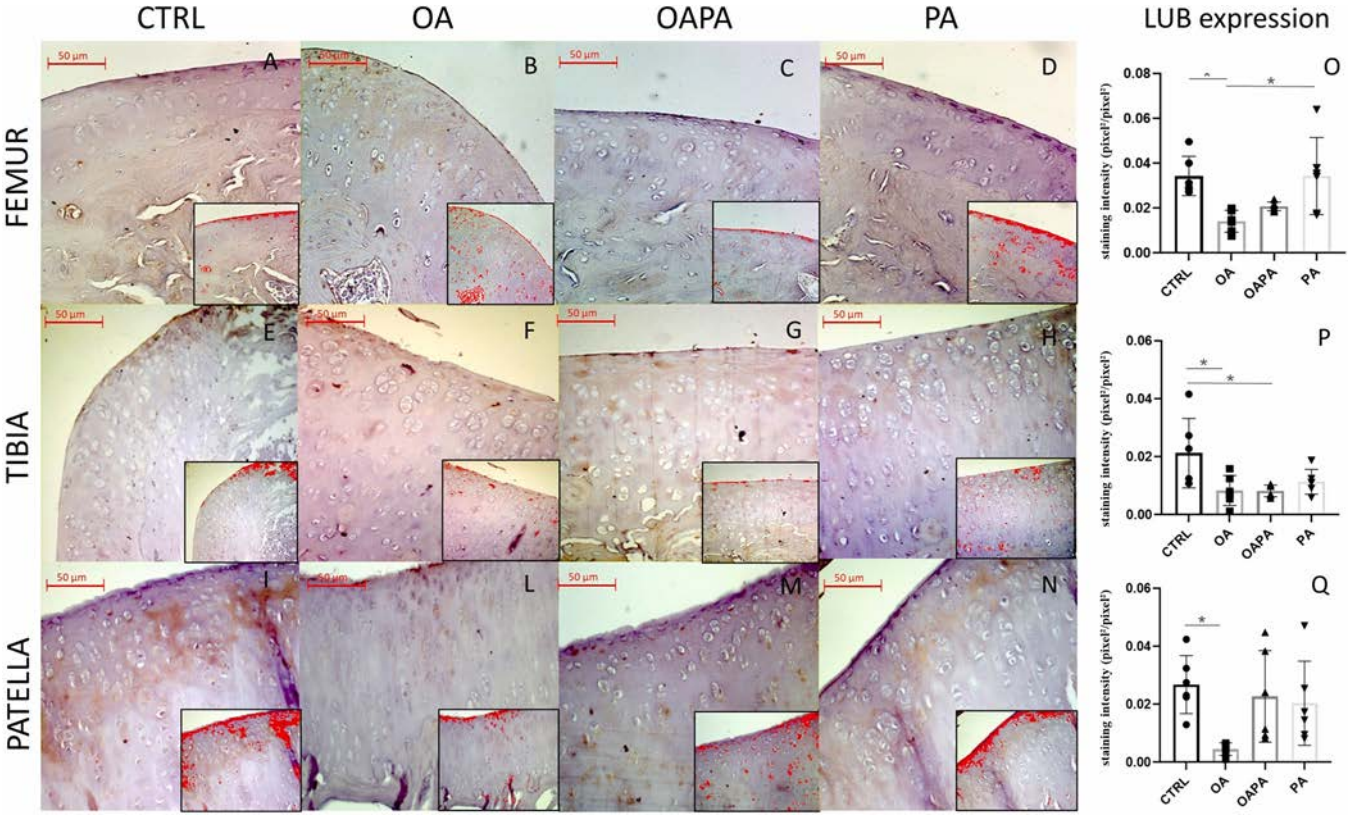

Figure 2. Lubricin immunostaining (A-N). Representative images of Lubricin immunostaining for cartilaginous tissue in femur (**A-D**), tibia (**E-H**) and patella (**I-N**) in CTRL (**A, E, I**), OA (**B,F,L**), OAPA (**C,G,M**) and PA (**D,H,N**). (**O-Q**) Statistical analysis of Lubricin expression and comparison between groups in femur (**O**), tibia (**P**) and patella (**Q**). Each point on the graphs represents a different animal. Five representative fields scattered in the preparation were selected from three different slides for each animal. 20x magnification, scale bars: 50 µm.

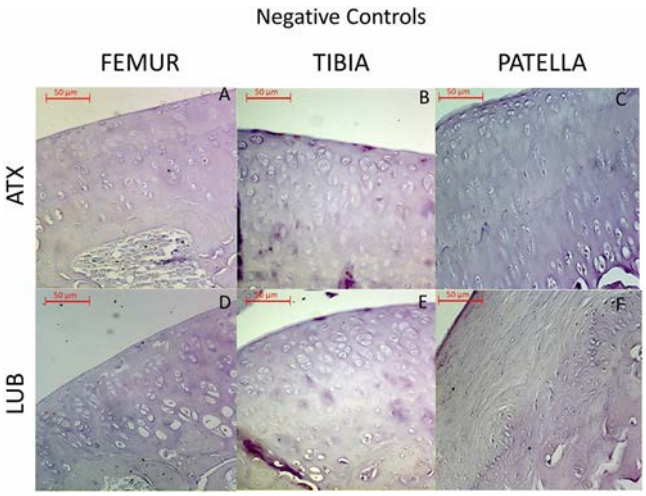

Figure 3 Negative controls (A-F). Representative images of negative staining for ATX (**A-C**) and Lubricin (**D-F**) in femur (**A, D**), tibia (**B, E**) and patella (**C,F**). Five representative fields scattered in the preparation were selected from three different slides for each animal. 20x magnification, scale bars: 50 µm.

5.4 Discussion

The therapeutic options for the treatment of OA still suffer from limitations, therefore extensive efforts have been made to identify novel genes and biomarkers that can characterize pathological imbalances and disease progression (Bernotiene et al., 2020). Understanding the molecular mechanisms that regulate function of articular chondrocyte as well as that of all the main players involved in the onset of osteoarthritic metabolic changes is paramount in the clinical setting and in tissue engineering. The expression of ATX and Lubricin in the hyaline cartilage of three components of the knee joint (femur, tibia and patella) was the object of this study performed on OA rats. In addition, we also observed the effect of exercise aimed at encouraging the movement of the lower limbs and improving pathological condition. Radiographic and symptomatic severity of knee OA have been correlated with ATX concentrations in the synovial fluid and plasma of patients (Mabey et al., 2015). This molecule appears to participate in systemic and local manifestation of OA, although it does not directly affect cellular activity. It leads to the synthesis of the phospholipid LPA which actively binds LPA receptors in the cell membrane. LPA is involved in macrophagic migration towards OA tissues (Miyabe et al., 2013), in the regulation of bone remodeling (David et al., 2014) and in the increase of expression of angiogenic factors and vascular endothelial growth factor (VEGF) through Gi/NF-κB pathway (Chuang et al., 2014). Consistent with its inflammatory contribution, genetic suppression of ATX in mesenchymal cells leads to pathological attenuation in mice model of OA, suggesting that ATX/LPA axis could represent a target in the disease (Nikitopoulou et al., 2021;

Datta et al., 2020). Inhibition of ATX has also been linked to reduced pain in animal model of the pathology (Thirunavukkarasu et al., 2017), as well as lower synovitis and cartilage degeneration, therefore leading to enhanced chondrocyte survival and lower catabolic activity, like MMPs-mediated type II collagen breakdown (Datta et al., 2020). In this study, statistical analysis of the staining intensity of ATX expression showed that it was significantly increased in articular cartilage of femur and tibia of OA rats in respect to healthy controls (* $p < 0.05$) (Fig. 1O and P), while no differences were evidenced in the patella (Fig. 1Q). These results suggest that the molecule could be involved during the imbalances within the cartilage in presence of mild OA and that could be an indicator of degenerative processes. Inversely, statistical analysis of the staining intensity of Lubricin showed similar expression patterns in femur, tibia and patella, reporting significant lower expression of the molecule in OA groups vs healthy CTRLs (* $p < 0.05$) (Fig. 2O-Q). This observation is in line with the current literature that suggests Lubricin role in maintaining joint integrity, preventing tissue breakdown and lowering the extent of friction between the articular surfaces. For this reason, failing in Lubricin production might be participating in the progression of arthritic events (Szychlinska et al., 2016; Musumeci et al., 2011). Physical activity has showed to stimulate the production of Lubricin and therefore slow down degeneration processes, furthermore, sustaining chondroprotection (Ogawa et al., 2014; Musumeci et al., 2015). In the presented results, we did not find significant differences between OA and OAPA groups in Lubricin expression in femur, tibia, and patella (Fig. 2O-Q). It cannot be excluded that the loss of superficial zone could be linked to reduced detection of molecule, but since the used model for this experiment was early/mild OA, mainly characterized by structural alterations, poorly organization and reduction of thickness rather than great loss of tissue, we retain plausible that the difference noticed with the CTRL group could be addressed to the lack of production of Lubricin by the populating cells. Nevertheless, in the femur, OAPA group showed lower expression of ATX when compared to OA, suggesting that moderate physical activity would be able to reduce the expression of this inflammatory mediator at least in the femur cartilage (* $p < 0.05$) (Fig. 1O). We hypothesize that to induce a significant impact though physical activity in the osteoarthritic cartilage, exercise should be potentially administered for longer time or more intensely, and this should be listed among the limitations of the study. To summarize, higher expressions of ATX in femur and tibia of mild OA rats suggest that this molecule could participate in the progression of the degenerative disease, although not involved in the patella. In the femur, moderate physical activity performed by mild osteoarthritic rats was able to lower the expression of ATX, encouraging the evidence that joint movement could be beneficial for the cartilage, especially in pathological conditions. As opposed to ATX, physical activity did not increase Lubricin levels in OA rats, although its expression was lower in respect to CTRLs, in femur, tibia and patella. The preliminary results of

this basic and morphological study suggest that these two molecules may be affected by changes in the tissue environment under conditions of pathological alteration involving chondrocytes and ECM, and in response to an exercise regimen. According to the clinical study of Mabey et al. (2015) plasma and synovial fluid levels of ATX are correlated with severity of knee OA, moreover, Ludwig et al. (2012) showed that Lubricin concentration in synovial fluid is diminished in many patients with OA. Although the synovial fluid and plasma are compositionally different, the evaluation of the presence of these two molecules in biological fluids is necessary to translate from rat to human and may not necessarily reflect the results found in cartilage tissue. Therefore, to deepen our results, further research is needed to analyse the expression levels of these biomarkers in serological and synovial fluid and to cross-validate these results with other biomolecular assays. Furthermore, synovial fluid biomarkers, associated with radiographic imaging of the knee, could provide a molecular biological profile to identify the severity of OA and this represents the future perspective of this study.

5.5 Conclusions

OA management still requires several efforts in medical science. Indeed, the understanding of pathophysiological process at molecular level is fundamental in order to prospect therapeutical and pharmaceutical strategies. In this study, we highlighted a possible involvement of ATX in the pathological scenario of mild OA, the altered lubricating property of the joint, as well as the role of mechanical stimulation, i.e., moderate exercise, in reducing ATX expression in the femur. Our findings might encourage further studies on the potential usefulness of ATX and Lubricin, as biochemical markers of disease progression, and of exercise to prevent/attenuate the osteoarthritic process.

5.6 References

Abdel-Magid, A.F., 2014. Autotaxin inhibitors may treat pain and osteoarthritis. ACS Med. Chem. Lett. 5, 1072–1073. https://doi.org/10.1021/ml5003103.

Arifin, W.N., Zahiruddin, W.M., 2017. Sample size calculation in animal studies using resource equation approach. Malays. J. Med. Sci. 24, 101–105.

Bernotiene, E., Bagdonas, E., Kirdaite, G., Bernotas, P., Kalvaityte, U., Uzieliene, I., Thudium, C.S., Hannula, H., Lorite, G.S., Dvir-Ginzberg, M., Guermazi, A.,

Mobasheri, A., 2020. Emerging technologies and platforms for the immunodetection of multiple biochemical markers in osteoarthritis research and therapy. Front. Med. 7, 572977 https://doi.org/10.3389/fmed.2020.572977.

Castrogiovanni, P., Di Rosa, M., Ravalli, S., Castorina, A., Guglielmino, C., Imbesi, R., Vecchio, M., Drago, F., Szychlinska, M.A., Musumeci, G., 2019. Moderate physical activity as a prevention method for knee osteoarthritis and the role of synoviocytes as biological key. Int. J. Mol. Sci. 20.

Chen, D., Shen, J., Zhao, W., Wang, T., Han, L., Hamilton, J.L., Im, H.J., 2017.

Osteoarthritis: toward a comprehensive understanding of pathological mechanism. Bone Res. 5, 16044. https://doi.org/10.1038/boneres.2016.44.

Chen, T., Weng, W., Liu, Y., Aspera-Werz, R.H., Nüssler, A.K., Xu, J., 2021. Update on novel non-operative treatment for osteoarthritis: current status and future trends. Front. Pharmacol. 12, 755230 https://doi.org/10.3389/fphar.2021.755230.

Chuang, Y.W., Chang, W.M., Chen, K.H., Hong, C.Z., Chang, P.J., Hsu, H.C., 2014. Lysophosphatidic acid enhanced the angiogenic capability of human chondrocytes by regulating gi/nf-kb-dependent angiogenic factor expression. PLoS ONE 9, e95180.

Datta, P., Nakamura, S., Rossomacha, E., Endisha, H., Younan, C., Borada, K.H., Perry, K., Mahomed, N.N., Gandhi, R., Rockel, J., Kapoor, M., 2019. Attenuation of surgically-induced osteoarthritis (OA) by inhibition of autotaxin. Osteoarthr. Cartil. 27, S426–S427. https://doi.org/10.1016/j.joca.2019.02.446.

Datta, P., Gandhi, R.A., Nakamura, S., Lively, S., Rossomacha, E., Potla, P., Shestopaloff, K., Endisha, H., Pastrello, C., Jurisica, I., Rockel, J.S., Kapoor, M., 2020. Effect of autotaxin inhibition in a surgically-induced mouse model of osteoarthritis. Osteoarthr. Cartil. Open 2, 100080. https://doi.org/10.1016/j. ocarto.2020.100080.

David, M., Machuca-Gayet, I., Kikuta, J., et al., 2014. Lysophosphatidic acid receptor type 1 (LPA1) plays a functional role in osteoclast differentiation and bone resorption activity. J. Biol. Chem. 289, 6551–6564.

Gerwin, N., Bendele, A.M., Glasson, S., Carlson, C.S., 2010. The OARSI histopathology initiative—recommendations for histological assessments of osteoarthritis in the rat. Osteoarthr. Cartil. 18, S24–S34.

Hayashi, K., Piras, V., Tabata, S., et al., 2013. A systems biology approach to suppress TNF-induced proin-flammatory gene expressions. Cell Commun. Signal. 11, 84. https://doi.org/10.1186/1478-811X-11-84.

Iqbal, S., Leonard, C., C. Regmi, S., et al., 2016. Lubricin/proteoglycan 4 binds to and regulates the activity of toll-like receptors in vitro. Sci. Rep. 6, 18910. https://doi. org/10.1038/srep18910.

Jones, S.B., Pfeifer, L.A., Bleisch, T.J., Beauchamp, T.J., Durbin, J.D., Klimkowski, V.J., Hughes, N.E., Rito, C.J., Dao, Y., Gruber, J.M., Bui, H., Chambers, M.G., Chandrasekhar, S., Lin, C., McCann, D.J., Mudra, D.R., Oskins, J.L., Swearingen, C. A., Thirunavukkarasu, K., Norman, B.H., 2016. Novel auto-taxin inhibitors for the treatment of osteoarthritis pain: lead optimization via structure-based drug de-sign. ACS Med. Chem. Lett. 7, 857–861. https://doi.org/10.1021/ acsmedchemlett.6b00207.

Kakiuchi, Y., Nagai, J., Gotoh, M., Hotta, H., Murofushi, H., Ogawa, T., Ueda, H., Murakami-Murofushi, K., 2011. Antinociceptive effect of cyclic phosphatidic acid and its derivative on animal models of acute and chronic pain. Mol. Pain 7, 33. https://doi.org/10.1186/1744-8069-7-33.

Leonardi, R., Rusu, M.C., Loreto, F., Loreto, C., Musumeci, G., 2012. Immunolocalization and expression of lubricin in the bilaminar zone of the human temporomandibular joint disc. Acta Histochem. 114, 1–5. https://doi.org/10.1016/j.acthis.2010.11.011. Epub 2011 Sep 28. PMID: 21955422.

Loreto, C., Musumeci, G., Leonardi, R., 2009. Chondrocyte-like apoptosis in temporomandibular joint disc internal de-rangement as a repair-limiting mechanism. An in vivo study. Histol. Histopathol. 24, 293–298. https://doi.org/ 10.14670/HH-24.293. PMID: 19130398.

Ludwig, T.E., McAllister, J.R., Lun, V., Wiley, J.P., Schmidt, T.A., 2012. Diminished cartilage-lubricating ability of human osteoarthritic synovial fluid deficient in proteoglycan 4: Restoration through proteoglycan 4 supplementation. Arthritis Rheum. 64, 3963–3971. https://doi.org/10.1002/art.34674.

Mabey, T., Taleongpong, P., Udomsinprasert, W., Jirathanathornnukul, N., Honsawek, S., 2015. Plasma and synovial fluid autotaxin correlate with severity in knee osteoarthritis. Clin. Chim. Acta 444, 72–77. https://doi.org/10.1016/j. cca.2015.01.032.

Makarczyk, M.J., Gao, Q., He, Y., Li, Z., Gold, M.S., Hochberg, M.C., Bunnell, B.A.,

Tuan, R.S., Goodman, S.B., Lin, H., 2021. Current models for development of disease-modifying osteoarthritis drugs. Tissue Eng. Part C Methods 27, 124–138. https://doi.org/10.1089/ten.TEC.2020.0309.

Man, G.S., Mologhianu, G., 2014. Osteoarthritis pathogenesis - a complex process that involves the entire joint. J. Med. Life 7, 37–41.

Martínez-Moreno, D., Jim´enez, G., Galvez-Martín, P., Rus, G., Marchal, J.A., 2019. ´ Cartilage biomechanics: a key factor for osteoarthritis regenerative medicine. Biochim. Biophys. Acta Mol. Basis Dis. 1865, 1067–1075. https://doi.org/10.1016/j. bbadis.2019.03.011.

Miyabe, Y., Miyabe, C., Iwai, Y., 2013. Necessity of lysophosphatidic acid receptor 1 for development of arthritis. Arthritis Rheum. 65, 2037–2047.

Mora, J.C., Przkora, R., Cruz-Almeida, Y., 2018. Knee osteoarthritis: pathophysiology and current treat-ment modalities. J. Pain Res. 11, 2189–2196. https://doi.org/ 10.2147/JPR.S154002.

Musumeci, G., Loreto, C., Carnazza, M.L., Coppolino, F., Cardile, V., Leonardi, R., 2011. Lubricin is ex-pressed in chondrocytes derived from osteoarthritic cartilage encapsulated in poly (ethylene glycol) di-acrylate scaffold. Eur. J. Histochem. 55, e31 https://doi.org/10.4081/ejh.2011.e31.

Musumeci, G., Carnazza, M.L., Leonardi, R., Loreto, C., 2012. Expression of β-defensin-4 in "an in vivo and ex vivo model" of human osteoarthritic knee meniscus. Knee Surg. Sports Traumatol. Arthrosc. 20 (2), 216–222. https://doi.org/10.1007/s00167-011- 1630-x.

Musumeci, G., Loreto, C., Carnazza, M.L., Cardile, V., Leonardi, R., 2013. Acute injury affects lubricin expression in knee menisci: an immunohistochemical study. Ann. Anat. 195, 151–158. https://doi.org/10.1016/j.aanat.2012.07.010.

Musumeci, G., Trovato, F.M., Loreto, C., Leonardi, R., Szychlinska, M.A., Castorina, S., Mobasheri, A., 2014. Lubricin expression in human osteoarthritic knee meniscus and synovial fluid: a morphological, immunohistochemical and biochemical study. Acta Histochem. 116 (5), 965–972. https://doi.org/10.1016/j.acthis.2014.03.011.

Musumeci, G., Castrogiovanni, P., Trovato, F.M., Imbesi, R., Giunta, S., Szychlinska, M. A., Loreto, C., Castorina, S., Mobasheri, A., 2015. Physical activity ameliorates cartilage degeneration in a rat model of aging: A study on lubricin expression. Scand. J. Med. Sci. Sports 25, e222–e230.

Neogi, T., 2013. The epidemiology and impact of pain in osteoarthritis. Osteoarthr. Cartil. 21, 1145–1153. https://doi.org/10.1016/j.joca.2013.03.018.

Nikitopoulou, I., Oikonomou, N., Karouzakis, E., Sevastou, I., Nikolaidou-Katsaridou, N., Zhao, Z., et al., 2021. Autotaxin expression from synovial fibroblasts is essential for the pathogenesis of modeled arthritis. J. Exp. Med. 209, 925–933.

Ogawa, H., Kozhemyakina, E., Hung, H.H., Grodzinsky, A.J., Lassar, A.B., 2014. Mechanical motion promotes expression of Prg4 in articular cartilage via multiple CREB-dependent, fluid flow shear stress-induced signaling pathways. Genes Dev. 28, 127–139.

Oo, W.M., Little, C., Duong, V., Hunter, D.J., 2021. The development of disease- modifying therapies for osteoarthritis (DMOADs): the evidence to date. Drug Des. Dev. Ther. 15, 2921–2945. https://doi.org/10.2147/DDDT.S295224.

Ostergaard, K., Petersen, J., Andersen, C.B., Benutzen, K., Salter, D.M., 1997. Histologic/ histochemical grading system for osteoarthritic articular cartilage: reproducibility and validity. Arthritis Rheum. 40, 1766–1771.

Ravalli, S., Szychlinska, M.A., Lauretta, G., Di Rosa, M., Musumeci, G., 2020. Investigating lubricin and known cartilage-based biomarkers of osteoarthritis. Expert Rev. Mol. Diagn. 20, 443–452. https://doi.org/10.1080/ 14737159.2020.1733978.

Schulze-Tanzil, G., 2021. Experimental therapeutics for the treatment of osteoarthritis. J. Exp. Pharmacol. 2021 (13), 101–125. https://doi.org/10.2147/JEP.S237479.

Szychlinska, M.A., Trovato, F.M., Di Rosa, M., Malaguarnera, L., Puzzo, L., Leonardi, R., Castrogiovanni, P., Musumeci, G., 2016. Co-expression and co-localization of cartilage glycoproteins CHI3L1 and lu-bricin in osteoarthritic cartilage: morphological, immunohistochemical and gene expression profiles. Int. J. Mol. Sci. 17, 359. https://doi.org/10.3390/ijms17030359.

Thirunavukkarasu, K., Swearingen, C.A., Oskins, J.L., et al., 2017. Identification and pharmacological characterization of a novel inhibitor of autotaxin in rodent models of joint pain. Osteoarthr. Cartil. 25, 935–942. https://doi.org/10.1016/j.joca.2016.09.006.

Yuelling, L.M., Fuss, B., 2008. Autotaxin (ATX): a multi-functional and multi-modular protein possessing enzymatic lysoPLD activity and matricellular properties. Biochim. Biophys. Acta 1781, 525–530. https://doi.org/10.1016/j.bbalip.2008.04.009.

Zhang, X., Li, M., Yin, N., Zhang, J., 2021a. The expression regulation and biological function of autotaxin. Cells 10, 939. https://doi.org/10.3390/cells10040939.

Zhang, X.X., He, S.H., Liang, X., Li, W., Li, T.F., Li, D.F., 2021b. Aging, cell senescence, the pathogenesis and targeted therapies of osteoarthritis. Front. Pharmacol. 12, 728100 https://doi.org/10.3389/fphar.2021.728100.

6 Morphological Evidence of Telocytes in Skeletal Muscle Interstitium of Exercised and Sedentary Rodents

Silvia Ravalli[1], Concetta Federico[2], Giovanni Lauretta[1], Salvatore Saccone[2], Elisabetta Pricoco[1], Federico Roggio[1,3], Michelino Di Rosa[1], Grazia Maugeri[1] and Giuseppe Musumeci[1,4,5,]*

[1]Department of Biomedical and Biotechnological Sciences, Human, Histology and Movement Science Section, University of Catania, Via S. Sofia 87, 95123 Catania, Italy

[2]Department of Biological, Geological and Environmental Sciences, Section of Animal Biology, University of Catania, Via Androne 81, 95124 Catania, Italy

[3]Department of Psychology, Educational Science and Human Movement, University of Palermo, Via Giovanni Pascoli 6, 90144 Palermo, Italy

[4]Research Center on Motor Activities (CRAM), University of Catania, Via S. Sofia 97, 95123 Catania, Italy

[5]Department of Biology, College of Science and Technology, Temple University, Philadelphia, PA 19122, USA
*Correspondence: g.musumeci@unict.it; Tel.: +095-378-2036

Biomedicines 2021, 9(7), 807; DOI:10.3390/biomedicines9070807

6.1 Introduction

The skeletal muscle is a highly dynamic and plastic tissue that promptly responds to physical activity and sedentary behavior [1]. Skeletal muscle disuse atrophy (SMDA) refers to biochemical, morphological, and functional changes in skeletal muscle that may result from states of hypokinesis or immobilization, e.g., following fractures or elective orthopedic surgery, and represents a major topic in the fields of regenerative and rehabilitation medicine [2,3]. On the contrary, both resistance and aerobic training induce metabolic changes within the muscle by altering protein synthesis, muscle proteolysis, therefore inducing molecular and cellular adaptations that regulate homeostasis and hypertrophy [4–6]. A large variety of stromal cells are involved during physiological processes following physical exercise, in order to sustain remodeling and regeneration [7,8]. More specifically, the involvement of Pax+ cells, side population cells (SP cells), pericytes, fibro/adipogenic progenitor cells (FAPs), and PW1+/Pax7– interstitial progenitor cells (PICs), has received attention to investigate exercise-based interventions preventing sarcopenia or in response to injury [8–13].

Alexander Mauro described, for the first time, in 1961, a population of mononucleated cells which had been called “satellite cells” (SCs) by virtue of their localization: underneath the surrounding basal lamina and outside the plasma membrane of the muscle fiber they are associated with [14]. These cells have been immunophenotypically identified by Pax7 [15], M-cadherin [16], CD34 [17], and α7-integrin [18] and originate from Pax3+ progenitors in the somites of the embryo that migrate to the limb bud [19–21]. In his dissertation, Mauro speculated about the role of these cells to be involved in muscle regeneration as dormant myoblasts, able to initiate the development of skeletal muscle fibers in the event of damage or exogenous triggers [14,22,23]. Besides SCs, other cells concur to the maintenance of skeletal muscle homeostasis and contribute to stem cell niche [24]. Fibroblasts proliferate in close proximity to satellite cells [25], providing structural reliability through assembly of collagen, elastic fibers, and other matrix substances [12,26–28]. FAPs are mesenchymal resident cells able to sustain SCs differentiation during tissue regeneration [29–31]. Furthermore, muscle-associated vessels accommodate pericytes and mesoangioblasts, participating in endothelial cell communication, angiogenesis, mechanisms of survivals, and cross-talk [32].

Lastly, another type of cell, recently identified in the muscle interstitium, is represented by the so-called “Telocytes” (TCs), which appear to physically reside near satellite cells, nerve, and microvascular network [13]. The discovery of this population is referred to as a case of serendipity by the Romanian research group led by Professor Laurentiu M. Popescu, just ten years ago [33]. To understand the road that leads to the definition of these new type of cells, it needs to be reminded the work of Santiago Ramón y Cajal, who described, at the beginning of 1900, the presence of unknown

cells in the loose connective tissue of the tunica muscularis of the gut, considering them as primitive interstitial neurons [34]. Although their existence was not fully recognized by the scientific community for half a century, M.S. Faussone-Pellegrini [35] and, independently, L. Thuneberg [36] acknowledged that these cells were not neurons and called them “Interstitial Cells of Cajal (ICCs)”. Extended studies, following the annotation of Cajal, lead to the identification of Interstitial Cajal-like Cells (ICLCs), named “Telocytes” in 2010, in many organs [33], testifying the ubiquity of the novel cell type [37]. Since they were identified, the number of scientific works on TCs is growing exponentially [38] (Figure 1).

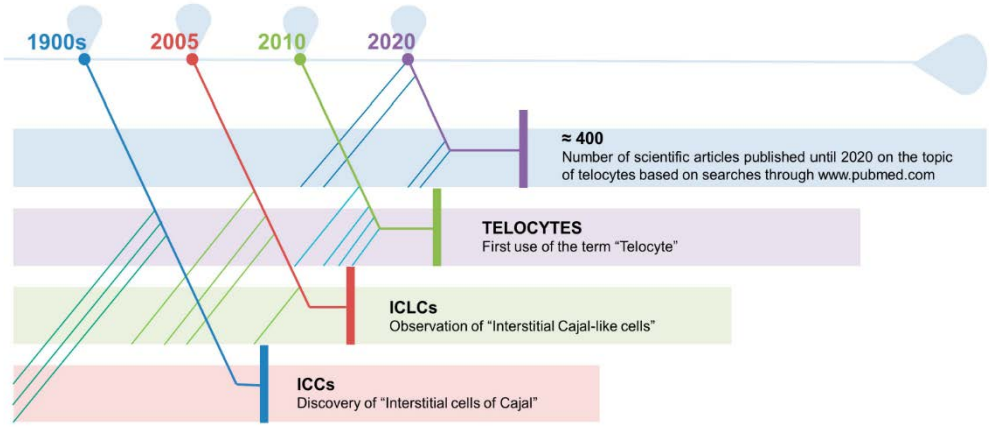

Figure.1. At the beginning of 1900, Santiago Ramón y Cajal described the presence of what he considered primitive interstitial neurons in the loose connective tissue of the tunica muscularis of the gut. Half a century later, M.S. Faussone-Pellegrini and L. Thuneberg observed that these cells were not neurons and called them “Interstitial Cells of Cajal (ICCs)”. These type of cells were then found in many other organs. Finally, Faussone-Pellegrini together with L. M. Popescu, proposed, in 2010, to use the term “Telocyte” to indicate an ICLC. Since their identification, TCs have received attention and the number of scientific articles on the topic is growing considerably.

It is noteworthy to mention that this discovery raised skepticism and controversy, since ICLCs were also described merely as CD34-positive stromal cells acting as stem cells during regeneration processes [39,40], or the term was used interchangeably to describe fibroblasts [41]. Therefore, there is a need for new evidence that can discriminate the different populations hosted in the stem cell niche of the tissues, not only for their morphology but also for their function. TCs are typically described as cells with small bodies, reported as pear-, spindle-, triangular-shaped, and very long cytoplasmic processes, up to hundreds of micrometers but only approximately 0.2 µm thick [42,43]. The identification of TCs, via transmission electron microscopy, showed characteristic features [33,44] (Table 1).

Although it is still unclear, the role of TCs seems to participate in sustaining cross-talk communication between stromal cells through signaling transmission via exosomes [13,45], secreting vascular endothelial growth factor (VEGF) and, broadly, promoting myofibers regenerative

mechanisms by supporting local stem cell niche differentiation, vasculogenesis, and preventing fibrosis [46]. The presence of this population has been observed, under physiological conditions, in numerous organs and tissues [47,48], and also following pathologic situations, such as musculoskeletal injuries [49], suggesting their role in healing processes and their function for regenerative medicine strategies [50–53]. As already mentioned, physical inactivity and activity have been extensively studied in relation to stem cell niche and, more recently, are also attracting attention with regard to TCs [49,54,55]. Finally, the aim of this morphologic study was to investigate the presence/absence of TCs in tibialis anterior muscle of healthy rats who underwent a protocol of endurance training for either 4 weeks or 16 weeks in comparison to sedentary rats who were inactive, i.e., not engaging in any physical exercise, throughout the duration of the experiment.

Cell Structure	**Characteristic Features of Telocytes**	
Body	small, oval- pear- spindle- triangular-shaped; average dimensions: 9.39 µm ± 3.26 µm; the nucleus occupies about 25% of the cell volume and contains clusters of heterochromatin attached to the nuclear envelope	
Cytoplasm	mitochondria: approximately 5%–10% of the cytoplasmic volume; small Golgi complex; endoplasmic reticulum: 1%–2% of the cyto-plasmic volume	
Plasmalemma	thin or absent basal lamina;	Caveolae occupy about 2–3% of cytoplasmic volume;
Telopodes	Number	on average from 1 to 5;
	Length	up to hundreds of µm;
	Thickness	uneven calibre, mostly below 0.2 µm;
	Aspect	moniliform with dilations and branches;
	Organization	three-dimensional network communicating through gap junctions;

Table1. Characteristic features of TCs and of their telopodes.

6.2 Materials and Methods

6.2.1 Ethical Approval

All the procedures involving alive animals were performed at the Center for Advanced Preclinical In Vivo Research (CAPIR), University of Catania. The guidelines of the Institutional Animal Care and Use Committee (I.A.C.U.C.) of the University of Catania (Approved protocol n. 2112015-PR of the 14.01.2015, Italian Ministry of Health) have been complied with. Animal care and handling were carried out in accordance with the EU Directive 2010/63/EU, as well as the Italian law (D.Lgs. 26/2014).

6.2.2 Animals: Housing and Breeding

Two-month-old healthy female Wistar outbred rats, with a bodyweight of 200 ± 20 g, were purchased from Charles River Laboratories, Milan, Italy and bred in the animal facilities at the University of Catania. Rats were maintained and kept in polycarbonate cages (10.25^{00} W × 18.75^{00} D × 8^{00} H) in stable hygrometric and thermic conditions (20– 23 ˚C) on 12 h light/dark cycle with ad libitum access to water and food, throughout the whole period of the experiment. It was used a standard rat chow: carbohydrates (40%), proteins containing all essential amino acids (30%), and lipids (30%). Lipids were a mixture of neutral fatty acids, saturated fatty acids, and unsaturated fatty acids. Diets were provided by Laboratorio Dottori Piccioni, Gessate (Milan), Italy. Twenty rats were used in this study equally divided into two groups, sedentary and undergoing physical exercise, respectively CTRL and PA, sacrificed at two different time points, 4 and 16 weeks: CTRL4W, control sedentary rats sacrificed at 4 weeks; PA4W, rats performing physical exercise sacrificed at 4 weeks; CTRL16W, control sedentary rats sacrificed at 16 weeks; PA16W, rats performing physical exercise sacrificed at 4 weeks. All animals were randomly distributed to groups. All efforts were made to minimize the number of mice, according to the principles of the 3Rs and the resource equation approach, and reduce their suffering [56]. Throughout the whole period of the experiment, the animals were free to move in the cages and their wellness was monitored through objective observation and daily checks (weight, claudication, fur and eyes appearance, consumption of food and water, lethargy) [57]. The animals were sacrificed by carbon dioxide (CO2) overdose, at the established time points. After euthanasia, tibialis anterior muscles were explanted and processed for the planned experiments since the high responsivity of this muscle to exercise [58].

6.2.3 Treadmill Training

Two groups of rats (PA4W and PA16W) performed physical activity in the form of running on a treadmill (2Biological instrument, Varese, Italy) (Figure 2). Rats were made familiar with the instrument for 1 week prior to surgery, at a speed of 10 m/min (type of exercise: interval training, between mild and moderate) for 5 min daily. This type of exercise is used to stimulate the muscles, joints, and bones in the work of flexion-extension of the limbs. The rats exercised 3 days a week and, in order to adapt the settings to the time-dependent ability of the rats to perform the exercise, the speeds and the durations were gradually incremented from 10–15 m/min for 5 min to 20–30 m/min for 15 min (from week 1 to week 4), from 10–15 m/min for 5 min to 30–40 m/min for 20 min (from week 1 to week 8), from 10–15 m/min for 5 min to 40–50 m/min for 25 min (from week 1 to week 16). The treadmill was gradually inclined between 2° and 6° degrees. A minimal electric shock (0.2 mA) was used to avoid the rat to stop running, if distracted, to stimulate the walking and to instruct the rats in the first place. All-electric shock bouts were closely monitored in real-time and acquired by the embedded data acquisition software (2Biological instrument, Varese, Italy). Rats that exceeded the number of five electric shocks, in one session, were suspended from the exercise.

Figure 2. Rats exercising on the treadmill. Speeds and the durations were gradually incremented, respectively, from 10–15 m/min for 5 min to 40–50 m/min for 25 min (from week 1 to week 16).

6.2.4 Histology Analysis

Tibialis anterior muscle samples were washed in phosphate-buffered saline (PBS, Bio-Optica, Milano, Italy), fixed in 10% buffered-formalin (Bio-Optica, Milan, Italy) for 24 h at room temperature. Afterwards, the samples were dehydrated in graded ethanol (BioOptica, Milan, Italy), cleaned in xylene (Bio-Optica, Milan, Italy) and paraffin-embedded (Bio-Optica, Milan, Italy), being careful to preserve the desired anatomical orientation. Slides of 5 µm thickness were cut from the obtained paraffin blocks and hematoxylin and eosin-stained (H&E, Bio-Optica, Milan, Italy) following a protocol described elsewhere [59]. The samples were then examined in triplicate for morphological evaluation with a Zeiss Axioplan light microscope (Carl Zeiss, Oberkochen, Germany) and by a digital camera (AxioCam MRc5, Carl Zeiss, Oberkochen, Germany), used to take images.

6.2.5 Histomorphometric Analysis

Each H&E stained muscle cross section was subjected in triplicate to morphometric analysis by calculating the area of twenty muscle fibers of five randomly selected fields with a total area of about 35.000 µm2, using a software for image acquisition (AxioVision Release 4.8.2—SP2 Software, Carl Zeiss Microscopy GmbH, Jena, Germany) [60]. Data were then expressed as diameter mean ± standard deviation (SD). Statistical significance of results was thus accomplished. Three investigators (two anatomical morphologists and one histologist) made the morphological assessment. If disputes occurred, a unanimous agreement was reached after section re-evaluation and before proceeding with data interpretation.

6.2.6 Double Immunofluorescence Analysis

Paraffin-embedded muscle tissue sections of 5 µm thickness were subjected in triplicate to double immunofluorescence (IF) combining anti-mouse and anti-rabbit goat secondary antibodies with either mouse or rabbit primary antibodies. Muscle sections were deparaffinized with xylene and rehydrated in graded ethanol scale. Afterwards, the slides were cleaned for 20 min with phosphate-buffered saline (PBS; Bio-Optica, Milan, Italy) and unmasked in citrate buffer (pH 6.0; Bio-Optica, Milan, Italy), or in ethylenediaminetetraacetic acid-Tris buffer (Tris-EDTA pH 8.0, Bio-Optica, Milan, Italy) for the antigenic retrieval and incubated in 0.3% H_2O_2/PBS, for 30 min, to block endogenous peroxidase activity. Non-specific antibody binding sites were blocked by applying a solution of 1% bovine serum albumin (BSA; Sigma-Aldrich, Saint Louis, MO, USA) in PBS 1X for 1 h at room temperature. Tissue slides were washed in PBS and, then, incubated overnight at +4 °C with a mixture

of mouse and rabbit primary antibodies at appropriate dilution in antibody dilution buffer: mouse monoclonal anti-CD34 (1:100; Dako, Agilent, Santa Clara, CA, USA), rabbit monoclonal anti-CD34 (1:100; Invitrogen, Thermo Fisher Scientific,Waltham, MA, USA), rabbit polyclonal anti-CD117 (1:500; Dako, Agilent, Santa Clara, CA, USA), mouse monoclonal anti-Vimentin (VIM, 1:200; Dako, Agilent, Santa Clara, CA,USA). Primary antibodies were revealed using specific fluorescent-dye Goat anti-Mouse Alexa Fluor 488-conjugated IgG (1 µg/mL; Invitrogen, Thermo Fischer Scientific, Waltham, MA, USA) and Goat anti-Rabbit 594-conjugated IgG (2 µg/mL; Invitrogen, Thermo Fisher Scientific, Waltham, MA, USA) for 1 h at room temperature. Details on primary and secondary antibody sources and dilutions are shown in Table 2. Negative controls were performed by replacing primary antibodies with non-immune serum, while cross reactivity of secondary antibodies was verified by omitting primary antibodies. Immunolabeled samples were rinsed in PBS and mounted using an anti-fade mounting medium containing 4',6-diamidino-2-phenylindole (DAPI) for nuclear counterstaining (Vectashield, Vector Laboratories, Burlingame, CA, USA) and sealed with nail polish.

Primary Antibody	Host Species	Producer	Dilution	Secondary Antibody	Producer	Dilution
Anti-CD34	MOUSE	Dako	1:100	AF488	Invitrogen	1 µg/mL
Anti-CD117	RABBIT	Dako	1:500	AF594	Invitrogen	2 µg/mL
Anti-CD34	RABBIT	Invitrogen	1:100	AF594	Invitrogen	2 µg/mL
Anti-VIM	MOUSE	Dako	1:200	AF488	Invitrogen	1 µg/mL

Table 2.Primary and secondary antibody used in IF and their dilutions.

6.2.7 Computerized Densitometric Measurements and Image Analysis

Digital micrographs of double immunofluorescence sections were taken using a confocal laser scanning microscopy (CLSM, Zeiss LSM700, Carl Zeiss, Oberkochen, Germany) with ZEN-2010 software. In order to detect the fluorophore signal, three lasers with 405, 488, and 555 nm wavelengths were used for the analysis of blue, green, and red signals, respectively. Image analysis software (AxioVision Release 4.8.2-SP2 Software, Carl Zeiss Microscopy GmbH, Jena, Germany), which quantifies the level of double positive staining of anti-CD34/anti-CD117 and anti-CD34/anti-Vimentin immunolabeling, was used to calculate the densitometric count in five fields, 10× magnification, randomly selected from each section. Statistical results are expressed as densitometric count ($pixel^2$)/($pixel^2$) of double immunostaining on muscle tissue. Three blinded investigators (two anatomical morphologists and one histologist) made the evaluations that were assumed to be correct

if values have not statistically significant difference. If disputes concerning interpretation occurred, unanimous agreement was reached after sample re-evaluation.

6.2.8 Immunohistochemistry

Skeletal muscle samples, 5 µm-thick, were processed for immunohistochemical analysis. Briefly, the slides were dewaxed in xylene, hydrated using graded ethanols, and therefore heated (5 min × 3) in capped polypropylene slide-holders with citrate buffer— pH 6 (Bio-Optica, Milan, Italy), using a microwave oven (750 W, LG Electronics Italia S.p.A., Milan, Italy) to unmask antigenic sites. The slides were incubated for 30 min in 0.3% H_2O_2/PBS to quench endogenous peroxidase activity before being rinsed for 20 min with PBS (Bio-Optica, Milan, Italy). After blocking, the sections were incubated overnight at 4 °C with rabbit monoclonal anti-CD34 (1:100; Invitrogen, Thermo Fisher Scientific, Waltham, MA USA). Immune complexes were then treated with biotinylated link antibodies (horseradish peroxidase polymer (HRP)-conjugated anti-rabbit and anti-mouse were used as secondary antibodies) and then detected with peroxidase-labelled streptavidin, both incubated for 10 min at room temperature (LSAB + System-HRP, K0690, Dako, Glostrup, Denmark). Immunoreactivity was visualized by incubating the sections for 2 min in 0.1% 3,3'-diaminobenzidine (DAB) (DAB substrate Chromogen System, Dako, Glostrup, Denmark). The sections were lightly counterstained with Mayer's hematoxylin (Histolab Products AB, Göteborg, Sweden), mounted in Glycerol Vinyl Alcohol (GVA) (Zymed Laboratories, San Francisco, CA, USA), observed with an Axioplan Zeiss light microscope (Carl Zeiss, Oberkochen, Germany), and photographed with a digital camera (AxioCam MRc5, Carl Zeiss, Oberkochen, Germany).

6.2.9 Statistical Analysis

Statistical analysis was performed using GraphPad Instat® Biostatistics version 8.0 software (GraphPad Software, Inc., La Jolla, CA, USA). The sample size calculation for this study was established using the resource equation approach, including minimum and maximum sample sizes, because it was not possible to assume standard deviation and effect size [56]. Data were tested for normality with the Kolmogorov–Smirnov and Shapiro–Wilk test. All variables were normally distributed. Differences between experimental groups were evaluated by using one-way ANOVA (histomorphometric and immunofluorescence analysis) and two-way ANOVA (weights) followed by Tukey's multiple comparison post hoc test. For all experiments, p-values of less than 0.05 ($p < 0.05$) were considered statistically significant; p values of less than 0.01 ($p < 0.01$) were considered to be highly statistically significant. The data are presented as the mean value ± SD. Cohen's κ was applied

to measure the agreement between the three blinded observers and averaged to evaluate overall agreement.

6.3 Results

6.3.1 Body Weight

Body weights and food and drink consumption were monitored throughout the experiment, 3 days per week, for a total of 48 time points. A physiological increase in body weight during the weeks in all groups was observed since the differences between groups, for each time point, are never significant ($p > 0.05$), as expected (Figure 3). At the start of the experiment, the mean ± SD body weight of all rats was 209.4 ± 13.52 g, at the end of the fourth week, it was 240.95 ± 10.95 g, reaching 290.7 ± 15.97 g, at the end of the sixteenth week, for the remaining animals.

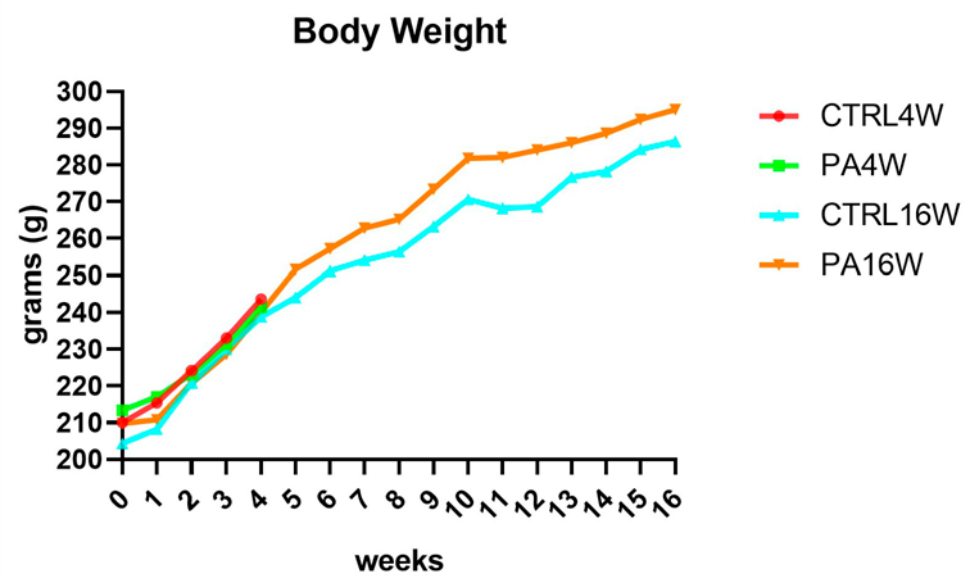

Figure.3. Body weight variations over 16 weeks, showing a physiological increase in all groups. The differences between groups, analyzed by two-way ANOVA followed by Tukey's multiple comparison post hoc test, are not significant, as expected ($p > 0.05$). CTRL4W, control sedentary rats sacrificed at 4 weeks; PA4W, rats performing physical exercise sacrificed at 4 weeks; CTRL16W, control sedentary rats sacrificed at 16 weeks; PA16W, rats performing physical exercise sacrificed at 4 weeks.

6.3.2 Histology and Histomorphometry

Histological analysis with H&E were examined to highlight the possible structural alterations in muscle tissue of all experimental groups. No cytological alteration is detected in the muscle fibers of all groups. The morphometric analysis of the diameter (µm) (mean ± SD) of the muscle fibers highlights a significant hypertrophy of the groups PA16W (30.46 ± 1.43 µm) (** $p < 0.0001$) and PA4W (27.47 ± 1.61 µm) (* $p < 0.001$) vs. CTRL16W (21.39 ± 2.19 µm). PA16W (27.47 ± 1.61 µm) also shows a predictable hypertrophy when compared to CTRL4W (24.01 ± 1.57 µm), (* $p < 0.001$). On the contrary, PA16W (30.46 ± 1.43 µm) does not show a statistically significant hypertrophy when compared with group PA4W (27.47 ± 1.61 µm), (ns) (Figure 4). No significant differences are revealed when compared CTRL4W vs. CTRL16W and PA4W vs. CTRL4W.

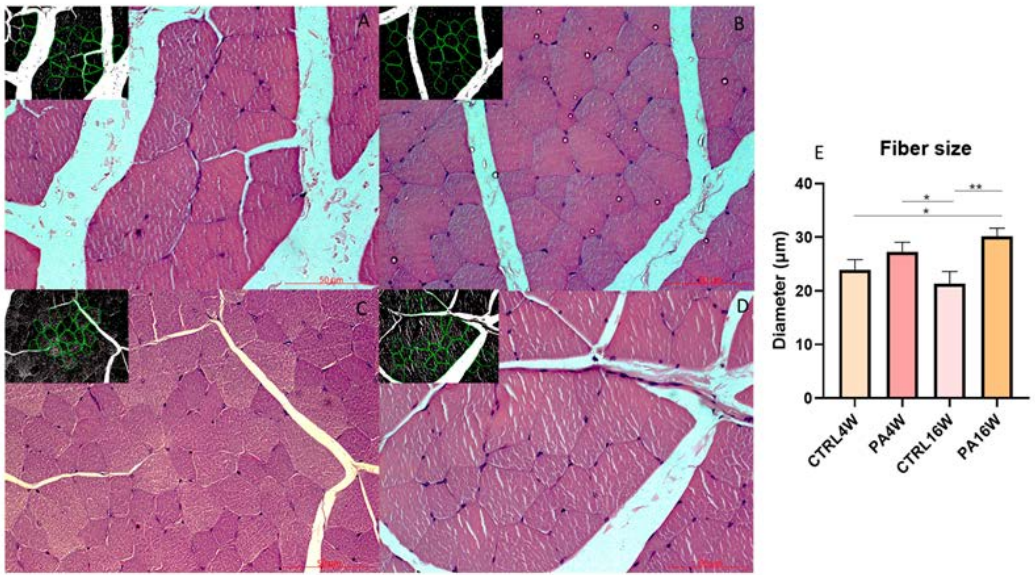

Figure 4. **Hematoxylin and eosin staining (A–D) and morphometric analysis of the diameter (µm) (mean ± SD) of the muscle fibers (E).** (**A–D**) (**A**) group CTRL4W and in the inset morphometric analysis by the software; (**B**) group PA4W and in the inset morphometric analysis by the software; (**C**) group CTRL16W and in the inset morphometric analysis by the software; (**D**) group PA16W and in the inset morphometric analysis by the software. (**E**) The morphometric analysis highlights a significant hypertrophy of the groups PA16W (30.46 ± 1.43 µm) (** $p < 0.0001$), and to PA4W (* $p < 0.001$) when compared to CTRL16W (21.39 ± 2.19 µm). Comparison between CTRL4W and PA16W highlights a significant hypertrophy of the latter group (* $p < 0.001$). No other comparisons show to be significant. Data were tested for normality with the Kolmogorov–Smirnov and Shapiro– Wilk test, and differences between experimental groups were evaluated by using one-way ANOVA, followed by Tukey's multiple comparison post hoc test. Lens magnification: ×20. Scale bars: 50 µm. ** $p < 0.0001$, * $p < 0.001$. CTRL4W, control sedentary rats sacrificed at 4 weeks; PA4W, rats performing physical exercise sacrificed at 4 weeks; CTRL16W, control sedentary rats sacrificed at 16 weeks; PA16W, rats performing physical exercise sacrificed at 4 weeks.

6.3.3 Double Immunofluorescence and Densitometric Analysis

Although transmission electron microscopy (TEM) examination is the golden standard for TCs identification [33,61], double-immunostaining is currently the most common tool for semi-quantitative analysis of TCs [62–64], since it can help in discriminate this population from other interstitial cells. In this work, double positive immunofluorescences for CD34/CD177 and CD34/VIM were used to identify TCs in sedentary and exercised muscle rat tissue at 4 and 16 weeks (Figures 5A and 6A). Statistical results are expressed as mean ± SD of the densitometric count (pixel^2)/(pixel^2) of double immunostaining on muscle tissue. CD34 and CD117 double labeling analysis indicates a statistically significant increase in the expression of TCs in PA16W ($7.7 \times 10^{-4} \pm 1.3 \times 10^{-4}$ (pixel^2)/(pixel^2)) vs. CTRL16W ($3.9 \times 10^{-4} \pm 2 \times 10^{-4}$ (pixel^2)/(pixel^2)) (* $p < 0.05$) (Figure 5B). Densitometric values for CTRL4W and PA4W groups are, respectively, $4.9 \times 10^{-4} \pm 1.4 \times 10^{-4}$ (pixel^2)/(pixel^2) and $6.1 \times 10^{-4} \pm 2.5 \times 10^{-4}$ (pixel^2)/(pixel^2). Similarly, the number of interstitial TCs is highly significant higher in PA16W ($1.3 \times 10^{-3} \pm 3.1 \times 10^{-4}$ (pixel^2)/(pixel^2)), vs. CTRL16W ($6.9 \times 10^{-4} \pm 1 \times 10^{-4}$ (pixel^2)/(pixel^2)) (** $p < 0.01$) as determined by CD34/VIM double-immunostaining (Figure 6B). Densitometric values for CTRL4W and PA4W groups are, respectively,$1 \times 10^{-3} \pm 2.6 \times 10^{-4}$ (pixel^2)/(pixel^2) and $9.3 \times 10^{-4} \pm 2.5 \times 10^{-4}$ (pixel^2)/(pixel^2). No other statistically significant differences are highlighted between groups, in both experiments.

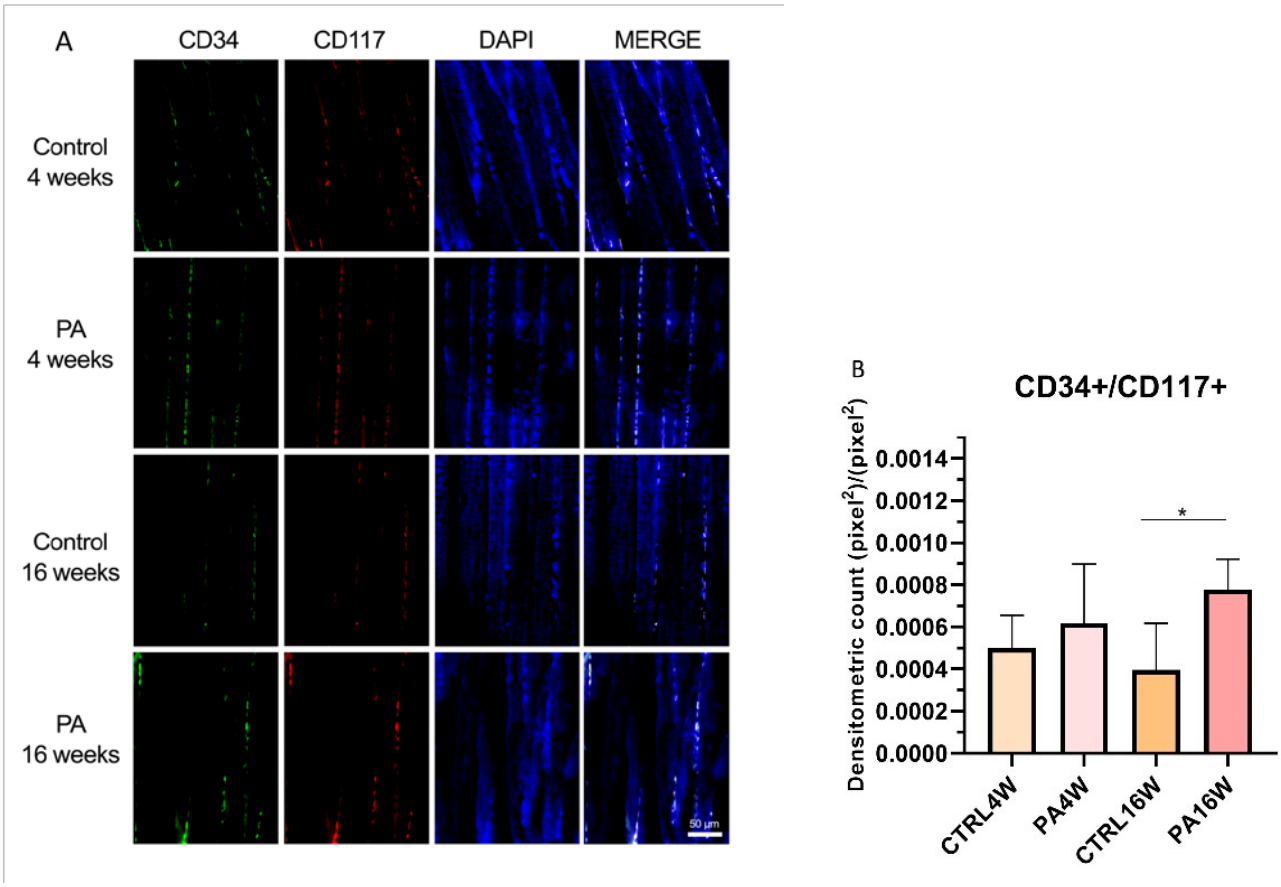

Figure 5. (**A**) Representative images of double immunofluorescence staining for muscle tissue TCs as determined by CD34+/CD117+. CD34 (green) and CD117 (red) immunostaining with 4',6-diamidino-2-phenylindole (DAPI; blue) counterstain for nuclei. (**B**) Comparison between PA16W and CTRL16W highlights a significant higher expression of TCs in exercised rats at 16 weeks (* $p < 0.05$). No other comparisons show to be significant. Data were tested for normality with the Kolmogorov–Smirnov and Shapiro–Wilk test, and differences between experimental groups were evaluated by using one-way ANOVA, followed by Tukey's multiple comparison post hoc test. The slides are scanned by confocal laser scanning microscopy (CLSM; Zeiss LSM700, Oberkochen, Germany) at 200× magnification. Scale bars: 50 µm. CTRL4W, control sedentary rats sacrificed at 4 weeks; PA4W, rats performing physical exercise sacrificed at 4 weeks; CTRL16W, control sedentary rats sacrificed at 16 weeks; PA16W, rats performing physical exercise sacrificed at 4 weeks.

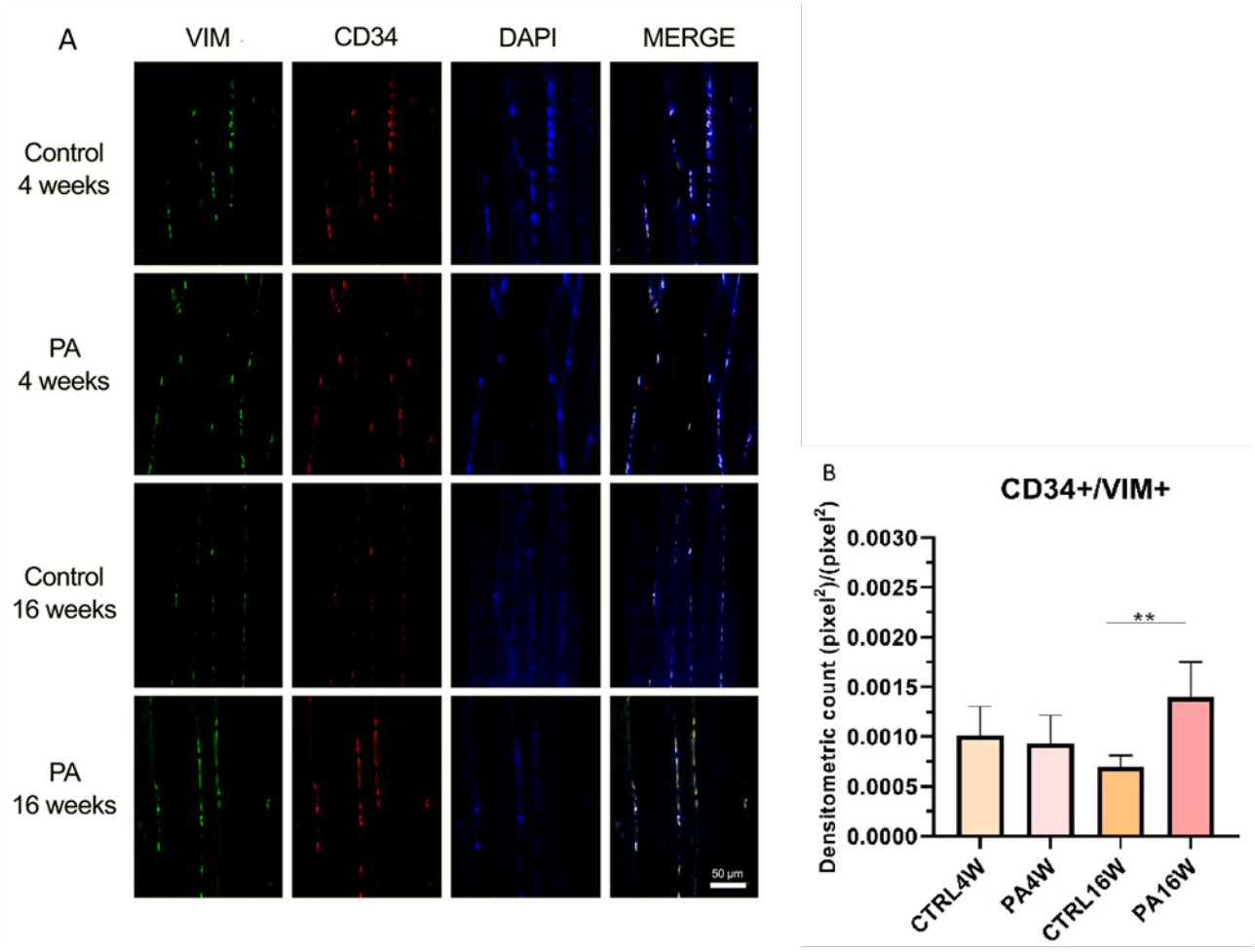

Figure 6. (**A**) Representative images of double immunofluorescence staining for muscle tissue TCs as determined by CD34+/VIM+. CD34 (red) and VIM (green) immunostaining with 4′,6-diamidino-2-phenylindole (DAPI; blue) counterstain for nuclei. (**B**) Comparison between PA16W and CTRL16W highlights a highly significant higher expression of TCs in exercised rats at 16 weeks (** $p < 0.01$). No other comparisons show to be significant. Data were tested for normality with the Kolmogorov–Smirnov and Shapiro–Wilk test, and differences between experimental groups were evaluated by using one-way ANOVA, followed by Tukey's multiple comparison post hoc test. The slides are scanned by confocal laser scanning microscopy (CLSM; Zeiss LSM700, Oberkochen, Germany) at 200× magnification. Scale bars: 50 µm. CTRL4W, control sedentary rats sacrificed at 4 weeks; PA4W, rats performing physical exercise sacrificed at 4 weeks; CTRL16W, control sedentary rats sacrificed at 16 weeks; PA16W, rats performing physical exercise sacrificed at 4 weeks.

6.3.4 Immunohistochemistry

Skeletal muscle sections showed CD34+ cells at the periphery of the fibers, within the interstitium between muscle fibers (Figure 7). These cells appear to exhibit morphological features of TCs, i.e., spindle nuclei, approximately 5–10 µm in diameter, and multiple long cytoplasmic processes, approximately 10–25 µm in length and 0.1–0.2 µm in thickness, identifiable with telopodes.

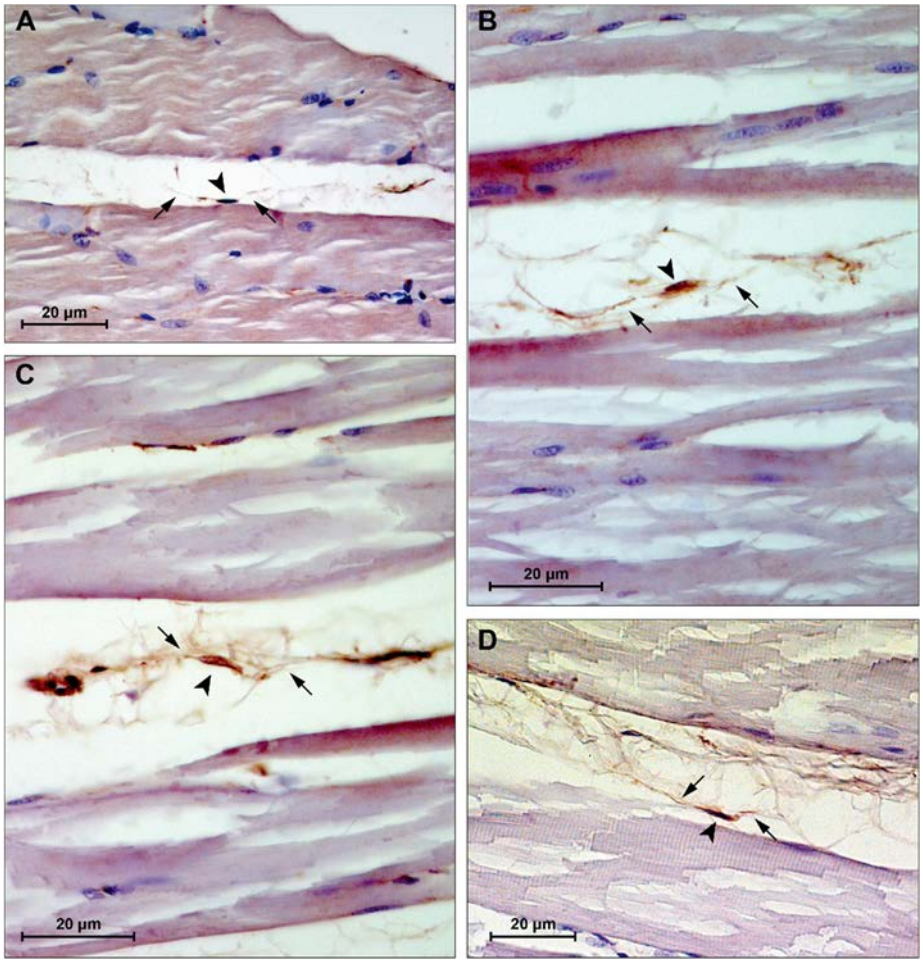

Figure 7. **Representative images of immunohistochemistry staining for muscle tissue CD34+ cells.** (**A**) group CTRL4W, estimated size body (arrowhead): 5.23 µm, estimated cytoplasmic processes length (arrows): 13.28 and 24.28 µm; (**B**) group PA4W, estimated size body (arrowhead): 5.04 µm, estimated cytoplasmic processes length (arrows): 26.68 and 11.94 µm; (**C**) group CTRL16W, estimated size body (arrowhead): 8.69 µm, estimated cytoplasmic processes length (arrows): 13.07 and 20.56 µm; (**D**) group PA16W, estimated size body (arrowhead): 9.56 µm, estimated cytoplasmic processes length (arrows): 22.03 and 13.36 µm. Lens magnification: ×40. Scale bars: 20 µm. CD34+ cells nuclei and cytoplasmic processes were measured using a caliper tool of the software for image acquisition (AxioVision Release 4.8.2—SP2 Software, Carl Zeiss Microscopy GmbH, Jena, Germany). CTRL4W, control sedentary rats sacrificed at 4 weeks; PA4W, rats performing physical exercise sacrificed at 4 weeks; CTRL16W, control sedentary rats sacrificed at 16 weeks; PA16W, rats performing physical exercise sacrificed at 4 weeks.

6.4 Discussion

TCs have been largely identified, over the last ten years, as populating the stromal compartments of a variety of organs, belonging to the tissue stem cell niche [33,49,65]. Within the skeletal muscle tissue, TCs are distributed throughout the perimysium and endomysium and could reach long-distances through their telopodes which allow these cells to make contact with myofibers, nerve terminals, blood vessels, and other stromal populations, including SCs, sited beneath the surrounding basal lamina of the myofiber.

In the present morphological study, the presence of TCs in tibialis anterior muscle of healthy rats who underwent a protocol of endurance training for either 4 weeks or 16 weeks was investigate in relation to sedentary rats who were inactive, i.e., not engaging in any physical exercise, throughout the duration of the experiment.

H&E staining shows no cytological alteration in the muscle tissue of all groups, although the morphometric analysis of the size of the muscle fibers highlights a significant atrophy, defined as a decrease in the size of myofibers, of the sedentary control group at 16 weeks (CTRL16W) when compared to physically active rats undergoing treadmill training for both 16 weeks (** $p < 0.0001$) and 4 weeks (* $p < 0.001$) (Figure 4). Muscle morphological adaptations to active/inactive styles were not, however, accompanied by statistically significant differences ($p > 0.05$) in body weights in all groups, indicating a physiological growth of the rats during the weeks, as expected (Figure 3).

Whether atrophy may affect muscle stem cells numbers or behavior is still controversial and should be further elucidated to assess the role of daily mechanical stress administered through exercise [66]. Mitchell et al. [67] reported that the number of stem cells in hindlimb muscles of mice was reduced after 2 weeks of hind limb suspension, and Verdijk et al. [68] observed similar decline in human vastus lateralis muscle following sarcopenia, reversed by resistance training which increased satellite cell content and type II muscle fiber size. Conversely, aerobic and resistance training have been reported to be a stimulus for the formation of new muscle fibers and maintain their homeostasis [4,5].

Although SCs are the main characters of renewal programme in skeletal muscle, other tissue residents and recruited stromal cells, e.g., fibroblasts, fibro-adipogenic progenitors, endothelial cells, perycites, and macrophages, are paramount supporting players [16,22,69]. Among these cell-cell interactions, TCs and SCs seem to interact by juxtacrine and paracrine intercellular signaling, in order to support in a concerted manner [13] the network mediating new tissue organization [70]. However, the interplay between these two cell types, especially in skeletal muscle injury [49], has yet to be elucidated in depth since cue-based investigations rely mainly on knowledge of the close proximity of TCs to SCs and their ability to communicate.

This study provides a novel finding that interstitial TCs are decreased in the muscles of sedentary rats compared to exercised rats, supporting the recent reports that TCs are, otherwise, increased in exercise-induced cardiac growth [55], participate in early moderate exercise-induced remodelling after acute myocardial infarct [71] and in eccentric contraction induced skeletal muscle injury, in rodents. Since their discovery is relatively recent, TCs are not yet defined by specific antigenic markers, although CD34 is the most commonly used antigen to characterize their presence [48,72]. Vimentin, CD117/c-kit, PDGFR-β (platelet derived growth factor receptor β), and SMA (smooth muscle actin) are the antigens most frequently associated with TCs [47,62,73,74]. Bei et al. analysed immunofluorescence double staining for cardiac TCs and fibroblasts in vitro. CD34/CD117, CD34/vimentin, and CD34/PDGFR-β were positive for TCs, whereas fibroblasts showed positivity only for vimentin and PDGFR-β [75].

In this work, double positivity for CD34+/CD117+ and CD34+/vimentin+ were used to individuate TCs and to discriminate this population from fibroblasts which are CD34/CD117-/vimentin+. CD34 is a sialomucin mainly expressed in hematopoietic stem cells (HSCs) surface but it has also been found in other tissue-specific stem cells [76]. Vimentin is cytoskeletal type III intermediate filament protein found in mesenchymal-derived cells that provides an architectural network for organelles anchoring to cytoplasm [73]. CD117 is a transmembrane receptor tyrosine kinase widely used for TCs identification which is active in proliferation and differentiation [77]. Based on two distinct double-immunostainings for CD34/CD117 and CD34/Vimentin, skeletal muscle TCs were identified in all groups. CD34/CD177 statistical analysis indicates a significant difference in the higher level of TCs in exercised rats at 16 weeks in relation to their control group (* $p < 0.05$) (Figure 5).

This result is also more significantly supported by CD34/VIM double-immunostaining (** $p < 0.01$) (Figure 6). These results indicate a potential targeting of TCs, as belonging to muscle stem cell niche, in cell dysfunction associated with atrophic condition [67]. This latter negatively affects stem cells via presence of catabolic factors such as myostatin [78] and tumor necrosis factor α [79] as well as decreases in trophic factors [80]. In contrast, in this work, rats subjected to regular physical training for 16 weeks maintained a stable TCs population, although not statistically increased compared to rats who performed exercise for only 4 weeks.

Finally, immunohistochemistry showed CD34+ cells, within the interstitium between muscle fibers (Figure 7), with characteristic features of TCs and telopodes, i.e., spindle nuclei and multiple long cytoplasmic processes. These observations are in support with current evidence suggesting TCs' role in intercellular signaling through their strategic position and organized network of telopodes with local cellular neighborhood, nerves, and capillaries [33,81,82]. Homo- and heterocellular communication seems to be carried out via small molecules and shedding microvesicles carrying

various molecules like proteins, RNAs, and microRNA [49,83,84]. These mechanisms of transmission allow rapid cell engagement in the tissue milieu, in order to approach adaptations to biochemical and physical changes. The use of TEM would have been useful to determine the ultrastructural features of TCs in exercised rats and this should be noticed as a limitation of this study.

6.5 Conclusions

These findings herein are intended to encourage knowledge about TCs population and their role in the stem cells niche of skeletal muscles. Further studies investigating TCs in response to different types of exercise (resistance, aerobic, isotonic, flexibility), sedentary behavior, ageing, and pathophysiological conditions, as well as studies on the possibility of triggering TCs through exercise to reverse atrophic conditions, would be scientifically valuable.

This study may be framed in a field still in its infancy, although it is rapidly attracting the attention of the scientific community. The understanding of the above-mentioned mechanisms between the cells involved in the tissue remodeling process could offer new chances in regenerative tissue strategies and insights about finding possible triggers for TCs in sarcopenia and other musculoskeletal disorders, in clinical medicine.

Finally, since exercise training has been shown to exert protective effects against sedentary-induced atrophy, rather by sustaining muscle remodeling and maintenance of TCs, this finding might promote further skeletal muscle adapted physical activity and rehabilitation programmes for humans.

6.6 References

1. Marini, M.; Veicsteinas, A. The exercised skeletal muscle: A review. *Eur. J. Transl. Myol.* **2010**, *20*, 105. [CrossRef]
2. Zhang, S.F.; Zhang, Y.; Li, B.; Chen, N. Physical inactivity induces the atrophy of skeletal muscle of rats through activating AMPK/FoxO3 signal pathway. *Eur. Rev. Med. Pharmacol. Sci.* **2018**, *22*, 199–209.
3. Rudrappa, S.S.; Wilkinson, D.J.; Greenhaff, P.L.; Smith, K.; Idris, I.; Atherton, P.J. Human skeletal muscle disuse atrophy: Effects on muscle protein synthesis, breakdown, and insulin resistance-A qualitative review. *Front. Physiol.* **2016**, *7*, 361. [CrossRef]
4. Konopka, A.R.; Harber, M.P. Skeletal muscle hypertrophy after aerobic exercise training. *Exerc. Sport Sci. Rev.* **2014**, *42*, 53–61. [CrossRef] [PubMed]
5. Minetto, M.A.; Giannini, A.; McConnell, R.; Busso, C.; Massazza, G. Effects of exercise on skeletal muscles and tendons. *Curr. Opin. Endocr. Metab. Res.* **2019**, *9*, 90–95. [CrossRef]
6. Musumeci, G.; Maria Trovato, F.; Imbesi, R.; Castrogiovanni, P. Effects of dietary extra-virgin olive oil on oxidative stress resulting from exhaustive exercise in rat skeletal muscle: A morphological study. *Acta Histochem.* **2014**, *116*, 61–69. [CrossRef] [PubMed]
7. Bani, D.; Nistri, S. New insights into the morphogenic role of stromal cells and their relevance for regenerative medicine. lessons from the heart. *J. Cell. Mol. Med.* **2014**, *18*, 363–370. [CrossRef]
8. Ceccarelli, G.; Benedetti, L.; Arcari, M.L.; Carubbi, C.; Galli, D. Muscle stem cell and physical activity: What point is the debate at? *Open Med.* **2017**, *12*, 144–156. [CrossRef]
9. Brett, J.O.; Arjona, M.; Ikeda, M.; Quarta, M.; de Morrée, A.; Egner, I.M.; Perandini, L.A.; Ishak, H.D.; Goshayeshi, A.; Benjamin, D.I.; et al. Exercise rejuvenates quiescent skeletal muscle stem cells in old mice through restoration of Cyclin D1. *Nat. Metab.* **2020**, *2*, 307–317. [CrossRef]
10. Boppart, M.D.; De Lisio, M.; Witkowski, S. Exercise and Stem Cells. *Prog. Mol. Biol. Transl. Sci.* **2015**, *135*, 423–456.
11. Kadi, F.; Charifi, N.; Denis, C.; Lexell, J.; Andersen, J.L.; Schjerling, P.; Olsen, S.; Kjaer, M. The behaviour of satellite cells in response to exercise: What have we learned from human studies? *Pflugers Arch. Eur. J. Physiol.* **2005**, *451*, 319–327. [CrossRef]
12. Marini, M.; Rosa, I.; Ibba-Manneschi, L.; Manetti, M. Telocytes in skeletal, cardiac and smooth muscle interstitium: Morphological and functional aspects. *Histol. Histopathol.* **2019**, *33*, 1151–1165.
13. Popescu, L.M.; Manole, E.; S¸erboiu, C.S.; Manole, C.G.; Suciu, L.C.; Gherghiceanu, M.; Popescu, B.O. Identification of telocytes in skeletal muscle interstitium: Implication for muscle regeneration. *J. Cell. Mol. Med.* **2011**, *15*, 1379–1392. [CrossRef]
14. Mauro, A. Satellite cell of skeletal muscle fibers. *J. Biophys. Biochem. Cytol.* **1961**, *9*, 493–495. [CrossRef]
15. Sambasivan, R.; Yao, R.; Kissenpfennig, A.; van Wittenberghe, L.; Paldi, A.; Gayraud-Morel, B.; Guenou, H.; Malissen, B.; Tajbakhsh, S.; Galy, A. Pax7-expressing satellite cells are indispensable for adult skeletal muscle regeneration. *Development* **2011**, *138*, 3647–3656. [CrossRef]
16. Kyryachenko, S.; Formicola, L.; Ollitrault, D.; Correra, R.; Denizot, A.L.; Kyrylkova, K.; Marazzi, G.; Sassoon, D.A. The Adult Stem Cell Niche: Multiple Cellular Players in Tissue

Homeostasis and Regeneration. In *Encyclopedia of Cell Biology*; Bradshaw, R.A., Stahl, P.D., Eds.; Academic Press: Waltham, MA, USA, 2016; Volume 3, pp. 794–806.
17. Beauchamp, J.R.; Heslop, L.; Yu, D.S.W.; Tajbakhsh, S.; Kelly, R.G.; Wernig, A.; Buckingham, M.E.; Partridge, T.A.; Zammit, P.S. Expression of CD34 and Myf5 defines the majority of quiescent adult skeletal muscle satellite cells. *J. Cell Biol.* **2000**, *151*, 1221–1233. [CrossRef]
18. LaBarge, M.A.; Blau, H.M. Biological progression from adult bone marrow to mononucleate muscle stem cell to multinucleate muscle fiber in response to injury. *Cell* **2002**, *111*, 589–601. [CrossRef]
19. Kassar-Duchossoy, L.; Giacone, E.; Gayraud-Morel, B.; Jory, A.; Gomès, D.; Tajbakhsh, S. Pax3/Pax7 mark a novel population of primitive myogenic cells during development. *Genes Dev.* **2005**, *19*, 1426–1431. [CrossRef]
20. Gros, J.; Manceau, M.; Thomé, V.; Marcelle, C. A common somitic origin for embryonic muscle progenitors and satellite cells. *Nature* **2005**, *435*, 954–958. [CrossRef] [PubMed]
21. Musumeci, G.; Castrogiovanni, P.; Coleman, R.; Szychlinska, M.A.; Salvatorelli, L.; Parenti, R.; Magro, G.; Imbesi, R. Somitogenesis: From somite to skeletal muscle. *Acta Histochem.* **2015**, *117*, 313–328. [CrossRef] [PubMed]
22. Pannérec, A.; Marazzi, G.; Sassoon, D. Stem cells in the hood: The skeletal muscle niche. *Trends Mol. Med.* **2012**, *18*, 599–606. [CrossRef] [PubMed]
23. Montarras, D.; Morgan, J.; Colins, C.; Relaix, F.; Zaffran, S.; Cumano, A.; Partridge, T.; Buckingham, M. Developmental biology: Direct isolation of satellite cells for skeletal muscle regeneration. *Science* **2005**, *309*, 2064–2067. [CrossRef] [PubMed]
24. Zickri, M.B. Possible local stem cells activation by microcurrent application in experimentally injured soleus muscle. *Int. J. Stem Cells* **2014**, *7*, 79–86. [CrossRef] [PubMed]
25. Murphy, M.M.; Lawson, J.A.; Mathew, S.J.; Hutcheson, D.A.; Kardon, G. Satellite cells, connective tissue fibroblasts and their interactions are crucial for muscle regeneration. *Development* **2011**, *138*, 3625–3637. [CrossRef]
26. Balduino, A.; Leite Duarte, M.E.; Taichman, R.S. Skeletal Resident Stem Cells. In *Resident Stem Cells Regenerative Therapy*; Dos Santos Goldenberg, R.C., Campos, A.C., Eds.; Academic Press: Cambridge, MA, USA, 2013; pp. 123–140.
27. Kang, Y.; Zhu, Z.; Zheng, Y.; Wan, W.; Manole, C.G.; Zhang, Q. Skin telocytes versus fibroblasts: Two distinct dermal cell populations. *J. Cell. Mol. Med.* **2015**, *19*, 2530–2539. [CrossRef]
28. Gatchalian, C.L.; Schachner, M.; Sanes, J.R. Fibroblasts that proliferate near denervated synaptic sites in skeletal muscle synthesize the adhesive molecules tenascin(J1), N-CAM, fibronectin, and a heparan sulfate proteoglycan. *J. Cell Biol.* **1989**, *108*, 1873–1890.[CrossRef]
29. Biferali, B.; Proietti, D.; Mozzetta, C.; Madaro, L. Fibro–Adipogenic Progenitors Cross-Talk in Skeletal Muscle: The Social Network. *Front. Physiol.* **2019**, *10*, 1074. [CrossRef]
30. Joe, A.W.B.; Yi, L.; Natarajan, A.; Le Grand, F.; So, L.; Wang, J.; Rudnicki, M.A.; Rossi, F.M.V. Muscle injury activates resident fibro/adipogenic progenitors that facilitate myogenesis. *Nat. Cell Biol.* **2010**, *12*, 153–163. [CrossRef]
31. Uezumi, A.; Fukada, S.I.; Yamamoto, N.; Takeda, S.; Tsuchida, K. Mesenchymal progenitors distinct from satellite cells contribute to ectopic fat cell formation in skeletal muscle. *Nat. Cell Biol.* **2010**, *12*, 143–152. [CrossRef]
32. Gautam, J.; Yao, Y. Pericytes in skeletal muscle. *Adv. Exp. Med. Biol.* **2019**, *1122*, 59–72.

33. Popescu, L.M.; Faussone-Pellegrini, M.S. TELOCYTES—A case of serendipity: The winding way from Interstitial Cells of Cajal (ICC), via Interstitial Cajal-Like Cells (ICLC) to TELOCYTES. *J. Cell. Mol. Med.* **2010**, *14*, 729–740. [CrossRef]
34. Ramón y Cajal, S. *Histologie du Systeme Nerveux de l'Homme & des Vertébrés*; Tome II.; Maloine: Paris, France, 1911.
35. Faussone Pellegrini, M.S.; Cortesini, C.; Romagnoli, P. Sull'Ultrastruttura Della Tunica Muscolare Della Porzione Cardiale Dell'Esofago E Dello Stomaco Umano Con Particolare Riferimento Alle Cosiddette Cellule Interstiziali Di Cajal. *Arch. Ital. Anat. Embriol.* **1977**, *82*, 157–177.
36. Thuneberg, L. Interstitial cells of Cajal: Intestinal pacemaker cells? *Adv. Anat. Embryol. Cell Biol.* **1982**, *71*, 1–130. [PubMed]
37. Pieri, L.; Vannucchi, M.G.; Faussone-Pellegrini, M.S. Histochemical and ultrastructural characteristics of an interstitial cell type different from ICC and resident in the muscle coat of human gut. *J. Cell. Mol. Med.* **2008**, *12*, 1944–1955. [CrossRef]
38. Aleksandrovych, V.; Pasternak, A.; Basta, P.; Sajewicz, M.; Walocha, J.A.; Gil, K. Telocytes: Facts, speculations and myths. *Folia Med. Cracov.* **2017**, *57*, 5–22.
39. Díaz-Flores, L.; Gutiérrez, R.; García, M.P.; González, M.; Sáez, F.J.; Aparicio, F.; Díaz-Flores, L.; Madrid, J.F. Human resident CD34+ stromal cells/telocytes have progenitor capacity and are a source of αSMA+ cells during repair. *Histol. Histopathol.* **2015**, *30*, 615–627.
40. Díaz-Flores, L.; Gutiérrez, R.; Goméz, M.G.; Sáez, F.J.; Madrid, J.F. Behaviour of telocytes during physiopathological activation. *Semin. Cell Dev. Biol.* **2016**, *55*, 50–61. [CrossRef]
41. Ivey, M.J.; Tallquist, M.D. Defining the cardiac fibroblast. *Circ. J.* **2016**, *80*, 2269–2276. [CrossRef]
42. Kucybala, I.; Janas, P.; Ciuk, S.; Cholopiak, W.; Klimek-Piotrowska, W.; Holda, M.K. A comprehensive guide to telocytes and their great potential in cardiovascular system. *Bratislava Med. J.* **2017**, *118*, 302–309. [CrossRef]
43. Cretoiu, M.S.; Cretoiu Anca Simionescu, D.; Popescu, L.M. Telocytes in Human Fallopian Tube and Uterus Express Estrogen and Progesterone Receptors. In *Sex Steroids*; Kahn, S.M., Ed.; IntechOpen, 2012; pp. 91–114. Available online: https://www.intechopen.com/books/sex-steroids/telocytes-in-human-fallopian-tube-and-uterus-express-estrogen-andprogesterone-receptors (accessed on 7 June 2021).
44. Gherghiceanu, M.; Popescu, L.M. Interstitial Cajal-like cells (ICLC) in human resting mammary gland stroma. Transmission electron microscope (TEM) identification. *J. Cell. Mol. Med.* **2005**, *9*, 893–910. [CrossRef] [PubMed]
45. Valadi, H.; Ekström, K.; Bossios, A.; Sjöstrand, M.; Lee, J.J.; Lötvall, J.O. Exosome-mediated transfer of mRNAs and microRNAs is a novel mechanism of genetic exchange between cells. *Nat. Cell Biol.* **2007**, *9*, 654–659. [CrossRef]
46. Deasy, B.M.; Feduska, J.M.; Payne, T.R.; Li, Y.; Ambrosio, F.; Huard, J. Effect of VEGF on the regenerative capacity of muscle stem cells in dystrophic skeletal muscle. *Mol. Ther.* **2009**, *17*, 1788–1798. [CrossRef]
47. Cretoiu, D.; Radu, B.M.; Banciu, A.; Banciu, D.D.; Cretoiu, S.M. Telocytes heterogeneity: From cellular morphology to functional evidence. *Semin. Cell Dev. Biol.* **2017**, *64*, 26–39. [CrossRef] [PubMed]
48. Díaz-Flores, L.; Gutiérrez, R.; García, M.P.; Sáez, F.J.; Díaz-Flores, L.; Valladares, F.; Madrid, J.F. CD34+ stromal cells/fibroblasts/ fibrocytes/telocytes as a tissue reserve and a principal

source of mesenchymal cells. Location, morphology, function and role in pathology. *Histol. Histopathol.* **2014**, *29*, 831–870.
49. Manetti, M.; Tani, A.; Rosa, I.; Chellini, F.; Squecco, R.; Idrizaj, E.; Zecchi-Orlandini, S.; Ibba-Manneschi, L.; Sassoli, C. Morphological evidence for telocytes as stromal cells supporting satellite cell activation in eccentric contraction-induced skeletal muscle injury. *Sci. Rep.* **2019**, *9*, 14515. [CrossRef] [PubMed]
50. Ibba-Manneschi, L.; Rosa, I.; Manetti, M. Telocyte implications in human pathology: An overview. *Semin. Cell Dev. Biol.* **2016**, *55*, 62–69. [CrossRef] [PubMed]
51. Boos, A.M.; Weigand, A.; Brodbeck, R.; Beier, J.P.; Arkudas, A.; Horch, R.E. The potential role of telocytes in Tissue Engineering and Regenerative Medicine. *Semin. Cell Dev. Biol.* **2016**, *55*, 70–78. [CrossRef]
52. Richter, M.; Kostin, S. The failing human heart is characterized by decreased numbers of telocytes as result of apoptosis and altered extracellular matrix composition. *J. Cell. Mol. Med.* **2015**, *19*, 2597–2606. [CrossRef]
53. Manetti, M.; Guiducci, S.; Ruffo, M.; Rosa, I.; Faussone-Pellegrini, M.S.; Matucci-Cerinic, M.; Ibba-Manneschi, L. Evidence for progressive reduction and loss of telocytes in the dermal cellular network of systemic sclerosis. *J. Cell. Mol. Med.* **2013**, *17*, 482–496. [CrossRef]
54. Pimentel Neto, J.; Rocha, L.C.; Barbosa, G.K.; dos Santos Jacob, C.; Krause Neto, W.; Watanabe, I.S.; Ciena, A.P. Myotendinous junction adaptations to ladder-based resistance training: Identification of a new telocyte niche. *Sci. Rep.* **2020**, *10*, 14124. [CrossRef]
55. Xiao, J.; Chen, P.; Qu, Y.; Yu, P.; Yao, J.; Wang, H.; Fu, S.; Bei, Y.; Chen, Y.; Che, L.; et al. Telocytes in exercise-induced cardiac growth. *J. Cell. Mol. Med.* **2016**, *20*, 973–979. [CrossRef]
56. Arifin, W.N.; Zahiruddin, W.M. Sample size calculation in animal studies using resource equation approach. *Malaysian J. Med. Sci.* **2017**, *24*, 101–105.
57. Castrogiovanni, P.; Di Rosa, M.; Ravalli, S.; Castorina, A.; Guglielmino, C.; Imbesi, R.; Vecchio, M.; Drago, F.; Szychlinska, M.A.; Musumeci, G. Moderate physical activity as a prevention method for knee osteoarthritis and the role of synoviocytes as biological key. *Int. J. Mol. Sci.* **2019**, *20*, 511. [CrossRef]
58. Ishihara, A.; Hirofuji, C.; Nakatani, T.; Itoh, K.; Itoh, M.; Katsuta, S. Effects of running exercise with increasing loads on tibialis anterior muscle fibres in mice. *Exp. Physiol.* **2002**, *87*, 113–116. [CrossRef]
59. Fischer, A.H.; Jacobson, K.A.; Rose, J.; Zeller, R. Hematoxylin and eosin staining of tissue and cell sections. *Cold Spring Harb. Protoc.* **2008**, *3*. [CrossRef]
60. Trovato, F.M.; Castrogiovanni, P.; Szychlinska, M.A.; Purrello, F.; Musumeci, G. Impact of western and mediterranean diets and vitamin D on muscle fibers of sedentary rats. *Nutrients* **2018**, *10*, 231. [CrossRef]
61. Bei, Y.; Wang, F.; Yang, C.; Xiao, J. Telocytes in regenerative medicine. *J. Cell. Mol. Med.* **2015**, *19*, 1441–1454. [CrossRef]
62. Cretoiu, S.M.; Popescu, L.M. Telocytes revisited. *Biomol. Concepts* **2014**, *5*, 353–369. [CrossRef]
63. Fu, S.; Wang, F.; Cao, Y.; Huang, Q.; Xiao, J.; Yang, C.; Popescu, L.M. Telocytes in human liver fibrosis. *J. Cell. Mol. Med.* **2015**, *19*, 676–683. [CrossRef]
64. Wang, F.; Bei, Y.; Zhao, Y.; Song, Y.; Xiao, J.; Yang, C. Telocytes in pregnancy-induced physiological liver growth. *Cell. Physiol. Biochem.* **2015**, *36*, 250–258. [CrossRef]

65. Díaz-Flores, L.; Gutiérrez, R.; García, M.P.; González-Gómez, M.; Carrasco, J.L.; Alvarez-Argüelles, H.; Díaz-Flores, L. Telocytes/cd34+ stromal cells in pathologically affected white adipose tissue. *Int. J. Mol. Sci.* **2020**, *21*, 9694. [CrossRef]
66. Fukada, S.I. The roles of muscle stem cells in muscle injury, atrophy and hypertrophy. *J. Biochem.* **2018**, *163*, 353–358. [CrossRef]
67. Mitchell, P.O.; Pavlath, G.K. Skeletal muscle atrophy leads to loss and dysfunction of muscle precursor cells. *Am. J. Physiol. Cell Physiol.* **2004**, *287*, C1753–C1762. [CrossRef]
68. Verdijk, L.B.; Snijders, T.; Drost, M.; Delhaas, T.; Kadi, F.; Van Loon, L.J.C. Satellite cells in human skeletal muscle; From birth to old age. *Age* **2014**, *36*, 545–557. [CrossRef] [PubMed]
69. Scharner, J.; Zammit, P.S. The muscle satellite cell at 50: The formative years. *Skelet. Muscle* **2011**, *1*, 28. [CrossRef]
70. Albulescu, R.; Tanase, C.; Codrici, E.; Popescu, D.I.; Cretoiu, S.M.; Popescu, L.M. The secretome of myocardial telocytes modulates the activity of cardiac stem cells. *J. Cell. Mol. Med.* **2015**, *19*, 1783–1794. [CrossRef]
71. Liao, Z.; Li, D.; Chen, Y.; Li, Y.; Huang, R.; Zhu, K.; Chen, H.; Yuan, Z.; Zheng, X.; Zhao, H.; et al. Early moderate exercise benefits myocardial infarction healing via improvement of inflammation and ventricular remodelling in rats. *J. Cell. Mol. Med.* **2019**, *23*, 8328–8342. [CrossRef]
72. Romano, E.; Rosa, I.; Fioretto, B.S.; Lucattelli, E.; Innocenti, M.; Ibba-Manneschi, L.; Matucci-Cerinic, M.; Manetti, M. A two-step immunomagnetic microbead-based method for the isolation of human primary skin telocytes/cd34+ stromal cells. *Int. J. Mol. Sci.* **2020**, *21*, 5877. [CrossRef]
73. Varga, I.; Kyselovicˇ, J.; Danišovicˇ, L'.; Gálfiová, P.; Kachlík, D.; Polák, Š.; Klein, M. Recently discovered interstitial cells termed telocytes: Distinguishing cell-biological and histological facts from fictions. *Biologia* **2019**, *74*, 195–203. [CrossRef]
74. Lis, G.J.; Dubrowski, A.; Lis, M.; Solewski, B.; Witkowska, K.; Aleksandrovych, V.; Jasek-Gajda, E.; Hołda, M.K.; Gil, K.; Litwin, J.A. Identification of cd34+/pgdfrα+ valve interstitial cells (Vics) in human aortic valves: Association of their abundance, morphology and spatial organization with early calcific remodeling. *Int. J. Mol. Sci.* **2020**, *21*, 6330. [CrossRef]
75. Bei, Y.; Zhou, Q.; Fu, S.; Lv, D.; Chen, P.; Chen, Y.; Wang, F.; Xiao, J. Cardiac telocytes and fibroblasts in primary culture: Different morphologies and immunophenotypes. *PLoS ONE* **2015**, *10*, e0115991. [CrossRef] [PubMed]
76. Nielsen, J.S.; McNagny, K.M. Erratum: Novel functions of the CD34 family. *J. Cell Sci.* **2008**, *121*, 3683–3692. [CrossRef]
77. Klein, M.; Urban, L.; Deckov, I.; Danisovic, L.; Polak, S.; Danihel, L.; Varga, I. Distribution of telocytes in the corpus and cervix of human uterus: An immunohistochemical study. *Biologia* **2017**, *72*, 1217–1223. [CrossRef]
78. Reardon, K.A.; Davis, J.; Kapsa, R.M.I.; Choong, P.; Byrne, E. Myostatin, insulin-like growth factor-1, and leukemia inhibitory factor mRNAs are upregulated in chronic human disuse muscle atrophy. *Muscle Nerve* **2001**, *24*, 893–899. [CrossRef] [PubMed]
79. Reid, M.B.; Li, Y.P. Tumor necrosis factor-α and muscle wasting: A cellular perspective. *Respir. Res.* **2001**, *2*, 269–272. [CrossRef]
80. Stevenson, E.J.; Giresi, P.G.; Koncarevic, A.; Kandarian, S.C. Global analysis of gene expression patterns during disuse atrophy in rat skeletal muscle. *J. Physiol.* **2003**, *551*, 33–48. [CrossRef]

81. Cretoiu, D.; Roatesi, S.; Bica, I.; Plesca, C.; Stefan, A.; Bajenaru, O.; Condrat, C.E.; Cretoiu, S.M. Simulation and modeling of telocytes behavior in signaling and intercellular communication processes. *Int. J. Mol. Sci.* **2020**, *21*, 2615. [CrossRef]
82. Vannucchi, M.G. The telocytes: Ten years after their introduction in the scientific literature. An update on their morphology, distribution, and potential roles in the gut. *Int. J. Mol. Sci.* **2020**, *21*, 4478. [CrossRef]
83. Cocucci, E.; Racchetti, G.; Meldolesi, J. Shedding microvesicles: Artefacts no more. *Trends Cell Biol.* **2009**, *19*, 43–51. [CrossRef]
84. Gandahi, N.S.; Ding, B.; Shi, Y.; Bai, X.; Gandahi, J.A.; Vistro, W.A.; Chen, Q.; Yang, P. Identification of telocytes in the pancreas of Turtles—A role in cellular communication. *Int. J. Mol. Sci.* **2020**, *21*, 2057. [CrossRef]

7 General Conclusions

Traditional treatments for OA involving the use of non-steroidal anti-inflammatory drugs (NSAID) and opioids are effective as pain reliefers but fail in restoring tissue degeneration and commonly present several adverse events. Current efforts in scientific research of OA are devolved to understanding the morpho-molecular mechanisms and pathophysiological changes occurring in the tissue, in order to plan future preventive measure and treatments for this complex and spreading disease. Regenerative engineering for cartilage, in the means of use of progenitor cells, scaffolds and biological and biophysical stimuli, is emerging as a promising alternative and solution to tissue defects for the support of neocartilage formation. Nevertheless, application of engineered structures deals with phenotypic instability of the cells in long-term cultures and, consequently, poor neo-tissue morphological properties. For this reason, in the first presented study, the work was addressed to investigate and improve the chondrogenic differentiation of hBM-MSCs in two different in vitro models represented by pellets and GelMA/HA hydrogels The results showed that the pellets after 21 days of culture and TGFβ1 supplementation, with different exposure times, showed a proper chondrogenic differentiation, but at the same time high hypertrophic factors expression levels were also highlighted, confirming the TGFβ1 “double effect”. These observations were important for the second part of the study in which the chondrogenic differentiation of hBM-MSCs was evaluated in a more complex in vitro system by seeding the hBM-MSCs in GelMA/HA hydrogels and subjecting the constructs to TGFβ1 priming for one-week and mechanical stimulation. The results showed that the cells inside the hydrogels exposed to mechanical stimulation alone did not give, or in some cases very weak, a significant differentiation response, while the cells inside the hydrogels exposed to TGFβ1 priming and mechanical stimulation combination were able to differentiate in the chondrogenic sense demonstrated a chondron-like organisation. The preliminary results of this work therefore encourage further study of this combination of elements which appears to be promising for tissue engineering for cartilage repair. In the second study the collagen I-based scaffolds were confirmed to be biocompatible after orthotopic implantation in vivo rat model by histological, histochemical, immunohistochemical and gene expression analysis, as suggested by total biodegradation and replacement of the biomaterial with the newly formed cartilage-like tissue at 16-weeks post-implantation, and absence of scar-like tissue formation and inflammatory cell infiltration at the interface between the scaffold and peri-native cartilage tissue.

Also regarding to prevention, the benefits of physical activity in OA patients have demonstrated to exert protective effect on joints as a non-surgical and non-pharmacological treatment, re-establishing the physiological function of cell populations, preventing the onset of OA, and/or postponing the need

for joint replacement. The purpose of the third study was to highlight the role of mechanical stimulation, i.e., moderate exercise, in reducing ATX expression in healthy and mild OA rat articular cartilage. Higher expressions of ATX were found in femur and tibia of OA rats, suggesting that this molecule could participate in the progression of the disease. Interestingly, in the femur, physical activity performed by OA rats was able to lower ATX expression, encouraging the evidence that joint movement is beneficial for the cartilage, and further studies on the potential usefulness of ATX, as biochemical markers of disease progression, and of exercise to prevent/attenuate the osteoarthritic process. Finally, last morphological study was intended to observe the presence of telocytes in tibialis anterior muscle of healthy rats who underwent a protocol of endurance training. The understanding of the mechanisms between the cells involved in the muscle tissue remodelling offers new chances in regenerative tissue strategies and insights about finding triggers in sarcopenia and other musculoskeletal disorders like OA that are affected by muscle integrity. Exercise training has been shown to sustaining muscle maintenance of telocytes, therefore promoting adapted physical activity and rehabilitation programmes for healthy subjects and OA patients.

The therapeutic and preventive approaches for OA still represent a difficult challenge for the clinical and scientific research fields. In conclusion, the present PhD thesis highlights some potential useful aspects concerning tissue engineering strategies and preventive methods based on physical activity aimed, respectively, to resolve and avoid osteoarthritic disease and cartilage degeneration.

List of Pubblications

1) Ravalli S, Szychlinska MA, **Lauretta G**, Di Rosa M, Musumeci G. Investigating lubricin and known cartilage-based biomarkers of osteoarthritis. *Expert Rev Mol Diagn.* 2020 Apr;20(4):443-452. doi: 10.1080/14737159.2020.1733978. Epub 2020 Feb 24. PMID: 32085680.

2) Ravalli S, Szychlinska MA, **Lauretta G**, Musumeci G. New Insights on Mechanical Stimulation of Mesenchymal Stem Cells for Cartilage Regeneration. *Appl. Sci.* 2020, 10(8), 2927; doi.org/10.3390/app10082927.

3) Szychlinska MA, Calabrese G, Ravalli S, Dolcimascolo A, Castrogiovanni P, Fabbi C, Puglisi C, **Lauretta G**, Di Rosa M, Castorina A, Parenti R, Musumeci G. Evaluation of a Cell-Free Collagen Type I-Based Scaffold for Articular Cartilage Regeneration in an Orthotopic Rat Model. *Materials* (Basel). 2020 May 21;13(10):2369. doi: 10.3390/ma13102369. PMID: 32455683;

4) **Lauretta G**, Ravalli S, Szychlinska MA, Castorina A, Maugeri G, D'Amico AG, D'Agata V, Musumeci G. Current knowledge of pituitary adenylate cyclase activating polypeptide (PACAP) in articular cartilage. *Histol Histopathol*. 2020 Nov;35(11):1251-1262. doi: 10.14670/HH-18-233. Epub 2020 Jun 16. PMID: 32542641.

5) Ravalli S, Federico C, **Lauretta G**, Saccone S, Pricoco E, Roggio F, Di Rosa M, Maugeri G, Musumeci G. Morphological Evidence of Telocytes in Skeletal Muscle Interstitium of Exercised and Sedentary Rodents. *Biomedicines*. 2021 Jul 13;9(7):807. doi: 10.3390/biomedicines9070807. PMID: 34356871

6) Ravalli S, Roggio F, **Lauretta G**, Di Rosa M, D'Amico AG, D'agata V, Maugeri G, Musumeci G. Exploiting real-world data to monitor physical activity in patients with osteoarthritis: the opportunity of digital epidemiology. *Heliyon*. 2022 Feb 22;8(2):e08991. doi: 10.1016/j.heliyon.2022.e08991. PMID: 35252602.

7) **Lauretta G**, Ravalli S, Maugeri G, D'Agata V, Rosa MD, Musumeci G. The Impact of Physical Exercise on the Hippocampus in Physiological Condition and Ageing-Related Decline: Current Evidence from Animal and Human Studies. *Curr Pharm Biotechnol.* 2022;23(2):180-189. doi: 10.2174/1389201022666210405142611. PMID: 33820516.

8) Ravalli S, Roggio F, Magrì B, **Lauretta G**, Broggi G, Caltabiano R, Vecchio GM, Magro G, Loreto C, Castorina A, Musumeci G. Immunohistochemical evaluation of autotaxin and

lubricin in mild osteoarthritic rat model performing moderate physical activity. *Acta Histochem.* 2022 Aug;124(6):151936. doi: 10.1016/j.acthis.2022.151936. Epub 2022 Jul 30. PMID: 35917632.

MANUSCRIPTS IN PREPARATION:

1) **Lauretta G**, Armiento AR, Stoddart MJ, Musumeci G. Evaluation of chondrogenic differentiation donor-dependent of Human bone marrow mesenchymal stem cells (hBM-MSCs) in Pellet cultures.

2) **Lauretta G**, Armiento AR, Stoddart MJ, Musumeci G. Effects of TGFβ1 Priming and Mechanical loading on Human bone marrow mesenchymal stem cells (hBM-MSCs) within GelMA/HA Hydrogels.